Influences on the Cold Start Behaviour of a Diesel Engine at Reduced Compression Ratio

David James MacMillan, MEng.

Submitted to the University of Nottingham for the degree of Doctor of Philosophy,
May 2009.

Contents

Abstract **vi**

Acknowledgements **viii**

Abbreviations **ix**

Nomenclature **xi**

1 Introduction **1**

1.1 Overview 1

1.2 Historical Background 2

1.2.1 Key Technological Contributions to Diesel Engine Performance Improvement 3

1.2.2 More Recent Motivators for Technology 7

1.3 Aims 12

1.4 Thesis Structure 13

1.5 Summary 14

2 Literature Review **15**

2.1 Introduction 15

2.2 Theory Behind Reduction in Compression Ratio 16

2.3 The Diesel Autoignition Process 19

2.4 Diesel Engine Cold Start 24

2.4.1 Modern Fuel Injection Equipment 29

2.4.2 Starting Aids 30

2.5 Cold Idle 31

2.6 General Compression Ratio Effects 33

2.7 Summary 34

3 Experimental Facilities and Test Procedure **36**

3.1 Introduction 36

3.2 Single Cylinder Engine 37

3.3 Cold Starting Modifications 39

3.4 Instrumentation and Data Acquisition 40

3.5 Experimental Technique 43

3.5.1 Steps to Ensure Repeatability 43

3.5.2 Performing a Cold Start Test Point 46

3.5.3 Modification for Cold Idle Test Points 47

3.6 Summary 47

4 Key Response Variables **48**

4.1 Introduction 48

4.2 Indicated Mean Effective Pressure 49

4.3 Heat Release Rate 52

4.3.1 Heat Transfer and Blowby 53

4.3.2 Further Uses of Heat Release 56

4.4 Summary 57

5 Combustion Characteristics — Effect of Injection Parameters **59**

5.1 Introduction 59

5.2 Varying Injection Timing 60

5.3 Varying Injection Quantity 64

5.3.1 Variations over 30 Injected Cycles 67

5.4 Varying Ambient Temperature 75

5.5 Varying Number of Injections 82

5.5.1 Pilot Injection 83

5.5.2 Twin Pilot Injection 89

5.6 Varying Engine Speed 96

5.6.1 Importance of Pilot Injection at Cold Idle 96

5.6.2 Effect of Engine Speed on IMEPg 98

5.6.3 Effect of Engine Speed on Coefficient of Variation of IMEPg 105

5.6.4 Effect of Multiple Injection on Cold Idle 110

5.7 Computational Validation of Mixture Distribution 125

5.8 Summary 138

6 Effects of Reducing Compression Ratio 140

6.1 Introduction 140

6.2 Method for Reducing Compression Ratio 141

6.3 Primary Effects of Compression Ratio 141

6.4 Cold Start Comparisons 149

6.5 The Effect of Reducing Temperature on LCR Cold Start 169

6.6 Cold Idle Comparisons 171

6.7 Multiple Pilot Injection at LCR 178

6.8 Summary 182

7 The effects of Glow Plug operation 184

7.1 Introduction 184

7.2 Impact of Glow Plug Operation on Cold Start 185

7.3 The Effect of Varying Glow Plug Temperature 189

7.3.1 Effect of Glow Plug Temperature on 300 rpm Cold Start 191

7.3.2 Effect of Glow Plug Temperature on Cold Idle 197

7.4 The Effect of Glow Plug Protrusion on Idle Stability 205

7.5 Summary 209

8 Discussion, Future Work and Conclusions 211

8.1 Introduction 211

8.2 Discussion of Key Findings 212

8.2.1 General Validity of Test Procedure 212

8.2.2 Low Speed Findings 212

8.2.3 Idle Speed Findings 214

8.2.4 The Place of Cold Start in General Engine Development 217

8.3 Future Work 220

8.4 Conclusions 223

References 227

Appendix 237

Abstract

The design trend for light duty diesel engines is towards lower compression ratio and higher turbocharger boost. This can enable higher specific power and lower pollutant emissions to be achieved, but raises concerns that cold start operation might be adversely affected. This is investigated and quantified through the study of a modern light duty diesel engine at two compression ratios and temperatures down to $-20°C$.

Key indicators of cold start performance are the magnitude and cycle-to-cycle variation of indicated mean effective pressure. Initial studies were carried out at 300 rpm, a speed representative of post-first-fire conditions. Studies were then conducted at higher engine speeds representative of cold idle. The utility of different injection strategies, timings and quantities is investigated when varying test temperature and engine speed through a range of values encountered during the cold start phase of engine operation. The importance of the glow plug as a cold start aid is also investigated by varying its operating temperature and protrusion into the combustion chamber. The indicated mean effective pressure was used to assess the effects of varying input parameters, and gross heat release rate information is used to identify the phenomena responsible for desirable or undesirable characteristics.

Reduction in compression ratio led to no deterioration of initial start performance from speeds just above cranking, provided an appropriate injection strategy was chosen. Higher indicated mean effective pressure was possible at low speeds using low compression ratio due to reduced losses and more complete combustion. Cycle-to-cycle variability in indicated mean effective pressure increased markedly for both compression ratios at engine speeds representative of cold idle, especially when test temperature was reduced. Stability reduction was more severe at low compression ratio.

Multiple pilot injections at high compression ratio cold idle resulted in better cycle-to-cycle stability. Analysis of heat release profiles suggested that additional pilots assisted fuel mixing, a conclusion supported by a computational fluid dynamics model. Multiple pilots created a more homogeneous fuel distribution through the bowl at time of main injection. Multiple pilots could not stabilise operation at low compression ratio.

Improvement in cold idle at low compression ratio was achieved by increasing glow plug temperature, which significantly increased the rate of fuel preparation. This increased the initial rate of heat release and resulted in significantly less variation in the heat release rate profiles. Small changes in glow plug protrusion rapidly degraded cold idle performance, indicating the importance of correct design.

Acknowledgements

First of all, thanks go to Professor Paul Shayler for giving me the opportunity to do research with him over the past years, and for all the support and advice given since I took him up on the kind offer.

To those I worked with within the group, both still present and gone on to pastures new, I thank them for providing the best working environment I could have hoped for. Among the technical staff special thanks go out to the two Johns and a Geoff who were especially involved with my project and kept me testing when others would surely have failed, greeting adversity with old school humour to the end. In the office I thank Antonino in particular for being my chiller monkey and sharing the pleasures of innumerable meetings.

I am deeply indebted to the Ford Motor Company, both for financial support and the infinitely valuable contributions of years of experience in the form of Mike Murphey, Mike Watts, Ian Pegg and Tim Morris in particular.

To my friends and family, for providing me with a fantastic world outside of work in the form of both support and entertainment. I could not have done or done it without you, you know who you are. The final thanks must to go to my parents who have provided me with every opportunity and encouragement from the year dot. I could not and would never wish for more.

Abbreviations

CO	Carbon Monoxide
CO_2	Carbon Dioxide
HC	Hydrocarbons
NO	Nitric Oxide
NO_2	Nitrogen Dioxide
NO_x	Oxides of Nitrogen
ATDC	After Top Dead Centre
BDC	Bottom Dead Centre
BSFC	Brake Specific Fuel Consumption
BTDC	Before Top Dead Centre
CA	Crank Angle
CFD	Computational Fluid Dynamics
CI	Compression Ignition
CR	Compression Ratio
DI	Direct Injection
EGR	Exhaust Gas Recirculation
EOC	End of Combustion

EVO	Exhaust Valve Opening
FIE	Fuel Injection Equipment
HCCI	Homogeneous Charge Compression Ignition
HCR	High Compression Ratio
HPCR	High Pressure Common Rail
IDI	Indirect Injection
LCR	Low Compression Ratio
LHV	Lower Heating Value
MEP	Mean Effective Pressure
ppm	parts per million
rpm	revolutions per minute
SI	Spark Ignition
SOC	Start of Combustion
TDC	Top Dead Centre

Nomenclature

γ	ratio of specific heats c_p/c_v
ϕ	Equivalence Ratio [-]
ρ_{air}	Density of Air [kg/m^3]
A	Area [m^2]
A_{ring}	Effective Ring Gap Area [m^2]
c_p	specific heat at constant pressure [kJ/kg$K$]
c_v	specific heat at constant volume [kJ/kg$K$]
$\mathrm{CoV}_{\mathrm{IMEPg}}$	Coefficient of Variation of IMEPg [%]
Cum GHR	Cumulative Gross Heat Release [J]
FMEP	Friction Mean Effective Pressure [bar]
h_c	Heat Transfer Coefficient [W/m^{2}K]
GHRR	gross Heat Release Rate [J/°]
NHRR	net Heat Release Rate [J/°]
IMEP	Indicated Mean Effective Pressure [bar]
IMEPg	gross indicated Mean Effective Pressure [bar]

$\overline{IMEPg}_n$	average gross Indicated Mean Effective Pressure for first n injected cycles [bar]
$\dot{m}$	Mass Flow Rate [kg/s]
m	mass [kg]
$m_{trapped}$	Trapped Mass [kg]
N	Engine Speed [rpm]
n_c	Indicated Combustion Efficiency [%]
n_f	Indicated Fuel Conversion Efficiency [%]
n_t	Indicated Thermal Efficiency [%]
p	Pressure [Pa]
Q_l	Energy Loss [J]
Q_{bby}	Energy Loss to Blowby [J/$\frac{1}{2}$CA]
Q_{ht}	Energy Loss to Heat Transfer [W]
Q_{LHV}	Lower Heating Value [MJ/l]
R	Specific Gas Constant
$\bar{S}_p$	Mean Piston Speed [m/s]
StD_{IMEPg}	Standard Deviation of IMEPg [bar]
T	Temperature [K]
U	Internal Energy [J]
V	Volume [m^3]
V_c	clearance Volume [m^3]
V_s	swept Volume [m^3]
W	Work [J]

Chapter 1

Introduction

1.1 Overview

There has been much development in passenger vehicle diesel engine technology in the last ten years. The introduction of turbocharged direct injection engines with high pressure common rail injection has produced improvements in specific power, economy and refinement which has increased consumer demand, especially in Europe. Development is generally a trade-off between improving desired factors and reducing unwanted side-effects. In this case, diesel engine technology development in recent years has been driven primarily by consumer demand for higher performance and driveability combined with legislative requirements for lower emissions of oxides of nitrogen and soot. Reduced compression ratios with higher levels of boost have enabled manufacturers to attain greater specific power with lower levels of NO_x formation at part load and reduced soot due to lower dependency on exhaust gas recirculation. The side-effect of lowering compression ratio is potential degradation of performance at cold start. Under these conditions the priority for engine development shifts from emissions reduction and fuel consumption to simply ensuring the vehicle will start, followed by acceptable idling behaviour.

The investigation reported in this thesis focuses on combustion phenomena associated with

cold start, and makes use of a single cylinder research engine. The aim was to gain an insight into and understanding of cold start behaviour and the problems which might arise as a consequence of design trends towards lower compression ratios. Investigations were performed at two compression ratios, where techniques to improve performance were developed, primarily through the optimisation of fuel injection. Conclusions are presented and recommendations made for application to future engine development.

A broad review of the development which has led to the modern turbocharged diesel engine with high pressure common rail fuel injection is presented in this chapter. Key technological innovations are briefly introduced as well as the tightening legislation which has driven much recent development. The trend of reducing compression ratio is also introduced. Thesis aims are highlighted and finally the thesis layout is presented.

1.2 Historical Background

By the end of the 19th century the Otto cycle spark ignition petrol engine, as patented by Eric B. Davidson and Felice Matteucci in 1854, was emerging as the principal prime mover in the fledgling automotive market. Rudolf Diesel patented his New Rational Combustion Engine in 1892 and succeeded in building the first working model in 1897. However, the first commercially available diesel automobiles did not come onto the market until the 1933 Citroen Rosalie and 1936 Mercedes-Benz 260 D. By this time petrol and spark ignition engines were firmly established as the leading combination for automotive power.

Heavy duty diesel engines, those with large displacement operating at lower engine speeds, have been widely used in road and rail haulage, marine or power generation applications. It is only in the last ten years that demand has increased rapidly for light duty diesel engines in passenger vehicles. Possibly the most significant driver for this trend has been much improved specific power output resulting from exploitation of turbocharging and common rail direct fuel injection. Figure 1.1 presents information on production diesel engines from four technological leaders, showing how the adoption of turbocharging in the 1980s and

direct injection in the 1990s has enabled a doubling of specific power after the demise of the naturally aspirated (N/A) engine.

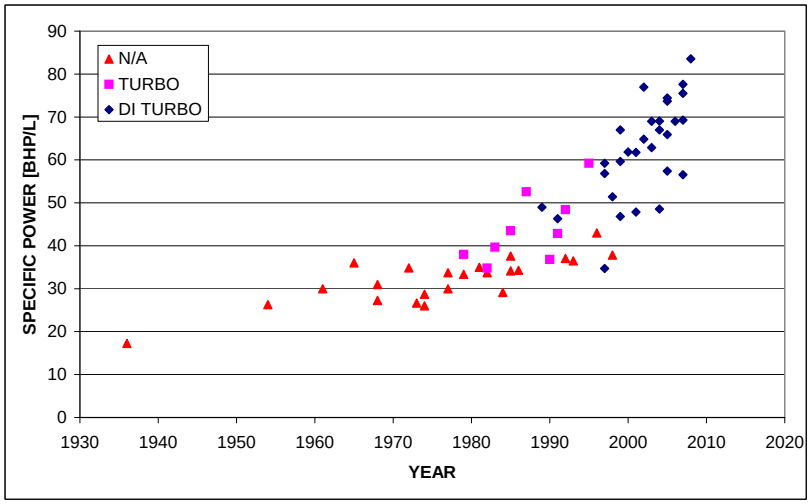

Figure 1.1: Diesel specific power output 1936–2008 — Source of data Carfolio [1]

1.2.1 Key Technological Contributions to Diesel Engine Performance Improvement

One of the most significant reasons why petrol engines established themselves so swiftly as the best choice for automotive applications was early success in the field of fuel delivery and mixing. Karl Benz's carburettor (patented in 1886) was able to draw petrol simply by using the low pressure within the fast moving stream of intake air before it enters the cylinder. The high volatility of petrol (vapour pressure 30–100kPa @ $20°C$, 1 bar [2]) ensures that fuel is well mixed and evaporated in the intake charge before combustion commences at spark timing. This technique is inherently inapplicable for diesel, due both to the low fuel volatility (approx 0.05kPa @ $20°C$, 1 bar [3]), and the unthrottled operating principle with lean running conditions. Despite this, a similar principle was applied for early engines using air-blast injection. High pressure air was used to spray fuel into the combustion chamber in a similar manner to an aerosol can, with some degree of atomisation. This technique required a large air compressor which reduced efficiency. It was also not capable of operating at the rate required for high speed engines suitable for automobile applications. Another means for mixing the fuel with air was required. The chief aims for diesel injection are

to ensure that the correct amount of fuel is delivered, at the correct time, in such a way that the charge is suitably broken up to ensure that there is oxygen available to thoroughly react with all fuel injected. The impracticality of vaporising diesel means that fuel must be injected in liquid form into the cylinder or a pre-chamber directly connected to it so that it is exposed to the high temperatures and pressures required for evaporation and autoignition. This requires high pressure injection, sufficiently high enough to ensure that there is always a positive pressure differential between the fuel supply and in-cylinder conditions during compression and combustion.

The optimisation of injection parameters is expected to play a major role in diesel engine cold start. Modern fuel injection equipment (FIE) enables much flexibility in injection strategy, but this is a relatively recent capability. An understanding of the historical development of the current high pressure common rail direct injection engine will be useful. Robert Bosch first solved the fuel injection problem commercially with series production of the PE-A in-line fuel injection pump in 1927 [4]. A cam driven plunger slides within a pump cylinder for each engine cylinder. Inlet fuel is pressurised and delivered to the injector. Quantity is varied with a control rod which moves a helix connecting the high pressure chamber to the fuel inlet, changing the effective stroke. The addition of a control sleeve allows variable start of injection by moving the relative position of the inlet to the plunger. The general operating principle of this pump is shown diagrammatically in Figure 1.2(a).

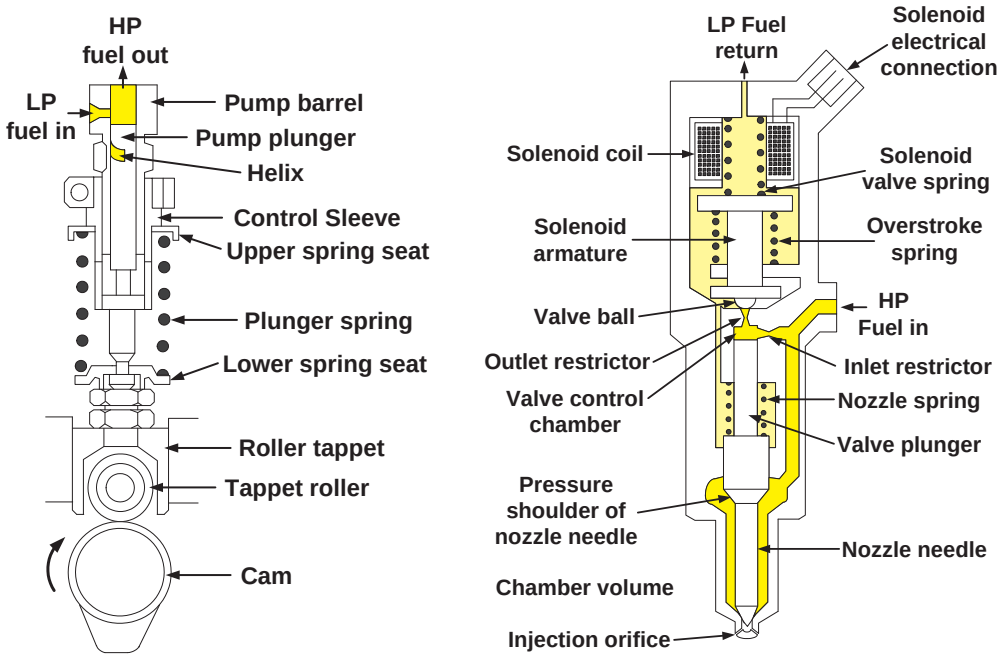

(a) Representation of the drive system of the Bosch PE-A fuel pump.

(b) Representation of the internals of a solenoid type fuel injection.

Figure 1.2: Internal detail of an in-line type pump from the early history of the diesel engine and a more modern solenoid injector. Both reproduced from [4]

Developments of this system led to the 1962 axial distributor pump with a single pump driving all cylinders. A control sleeve connects the required injector to the high pressure fuel at the appropriate point in the engine cycle. Electronic control was realised in 1986 with the solenoid valve distributor pump, allowing a degree of control not possible using mechanical means. Typically these systems were employed with pintle hole injectors in indirect injection (IDI) engines. Indirect injection engines have a small pre-combustion chamber connected to the cylinder by at least one channel. Fuel is injected through a single nozzle hole into this chamber, where it combusts. Rapid expansion forces the charge into the main cylinder where the remainder of the combustion and expansion occurs as more oxygen is available. The high gas velocity of the charge emerging from the pre-combustion chamber ensures thorough air/fuel mixing. These systems commonly operated with a maximum fuel pressure of approximately 450 bar. There are, however, significant losses to heat transfer in the IDI engine. This, and the limited applicability of advanced injection strategies required for emissions control, led to IDI being slowly replaced by the direct injection (DI) concept.

In direct injection there is no pre-chamber. The problem this presents is that the fuel/air mixing cannot be achieved by the rapid expansion from the pre-chamber into the main cylinder. Fuel must be sprayed through a multi-hole nozzle to ensure an even distribution. Small nozzle holes promote atomisation of the spray. To achieve high loads at high speeds, very high rail pressures ($>$ 1000 bar) are required. The unit injector was released in 1994 as an early solution to the problem, dispensing with the high pressure fuel lines, allowing very high pressures ($>$ 2000 bar) and multiple injections per cycle. The unit injector combines a camshaft driven pump and injector in one unit for each cylinder with electronic solenoid control. A greater degree of control was realised with the 1997 introduction of common rail fuel injection. A high pressure pump driven from the crankshaft keeps a reservoir of fuel pressurised in the common rail. High pressure lines then supply each injector, which is again actuated with either a solenoid valve or a piezoelectric actuator. Having a constant supply of high pressure fuel enables multiple precisely controlled injections per cycle with maximum control over pressure. A representation of a solenoid injector with connection to a high pressure supply such as that of the common rail is given in Figure 1.2(b).

The advance which has enabled diesel engines to approach, and even exceed, the level of power delivered by the petrol spark ignition (SI) engine is the addition of the turbocharger. High pressure and temperature exhaust gas from combustion represents a significant waste of potential energy. By using this gas to drive a turbine, which in turn drives a compressor, some of this energy can be reclaimed to pressurise intake air. Greater oxygen content in the intake charge can then be reacted with an increased fuel delivery to produce more power. The first application was marine, boosting a 10 cylinder passenger liner engine from 1750 hp by 43% to 2500 hp in 1923. It was not until the late 1970s that the technology became viable for automotive turbodiesels, with introduction in the Mercedes-Benz 300SD and Peugeot 604. As previously shown in Figure 1.1, the turbocharger, in conjunction with direct injection, enabled a rapid increase in specific power output which continues to the present day. For the first time diesel engines were able to achieve similar peak performance to petrol engines without an accompanying increase in displacement, whilst also delivering desirable low and medium speed torque performance. High torque at low speed results in reduced frictional losses for a given power demand — hence fuel economy gains. As with fuel

injection, turbocharging has come a long way since the early developments. Turbocharging is not especially relevant at cold start, as increased oil viscosity with reduced temperature generally renders the turbine/compressor inoperable until temperatures rise, effectively creating backpressure. The application is however of interest, because compression ratio (CR) has had to be reduced as turbocharger boost has been increased to keep peak pressures within sensible limits at high loads. This is the root cause of cold start difficulties, as is explained in the following section.

1.2.2 More Recent Motivators for Technology

Increased demand from improvements in power output has been aided by financial benefits due to significant fuel economy gains compared to the equivalent petrol model. Increased energy prices and growing concern over global warming have made improving fuel economy and knock-on carbon dioxide (CO_2) emissions one of the principal targets for automobile development. Nationally and internationally there have been many conventions of industry and policy spokesmen addressing this matter. The largest of these was the 1997 Kyoto Protocol implemented into the Framework Convention on Climate Change. In general this protocol is an agreement to collectively reduce global greenhouse gas emissions by 5.2% compared to those in 1990 [5]. For their part, car manufacturers marketing cars in Europe have signed up to a voluntary agreement to reduce their fleet average CO_2 emissions to 140g/km in 2008 followed by a further proposal of meeting a 120g/km target by 2012. This is to be achieved by ensuring that fleet average CO_2 is no greater than 130g/km with the remainder achieved using complementary technology such as energy saving tyres, more efficient air conditioning systems and increased use of biofuels with lower well-to-wheel carbon footprints than fossil fuels [6, 7]. Figure 1.3(a) shows, to date, how effective the industry has been at achieving these goals based on UK sales. Figure 1.3(b) shows the changing market shares of different bands of vehicle CO_2 performance. The distribution is seen to be shifting markedly to the left with a greater number of low emission vehicles being purchased and fewer so called gas-guzzlers. Increasing new technology diesel penetration has been the prime motivator for this downward trend.

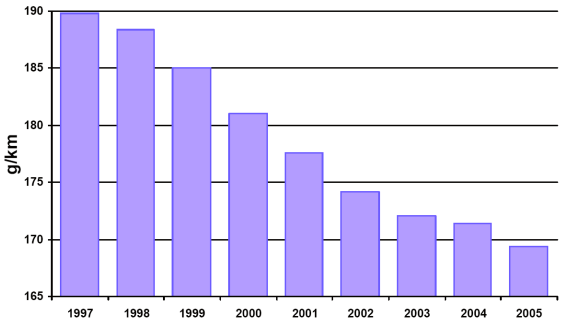

(a) UK Average CO_2 Emissions 1997–2005

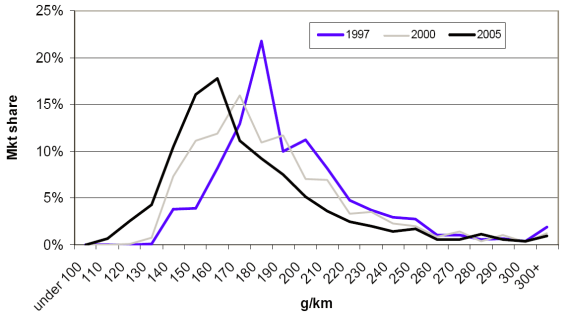

(b) UK Market Distribution, CO_2 emissions — 1997–2005

Figure 1.3: UK CO_2 Emissions and Diesel Penetration History, 1997–2005, source [8]

Zervas et al. [9] noted this and considered the potential for CO_2 reductions in Sweden, which has one of the lowest diesel penetrations in Europe (7% as of 2005). With various estimates of diesel and petrol fuel economy trends they calculated the effects of differing levels of diesel penetration in the Swedish market. Using the most likely scenarios they calculated that an increase in penetration to 30% would reduce CO_2 emissions by between 2.8% and 3.5%, whilst increasing to the European average of 50% would result in savings of between 7.5% and 9.1%.

Various governments have expressed their concern over human contribution to global warming, partly by introducing new CO_2 based taxation systems for vehicle licensing. Inherently more efficient diesel engines burn less fuel and release less CO_2, providing another financial incentive. Further developments have yielded quieter, more refined engine designs resulting in a more pleasurable driving experience. Other factors for increased diesel uptake include greater availability across all sectors of the vehicle market, emergence of Sports Utility Vehicle and Multi Purpose Vehicle sectors which are especially suited to diesel power, suitability of the low-revving diesel for more relaxed long motorway journeys and reduction of the perception that diesel is dirty and harmful. Focused marketing by manufacturers has also greatly influenced demand for diesel vehicles. This has included the introduction of diesel prestige and performance models such as the BMW 535D and VW Touareg V10 TDi as well as recent sporting success with the Audi R10 and Peugeot 908. Factors such as these have resulted in a Europe wide shift away from petrol, which dropped below 50%

penetration for the first time in 2005. Figure 1.4(a) charts the rise in popularity of the diesel automobile throughout Europe as a whole between 1990 and 2008 [8]. Figure 1.4(b) details the increasing penetration of diesel power in every individual sector between 1997 and 2005, from the mini segment through to luxury vehicles, both new sectors. A third entirely new segment, the diesel sports car, is also revealed, indicative of the significant shift in perception.

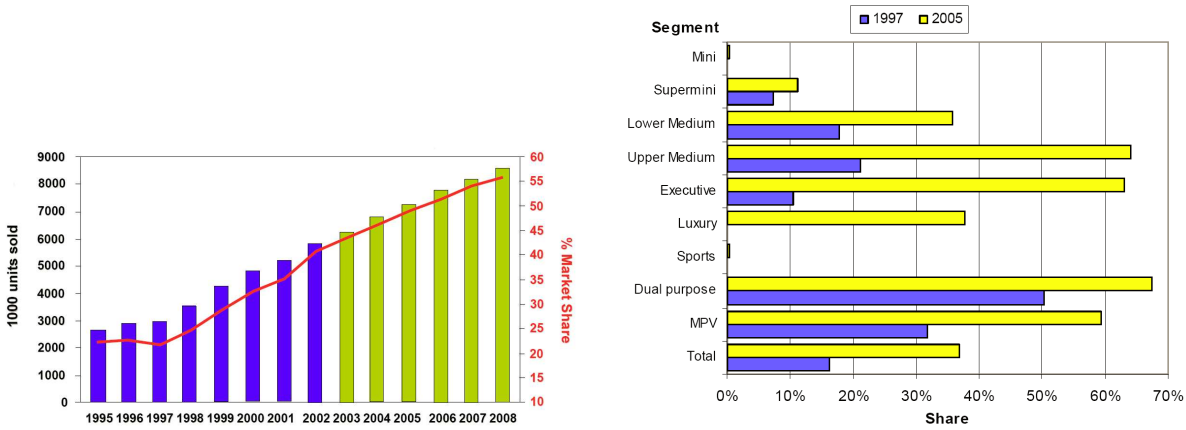

(a) European Diesel Penetration — 1990–2008 (b) UK Diesel Penetration — 1997 vs. 2005

Figure 1.4: Diesel Penetration History, Europe and UK, Source [10]

At the same time there has been incremental tightening of emissions legislation. All new cars must meet standards set by European Union directives, commonly referred to as Euro III, Euro IV and so on. Manufacturers have been forced to reduce emissions by up to 95% inside of 20 years with the latest proposals placing particular emphasis on oxides of nitrogen (NO_x) emissions for diesel engines as shown in Figure 1.5.

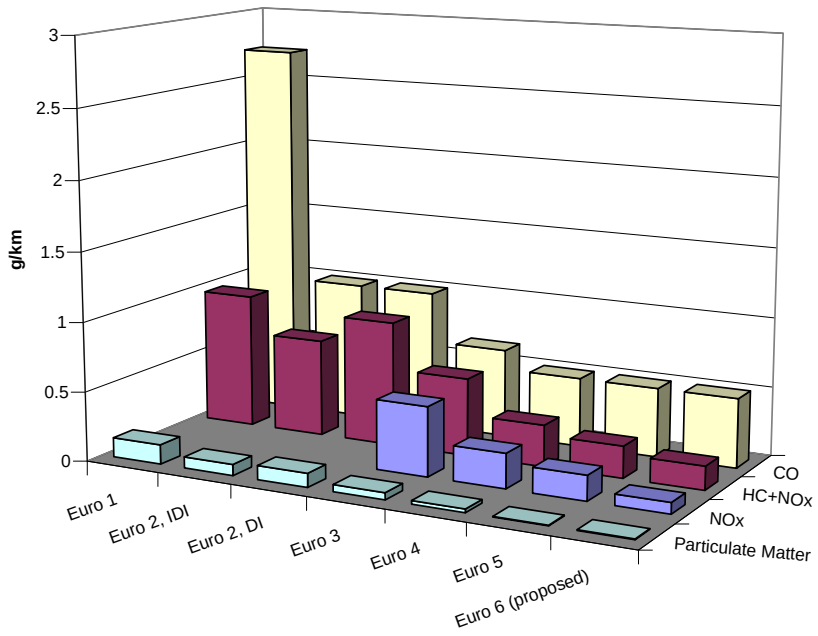

Figure 1.5: Euro Emissions Standards

Various oxides of nitrogen are produced during high temperature reactions in an internal combustion engine [11]. In the presence of excess oxygen, as exists in lean burning diesel engines, Nitrogen Oxide, NO, will be converted to Nitrogen Dioxide, NO_2. Collectively these gasses are referred to as NO_x and contribute to ground level smog as well as a variety of respiratory disorders. Added to this, oxides of nitrogen are dissolved in atmospheric moisture, forming various nitric acids which fall to the earth as acid rain.

Advances in diesel technology, such as high pressure common rail direct injection with multiple injection strategies, have helped manufacturers meet the targets set for NO_x and particulate emissions [12–15], and particulate filters look set to dramatically reduce remaining particulate matter emissions [16, 17]. However, lean burning diesel engines with high temperature operation are inherently prone to higher levels of NO_x than petrol engines.

To concurrently address the problem of NO_x formation whist satisfying consumer demand for performance and refinement, manufacturers are experimenting with a reduction in compression ratio and increased turbocharger boost. With reference to Figure 1.1, Figure 1.6 depicts the reduction in compression ratio from around 21:1 to 17.5:1 since the introduction of turbocharged, high pressure direct injection diesels.

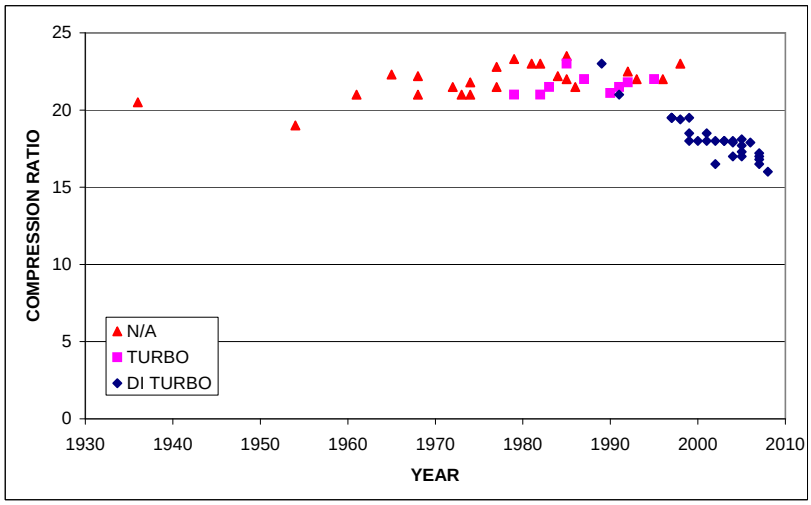

Figure 1.6: Diesel compression ratio 1936–2008 — Source of data Carfolio [1]

The reduction in compression ratio potentially affects other areas of performance, notably cold start behaviour. This forms the main area of study covered in this thesis. Under cold start conditions vehicle engines must operate reliably from cold in very low temperatures with acceptable refinement characteristics for the consumer. As diesel combustion relies on temperature rise caused by compression, it is possible that further reduction in compression ratio will bring cold operation into an unstable region, possibly even total failure to start.

There are several challenges that need to be addressed.

- Low temperatures increase engine friction, reducing cranking speed. Lower cranking speed allows more time for blowby and heat transfer, further reducing peak compression temperature and pressure. This will lead to reduced fuel vaporisation and poor mixture preparation. Depending on the severity there may be total misfire or poor combustion efficiency.
- If work output is not higher than friction the engine will not accelerate from cranking speed and the start will fail.
- Desirable cold start characteristics are low time to first fire, suppression of misfire/poor cycles and high work output to achieve idle speed within the minimum number of cycles.

- Once idle speed has been attained, concern shifts to maintaining that speed against friction and ancillary load demands. Variability in work output, especially poor cycles and misfire, will be evident to the consumer both in variable engine speed and audible deviations.

1.3 Aims

The work presented aims to produce a detailed study of phenomena encountered at cold start in the DI diesel engine. Cold start performance is frequently analysed on a multi-cylinder rig attempting unassisted starts from cold conditions [18–21]. Metrics such as time to first fire, time to idle speed or stability of idle speed have been measured to assess performance differences. The use of a single cylinder research facility with dynamometer control allows detailed analysis of combustion events by eliminating variables such as engine speed and cylinder to cylinder variations/interactions. Analysis of cylinder pressure data allows detailed performance assessment in terms of indicated work output and heat release rates — improving understanding of not only how much power is produced, but the way in which it is produced. Heat release analysis in particular allows phenomena such as ignition delay, combustion initiation and combustion propagation to be examined. Complete control over injection parameters has enabled optimisations to be performed.

Performance and heat release characteristics are examined with particular reference to the differences encountered when reducing compression ratio from conventional 18.4:1 to 15.4:1, a target level typical for next-generation engines. Problems encountered are quantified and potential solutions investigated. The effects of ambient temperature are also explored to determine critical conditions where solutions are required. Two regimes of operation are studied. These are referred to as cold start (300 rpm operation just above cranking speed) and cold idle (operation at higher engine speeds representative of idle). At cold start the principal objective is to suppress misfire and ensure high work output for acceleration to idle speed. At cold idle the objective is to meet a target load, representative of increased engine friction at low temperatures, with the minimum cycle-to-cycle variation to provide

a smooth idle speed. Study of the phenomena highlighted earlier is used to define desirable combustion characteristics and to investigate the techniques which may be used to ensure these characteristics are achieved despite reduced temperatures.

1.4 Thesis Structure

The work undertaken in this thesis is split up into 8 chapters. After this brief introduction to the topic area, previous work on diesel cold start and related areas of study are reviewed in Chapter 2. Areas that require further investigation are highlighted. The single cylinder rig which has been used for experimental investigation is described in Chapter 3. The hardware and software used is outlined along with modifications made for cold operation. The test procedure used for investigation is introduced. Key response variables used to quantify performance of the single cylinder rig are introduced in Chapter 4. Experimentation conducted at high compression ratio is presented in Chapter 5. This is the largest chapter as it defines baseline performance characteristics and studies the effects of changing input parameters on ignition, combustion, work output and other responses. Investigations are focused on two main areas; low speeds representative of cranking, and higher speeds representative of cold idle. Various injection strategies are considered to assess their impact on performance. This broad investigation enables a more focused study at low compression ratio, presented in Chapter 6. Direct comparisons are made which reveal the implications of a reduction in compression ratio in the cold start regime. Findings in Chapter 6 led to the acquisition of a new ceramic glow plug capable of very high temperature operation. The effect of glow plug operation is investigated to assess any impact on cold performance at both compression ratios. These findings are given in Chapter 7. A discussion is presented in Chapter 8 where the real world applicability and utility of the findings of the thesis are considered. Potential future work points are discussed before the key conclusions are listed.

1.5 Summary

The historical background of automotive applications for internal combustion engines has been detailed, revealing that increased performance has driven demand for the compression ignition diesel engine. Particular attention has been paid to technological advancements which have enabled the diesel engine to compete directly with the petrol engine for the first time, with power output approaching 100 bhp/litre whilst maintaining a fuel economy and CO_2 advantage. Increasingly tight legislation, especially relating to oxides of nitrogen and particulate matter, is forcing the industry to pursue designs which can both meet these targets whilst satisfying consumer demand for power and refinement. One such design is to reduce the compression ratio with an accompanying increase in turbocharger boost. This is discussed in more detail in Chapter 2. A reduction in compression ratio may result in degradation of start performance in extremes of cold weather, as temperature rise during the compression stroke will reduce. The aims of this thesis have been set out — in summary they are to quantify the extent of this effect and investigate solutions to any cold start problems encountered as a direct result of reducing compression ratio.

Chapter 2

Literature Review

2.1 Introduction

Much research and development has been conducted in the field of diesel engine technology over the past decade. This has been focused primarily on improvements to specific power output whilst meeting ever-tightening emission legislation and improving negative aspects of diesel such as noise and vibration. As discussed in Chapter 1, much has been achieved, resulting in a shift in consumer buying patterns towards diesel. The aim for this chapter has been to look in more detail at previous work completed in the specific field of diesel engine cold start. To date there is little work available to review that specifically tackles the cold start of diesel engines at reduced compression ratios. There are, however, many pieces of work detailing advances and studies in related fields where results are of use to this investigation. Reviews of several of these areas of interest are presented within this chapter. The broader area of why a reduction in compression ratio is being utilised is introduced, followed by a brief summary of the diesel autoignition process and works which have studied this in some detail. Previous work in the field of diesel cold start is then summarised, including topics considered relevant such as the impact of changes in injection strategy and cold start aids. Further work detailing the general effects of reducing compression ratio are then covered before the conclusions are presented.

2.2 Theory Behind Reduction in Compression Ratio

One method for simultaneously improving power output and reducing emissions of oxides of nitrogen is to reduce the compression ratio whilst increasing the level of turbocharger boost. More boost increases oxygen intake per cycle which can react with more fuel producing greater power when required. There are other factors to consider: part of what makes diesel combustion more efficient than petrol is that more work can be extracted by expanding the combustion gasses over a larger volume ratio — clearly there is a trade-off.

In fully warm operation, diesel combustion is initiated by the pressure and temperature rise due to compression. As temperatures increase, radicals with high volatility such as CH separate from the fuel which then go through further chemical processes until highly exothermal reactions such as $H_2 + OH \rightarrow H_2O + H$ begin to occur. Once these reactions reach a critical rate the process becomes self sustaining resulting in autoignition and a rapid rise in in-cylinder pressure and temperature. Temperature rise due to compression can be approximated by the following law in the ideal cycle

$$T_2 = T_1 {r_c}^{\gamma - 1} \tag{2.1}$$

Where T_1 is the temperature of charge gas at bottom dead centre, T_2 is the temperature at the end of compression, r_c is the compression ratio and γ is the adiabatic index of the gas, ratio of specific heat capacity at a constant pressure (c_p) to specific heat capacity at constant volume (c_v). A lower compression ratio therefore results in a lower temperature rise due to compression. If the same amount of fuel is burnt, the resulting bulk temperature will be lower for a low compression case. NO_x formation can occur either through the prompt mechanism within the flame front or by the Zeldovich mechanism in the hot burned gasses behind the flame [22, 23]. Modelling by Studzinski et al. [24] showed that small changes in bulk gas temperatures above 2000 K cause large increases in NO_x production, for example 2000 $\rightarrow$ 2050 K increased NO_x formation by over 44%.

Figure 2.1 is an example $\phi - T$ diagram from Pickett et al. [25] showing the regimes of soot and NO_x generation calculated for n-heptane mixing in air at ambient temperature of

1000 K and 1200 K.

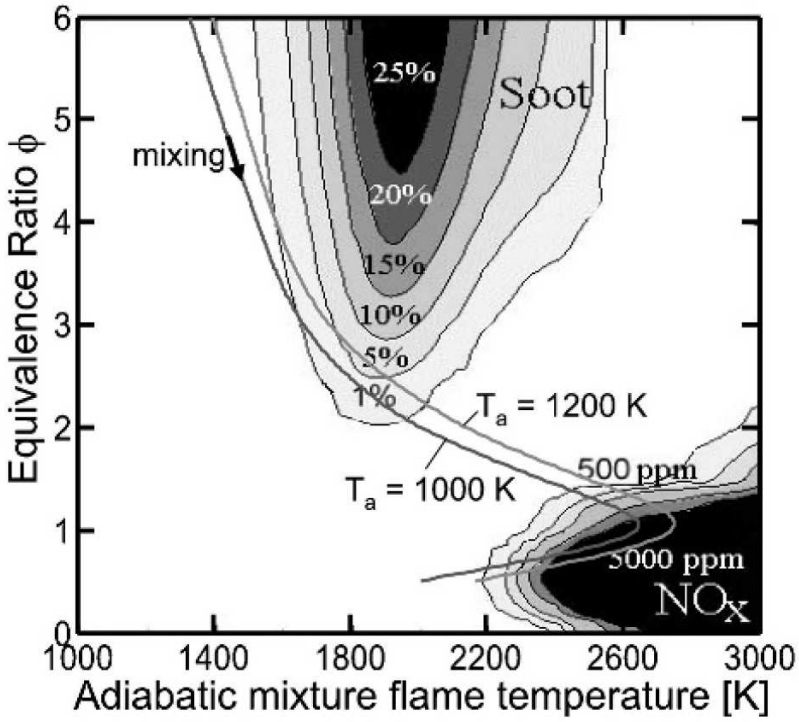

Figure 2.1: Calculated soot yield (% carbon atoms from fuel converted to soot) and NO_x formation paths for n-heptane combustion in ambient air at two different initial temperatures. Reproduced from [25]

As combustion begins in the rich mixture there is soot generation as the flame temperature increases before leaning out and reaching the hottest temperatures required for NO_x generation. It can be seen that a lower initial temperature reduces exposure to both pollutant formation zones with lower adiabatic flame temperature. Hence a reduction of compression ratio may be one way in which to implement low temperature combustion in an attempt to miss the soot and NO_x production regions. Kook et al. [26] experimented with different levels of EGR to reduce adiabatic flame temperature, finding that below flame temperatures of $\approx 2260\ K$, engine out NO_x was always < 10 parts per million (ppm), but as the temperature rose towards 2600 K this increased exponentially to > 400 ppm. Ladommatos et al. [27] varied intake temperature between $40°C$ and $120°C$ whilst fixing all other parameters on a 2.5 litre multi-cylinder DI diesel and noted that NO_x increased from ≈ 90 ppm to 170 ppm. Higher inlet temperatures reduced ignition delay from 12.5° at 2000 rpm to 7°. An ignition improver was used with inlet temperature fixed to $40°C$ to isolate the effect of start of combustion, and it was found NO_x only rose to just over 100 ppm. The remaining

70 ppm increase from the temperature effect again reveals how increased global temperature in the cylinder increase NO_x emissions.

This high level of temperature dependency means that a lower compression ratio will reduce NO_x emissions as found in the literature. Hountalas et al. [28] performed a computational investigation considering behaviour under various load conditions of a heavy duty diesel at compression ratios between 14:1 and 20:1 to assess the benefits of variable compression ratio. Low compression ratio was useful for limiting peak combustion pressures at high load, which in turn reduced NO emissions by between 5 and 20% when lowering CR from 18:1 to 14:1, dependent on load, with optimised injection timings. There was, however, a 4% fuel consumption penalty and a potentially significant soot increase. Sood et al. [29] modelled engine performance for a variable compression ratio engine such that compression ratio was adjusted to ensure optimum brake specific fuel consumption (BSFC) at all engine speeds. Load was varied at each condition to achieve the minimum BSFC. At 1900 rpm the optimum compression ratio was 16.4:1. At any other speed an increase in compression ratio up to 18.5:1 at 2700 rpm resulted in better BSFC. As compression ratio increased, peak in-cylinder pressures could be up to 100 K higher, resulting in a NO_x emissions penalty of up to 75%. An experimental investigation was carried out by Parlak et al. [30] whereby the compression ratio of a single cylinder IDI engine could be varied by altering the stroke. The unit was tested at CRs ranging from 16.1–18.2 with standard internals and then in a low heat rejection format where the internals (cylinder head, valves and piston) were coated with a ceramic material to reduce heat transfer. NO_x contour maps were produced for a range of speeds and loads. It was found that the low heat rejection engine always had greater NO_x output for any given speed and load at each compression ratio tested. A reduction in CR from 18.2–16.8 typically reduced NO_x by 14% without adverse effect on engine operation. Lower CR resulted in a performance reduction and high BSFC penalty.

Lower in-cylinder temperatures also open up the possibility of using lower EGR rates than currently required to meet emissions goals. This reduced dependency should allow more flexibility to reduce particulate matter when NO_x is not critical.

2.3 The Diesel Autoignition Process

Ignition delay in a compression ignition engine is the time between fuel injection and fuel ignition. During this ignition delay period, physical and chemical processes occur which enable fuel autoignition once they have progressed to a suitable degree. The physical processes are mainly to do with splitting the fuel injection into smaller, more ignitable parts by spray atomisation in the injector nozzle followed by evaporation. There are also air entrainment processes where the broken up fuel spray is surrounded and mixed with the oxygenated air essential for combustion. Rosseel et al. [31] considered each fuel droplet as a discrete sphere travelling across the combustion chamber against the resistive force of stationary high pressure air. Creation of an ignitable mixture was modelled as evaporation from the droplet surface due to high compression temperatures which created a wake of fuel/air mixture. As the temperature of the droplet increased and the speed reduced, the wake became progressively richer. If in-cylinder temperature is above the autoignition point, combustion occurs once the wake is in the ignitable region after a chemical ignition delay. Due to turbulence in the chamber, wakes would be expected to intersect and combustion would be expected to propagate throughout the charge to more droplets through all intersecting wakes of sufficient richness. In reality, the chemical processes are the oxidisation reactions in the fuel, air and residual gasses as well as cracking of hydrocarbon chains, producing more volatile species. Once reactions have progressed to a critical level, autoignition occurs, potentially at multiple independent locations — the end of the ignition delay period.

Ignition delay is an important factor in diesel engine operation. A long ignition delay can mean that a high degree of fuel air mixing has occurred before ignition, resulting in extremely rapid combustion and very high in-cylinder pressure. This can cause bearing, piston or con-rod damage and be audible in diesel engine knock — considered as a possible barrier to entry for automotive diesel engines by Dicksee as long ago as 1932 [32]. Low compression ratio reduces compression temperature and pressure, both detrimental to autoignition. As asserted by Dicksee, subsequently shown experimentally by Crua et al. [33] and numerically by Gonzalez et al. [34], high cylinder pressure reduces the ignition point of diesel fuel. Crua observed for 700 K and 65 bar cylinder pressure, ignition delay was

approximately 2 milliseconds. A reduction in pressure to approximately 42 bar increased ignition delay to 3 ms. This mimics previous research in the broader field of combustion, such as Caron et al. [35], where it was found that a methane/air (83% vol methane) mixture at $410°C$ started to undergo cool flame reactions after 100 s at 6 bar, reducing to 20 s at 11 bar. Too long a delay period in a diesel engine may lead to misfire where the correct conditions for combustion (sufficient temperature, pressure and local equivalence ratio at a potential ignition site) are never reached, or work is done late in the expansion stroke resulting in low indicated mean effective pressure (IMEP). It is crucial to avoid this situation during diesel engine cold start. A misfiring cycle results in no acceleration away from cranking or a drop in engine speed from idle speed, producing long start delays and poor quality idle. If injection is advanced in an attempt to avoid misfire, ignition may occur too soon in the compression stroke where significant work is done against the piston's upwards motion.

The delay period is defined as the time period or number of crank angle degrees between start of injection and start of combustion. Start of injection is often obtained from injector needle lift sensor readings. In the event of this option not being available, it can be obtained from a current clamp which detects the injector control signal. It is assumed that injection is instantaneously initiated with these signals. It is more difficult to accurately determine the start of combustion. There are two main methods used for the detection of ignition. Many studies use an optical method where a special optically accessible engine is required [36–38]. Part of the cylinder wall, head or piston is constructed from quartz crystal or sapphire, allowing a CCD camera or other form of optical sensor to measure light emissions. The second method is an analytical technique looking for heat release or a deviation in the pressure trace away from that expected in a motored cycle [39–41]. The heat release technique is a more robust way of locating start of combustion, as high heat releases can be seen for only moderate changes in pressure depending on injection parameters. Higgins et al. [42] revealed that a significant increase in flame luminosity associated with soot incandescence, visible to a normal camera, lags behind calculated heat release by approximately 1 ms. Acceptable accuracy may be obtained using the heat release technique with no requirement for complicated optical access and regular cleaning or expensive

chemiluminescence equipment to measure luminosity.

There have been many studies looking at ignition delay in compression ignition engines leading to the development of a model to predict ignition delay given certain input parameters. The correlations derived have often predicted ignition delay in the form of an Arrhenius equation as follows

$$\tau_{id}(ms) = Ap^{-n}e^{\frac{E_a}{\tilde{R}T}} \tag{2.2}$$

Where A and n are experimentally derived constants and $\tilde{R}$ is the universal gas constant (8.3144 J/(mol K)). E_a is the apparent activation energy for the fuel combustion, this may be derived experimentally, or by using a relationship of the form suggested by Heywood [23]

$$E_a = \frac{618840}{CN + 25} \tag{2.3}$$

where CN is the fuel cetane number. Table 2.1 from Heywood [23] illustrates the findings of previous attempts to predict ignition delay in this way.

	Conditions				Parameters		
Investigator	**Apparatus**	**Fuel**	p **[atm]**	T $[K]$	n	A	E_a
Spadaccini and TeVelde No.1 [43]	Steady Flow	No. 2 Diesel	Oct-30	650-900	2	2.43*10-9	20926
Spadaccini and TeVelde No.2 [43]	Steady Flow	No. 2 Diesel	Oct-30	650-900	1	4.00*10-10	20080
Stringer et al. [44]	Steady Flow	Diesel 45-50 octane	30-60	770-980	0.76	0.0405	5473
Wolfer [45]	Constant Volume Bomb	cetane 50	Aug-48	590-782	1.19	0.44	4650
Hiroyasu et al. [46]	Constant Volume Bomb	Kerosene	Jan-30	673-973	1.23	0.0276	7280
Watson [47]	Diesel Engine	diesel	Unknown	Unknown	3.45	1.02	2100

Table 2.1: Empirically derived ignition delay correlations from several investigations, source [23]

In these investigations, steady flow experiments were performed in apparatus similar to a jet engine, where pressurised and highly heated air flows down a length of tube and fuel is injected into this flow. A constant volume bomb is simply a self contained pressure vessel containing heated, pressurised air. The fuel is injected into this environment for measurement of ignition delay. The constants derived in these experiments are shown to vary by several orders of magnitude. The correlations are applicable to the study in question, but their applicability to any other test is questionable.

Hardenburg and Hase [48] performed similar experiments with an actual diesel engine and observed a greater number of factors in an attempt to derive a correlation which was more appropriate for use in real combustion engines. Their correlation takes the following form

$$\tau_{id}(CA) = (0.36 + 0.22\tilde{S}_p)e^{E_a(\frac{1}{\bar{R}T} - \frac{1}{17190})(\frac{21.2}{p-12.4})^{0.63}} \tag{2.4}$$

Where S_p is the mean piston speed. In reality it has been found that the constants for these ignition delay correlations require adjusting when attempting to match predictions to experimental data from alternate equipment, even when varying parameters such as intake temperature or pressure. As such they can only be of minor importance for cold start applications where input variables are distant from fully warm running and autoignition is thought to be at least aided by glow plug operation creating a hot spot.

The failure in general applicability of these relatively simple autoignition models led to consideration of the autoignition process in more detail. Rosseel et al. [31] split the ignition delay process into the physical and chemical processes that occur with a single fuel droplet. The effect of variations in the droplet diameter and its surroundings were considered and it was concluded that the chemical and physical processes were dependent upon each other and that the chemical portion of the ignition delay was more significant than the physical. This may not be the case at cold conditions where evaporation is expected to be reduced. Increased computational power and memory capacity have enabled advancements in numerical techniques including Computational Fluid Dynamics (CFD). Complex submodels of the physical and chemical processes have been developed, allowing solutions for spray atomisation, evaporation and combustion to be obtained more swiftly and with greater accuracy than previously possible. Professional codes such as CHEMKIN are available, which

can be trained to provide good results for each application.

2.4 Diesel Engine Cold Start

Combustion initiation in a diesel engine is primarily dependent on pressure and temperature rise due to compression. As demonstrated in equation 2.1, the compression of air from intake conditions to those at top dead centre (TDC) cause a temperature rise. In normal operation, when the engine is warm, the in-cylinder temperature is designed to be sufficient for reliable combustion on every cycle when fuel is injected. If temperatures drop significantly, and the engine is allowed to soak at a greatly reduced temperature, it is possible that this may no longer be the case. This has always been a concern in diesel engine design, leading to the introduction of cold start aids such as glow plugs to provide additional heat input or an ignition source. Glow plugs are now commonly utilised for a period of post-glow, reducing emissions during warm-up where low temperatures impact on complete hydrocarbon oxidation [49]. With the proposed reduction in compression ratio it is expected that problems with cold start will become more prevalent. The reduced air, fuel and cylinder wall temperatures, with the lower compression temperature increase, may combine to bring cold start into an unstable region.

There is much evidence in the literature that points to difficulties with diesel engine cold start, though work at reduced compression ratios is only just starting to emerge. The most directly relevant piece of work found to date was a low compression ratio cold start investigation performed by Pacuad et al. [50] in 2008. An extensive investigation was carried out involving experimental work, computational fluid dynamics and an optically accessible engine. A conventional high pressure common rail (HPCR) DI diesel engine with a CR of 17:1 was reduced to 13.7:1 CR by using a piston with increased bowl volume. For a motoring speed of 170 rpm at $-20°C$ this resulted in a reduced peak compression pressure of 25.5 bar compared to 28 bar at 17:1, and a calculated drop in peak compression temperature of 24 K. With no changes to injection calibration there was a dramatic extension of time to idling. At $20°C$, 17:1 idle speed was attained in only one second, at 13.7:1 this increased to

17.5 s. Starting was no longer possible at low compression ratio when reducing temperature to $0°C$ unless injection strategy was re-optimised.

Optical access confirmed significant increase in wall wetting, implying that fuel vaporisation is reduced due to the lower pressure and temperature and that the amount of vaporised fuel in close proximity to the glow plug at TDC is insufficient for autoignition. Start delay was brought back to acceptable levels at temperatures down to $-25°C$ with optimisation of injection strategy. Main timing and pilot quantity were found to have the largest impact on startability. Rail pressure was also found to be important — above 300 bar there was excessive penetration resulting in increased wall wetting and reduced time for vaporisation in the transit across the cylinder. Even when injection parameters were optimised for low compression ratio there was a 50% increase in ignition delay of the main.

A CFD investigation highlighted difficulties in cold start whereby the areas with richest fuel were also the coolest, making them less likely to undergo autoignition. Autoignition was found to occur in the CFD model not where the fuel jet first passes the glow plug tip, but when fuel vaporises along the wall and recirculates back to the glow plug with air motion in the cylinder. Variations in the pre-glow period and relative injector–glow plug positioning were found to have a strong effect on startability. Of particular interest to this investigation, it was found that rotating the injector away from stock format always resulted in an improvement of start delay independent of direction. The implications of this are that stock glow plug setup is optimised for normal running conditions, not cold start, and that swirl plays an important part in transporting fuel to the glow plug, even at low engine speed because the direction of glow plug rotation was not important. An improvement was seen either by causing one nozzle spray to directly impinge on the glow plug, or, if the first spray was moved away from the glow plug, swirl carried fuel from the adjacent nozzle towards the plug. Increasing cranking speed with a larger battery also reduced start delay because temperatures and pressures increased due to a reduction of available time for losses to heat transfer and blowby.

Whilst the Pacaud paper is a very recent addition to the literature dealing with the exact subject under consideration, there is significant earlier work on the broader subject of

diesel cold start. In 1932, Dicksee [32] provided an in depth discussion of various aspects of the possibilities of diesel engines being used for light duty automotive applications. The optimum compression ratio was discussed, and whilst as low as 13:1 was considered, it was ruled that a higher ratio would be required due to likely difficulties under cold conditions. Again in Vulliamy's [51] 1954 paper on matching diesel engines to light road vehicles, there is a thorough summary of the limited applications at the time and how cold starting was a known problem in the days before other factors had been addressed. The merits of various engines were assessed — particular credit was given to an electronic device similar to a petrol choke which delivered excess fuel at cold start. This enabled the minimum temperature for successful starting to be reduced by approximately $2.5°C$ to $\approx -6.5°C$. The possibility of using other cold starting aids was discussed, but these were generally considered inappropriate due to unwanted increase in engine complexity and size at the time.

More recently, Zahdeh et al. [52] performed motored cold start tests on a single cylinder direct injection diesel engine which was cold soaked at the test temperature for three hours before each attempt to start. They discovered that reduced temperatures led to many problems including lower cranking speeds resulting in higher blowby and heat transfer losses, a result also found by Pacaud and Gonzalez [34, 50]. This led to skipped cycles on starting at any ambient below $0°C$, resulting in either an 8 stroke or 12 stroke cycle, greatly extending start times. Shayler et al. [53] helped to explain reduced cranking speeds by performing teardown tests on four engines and calculating motored friction at various temperatures. It was found that friction mean effective pressure (FMEP) could increase by a factor of around three depending on engine design and motoring speed when reducing temperatures from $20°C$ to $-25°C$ during the first period of operation.

Burrows [54] investigated several aspects of cold start on four IDI and DI engines including one installed in a road vehicle, the engine bay section of which was entirely enclosed in a sealed cold chamber and mounted on a rolling road. Cooling was accomplished with forced circulation of chilled coolant and desiccated air. Start quality was assessed in terms of time to first fire, time to idle speed and percentage misfire. Stability was assessed using standard

deviation of ignition delay at a steady speed. Typically, swift starts were accomplished when soak temperature was above $-10°C$. Below this temperature the sum of starter motor and combustion mean effective pressure (MEP) was similar to FMEP. This extended start times to tens of seconds until FMEP reduced with heat addition from continued cranking. Appropriate fuel injection timings were critical, and excess fuel allowed greater air utilisation. Glow plug operation with surface temperature above $850°C$ was vital for low temperatures at all periods of cold start. Reduced glow plug protrusion actually aided startup by increasing MEP on firing cycles. This was attributed to less airflow obstruction resulting in improved mixing. Glow plugs had insignificant effect on charge or combustion wall temperature, so it was concluded they provide a hot spot for combustion initiation. There was significant variation in cold start performance between engines, revealing how cold start is an important parameter to consider in design.

Burrow's work was expanded by Tindle [55] who considered engine friction during the initial minute of operation. It was found that initial friction is twice the expected value at low temperatures in hydrodynamically lubricated components such as the crankshaft. It is these contributions to friction that significantly extend start time until local oil films reduce in viscosity after multiple revolutions. It was found that starving the engine of oil for the first few seconds of a free start from $-25°C$ reduced FMEP from a peak of ≈ 9 bar to ≈ 7 bar, cutting time to idle from 15–5 s. Improving air utilisation by oxygen enrichment, better atomisation of fuel, better fuel spray targeting, over-fuelling or adjusting injection timing could yield work output benefits, showing the need to re-optimise engine design and calibration for cold start compared to baseline settings. Differences in heat transfer and blowby between engines was found to be a key differentiator between cold start performance.

Osuka et al. [19] investigated the utility of modern HPCR direct injection hardware in assisting cold start of a 6 cylinder heavy duty DI diesel cranked by its own starter motor. It was found that two part injection greatly improved the cold start performance in comparison to single injection. The benefits were in lower misfire and shorter, more repeatable ignition delay. This led to startup times being reduced by over 50% at cold ambients. A similar investigation was performed by Zhong et al. [56] utilising a 4 cylinder light duty diesel

engine with common rail injection. It was found that a single injection was suitable for startup at $20°C$, but multiple injections had to be utilised below this level. Start times were greatly extended at $0°C$ and $-10°C$, no start was possible at $-20°C$ within a 60 cycle cranking period. Pressure based calculations for in-cylinder temperature agreed with previous investigations by Zheng et al. [57] using three single cylinder units where intake air temperature could be controlled between 393–600 K. It was found that combustion was impossible below bulk temperatures of ≈ 540 K as this is where the first volatile species begin to react. Combustion was principally initiated by homogeneous charge compression ignition (HCCI) type cool flame reactions of the split injection, some of which led to strong conventional combustion on that cycle, whilst others never surpassed these low levels of heat release.

Han et al. [58] uncovered similar relationships, linking combustion instability to ambient temperature, instantaneous engine speed and injection timing. Regions of injection timing at a range of engine speeds resulting in suppression of misfire were identified for use in a heavy duty diesel engine. Misfiring was also linked to a mismatch between injection parameters and instantaneous engine speed at injection, indicating that higher resolution control strategies would be required. Injection timing zones with reliable firing were shown to narrow with lower cetane fuels having a higher resistance to autoignition. Mitchell [59] conducted a real-world investigation on the effects of cetane number with an extensive investigation of 18 commercially available medium and heavy duty vehicles. Over 300 overnight cold soaks were performed and startability assessed with each vehicle and a selection of 14 fuels of varying parameters, with and without starting aids. The most important factor was engine design and calibration. Below this, fuel factors deemed critical were cetane number followed by volatility, especially mid boiling point. The use of a cetane booster was found to have the same positive effect as a natural increase in cetane from different fuel in the range tested.

2.4.1 Modern Fuel Injection Equipment

Many studies have been conducted considering the benefits of modern high pressure common rail technology, principally those of multiple injections per cycle. Although not generally related to cold start operation, many of the conclusions are of interest for this study. The benefits of latest generation technology are centred on the ability to deliver multiple well timed, precisely controlled quantities of fuel to the cylinder at high pressure on each firing cycle. The concept is not new as evidenced by work carried out in 1946 at Shell's Thornton Research Centre, later reported by Davies [60] in 1951. A single cylinder unit was initially modified with a second injector to deliver a small metered injection starting 25° before start of main injection. This resulted in a perceptible reduction in engine noise, reduced ignition delay of the main injection, reduced rate of pressure rise and no notable increase in specific consumption. This in turn reduced high frequency engine vibrations associated with knock. The engine ran as smoothly with low quality 30 cetane fuel as it had previously done with 50 cetane fuel. In an alternate experiment, a secondary pump was connected via non return valves to a standard 6 cylinder diesel engine and cam timed to inject the pilot as before. Similar results were found for this dual pump layout as for the original set-up, but only over a limited speed range. The dual pump layout was not capable of precise fuel delivery timing and metering as in the single cylinder twin injector layout. This revealed the importance of timing and quantity of pilot fuel delivery in fuel preparation.

Since these early experiments there has been considerable fuel injection equipment development to give greater control of injection parameters, resulting in the common rail direct injection technology used by the author. More recent work includes Carlucci et al. [61], who tested a 4 cylinder common rail DI diesel using a variety of levels and timings of both pilot and twin pilot (early + pilot) injections before the main. Engine speed and load conditions were selected to represent the steady speed phases of the European Driving Schedule. It was found that for levels above the minimum injection quantity in the pilot or early injection, ignition delay was reduced by around half at all engine conditions. A secondary effect was that the introduction of a highly advanced second pilot injection, referred to as an early injection, had the potential to either promote or suppress ignition of the pilot dependent

on injection quantity. The resulting different combustion profiles allowed much flexibility in obtaining desired emissions levels by varying phasing and premixed combustion depending on load requirements. This indicates that pilot injection is an important area for study at cold start, where ignition delay is subject to greater variability and may extend to misfire in the worst conditions. Much emissions investigation was conducted, which is not of direct interest to this study. The principal effect of reduced ignition delay is lower NO_x due to less pre-mixed high heat release rate combustion without a soot formation penalty in the later part of the burn, as well as the potential for reduced fuel consumption — all desirable side effects.

Ishida et al. [62] investigated the effects of pilot injection with two different diesel fuels, cetane ratings of 55 and 40. A high speed direct injection turbocharged and intercooled four cylinder diesel was tested at 1750 rpm across a variety of loads. Again, pilot injection resulted in a 50% decrease in ignition delay, improved emissions performance and greater fuel efficiency. Of interest to this study is the fact that the same performance gains were made for low cetane fuel as high cetane. When main timing is retarded the increase in ignition delay is more prominent with low cetane fuel. Pilot injection was therefore critical to maintain reliable combustion with reasonable ignition delays. In especially cold environments diesel engines must run on winter fuel to resist paraffin waxing [63]. One side effect of this is a lower cetane index, further compounding problems with cold start. It is useful to know that advantages seen in standard fuel may be carried over to low cetane fuels.

2.4.2 Starting Aids

Various work has been conducted on the use of starting aids to overcome the difficulties of diesel engine cold start. Lindl and Schmitz [64] compiled a useful summary of starting aids and their utility in the modern diesel engine. It was found that glow plugs are ideally suited for low displacement engines, achieving positive starts at $-20°C$ as long as the glow plug tip temperature was above $1100°C$. There was also a great emissions benefit, both at cold start and idle speed during the warm-up period. For piston displacements above 1000 cm^3,

intake air heaters, either electric, using a direct fuel flame burner, or catalytically ignited recirculated exhaust gas [21], provide the only reliable solution to the cold start problem. Work by Shen et al. [20] indicated that railplugs, capable of generating a high velocity stream of plasma, may provide a better starting aid than glow plugs under adverse conditions. Successful starts with no waiting time before cranking were achieved in only two seconds at $-29°C$ compared to $-24°C$ after an extended pre-glow and cranking period with standard glow plug configuration. This was shown with a 4 cylinder IDI diesel engine soaked in a cold room, but the authors considered results applicable to DI. Schatz [65] investigated the use of a heat battery to store exhaust heat in an efficiently insulated container, then utilised this store to assist cold start of various vehicles by heating coolant. Emissions data were collected for American Environmental Protection Agency driving cycles showing carbon monoxide (CO) and hydrocarbons (HC) were reduced by up to 80% at $-7°C$ cold start, startability and cabin heating were greatly improved at $-10°C$ and the limit of startability for the diesel engine tested was improved from $-16°C$ to $-28°C$ with much improved noise characteristics. There were fuel economy improvements using the heat battery of up to 13% during the early warm-up phase. This increased to 18% when the engine was pre-heated for 60 s using stored heat. These findings are of use as the reduced compression temperatures at low compression ratios will require a greater understanding of techniques that may be used to counter any difficulties that may arise.

2.5 Cold Idle

Another problem with reduced temperatures has proven to be increased cold idle instability. Typical warm condition starts are achieved in a matter of a few seconds from key-on, but this may extend to tens of seconds or even complete failure at reduced temperatures. Once the engine has reached idle and the load demand drops off, the idle governor can struggle to maintain the desired speed until the temperature of the system increases over time. There is indication in the literature that this is important, but little work appears to have been documented specifically concentrating on cold idle for diesel, especially considering lowered compression ratio where this problem is expected to be exacerbated. Pacaud et al. [50]

alludes to poor engine behaviour at cold idle for a the 13.7:1 compression ratio, but no data are presented.

Several studies have been carried out that focus on idle stability in the field of spark ignition engines. One common technique has been to monitor flywheel acceleration during idle and relate this to combustion instability. Chen et al. [66] applied this technique to an SI engine along with adaptive ignition time trimming to balance cylinder power output, reducing maximum crankshaft speed variation and $\frac{1}{2}$ engine order torque fluctuation by $\approx 90\%$ over a range of engine idle speeds. Martino et al. [67] performed a similar study for an on-vehicle idle quality perception test. There was a strong correlation with both flywheel acceleration perturbations and the reduced work output of the worst combustion cycle against perceived idle instability by the occupant. Teng [68] also used a flywheel acceleration monitoring technique to assess idle stability. The key results of interest for this study are that the standard deviation of the flywheel acceleration over a test period is proportional to the engine load and that there are two components to idle instability; cycle-to-cycle variation and cylinder to cylinder variation. From this it was deduced that higher load leads to higher stability and that some stability improvement can be obtained by better cylinder to cylinder matching, but the cycle-to-cycle variation remains constant. Cylinder matching is irrelevant for the single cylinder engine used in the current investigation, but effects of injection strategy on diesel idle combustion are likely to be significant as found by the adaptive ignition trimming performed by Chen.

By considering the factor effects of varying fuel supply, air mass supply and residual fraction for an SI engine at steady-state idle, Hinze et al. [69] showed that the amount of fuel supplied has the strongest percentage effect on coefficient of variation of IMEP for a percentage variation of that input. In the steady-state condition it was found that normal variations in residuals, intake air and fuel injection accounted for less than half of the total perturbations from mean work output. The remainder was attributed to field effects of flow and charge inhomogeneity, and was typically in the region of 7% coefficient of variation of IMEP. Simulated starts were performed by Chen et al. [70] to consider the effect of equivalence ratio and fuel composition on stability of IMEPg in an SI engine. In general it was found

that over-fuelling drastically reduced the start time for all fuels tested, typically by 80% from stoichiometric to an equivalence ratio of 1.5. At the same time the coefficeint of variation of IMEPg was found to drop from 15% to 3%. Increasing fuel volatility by using larger percentages of high volatility components, such as n-pentane (similar to light end petrol fractions) or MTBE (oxygenated fuel), improved the performance of the near stoichiometric mixtures to nearly the level of the very rich ones. The stability levels encountered at cold conditions in a diesel engine are likely to be lower than in a petrol one as there is no spark ignition to initiate combustion. The fuel volatility effect is of significant importance to this study, as diesel fuel is less volatile than petrol. The large improvement in stabilty when increasing volatility of the already volatile SI fuel is cause for concern.

2.6 General Compression Ratio Effects

The principal motivators for the reduction in compression ratio in this study are to facilitate higher levels of turbocharger boost whilst giving potential for NO_x reduction. As discussed earlier, Parlak et al. [30] noted that in a single cylinder IDI diesel engine a reduction in compression ratio could lead to unacceptable ignition delays, resulting in high pressure rise rates. This was countered with the use of a ceramic coated, low heat rejection engine design. Some benefits were found in a moderate reduction in CR from 18.2:1 to 16.8:1, but any further reduction caused a significant deterioration in running quality. Dhinagar et al. [71] made use of another low heat rejection design with direct injection and an extended electrode spark plug as an ignition source to reduce CR to as low as 10.5:1. This demonstrated that technology could allow multi-fuel capability. At 1500 rpm with variable load, the low compression engine generally exhibited similar performance to that of a normal diesel, with some potential for better thermal efficiency and smoke output, as well as significantly quieter operation due to low in-cylinder pressures and rates of pressure rise. Laguitton et al. [72] varied the compression ratio of a single cylinder engine to study combustion effects and found a reduction in CR from 18.4:1 to 16:1 simultaneously reduced soot and NO_x at medium and high loads with no associated penalty in fuel economy. A 2–4° increase in ignition delay was found which increased premixed burn percentage, but any detrimental

effects of this were countered by reduced temperatures at low CR and increased penetration of fuel, leaning out the overall mixture. Theoretical studies such as [73] and [74] focused on the effects of compression ratio on specific fuel consumption and power output. In both cases an optimum CR was found at approximately 15:1. This was attributed to the increased thermodynamic efficiency of higher compression being offset by higher heat transfer losses above this region.

2.7 Summary

The theory behind a reduction in compression ratio has been presented, showing how it offers the potential to reduce emissions of both NO_x and particulate matter by lowering bulk gas temperature and adiabatic flame temperature. This gives additional flexibility to avoid combustion occurring within key NO_x and soot formation regions, shown by a selection of published work.

Work considered relevant to the subject area of diesel cold start at reduced compression ratio has been reviewed to assess the current knowledge base, consider useful techniques which may be applied, and highlight areas where further work may be required. There is little published work in the specific field of low compression ratio diesel cold start. Whilst this makes direct comparisons with alternate studies difficult, it does mean that this study should shed light on an area of development which is likely to become crucial in the coming years. Encouraging results were obtained by Pacaud et al. [50] in the most applicable study, showing that re-optimisation of injection strategy during the cranking phase of cold start at low compression ratio can deliver comparable start times to a higher compression ratio. The importance of the glow plug was also highlighted as an area for potential development. The study suggests that there was poor quality cold idle which was not remedied, but no data were presented to quantify this. Cold idle operation, at any compression ratio, does not appear to be an area where much work has been published. It therefore makes an excellent subject for consideration within this work, where direct comparisons may be drawn between two compression ratios.

Reduced temperatures lead to increased friction, especially in hydrodynamically lubricated components. This friction lowers cranking speed, further increasing heat transfer and blowby. Previous work on cold start has constantly highlighted the utility of a pilot injection to reduce ignition delay and suppress misfire. This is important as the ambient temperature drops below $0°C$. Under warm conditions, a second pilot injection gave a greater degree of control over combustion. If these findings can be replicated under cold conditions, this may be one way to improve performance. As engine speed increases from cranking, injection parameters must be adjusted accordingly to avoid a mismatch and poor performance. Idle performance is vulnerable to small changes in input parameters, even at normal operating temperatures. Either a high resolution of control or a speed-stable strategy must be employed to obtain the desired swift time to idle. A variety of starting aids have been used to reduce the impact of low temperatures on starting performance. All studies considered here report that substantial improvements were made in terms of startability, with potential knock-on benefits for cold emissions compared to baseline glow plug performance. Previous studies suggest that if the standard engine configuration does not yield acceptable results, more advanced starting aids to assist cold start may need to be considered.

Chapter 3

Experimental Facilities and Test Procedure

3.1 Introduction

All experiments performed during this investigation have been conducted using a single cylinder research engine. Details of this unit, and how it has been modified to investigate the cold starting regime, are given in this chapter. Engine control, data acquisition and instrumentation utilised to gather results are discussed. A novel testing methodology is introduced which enabled a high rate of data collection. It was used throughout this investigation to investigate the cold start and cold idle regimes focusing on the combustion process whilst ensuring minimum deviation in operating parameters such as test temperature and compression pressure, ensuring repeatable results.

3.2 Single Cylinder Engine

All experiments were performed on a single cylinder rig as pictured in Figure 3.1. A single cylinder unit was selected primarily because it allows the tightest control over variables. Measurements taken are always independent of events in other cylinders and intake/exhaust characteristics are independent of demands in other cylinders. There is always some cylinder to cylinder variation due to manufacturing differences and variable mixture preparation, so only having one cylinder eliminates these. Secondary benefits are that a smaller capacity dynamometer and cooling tower can be used and increased simplicity improves reliability and speeds up maintenance/rebuilds.

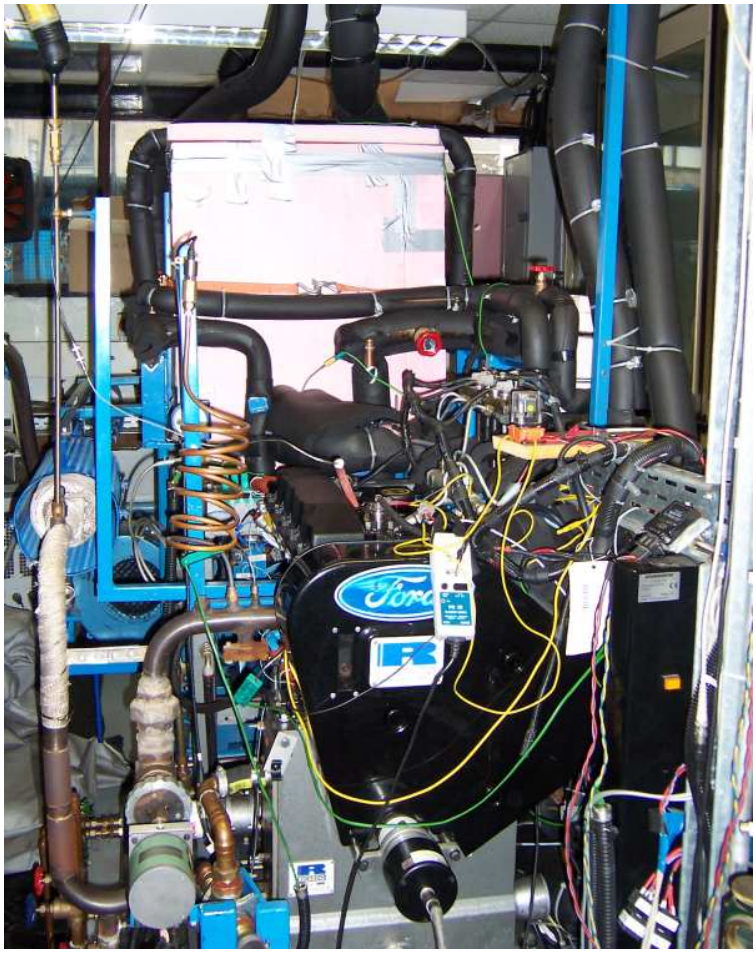

Figure 3.1: Single Cylinder Research Facility

The unit is a single cylinder variant of a production Ford 2.0 litre Puma direct injection

diesel engine. Ricardo Consulting Engineers manufacture this Hydra unit to the following specification.

Bore	86 mm
Stroke	86 mm
Displacement	499.56 cm^3
Initial Compression Ratio	18.4 : 1
Injection System	1350 bar Bosch HP Pump, Common Rail, Denso 6 hole centrally mounted solenoid injector
Valves	4 per cylinder — 2 inlet 2 exhaust
Swirl Ratio	1.4

Table 3.1: Single Cylinder specifications

The DENSO fuel injection equipment has been proven to be capable of reliable injection of quantities as low as 1 millimetre cubed per stroke (mm^3/str) and as high as 90 mm^3/str at temperatures as low as $-20°C$, (see Appendix A.1). The engine was mounted on a test-bed and connected to a David McClure swinging frame DC dynamometer with rated capacity of 60 kW at 4500 rpm. Dynamometer speed was regulated by a Control Techniques Mentor II DC drive unit capable of motoring and absorbing operation to maintain a steady speed against varying engine torque through the cycle. The Puma engine is rated to operate at up to 5500 rpm, but speed was limited to 3800 rpm to ensure operation within the limits of data capture equipment.

Diesel was supplied to the injectors via a low pressure fuel pump feeding a 1350 bar Bosch high pressure pump, pressurising the common rail. The single cylinder unit is not equipped with an alternator. Power is supplied to the engine control unit, low pressure fuel pump and glow plug by a 12 V automotive battery connected to a trickle charger. The diesel used for cold testing was Optifluid CS, a reference fuel for winter testing whose properties are given in Table 3.2.

Density @ $15°C$	$820 - 840\ kg/m^3$
Viscosity @ $40°C$	$1.9 - 2.3\ cSt$
Pour Point	$< -40°C$
Cloud Point	$< -40°C$
Cetane Index	> 47
Initial Boiling Point	$< 180°C$
T50	$< 255°C$
T90	$< 325°C$
Final Boiling Point	$< 360°C$

Table 3.2: Optifluid CS Diesel Fuel Properties [75]

3.3 Cold Starting Modifications

The optimisation of cold starting of a diesel engine is the major area of investigation in this thesis. Several modifications were made to adapt the rig for operation at low ambient temperatures. The principal method of cooling was the direct chilling of coolant by a F+R VP45WC 5.8 kW cooler, capable of chilling down to $-30°C$. The coolant was a 50/50 mixture of tap water and BS6580 ethylene glycol antifreeze, and was circulated around the engine block in the same way as in stock format. An 80 litre plenum before the intake was chilled using an atmospheric cooling radiator to provide a reservoir of low temperature intake air. Coolant passed through a water jacket around the intake manifold to ensure the chilled air remained at a low temperature. The fuel was chilled with a radiator to simulate as accurately as possible conditions for a vehicle attempting a cold start after prolonged periods at low temperature. Oil was not directly chilled, but was constantly pumped around the chilled engine, cooling it indirectly. When chilling down to $-20°C$, it became necessary to place insulating jackets around the engine block to maintain this low temperature.

For warm running during conditioning and alternative experiments, heaters were used to directly raise the temperature of coolant fluid (Watlow Industries 3 kW immersion heater) and oil (2x Eltron Chromalox sump mounted heaters), capable of indirectly heating the

block to temperatures above $80°C$ with no other heat input. These modifications were necessary as the single cylinder rig does not produce enough heat to achieve warm running temperatures on its own. In these experiments, heat was rejected from the system via a Carter M3 series Bantam cooling tower in place of the engine radiator.

A schematic of the coolant circuit is given in Appendix Figure b for reference.

3.4 Instrumentation and Data Acquisition

An important measurement for performance assessment is in-cylinder pressure. This was measured using a Kistler 6125B quartz pressure sensor rated to 250 bar peak pressure. This transducer was selected because of its high resistance to thermal shock. The signal from the 6125B was amplified to 0–$10V$ by a Kistler 5011 charge amplifier. The 6125B is a dynamic sensor, therefore there is significant signal drift after periods with little or no change in pressure. Due to this limitation, the signal was referenced at bottom dead centre (BDC) of the intake stroke with the signal from the intake manifold pressure transducer to give a baseline. The Kistler transducer was calibrated using a Budenberg hydraulic deadweight calibration bench to 0.05% accuracy.

The rig was equipped with many other pressure transducers and thermocouples to monitor operation. Sheathed TC Limited K-type Chomel-Alumel thermocouples were used to monitor temperature at key rig locations shown in Figure 3.2.

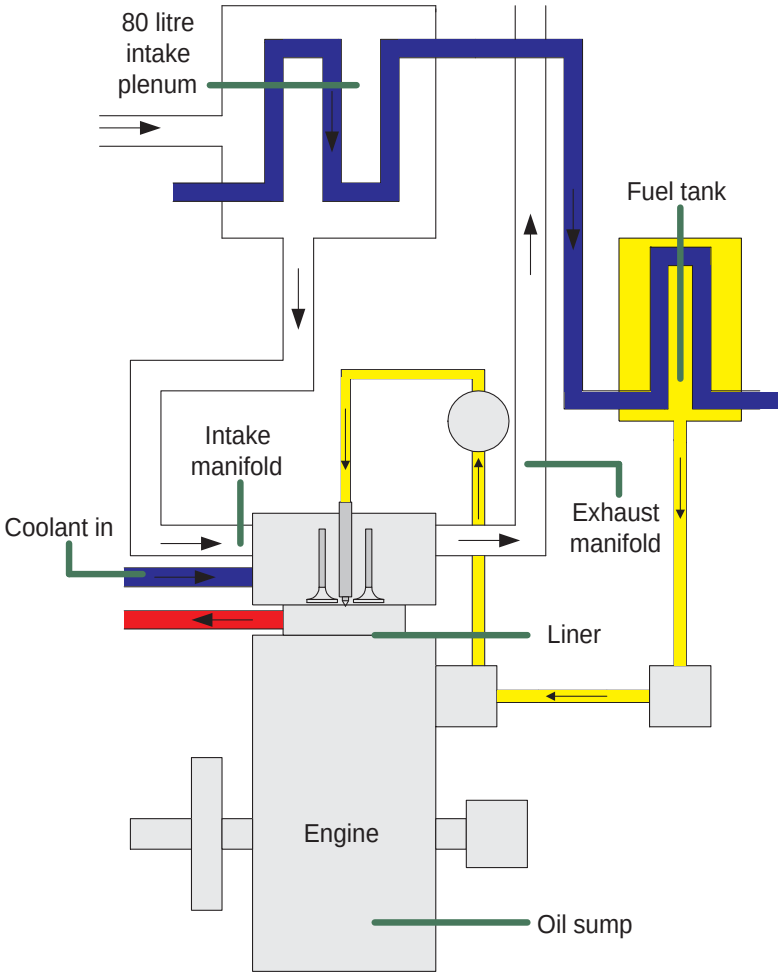

Figure 3.2: Location of thermocouples on single cylinder rig

Each thermocouple was calibrated in a crushed ice water bath at $0°C$ and then in a temperature controlled oil bath at 5–$10°C$ intervals up to $100°C$ to ensure sufficient accuracy within the range of expected operation. The exhaust thermocouple was calibrated to $300°C$ which is suitable for all but the hottest conditioning tests. Near linear fits were observed for all thermocouples tested and assumed to hold at higher temperatures, allowing accurate approximation of further increased gas temperatures. Fuel rail pressure was measured with a 2000 bar Leafield Engineering pressure transducer connected to a Vishay Measurements Group 2200 System Signal Conditioning Amplifier to produce a 0–10 V signal for input to dSPACE. A 7 bar Kulite pressure transducer monitored oil pressure whilst a 6 bar Kulite transducer was used to monitor the fuel feed from the low pressure pump, along with two 4 bar Kulite transducers for intake and exhaust manifold pressures. The Kulite sensors

output signals to in-house amplifiers which boost levels to 0–10 V. All pressures transducers were calibrated using the Budenberg hydraulic deadweight calibration bench.

A Hohner Automation optical shaft encoder with $\frac{1}{2}$ degree crank angle resolution outputs 720 DC pulses per engine revolution — 1440 per cycle. This signal is the trigger for crank based data acquisition through dSPACE which captures system variables at each $\frac{1}{2}$ crank angle step. An AVL 402 dynamic top dead centre (TDC) probe was used to locate dynamic TDC with high accuracy. Small errors in TDC location can result in large errors in calculations, as found in the literature. The shaft encoder was aligned to within 0.1° of true TDC which reduces IMEP calculation errors to less than 1% [76]. Secondary measurements which do not need to be resolved with such time accuracy, such as fuel or air temperature, are captured at the rate of 100 Hz using a separate time based trigger in dSPACE.

ATI Vision was used to isolate the engine control unit and give full control over injection parameters. This enabled investigation of injection strategies with up to five injections per cycle. Figure 3.3 illustrates the nomenclature used in this report. In a single injection case the entire quantity is delivered in injection B, otherwise A is always a pilot injection. Subsequent letters may designate further pilots or portions of the main as appropriate.

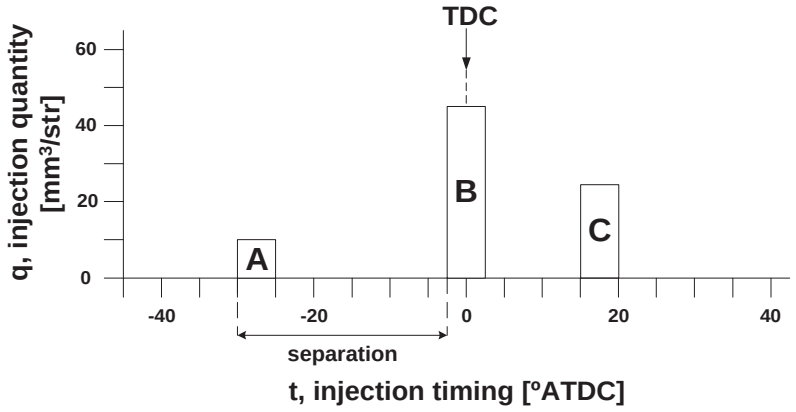

Figure 3.3: Injection Nomenclature

Appendix Figure c is a schematic detailing the major signals in the single cylinder rig. This follows the path of signals from the personal computer to the engine control unit and dSPACE data acquisition system. From there it shows how these interact with the various transducers and components of the rig itself. For simplicity, temperature and pressure

signals are not displayed on this diagram, apart from that of principal pressure transducer for in-cylinder measurement.

3.5 Experimental Technique

3.5.1 Steps to Ensure Repeatability

As with all investigation, it was important to ensure consistency both on a test-to-test and day-to-day basis. A novel experimental technique was developed and optimised to ensure a good level of repeatability over the course of these investigations. Variability was limited by controlling test-to-test variations in initial conditions and by use of post-test and end-of-day procedures to maintain the engine in the required condition.

There was a rigorously maintained procedure at the start of every day before any data acquisition was performed. This is detailed in Appendix A.3. The procedure ensured that the desired operating point was reached and held for a suitably long period for good soaking at target temperature. Various thermocouples monitor the engine, but the one used to define test temperature measured the temperature at the liner, as this is the reading closest to the combustion chamber. Other temperatures could be a few degrees lower during cold start. For example, to achieve $-20°C$ liner temperature the chiller would be set to $-28°C$, resulting in pre-engine coolant, fuel and intake air temperatures around $-25°C$. Three cleaning point tests were run to draw fuel through the injection system and condition ready for cold testing. After a one hour soaking period it was found that the first two to three tests exhibited a pattern of increasing performance until stable operation was encountered. Therefore a high fuelling test point was used to monitor performance and ensure that these first tests did not contribute to the data set.

After each test, a conditioning run was performed to purge the chamber of any remaining fuel residue, draw fresh air into the chamber and create a known starting condition for the next test. A set cleaning injection strategy with high combustion efficiency was run for 30

cycles and then the engine was motored for two minutes, drawing cool clean air through the chamber. The engine was reset to BDC intake and left to soak for 15 minutes before the next test point was initiated. This conditioning technique enabled around 20 tests a day to be performed with good repeatability. After this number there was potential for decreased stability in the value of peak compression pressure before injection as shown in Figure 3.4. Data are presented from three days of testing at $-20°C$.

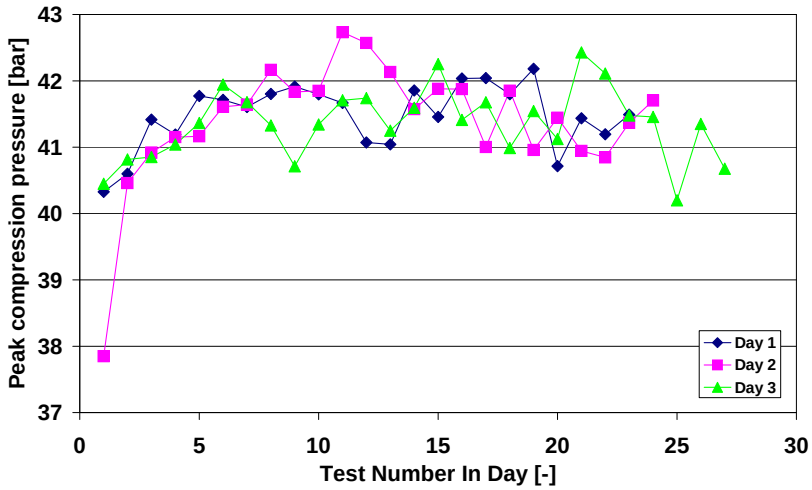

Figure 3.4: Variations in peak motored pressure before fuel injection throughout three days of testing at 300 rpm, $-20°C$

The previously mentioned increase in pressure for the first three tests is seen before settling into the 41-42 bar area for the following 20 tests. There was potential for variability, as seen in the middle section for day two. Such variability was monitored, and if considered out of the ordinary, the test was repeated. It can be seen that there was increased potential for variability towards the end of day three. Results were noted and a cap of tests of 25 points including the first three pre-data-collection tests was imposed whilst still monitoring variability. This provided an excellent balance between rapid population of testing matrices and validity of results.

The first test of the day was repeated at the beginning and end of each day of testing over a period of nearly four months. Ambient temperature outside the lab varied from $0°C$ to more than $20°C$, yet Figure 3.5 exhibits no evidence of long term drift, validating the testing process. End-of-day tests, ignoring outliers caused by low pressure, were typically

repeatable at 9.75 bar IMEPg ± 0.5 bar for a temperature of $-10°C$. This is representative of the high level of test-to-test variability due to cold conditions. Whilst this may be considered a broad margin in some fields, the investigations performed for this work are concerned with revealing trends and optimum regions, not precise numerical values as this is of limited applicability to multi-cylinder operation in a real vehicle under true cold start conditions. This margin is acceptable (and typical) for cold start study. Low peak pressure for the first test of the day means a reduction of up to 1 bar in IMEPg.

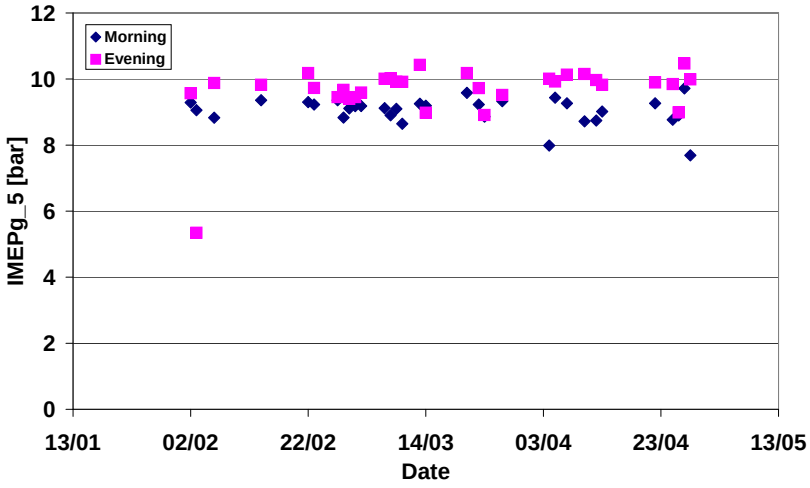

Figure 3.5: Variations in average indicated mean effective pressure of the first five injected cycles between February and May 2006, first and last test of day, [2,20,35] mm^3/str, Main timing 0.5°BTDC, $-20°C$, 300 rpm

In the sub-zero testing environment, often with large fuel excess, it is likely that significant accumulation of soot and unburned fuel within the combustion chamber may occur. Spray impingement on walls/piston is a known mechanism for this [77] and will be exacerbated by cool surface temperatures. Combined with this, there may be water as ice present. To return the engine to an initial condition for the start of testing on a subsequent day, a hot conditioning run was performed as detailed in Appendix A.4. In addition, engine oil was changed after every two days of testing and the oil filter was changed every two weeks. This ensured there could be no significant build up of contaminants in the oil. A brief conditioning run was performed at the start of a day if a period of two or more days had passed since the last engine operation. It was found that any long periods of engine rest could deteriorate repeatability until this brief spell of conditioning was performed.

3.5.2 Performing a Cold Start Test Point

The test procedure utilised for cold start tests was developed to mimic the low speed, cold surface conditions during the first few cycles of cold engine operation. The procedure was as follows:

- Program ATI with the desired injection strategy.
- Wait for the 15 minute soak time to elapse.
- Turn on glow plug for a pre-glow period of 4.5 seconds.
- Motor engine to 300 rpm.
- Engage fuelling on 11th cycle.
- Inject for 30 cycles.
- Stop engine.
- Perform cleaning test and cold soak as detailed in previous section.

There was a pre-glow period of 4.5 seconds to allow the glow plug to achieve operating temperature before fuel delivery, as would be the case in service settings. 300 rpm was chosen as it is just above cranking speed where a quick acceleration to idle speed is desired. It was not possible to operate below this level as the dynamometer was incapable of maintaining a set speed due to the rapidly varying resistive forces associated with compression, expansion, intake or exhaust phases. 300 rpm could be maintained with little variation through the cycle. Fuelling was engaged on the 11^{th} cycle to allow time for engine speed, cylinder pressure and fuel rail pressure to stabilise before injection. It was found that 400 bar was a good fuel injection pressure. This was based on experimental testing which was confirmed during personal communication with Ford Motor Company.

3.5.3 Modification for Cold Idle Test Points

Tests were performed at higher speeds to investigate operation within the idle regime. These tests are referred to as cold idle and were performed in the range 600–1500 rpm. Several minor modifications were required to achieve reliable operation at the higher speed. Glow plug pre-heat had to be extended to 8 seconds to compensate both for reduced time available to warm up before injection, and because there was increased convective cooling during the motoring section at higher speeds. Fuelling was delayed for a further 5 cycles as it took longer for engine speed to stabilise at the higher levels. This allowed more cycles of compression, simulating heat addition from previous cold start cycles.

3.6 Summary

The single cylinder research engine was introduced along with the modifications made to mimic operation in cold environments. The equipment is capable of chilling the entire unit, including air, fuel and coolant, to $-20°C$. The rig has been instrumented to monitor the temperature of various components as well as the pressure of oil, intake air and exhaust gasses to ensure consistency of results. Signals from the Kistler 6125B in-cylinder pressure transducer are referenced to the correct crank angle by a shaft encoder which outputs 720 pulses per crankshaft revolution. A dynamic calibration device has been used to ensure accuracy to approximately 0.1°. This minimises errors in calculated values dependent on accurate location of pressure readings in the cycle. A test technique has been developed which allows a significant number of experiments to be performed per day of testing, along with conditioning procedures to ensure a repeatable starting condition. This allows rapid completion of testing matrices, limiting time based variability. Typical test-to-test repeatability is expected to be approximately ±5% of IMEP for a stable 300 rpm test due to the cold surface conditions. The combination of a repeatable test procedure and well calibrated transducers should ensure minimum experimental and calculation error, and therefore trends can be interpreted without significant error contribution.

Chapter 4

Key Response Variables

4.1 Introduction

The data acquisition equipment was described in Chapter 3. The majority of the transducers were used to monitor operating conditions such as temperature, rail pressure and engine speed to ensure tests were performed within the desired operating parameters. Post processing of data produced many outputs from the inputs of the various transducers, but two outputs were of particular importance, gross Indicated Mean Effective Pressure (IMEPg) and gross Heat Release Rate (GHRR). Both are calculated primarily with the output of the in-cylinder pressure transducer and a knowledge of the combustion chamber geometry throughout the cycle. These output parameters will be derived in this chapter. The application throughout this work of IMEPg and GHRR, as well as other parameters which may be derived from them, will be explained.

4.2 Indicated Mean Effective Pressure

This quantity is expressed in bar (10^5 N/m^2) and represents work done per cycle per unit of swept cylinder volume. The term "work output" is used in some descriptive passages interchangeably with IMEP as the swept volume of the engine remains constant, therefore maximising work output is the same as maximising IMEP. When quantifying work output, IMEP is used and numbers are in bar. Net IMEP is the work done on the piston by the working gasses over the four engine strokes of a cycle per unit displaced volume. Gross IMEP is the work done on the piston over the compression and expansion strokes only (closed portion of the cycle) per unit displaced volume. Using these factors, the performance of engines of different sizes can be directly compared in terms of how efficiently they utilise their swept volume. IMEPg is used throughout this investigation as the single cylinder engine is motored by the dynamometer, therefore pumping work of the intake and exhaust strokes is not considered. The pumping work at these speeds in unthrottled diesel operation is very low, but there is the possibility of it obscuring trends in the data, so it is omitted from this point on.

IMEPg is the work done on the piston over the period from BDC intake to BDC expansion divided by the swept volume. Work done is defined as force in joules multiplied by distance moved in direction of force in metres ($W = Fx$). Force exerted on the piston is the projected area of the piston in square metres times the pressure that acts on it in Pascals ($F = pA$). The work done on the piston during the closed portion of the cycle is given by

$$W = \int_{BDC_{intake}}^{BDC_{expansion}} pA\,dx \tag{4.1}$$

and considering the area of the piston (effectively the cross sectional area of the cylinder bore) is constant, dividing by the swept volume of the engine results in the IMEPg.

$$IMEP_g = \frac{\int p\,dV}{V_s} \tag{4.2}$$

To solve this integral it is necessary to know the volume in the cylinder at any point in the cycle. The geometry of the internals must be known. The following equation gives the

distance from the crank axis to the piston axis, s, at any angle, θ.

$$s = a\cos\theta + l^2 - (a^2\sin^2\theta)^{\frac{1}{2}} \tag{4.3}$$

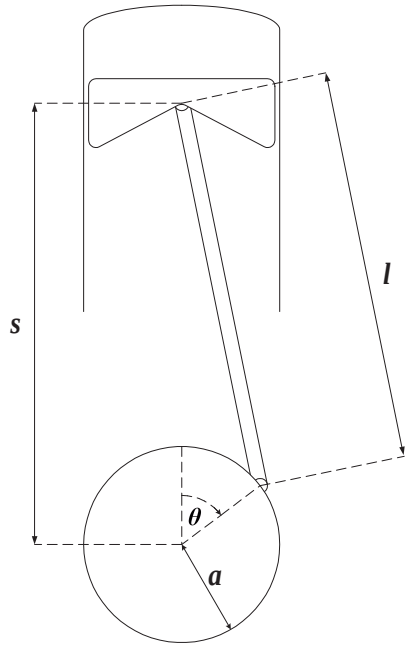

Figure 4.1: Cylinder Geometry Schematic

where a is the crank radius and l is the connecting rod length, as depicted in Figure 4.1. The total stroke is $2a$, with s varying between $l - a$ and $l + a$, therefore the volume in the cylinder at any time can be expressed as a fraction of the total swept volume plus the clearance volume at TDC, V_c

$$V = V_s\frac{(l + a) - s}{2a} + V_c \tag{4.4}$$

Knowing the volume at any angle allows the dV term to be derived for any given step from equation 4.2 and the IMEPg to be calculated with the pressure data. In this case data are acquired at every $\frac{1}{2}$ crank angle. A matrix for volume is generated to reflect this. Figure 4.2 shows a typical 300 rpm cycle with a small pilot followed by a large main at 20° after top dead centre (ATDC). this is indicated by the dashed black line, the output of a current clamp probe attached to an injector wire. The current clamp is used throughout this work, and units are assigned arbitrarily to ensure visibility on each scale. The blue line shows pressure rise up to TDC and the red the associated crank angle resolved IMEPg

contribution required for compression over that angle step. After TDC, expansion begins and the IMEPg contributions become positive. When ignition occurs there is a distinct pressure rise and associated increase in the IMEPg contributions. Expansion, and positive work output contribution, continues until BDC.

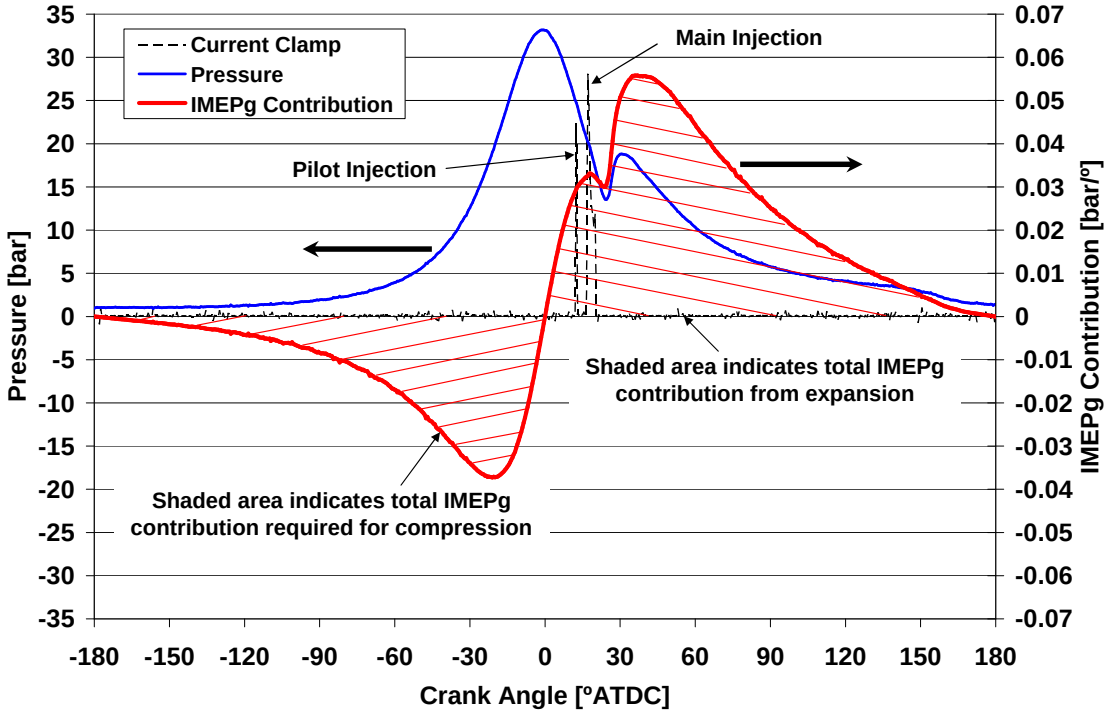

Figure 4.2: Example of IMEPg contributions, 300 rpm, LCR

IMEPg values are used directly to consider the work output (in specific form, by dividing by swept volume) of any specific cycle, or the average value. In general, for 300 rpm, tests the average of the first 5 injected cycles, $\overline{IMEPg}_5$, is considered, as the very first cycles are responsible for acceleration from cranking. At higher idle speeds, the average of the first 10, $\overline{IMEPg}_{10}$, is used due to greater variability and the interest of the study being in quasi-steady-state performance. IMEP is often used to consider cycle-to-cycle stability. This may be in terms of standard deviation ($\mathrm{StD}_{\mathrm{IMEPg}}$), the root of the averaged square of the differences between each cycle's IMEPg and the average value for all cycles between the first and the last considered, generally the first and last injected cycles.

$$\sigma_{IMEP_g} = \sqrt{\frac{1}{n}\sum_{1^{st}}^{n}(IMEP_{g_i} - \overline{IMEP}_g)^2} \tag{4.5}$$

More often the Coefficient of Variation of IMEPg ($\mathrm{CoV}_{\mathrm{IMEPg}}$) is used — the standard

deviation of IMEPg as a percentage of the mean

$$CoV_{IMEP_g} = 100\frac{\sigma_{IMEP_g}}{\overline{IMEP_g}} \tag{4.6}$$

This allows cycle-to-cycle variation to be more directly compared between tests of differing work outputs. $\mathrm{CoV_{IMEPg}}$ is an accepted standard for idle stability as found in the literature [78–80]. For the purposes of this investigation, the average IMEPg is taken as $\overline{IMEP}g_5$ or $\overline{IMEP}g_{10}$, whichever is currently being used to characterise performance.

4.3 Heat Release Rate

The second parameter used extensively in data analysis is Gross Heat Release Rate (GHRR). GHRR is the rate at which combustion converts energy stored in the chemical bonds of the reactants into sensible internal energy. This is expressed in J/°. To calculate the gross value, the net value (NHRR) must first be obtained from pressure data and cylinder volume. Knowing the rate at which the pressure is rising within a specific volume of gas will allow NHRR to be calculated. The net value is the apparent rate of heat release ignoring losses due to heat transfer and blowby. Losses must be approximated and added on to arrive at the gross value. The First Law of Thermodynamics states that the increase in internal energy of a closed system is equal to the amount of energy added to the system minus that lost to the surroundings through work or loss. In an internal combustion engine this can be written as

$$dQ_{hr} = dW + dU_s + dQ_l \tag{4.7}$$

where dQ_{hr} is the gross heat release caused by combusting fuel, dW is the work done by piston motion, dU_s is the change in sensible internal energy and dQ_l is a term which covers energy losses due to heat transfer and blowby. The following relationships can be substituted to obtain an equation that can be solved with the available data

$$dW = p\,dV \tag{4.8}$$

$$dU_s = m_{trapped}c_v\,dT_b \tag{4.9}$$

$$dT_b = \frac{d(pV)}{mR} \tag{4.10}$$

$$\frac{R}{C_v} = \gamma - 1 \tag{4.11}$$

where $m_{trapped}$ is the trapped mass, c_v is the specific heat at constant volume, T_b is the global bulk gas temperature, R is the specific gas constant and γ is the ratio of specific heats, c_p/c_v. Full details of this substitution are given in Appendix A.5, and result in equation 4.12 below.

$$dQ_{hr} = \frac{\gamma}{\gamma - 1} p\, dV + \frac{1}{\gamma - 1} V\, dP + dQ_l \tag{4.12}$$

It has been shown previously that a good approximation of γ is crucial to reliable heat release analysis, and that it varies greatly with temperature and composition. The work of Brunt et al., especially in [81] and [82], has yielded the following correlation for diesel operation. This is a development of previous work by authors such as Gatowski [83] and was found to offer good results across the wide range of charge composition found in diesel engine operation.

$$\gamma = 1.44 - 1.2 * 10^{-4} T_b + 1 * 10^{-8} T_b^2 \tag{4.13}$$

4.3.1 Heat Transfer and Blowby

Without the Q_l term, Equation 4.7 gives the net heat release rate. Net heat release rate is lower than gross because of heat transfer losses from the charge to the combustion system walls and escape of gasses past the piston rings. Generally speaking, the heat transfer is the dominant term, accounting for as much as 20% of total heat release [23]. Heat transfer can be modelled as follows

$$Q_{ht} = h_c A \Delta T \tag{4.14}$$

where h_c is a heat transfer coefficient, A is the total combustion chamber surface area at the given timestep and ΔT is the temperature difference between the charge in the cylinder and the walls into which heat is flowing. A is calculated in much the same way as V in equations 4.3 and 4.4. As reported by Pugh [84], there are many correlations which may be used to find appropriate values of h_c. His modification of the Hohenberg correlation [85] developed on an earlier version of this research engine was modified for use in this project as

all parameters are readily available from engine recordings. The coefficients were adapted to suit low temperature operation so that GHRR was zero on a motored cycle with no fuel injection. The correlation used is given in Equation 4.15.

$$h_c = 67.7V^{-0.06}p^{0.8}T_b^{-0.4}(1.49 + \bar{S_p})^{0.8} \tag{4.15}$$

where $\bar{S_p}$ is the mean piston speed in metres per second.

Blowby rate under fully warm conditions is generally very small, in the region of 1-2% [23]. It is often ignored in GHRR calculation, but is included here as it is important to attempt to model it for this cold, low speed operation. The approach adopted here follows Cheng [86], who represented blowby as flow through an orifice with upstream pressure equal to cylinder pressure and downstream pressure equal to that of the crankcase, giving an instantanious mass flow rate of

$$\dot{m} = A_{ring}\gamma^{\frac{1}{2}}(\frac{2}{\gamma+1})^{\frac{\gamma+1}{2(\gamma-1)}}(\rho p)^{\frac{1}{2}} \tag{4.16}$$

where ρ is the density of the blowby gasses and A_{ring} is the effective ring gap area. This may be determined by measuring blowby gasses vented from the crankcase and adjusting the value of A_{ring} so that the calculated value matches experimental. Direct measurement of blowby from a single cylinder engine is difficult due to large pulsating pressurisation of the crankcase from the single piston motion. In previous work with this engine, Pugh [84], in communication with Cheng, adjusted the value for a similar DI diesel multi-cylinder unit under fired conditions at $-20°C$. The adjusted value of $4.1E^{-8}$ m^2 will be used in this study. The energy loss to blowby for each half crank angle is modelled as

$$\frac{dQ_{bby}}{d\theta} = \frac{60\dot{m}}{720N}\frac{pV}{m_{trapped}}\frac{\gamma+1}{\gamma-1} \tag{4.17}$$

where N is the engine speed in rpm.

GHRR has been used to evaluate start of combustion, compare the different phases of burn (such as premixed mixing controlled combustion) and to investigate peak rates of heat release. The cumulative heat release rate has also been utilised to determine the total amount of fuel burnt in any given cycle. An enlarged view of a portion of Figure 4.2 is presented in Figure 4.3 with pressure data and the GHRR for each $\frac{1}{2}$ crank angle. Various markers indicate start of injection events and the three principal phases of combustion.

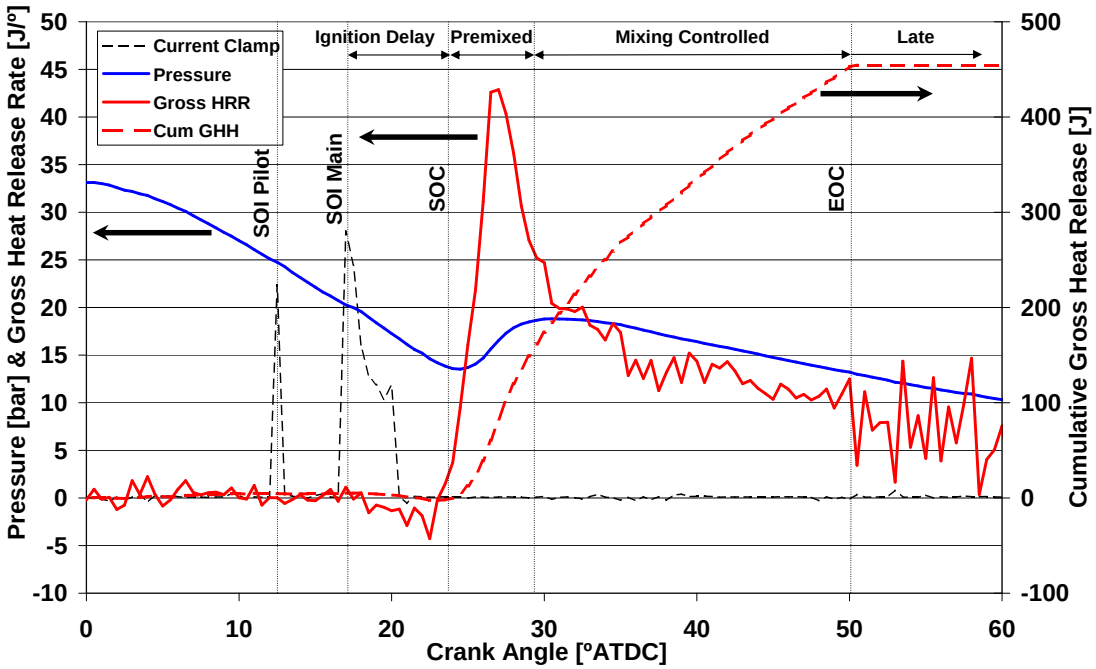

Figure 4.3: Example of Heat Release Rate, 300 rpm

In this example there is no notable pilot combustion, as seen through much of the work presented. Unless otherwise stated the term ignition delay refers to the period between injection of the main and Start of Combustion (SOC). SOC is defined here as the first instance where GHRR breaches 2.5 J/°, is higher than the previous reading and the subsequent reading is higher again. More simply, 3 consecutively rising readings, the middle of which is above 2.5 J/°. The period between start of main injection and SOC is the ignition delay period where fuel mixes with hot air and low level chemical reactions occur until there is a suitable fuel/air mixture and rapid acceleration of reactions occurs. Premixed combustion refers to the initial spike where a potentially large amount of appropriately mixed fuel and air combust immediately after initial ignition. The end of premixed combustion is defined to an extent subjectively, but generally occurs within a few crank angle degrees, when mixing controlled combustion becomes the primary burn mechanism. In this phase the propagation of the flame is defined by the rate at which fuel is liberated from rich areas and entrains in air to become appropriately mixed and continue the combustion process. Generally this period is characterised by a downward slope in heat release rate as the diffusion flame reaches the low, relatively steady levels indicative of late combustion. End of Combustion (EOC) was calculated by sampling the average rate of heat release at the bottom of the

power stroke, where there should be no combustion, and looking for the first point on the GHRR curve where the local average reached a certain small value above this point. This value was tuned depending on the form of test (low speed high fuelling vs. high speed low fuelling) as a wide range of GHRRs are considered in this study. The total cumulative heat release was therefore the addition of the $\frac{1}{2}$ crank angle degree resolved heat release rates between start of injection and the point determined to be the end of combustion, divided by two as GHRR is calculated in $J/^\circ$, not $J/\frac{1}{2}^\circ$. The combustion duration is defined as the interval between SOC and EOC and is expressed predominantly in milliseconds to account for variable engine speed. Negative heat release after main injection is evident in Figure 4.3. This is caused by fuel vaporisation before start of combustion around 23°ATDC. The swift rise to peak heat release rate, indicating premixed combustion, is followed by slow reduction in heat release rate, indicating diffusion burn. In this case the algorithm picks off end of combustion at 50°ATDC with just over 450 J of energy being released.

4.3.2 Further Uses of Heat Release

As well as enabling in-cylinder combustion events to be visualised, the cumulative value of the gross heat release through the whole combustion event can be used in calculations to give an indication of how much of the injected fuel is being burnt (n_c, indicated combustion efficiency) and the efficiency of conversion of this burnt fuel to IMEPg (n_t, indicated thermal efficiency). The multiple of these two efficiencies is the indicated fuel conversion efficiency, n_f, which reveals how well the total injected quantity of fuel is converted to IMEPg. Equations 4.18–4.20 below detail these calculations

$$n_c = 100\frac{\mathrm{GHR_{cum}}}{\mathrm{q_{fuel}Q_{LHV}}} \tag{4.18}$$

where $\mathrm{GHR_{cum}}$ is the cumulative gross heat release in Joules, $\mathrm{q_{fuel}}$ is the total fuel injected per cycle in litres and $\mathrm{Q_{LHV}}$ is the lower heating value of the fuel in Joules per litre. In this work 34.425 MJ/l [23] is used as the LHV for diesel fuel.

$$n_t = 100\frac{\mathrm{IMEP_g}V}{\mathrm{GHR_{cum}}} \tag{4.19}$$

where IMEPg is in SI units of pascals and V is the displaced volume in m^3, 0.0005. n_c is the percentage of the injected fuel energy available that is released in combustion and n_t is the work done as a percentage of that energy released. The multiple of the two gives the overall fuel conversion efficiency, a measure of how well the fuel injected is converted to IMEPg.

$$n_f = \frac{n_c n_t}{10000} \tag{4.20}$$

These values are of use in analysis of heat release to aid in characterising combustion. For example, it is possible for much of the injected fuel to be burnt, but due to poor combustion phasing, low thermal efficiency will result in a poor output. At fully warm conditions it is desirable to burn all of the fuel, rarely achieved in reality, but greater than 99% is targeted [23, 87]. Due to losses and variations in combustion phasing, indicated thermal efficiency can vary widely. At low speeds representative of cold start it is possible to combust much of the fuel at the small cylinder volumes around TDC, enabling high thermal efficiency.

4.4 Summary

The key response variables of Indicated Mean Effective Pressure and Rate of Heat Release have been introduced, with their derivations. In this thesis IMEPg, is used to characterise the work output of a given engine cycle, or an average such as $\overline{IMEPg}_5$ to characterise the average work output over a given number of cycles. This reduces the effect of cycle-to-cycle variation and ensures better trends. In some cased the term "work output" may be used interchangeably with IMEP, as only one engine is considered, hence the swept volume remains the same. Maximising IMEPg at cold start will enable a quick run-up to idle speed. Once cold idle speed has been reached, the priority shifts to maintaining engine speed against the load placed on the engine by friction and auxiliary demand. If the set-point IMEPg can be maintained with minimum deviation, this should ensure a stable idle speed which is a desirable cold idle target. Minimised $\mathrm{StD}_{\mathrm{IMEPg}}$ and $\mathrm{CoV}_{\mathrm{IMEPg}}$ parameters will achieve this goal.

Greater understanding of the processes involved in cold start may be obtained by considering the GHRR of a cycle, or an average GHRR for a number of cycles. This enables the bulk combustion process to be visualised, when and how the fuel is burnt, as well as how much is combusted overall. Different efficiencies may be calculated with these responses to understand what constitutes desirable performance at cold start. Detailed analysis of these results, in conjunction with other output indicators, should facilitate a better insight into the cold start process over the coming chapters.

Chapter 5

Combustion Characteristics — Effect of Injection Parameters

5.1 Introduction

The effects of varying injection parameters on work output and heat release characteristics under cold start conditions ranging from $10°C$ to $-20°C$ are investigated in this chapter. It represents a large collection of work, dealing with varying injection timing, quantity, number of injections and engine speed. It is necessarily the largest chapter in the thesis, laying down the baseline for later performance comparisons and aims to give a comprehensive summary of the cold start regime. By analysing factor effects on both gross Indicated Mean Effective Pressure and gross Heat Release Rate, areas which give the best performance are identified. In this section, results are given for high compression ratio (HCR) for later comparison at Low Compression Ratio (LCR). By identifying the reasons behind differing performance, a more focused approach may be applied when considering LCR.

At low engine speeds it is necessary to maximise work output to attain a swift run-up to idle speed. This chapter begins with investigations at 300 rpm, a speed representative of cycles just above initial cranking. A sweep of injection timing for a single injection at high fuelling

is analysed to locate optimum timings for work output. With optimum timing identified, the effect of fuel quantity is studied to assess if benefits may be obtained by varying the air/fuel ratio. The effect of test temperature on indicated work output is then studied to ascertain if performance will be compromised by further changes in temperature. The utility of one or two small pilot injections in advance of the main is considered to observe any improvements that may be offered.

The priority for higher speeds representative of cold idle shifts to meeting a set work output to counter engine friction and ancillary load. Good quality cold idle meets this target with minimum deviation to maintain a stable engine speed. The cold idle region is considered at the worst case $-20°C$ by varying engine speed in the range 600–1500 rpm and considering the effect of this variation on work output followed by the cycle-to-cycle variability of work output. A sweep of injection timings is performed to locate the best performance obtainable with a pilot plus main injection strategy for target IMEPg. Number of pilot injections and pilot quantity are found to have a strong effect on cold idle performance. Different combinations are assessed to study the effect of pilot injection strategy on variations in work output and heat release across a range of engine speeds and injection timings. The experimental study is finalised by investigating the effect of test temperature on the performance of different injection strategies. As pilot injection strategy was found to have significant effect on cold idle operation, and this was linked to differences in fuel mixing, a computational fluid dynamics investigation is presented which gives an insight into fuel distribution within the cylinder for a variety of pilot injection strategies.

5.2 Varying Injection Timing

Common rail fuel injection equipment allows for multiple precisely defined injection events per engine cycle. This allows the calibrator much freedom, but interactions of multiple factors may make correct observations and judgements difficult. In this section a single factor, injection timing, is varied. An engine speed of 300 rpm is used to simulate the first cycles just above cranking speed. High work output is desirable for swift engine acceleration

towards idle speed. The effect of varying main timing between TDC and 25°ATDC for a single injection of 60 mm^3/str at an ambient temperature of $-10°C$ on $\overline{IMEPg}_5$ is depicted in Figure 5.1.

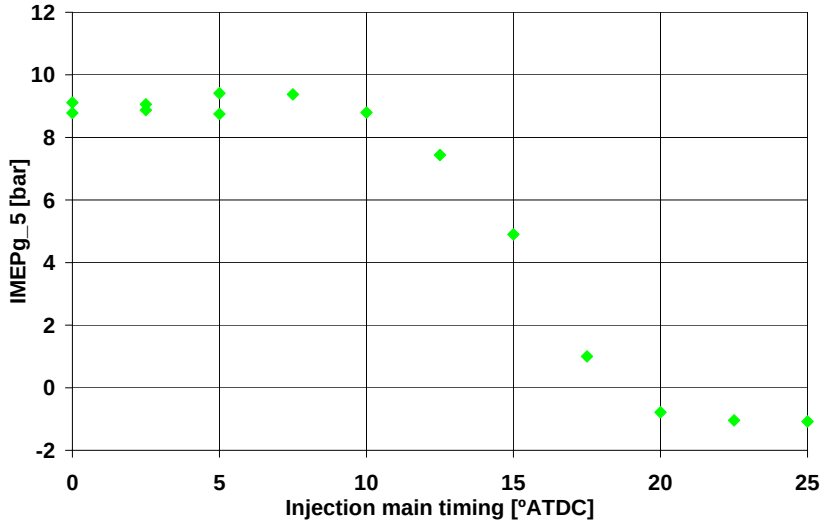

Figure 5.1: Effect of main timing on average IMEPg over the first 5 fired cycles, single injection, 60 mm^3/str, $-10°C$, 300 rpm, HCR

This high fuelling test point has a relatively flat region from TDC to 7.5°ATDC, where approximately 9 bar is produced. After this point IMEPg reduces until 20°ATDC where the value becomes negative, implying all five cycles misfire, resulting in only the losses of the system contributing to IMEPg. Timings in advance of TDC result in excessive cylinder pressure and have not been investigated, however from the gradient of the line it is apparent that this would result in lower IMEPg.

The Gross Heat Release Rate (GHRR) and Cumulative Gross Heat Release (Cum GHR) profiles for the first combusting cycles of the above test points, at 7.5° intervals, are presented in Figure 5.2. Ignition delay and combustion duration for each timing (calculated as described in Chapter 4) are depicted in the following figure, 5.3. Values are given for both the first cycle and average of all combusting cycles. The average value is used as there can be large variations cycle-to-cycle, especially over the first few cycles which can obscure trends as seen by comparing the two sets of results.

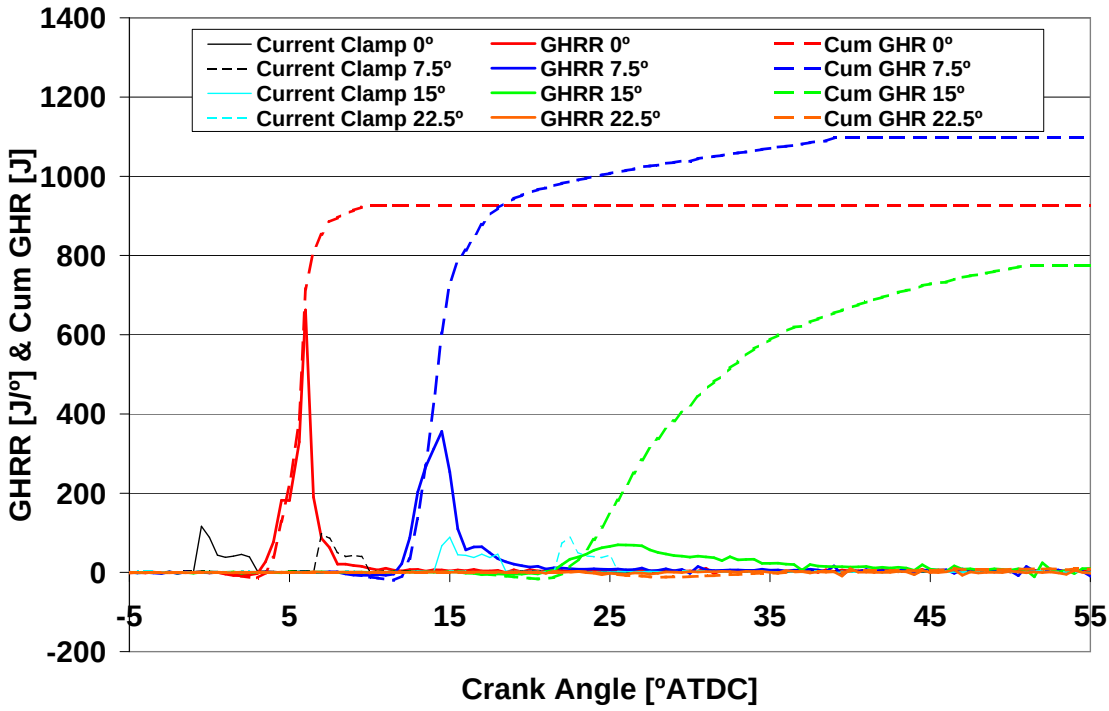

Figure 5.2: Effect of main timing on first cycle Gross Heat Release Rate and total Cumulative Gross Heat Release, single injection, 60 mm^3/str, $-10°C$, 300 rpm, HCR

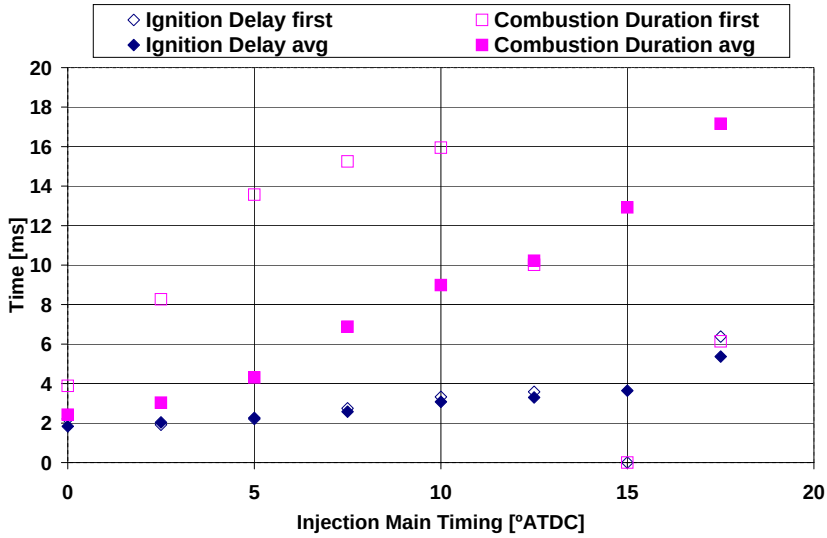

Figure 5.3: Effect of main timing on Ignition Delay and Combustion Duration (unfilled markers represent first combusting cycle values, solid markers represent average values for all combusting cycles), single injection, 60 mm^3/str, $-10°C$, 300 rpm, HCR

Considering the heat release profiles, the first effect of retarded timings is an extension of ignition delay due to injection into a cooler atmosphere, with lower heat input and vaporisation as timing is retarded. Despite an increase in ignition delay, there is a lower peak GHRR,

indicating a substantially lower mixing rate. The dominant factor in fuel/air preparation is therefore in-cylinder temperature and pressure during the ignition delay period, not time. As injection is retarded towards 20°ATDC, the ignition delay of combusting cycles extend until no combustion is achieved. The heat release profile for the most retarded injection plotted in Figure 5.2 becomes negative after injection, indicating evaporation, but does not rise above 0. This is a total combustion failure and results in a misfiring cycle. Due to this, data are only plotted up to 17.5°ATDC in Figure 5.3.

Considering the data in Figure 5.3 also reveals that combustion duration is directly related to injection timing. Average values of combustion duration increase with retarded injection producing long, low intensity diffusion burns with low peak rates of heat release. Comparing results for first and average cycles shows this trend holds until 10°ATDC and then first cycle combustion duration actually reduces. This is due to the extremely low heat release rates generated in the first cycles until some heat has been added by combustion. The zero values at 15°ATDC indicate a misfiring cycle.

Despite increased combustion duration there is only a very small increase in ignition delay for the first cycle compared to the average value. Heat addition from previous combustion is of low importance for combustion initiation times, but it has a great effect for combustion intensity. This implies ignition is initiated by the glow plug and that charge temperature dictates the intensity and duration of the combustion after ignition.

When Figures 5.1, 5.2 and 5.3 are considered together, it can be seen that peak IMEPg and cumulative heat release is achieved by ensuring combustion phasing is such that fuel is injected into the cylinder at the optimum conditions for thorough mixing with a moderate peak rate of heat release and combustion duration. Injection in advance of this results in higher peak rates of heat release, but a lower cumulative burn due to abrupt termination of combustion. This implies that there is not enough time for thorough mixing in the diffusion burn. Retarded timings result in long ignition delays, extending combustion into regions with lower temperatures and pressures, resulting in low rates of heat release which do not promote self sustaining combustion. This causes both low combustion efficiency and poor phasing for thermal efficiency.

Summarising, pilot injection timing was found to have limited effect on IMEPg between approximately TDC and 10°ATDC, after which there was a rapid degradation. Cumulative heat release increases over the first few degrees after TDC before reducing with retard. Peak rate of heat release reduces with retard and combustion duration extends significantly until the onset of misfire after 15°ATDC. Ignition delay approximately doubles between TDC and 15°ATDC.

5.3 Varying Injection Quantity

The most direct way of varying work output is to inject a different quantity of fuel. A sweep of fuellings between 30 mm^3/str and 80 mm^3/str is shown in Figure 5.4. The injection timing was fixed at 5°ATDC, which gave the highest $\overline{IMEP}g_5$ for the timing sweep previously presented in Figure 5.1. The value of the first cycle IMEPg is also given. Peak values of $\overline{IMEP}g_5$ are slightly higher for these tests compared to the earlier results for main timing. This has been linked to an increase in compression pressure of some 1 bar due to the timing sweeps being the first tests performed for this build. Although much hot conditioning had been performed before data acquisition, it is possible that cold temperature high fuelling runs help bed the rings in over time and/or a certain amount of oil/fuel/water mixture down the bore is actually beneficial for low speed sealing. By this point the compression pressure had stabilised. Selected first cycle heat release results are given in Figure 5.5 to analyse the IMEPg trends.

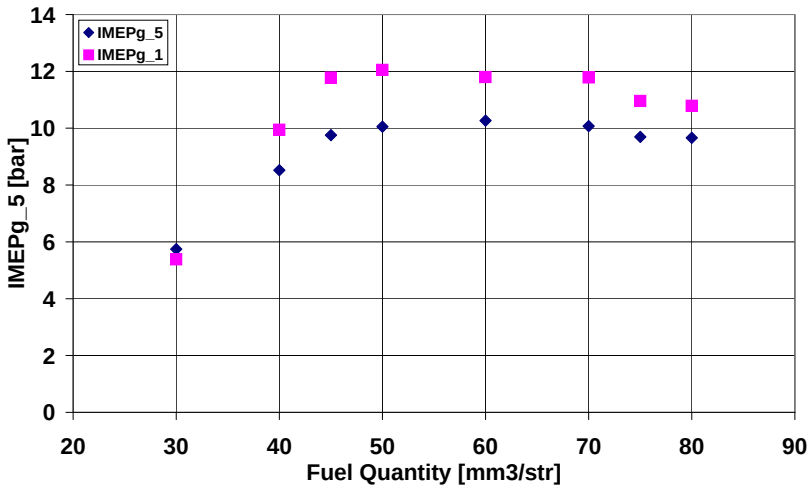

Figure 5.4: Effect of fuel quantity on IMEPg (first cycle and average of first five cycles), single injection, main timing 5°ATDC, $-10°C$, 300 rpm, HCR

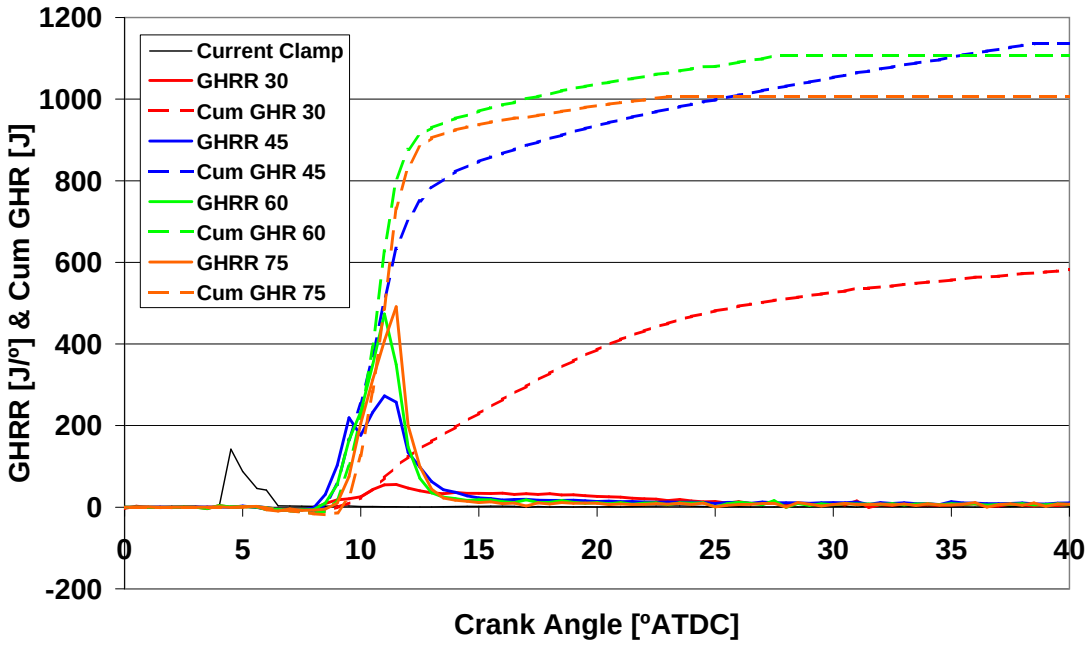

Figure 5.5: Effect of fuel quantity on first cycle Gross Heat Release Rate and total Cumulative Heat Release, single injection, main timing 5°ATDC, $-10°C$, 300 rpm, HCR

In Figure 5.4 there is a clear increase in IMEPg up to around 50 mm^3/str, then a plateau region before slightly reducing IMEPg above 70 mm^3/str. The heat release rate graph (5.5) helps to explain this. At the low fuelling there is a low faltering burn, which continues until 40°ATDC. The rate of heat release is greatly increased by injecting 45 mm^3/str. This, combined with a very long burn period, produces the highest overall heat release for this cycle, resulting in a near identical cycle resolved IMEPg to 60 mm^3/str. Increasing fuelling

above this level again increases peak rate of heat release and results in one distinct peak, followed by a shorter and lower diffusion burn. At the highest level there is no further significant increase in peak heat release rate. There is a longer fuel evaporation (negative heat release) period before combustion, as depicted by the detail view in Figure 5.6. An earlier termination of combustion is experienced, resulting in lower cumulative fuel burn and IMEPg despite increased fuel input. Ignition delay and combustion duration results are given in Figure 5.7.

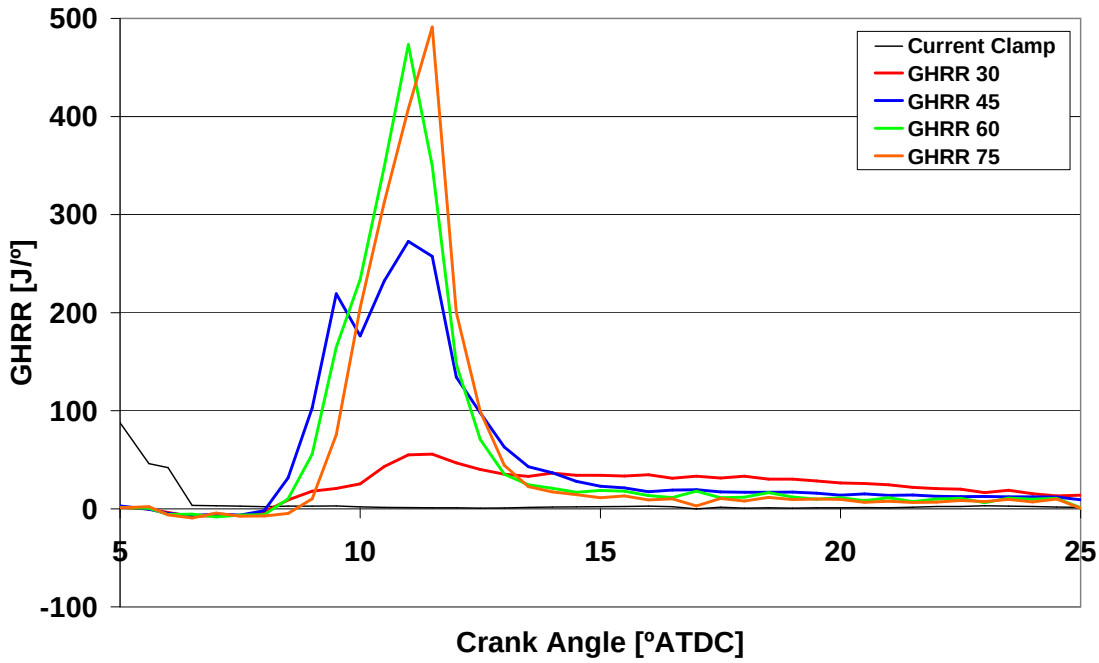

Figure 5.6: Detail view of effect of fuel quantity on first cycle Gross Heat Release Rate, single injection, main timing 5°ATDC, $-10°C$, 300 rpm, HCR

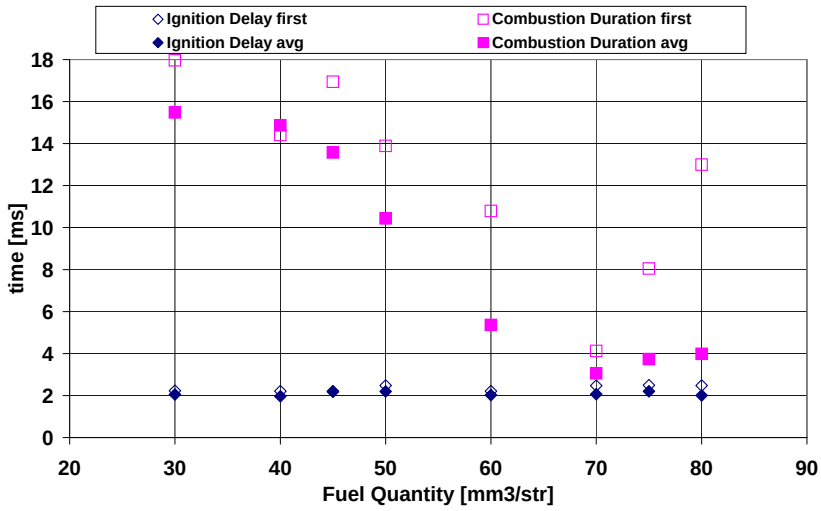

Figure 5.7: Effect of fuel quantity on Ignition Delay and Combustion Duration (unfilled markers represent first combusting cycle values, solid markers represent average values for all combusting cycles), single injection, main timing 5°ATDC, $-10°C$, 300 rpm, HCR

As previously seen at this timing, the first cycle and average ignition delay is very similar for all quantities, slightly extending with the highest values, especially in the first cycle due to extra heat required for vaporisation. Combustion duration of the first cycle is almost always longer, likely due to excessively faltering initial heat release at low fuellings and reduced initial peak rates of heat release increasing total time for mixing at high fuellings. As the test progressed, heat addition from previous combustion increased heat release from low fuellings and reduced ignition delay at high fuellings, allowing combustion to be completed in a more energetic environment, resulting in early termination.

In summary, as fuel quantity is increased from low values to 60 mm^3/str, the peak rate of heat release and IMEPg increase, whilst combustion duration reduces. Larger quantities of fuel have little further overall effect on performance.

5.3.1 Variations over 30 Injected Cycles

The difference between $\overline{IMEPg_5}$ and first cycle IMEPg was shown to be up to 2 bar, suggesting some rapid changes in performance over the first few cycles. Significant differences between first cycle and average combustion durations were also noted. This section aims

to explain some of these differences. Figure 5.8 compares the IMEPg of each fired cycle for the 45 and 60 mm^3/str cases.

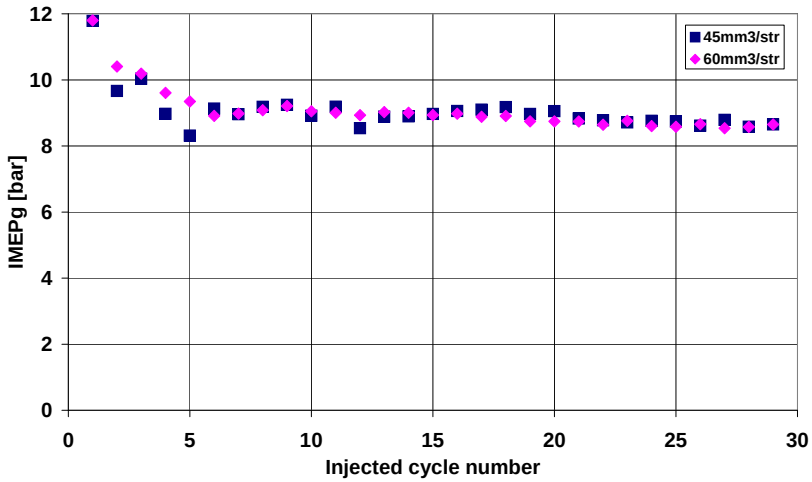

Figure 5.8: Cycle resolved IMEPg for single injection quantities of 45 mm^3/str and 60 mm^3/str, main timing 5°ATDC, $-10°C$, 300 rpm, HCR

It is worth noting that 45 mm^3/str is approximately stoichiometric for this combustion system, and therefore 60 mm^3/str represents an equivalence ratio (ϕ) $\approx$ 1.3. It is typical to run rich at cold start [76, 88], but it was shown in the previous section that excessively rich mixtures are detrimental. There appears to be no peak IMEPg benefit to increasing fuelling above 45 mm^3/str, however higher fuelling does give a more reliable IMEPg with no significant drops as experienced at 45 mm^3/str. The following figures give heat release rate profiles and cumulative heat release histories as the test progresses (first, second, fifth, 10$^{\text{th}}$, 20$^{\text{th}}$ and 29$^{\text{th}}$ injected cycles). Figures 5.9 and 5.10 present results for 45 mm^3/str, Figures 5.11 and 5.12 60 mm^3/str.

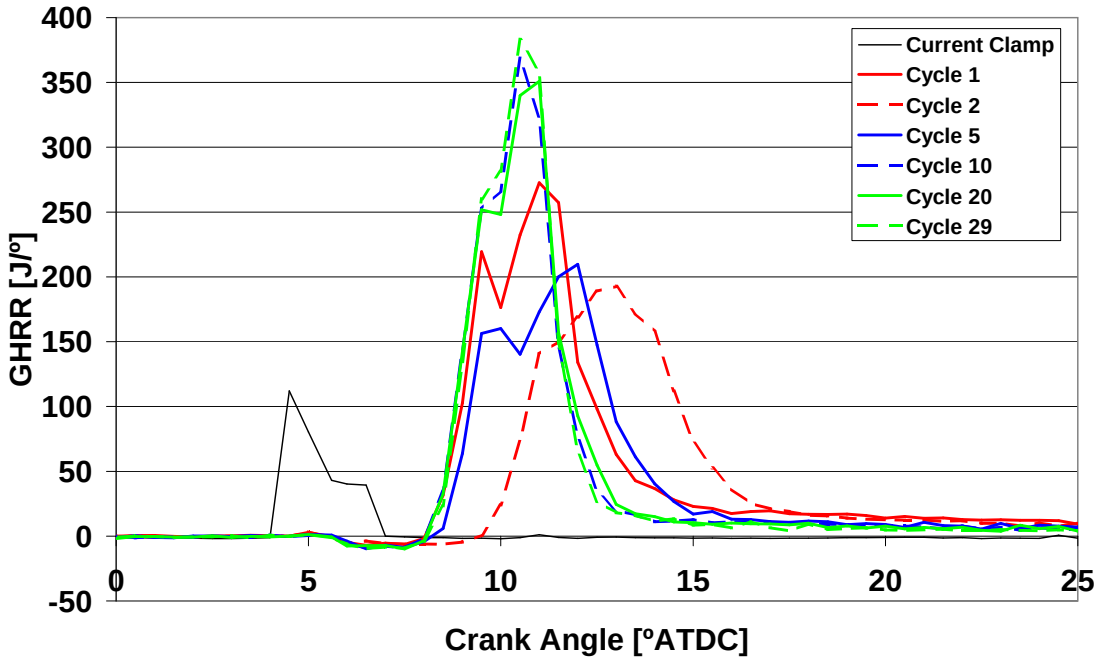

Figure 5.9: Gross Heat Release Rates as test progresses, 45 mm^3/str, main timing 5°ATDC, $-10°C$, 300 rpm, HCR

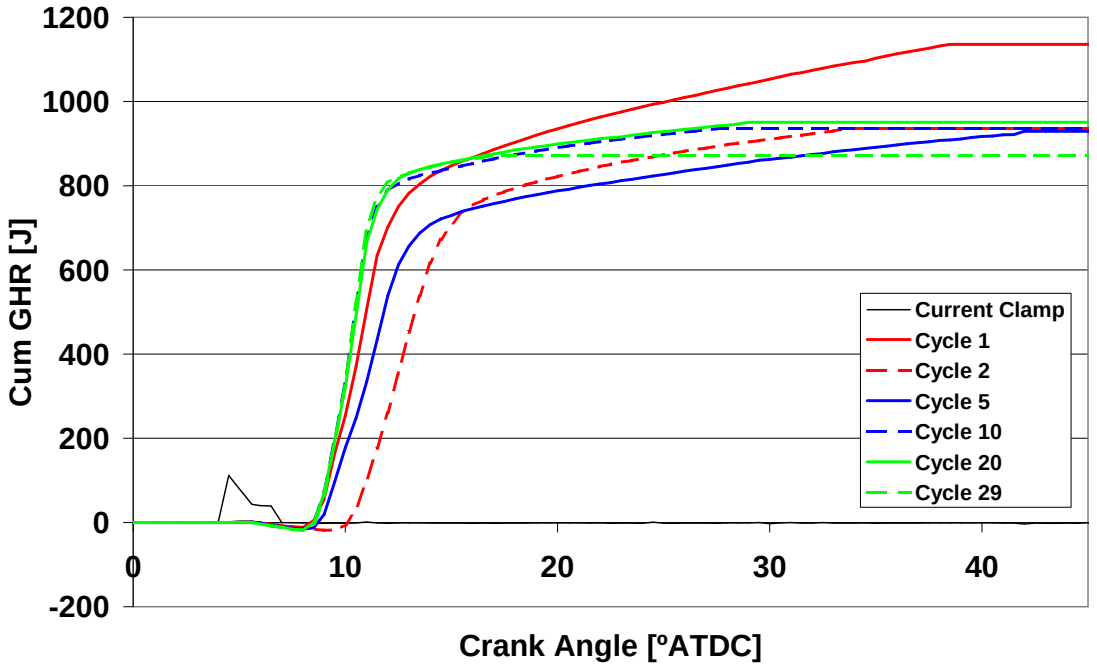

Figure 5.10: Cumulative Gross Heat Release as test progresses, 45 mm^3/str, main timing 5°ATDC, $-10°C$, 300 rpm, HCR

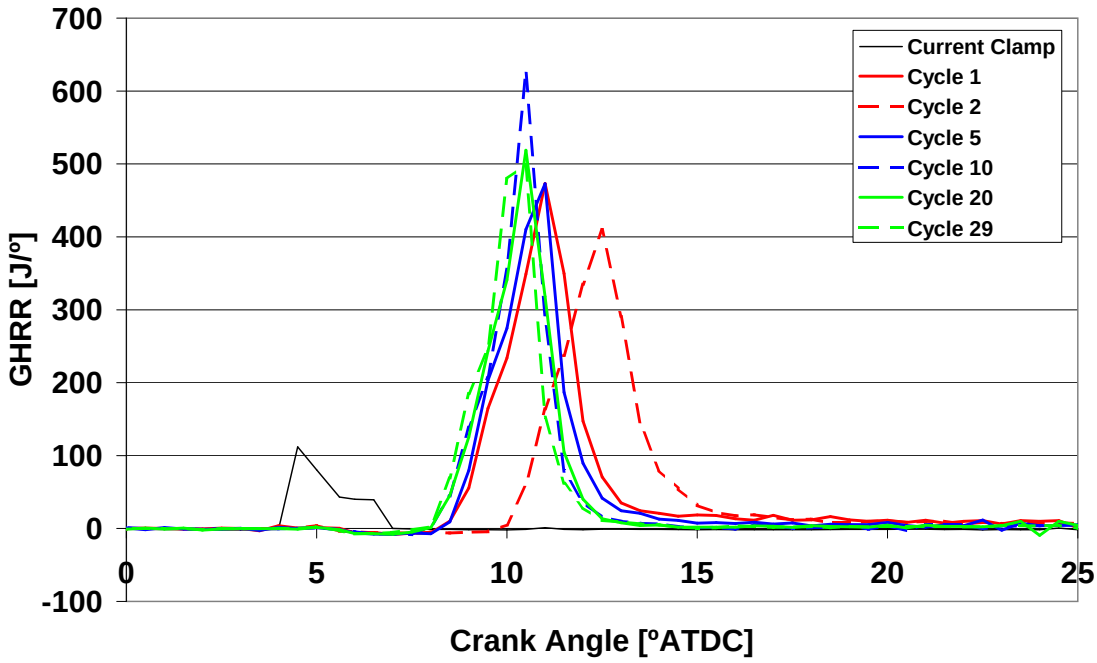

Figure 5.11: Gross Heat Release Rates as test progresses, 60 mm^3/str, main timing 5°ATDC, $-10°C$, 300 rpm, HCR

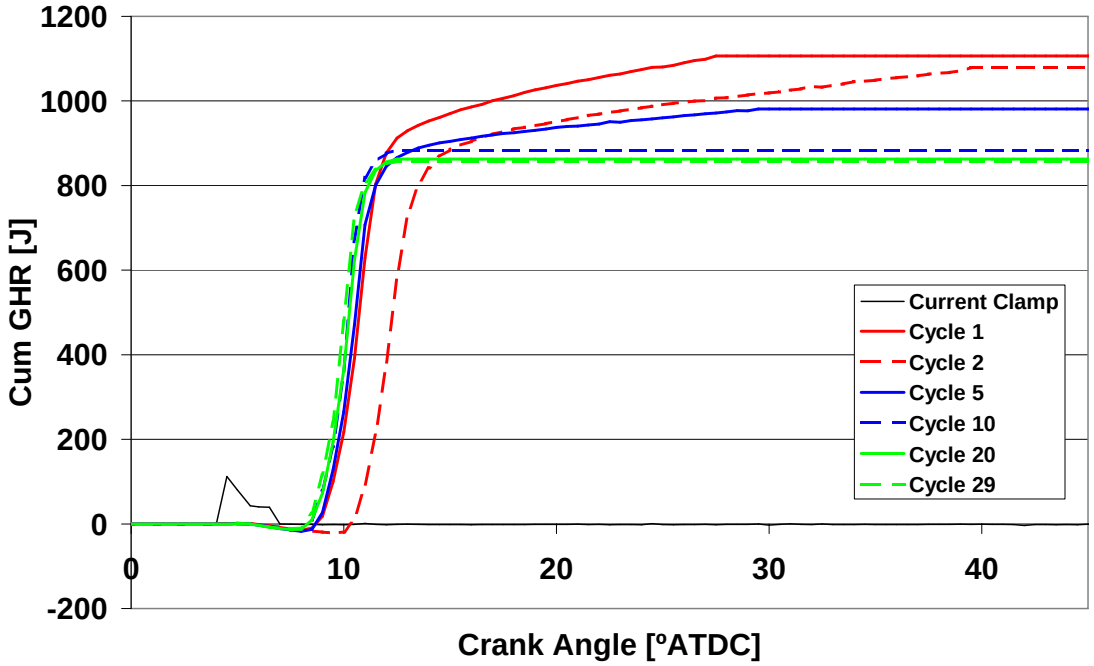

Figure 5.12: Cumulative Gross Heat Release as test progresses, 60 mm^3/str, main timing 5°ATDC, $-10°C$, 300 rpm, HCR

Both fuel quantities require some time to settle down to their approximate steady-state GHRR profile. The high fuel quantity has a higher peak rate of heat release for all cycles, and a shorter combustion duration, even after multiple fired cycles. The less stable output of 45 mm^3/str can be attributed to its lower peak rate of heat release for the poor cycles, resulting in poorer self sustaining combustion and excessively long combustion duration. This leads to both reduced cumulative burn and poor combustion phasing. There is an extended ignition delay for cycle two in both cases, but this is no longer apparent by the 5^{th} cycle. In the high fuelling case, the heat release rate profile has nearly reached steady-state by the 5^{th} cycle, whilst heat addition is still increasing initial rate of heat release for the low fuelling. Excess fuel ensures a high peak rate of premixed heat release and strong, self sustaining combustion, with no need for heat input from previous cycles as in the 45 mm^3/str case.

The first cycle or two are the most important when considering a quick acceleration to idle speed, however it is still of interest to consider why there is a drop in IMEPg over the first 5 cycles before reaching a relatively stable lower point. Considering Figures 5.11 and 5.12 again, it can be seen that the first fired cycle (red) is a hybrid of the steady-state (high rate of heat release) and the intermediate (cycles 2 and 5, long diffusion period before termination of combustion) cycles. This results in the highest overall burn. There is some extension of the ignition delay for the second cycle in the crank angle (CA) domain until cycle 5 settles towards the steady-state region of high GHRR, but lower cumulative burn for lower IMEPg. Figure 5.13 depicts the ignition delay of each cycle in this test in both the crank angle and time domain.

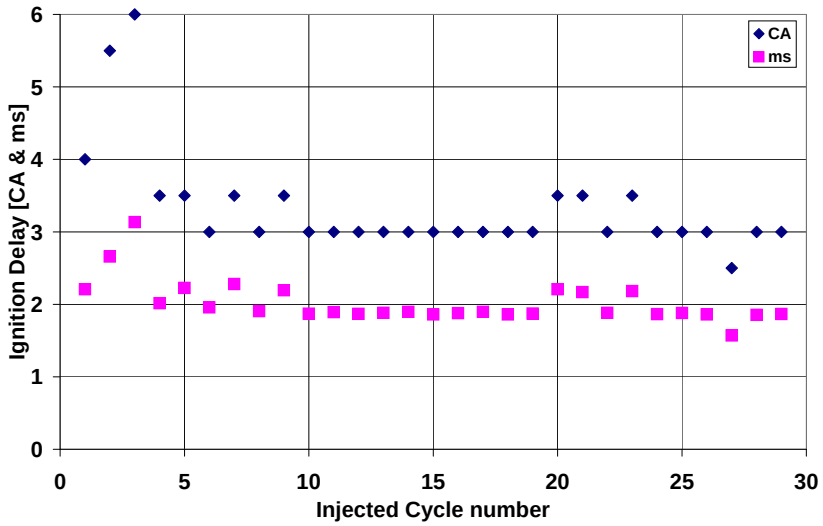

Figure 5.13: Ignition delay (Crank Angles and ms) as test progresses, 60 mm^3/str, main timing 5°ATDC, $-10°C$, 300 rpm, HCR

Whilst there is disparity of CA based ignition delay, much of this is removed when considering the actual time for ignition to occur. The implication of this is that there is significant variation in engine speed over the first few cycles. The cycle resolved average speed during the ignition delay period is given in Figure 5.14.

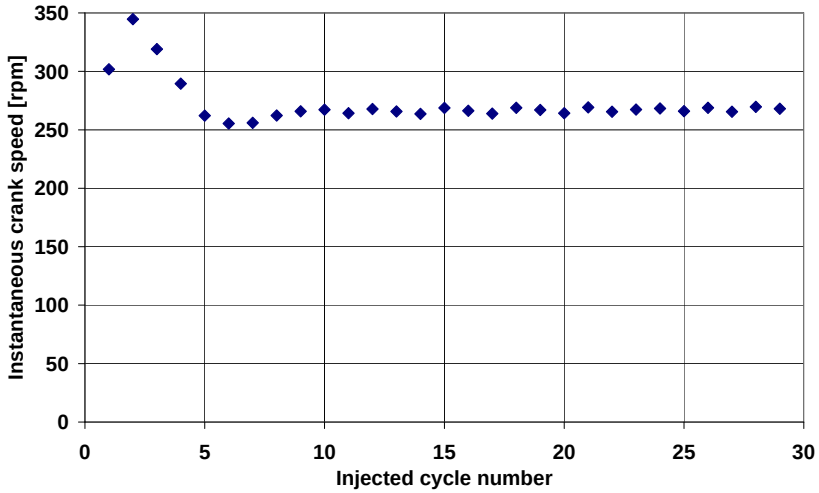

Figure 5.14: Average instantaneous crankshaft speed during the ignition delay period, 60 mm^3/str, main timing 5°ATDC, $-10°C$, 300 rpm, HCR

Crankshaft speed fluctuates throughout the cycle at 300 rpm due to varying loading from compression and expansion. There is a rapid rise in speed from the set point 300 rpm on the first injected cycle due to combustion such that the crank is rotating at $\approx$ 350 rpm

when fuel is injected for the second cycle. After this, the controller brings the speed down to approximately 260 rpm during this part of the cycle. The dynamometer/controller is unable to maintain a set speed during the expansion phase, and therefore compensates by a reduction in speed in the other portions of the cycle. Plotting cycle resolved IMEPg against average crankshaft speed during the ignition delay period in Figure 5.15 shows the effect of this initial speed flare on IMEPg over the first few cycles.

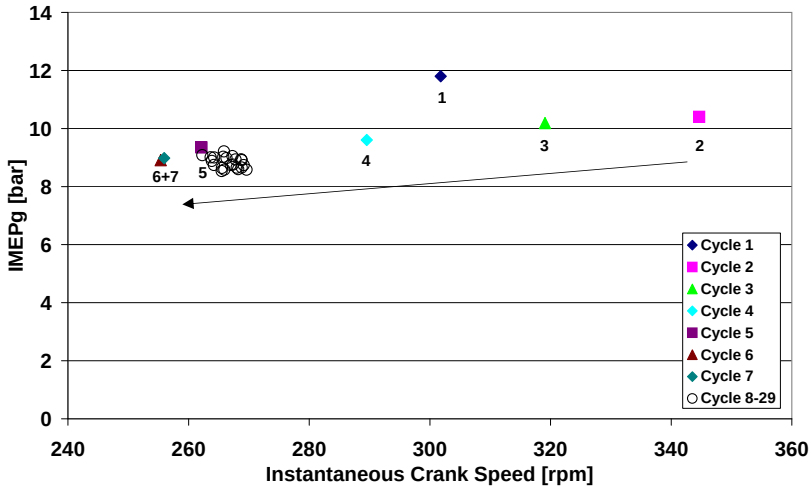

Figure 5.15: Relationship between instantaneous crankshaft speed during ignition delay period and IMEPg for that cycle throughout test, 60 mm^3/str, main timing 5°ATDC, $-10°C$, 300 rpm, HCR

Apart from cycle 1 there is a positive correlation with reducing engine speed leading to reducing IMEPg. This could be expected because at these cold start speeds there is much time for both heat transfer and blowby, which is exacerbated by poor sealing. The hypothesis is borne out, in general, by Figure 5.16.

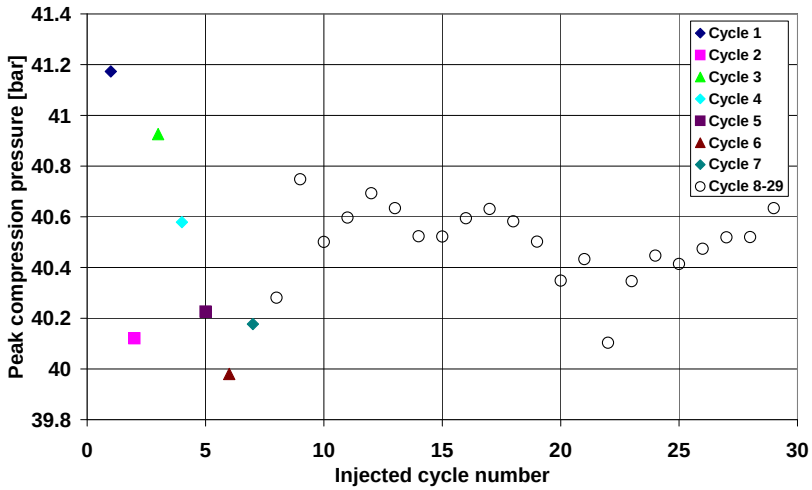

Figure 5.16: Peak compression pressure throughout the test, 60 mm^3/str, main timing 5°ATDC, $-10°C$, 300 rpm, HCR

As engine speed reduces over the first cycles, so too does peak pressure due to greater time under compression. The second cycle has a significantly lower peak pressure after the initial combustion cycle despite the highest engine speed. This suggests that the sudden impulse of pressure rise unsettles the rings, taking a further cycle to effectively seal again. Lower peak pressure at higher speed for cycle 3 compared to cycle 1 suggests that motored sealing is more effective than under fired conditions. High peak pressure and higher than steady-state speed, combined with entirely cool charge with no residuals from previous combustion, helps to explain why the highest IMEPg is achieved in cycle 1. Steady-state IMEPg cycle 8–29 is lower due to reduced speed, greater residuals and possibly warmer intake temperatures due to mixing with hot residuals and contact with warmer walls/piston, reducing density. At the levels dealt with in this investigation — each $°C$ increase in effective intake temperature will reduce density, and therefore oxygen availability, by around 0.37%. It is likely that there are very high levels of residuals in this untuned, naturally aspirated single cylinder unit at low speeds. Schwarz and Spicher [89] investigated a single cylinder SI engine and found that a complicated relationship with both speed and load existed. It is not clear what the effect of reducing speed below 2000 rpm would be from this investigation, but levels of residuals were found to be up to 20%. High residual fraction plus greater blowby and heat transfer under fired and reduced speed operation will contribute to the $\approx$ 25% reduction in IMEPg between cycle 1 and 7.

To summarise, fuelling above stoichiometric reduces cycle-to-cycle variability in work output in these unstable conditions by increasing initial rate of heat release which promotes strong self-sustaining combustion. At these fuelling levels there is a degradation in performance over the first few cycles which has been linked to a reduction in engine speed during the compression phase, increasing time for heat transfer and blowby, reducing peak compression pressure, as well as a possible reduction in charge density and higher residuals.

5.4 Varying Ambient Temperature

The data so far has been gathered at a test temperature of $-10°C$ measured at the liner. This is representative of extreme conditions encountered in the UK, but at higher latitude the vehicle must perform below this level. The cooling equipment available was able to reliably chill to $-20°C$ at the liner irrespective of external weather conditions. Fuel and intake air temperature would typically be around $-25°C$ for these tests. Data were also gathered stabilising the liner temperature at $10°C$ to compare performance with a typical morning cold start during much of the year in the UK.

A comparison of performance at the three temperatures with the same 60 mm^3/str timing sweep as previously presented for only $-10°C$ in Figure 5.1 is given in Figure 5.17.

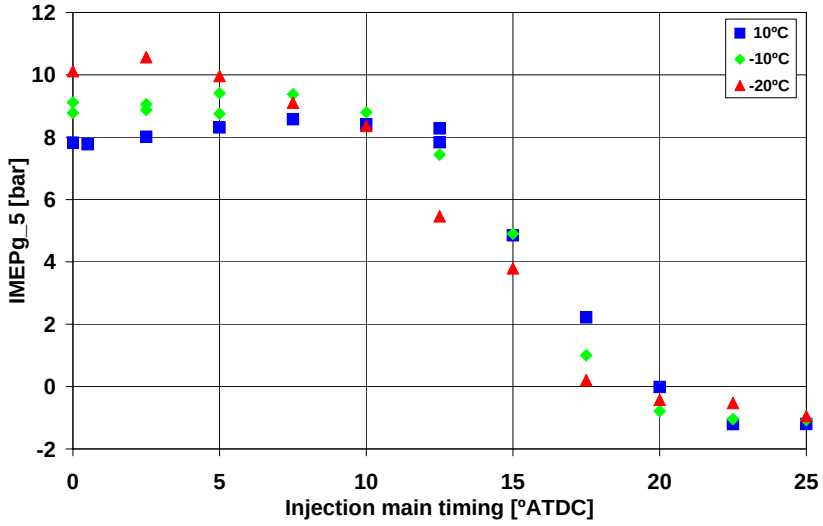

Figure 5.17: Effect of temperature on $\overline{IMEPg}_5$, 60 mm^3/str, 300 rpm, HCR

The most notable effect of an increase in test temperature is a *decrease* in peak $\overline{IMEP}g_5$. Reducing temperature to $-20°C$ gives a peak value around 10.6 bar at 2.5°ATDC compared to the $-10°C$ peak of 9.4 bar at 5°ATDC. Increasing temperature to $10°C$ results in a peak $\overline{IMEP}g_5$ of only 8.6 bar at 7.5°ATDC, suggesting a reduction in fuel burn as well as some degree of change in phasing. In the region just in advance of 10°ATDC, IMEPg is relatively independent of temperature in this range, in advance of this, colder temperatures produce higher $\overline{IMEP}g_5$, a trend reversed in the retard. Considering again the 5°ATDC case for all temperatures, Figure 5.18 shows the effects on GHRR and cumulative GHR.

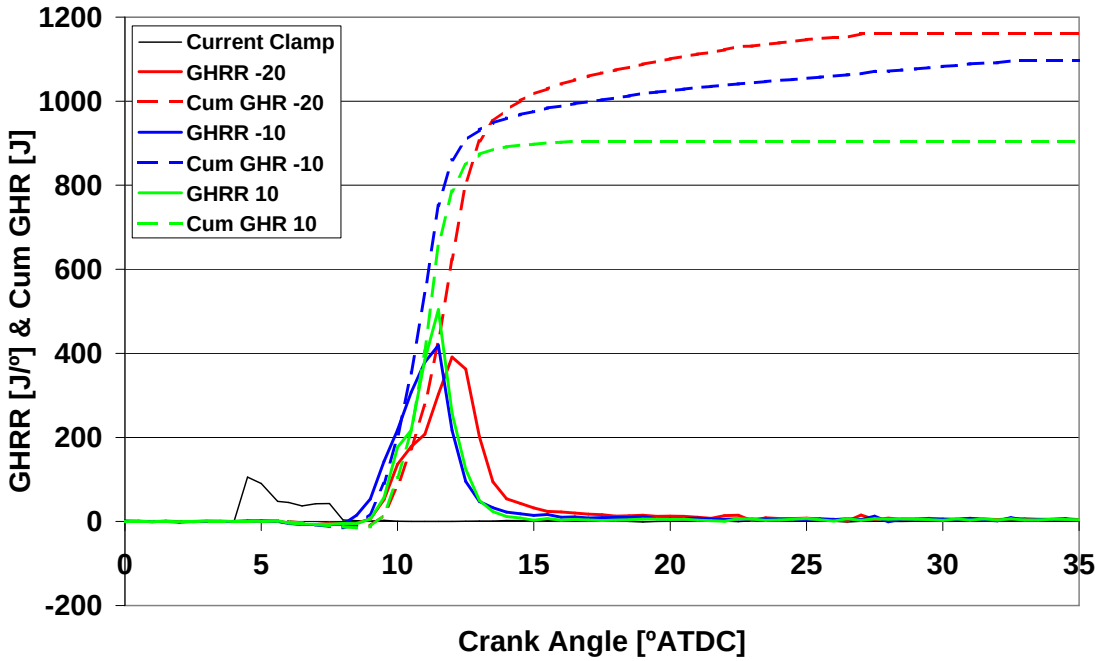

Figure 5.18: Effect of temperature on first cycle Gross Heat Release Rate and Cumulative Gross Heat Release, 60 mm^3/str main timing 5°ATDC, 300 rpm, HCR

These single cycle traces show that peak rate of heat release reduces with temperature, yet total cumulative heat release increases. As temperature increases, better fuel preparation leads to a greater peak rate of heat release and faster combustion which terminates at a less complete fraction than with lower temperatures. When averaged over all cycles, ignition delay was similar for the three temperatures but combustion duration reduced, as expected, with increased temperature. Approximate equivalence ratios are given for the three test temperatures in Table 5.1, based on the temperature of the intake air at that liner condition.

Temperature [$^{\circ}C$]	ρ_{air} [kg/m^3]	ϕ
-20	1.420	1.24
-10	1.367	1.29
10	1.246	1.41

Table 5.1: Properties of intake charge using a 60 mm^3/str injection

Whilst all tests are running very rich, it appears the greater oxygen density (higher intake ρ means there will be more O_2 in the charge) at low temperature combined with a lower peak rate of heat release allows better fuel/air mixing and a more complete combustion event. Peak compression pressures on the final motored cycle were recorded for each day of testing at a given temperature. At $10^{\circ}C$ the average was 39.0 bar, rising to 40.3 bar for $-10^{\circ}C$ and 41.1 bar at $-20^{\circ}C$. This effect was noted in numerical studies by Gonzalez [34], where cooler intake charge of higher density resulted in greater compression pressure, even though losses to heat transfer reduced compression temperature.

The effect of running lean at 30 mm^3/str was studied at $-10^{\circ}C$ in Section 5.3 at an optimum timing. It was found that combustion was weak with very long duration but reliable, resulting in $\overline{IMEPg_5}$ approximately half of the 60 mm^3/str case. Figure 5.19 gives a broad timing sweep for a 30 mm^3/str single injection at the three test temperatures to characterise the effect of temperature at lean conditions.

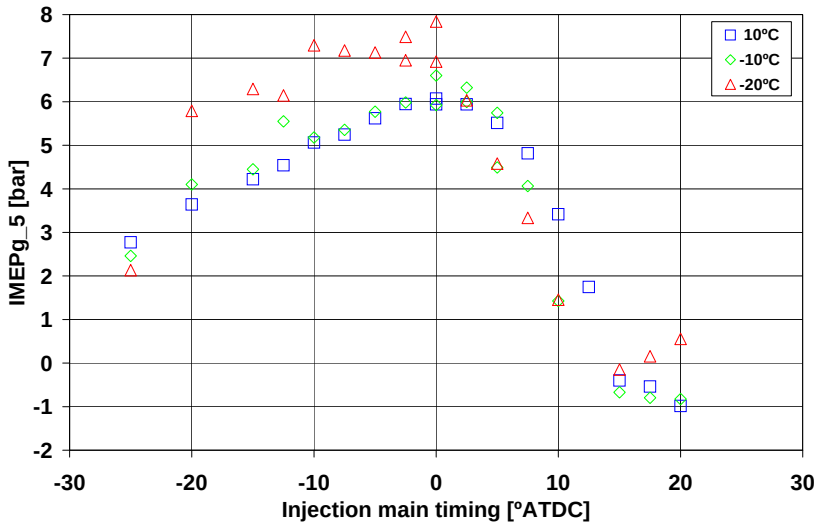

Figure 5.19: Effect of temperature on $\overline{IMEPg_5}$, 30 mm^3/str, 300 rpm, HCR

Results are similar to those at 60 mm^3/str in that a decrease in temperature causes both swifter reduction in IMEPg after TDC and the potential for slightly increased optimal IMEPg at the lowest temperature, although this is less evident as the benefits of extra oxygen availability are lower in the already lean environment. Injection before TDC is not necessarily beneficial apart from at the lowest temperature, otherwise IMEPg is relatively insensitive to temperature. There is more variability at $-20°C$ as indicated by the repeat points around TDC and reduced predictability of the curve with main timing. Figures 5.20, 5.21 and 5.22 contain first cycle heat release profiles for the three temperatures at a main timing of 10° before top dead centre (BTDC), TDC (lower repeat for $-20°C$) and 10°ATDC.

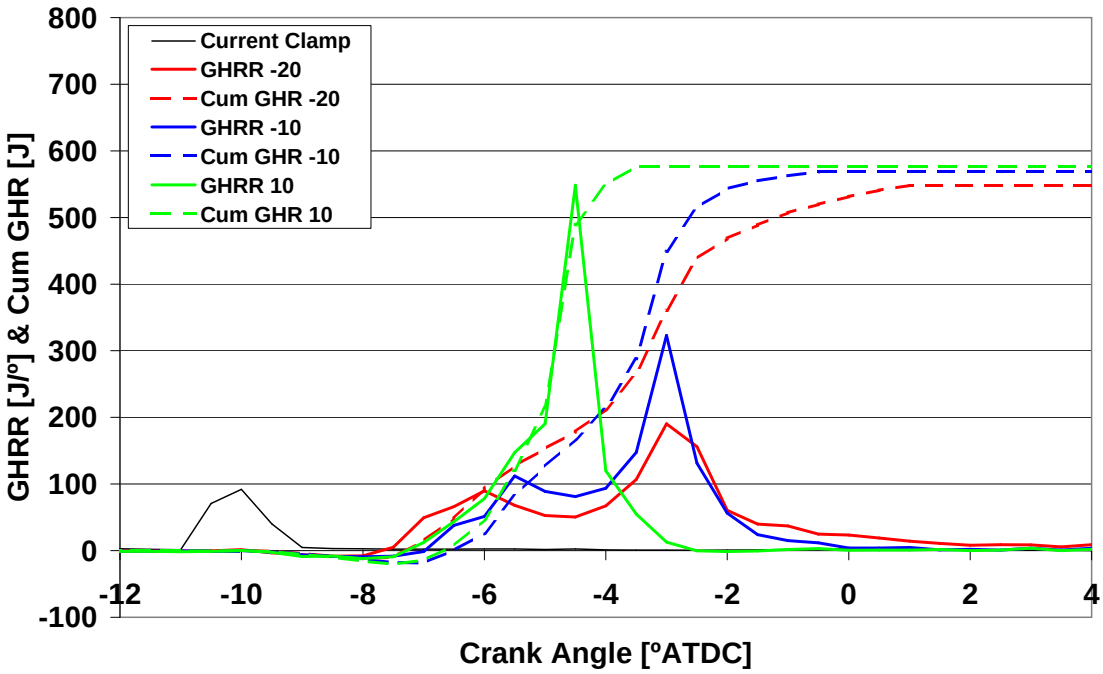

Figure 5.20: Effect of temperature on first cycle Gross Heat Release Rate and Cumulative Gross Heat Release, 30 mm^3/str main timing 10°BTDC, 300 rpm, HCR

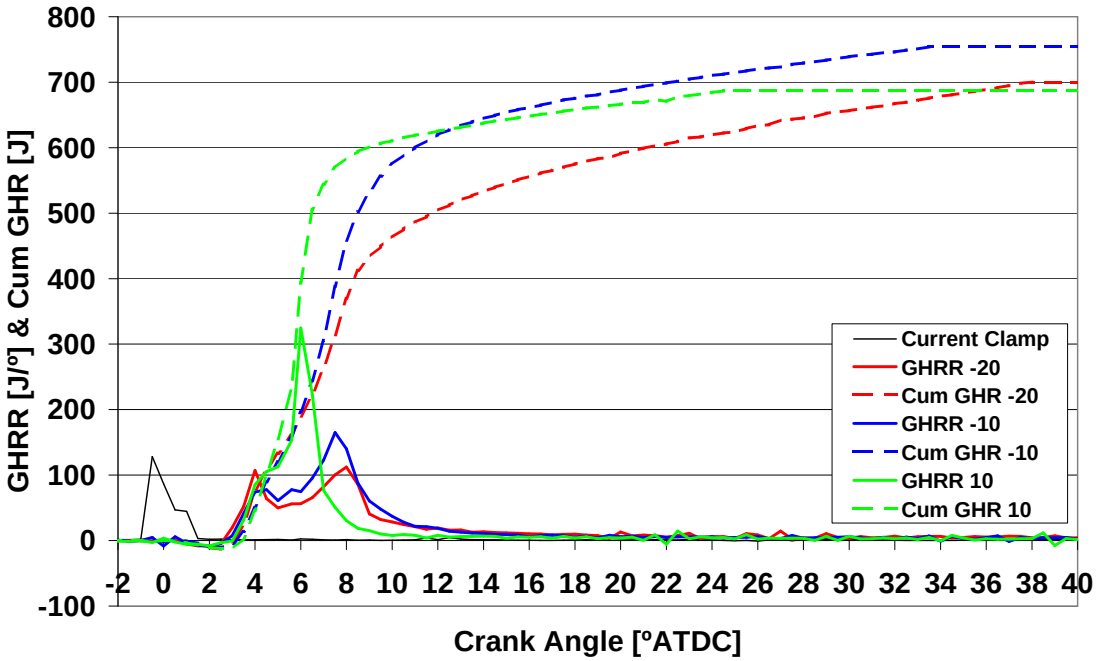

Figure 5.21: Effect of temperature on first cycle Gross Heat Release Rate and Cumulative Gross Heat Release, 30 mm^3/str main timing TDC, 300 rpm, HCR

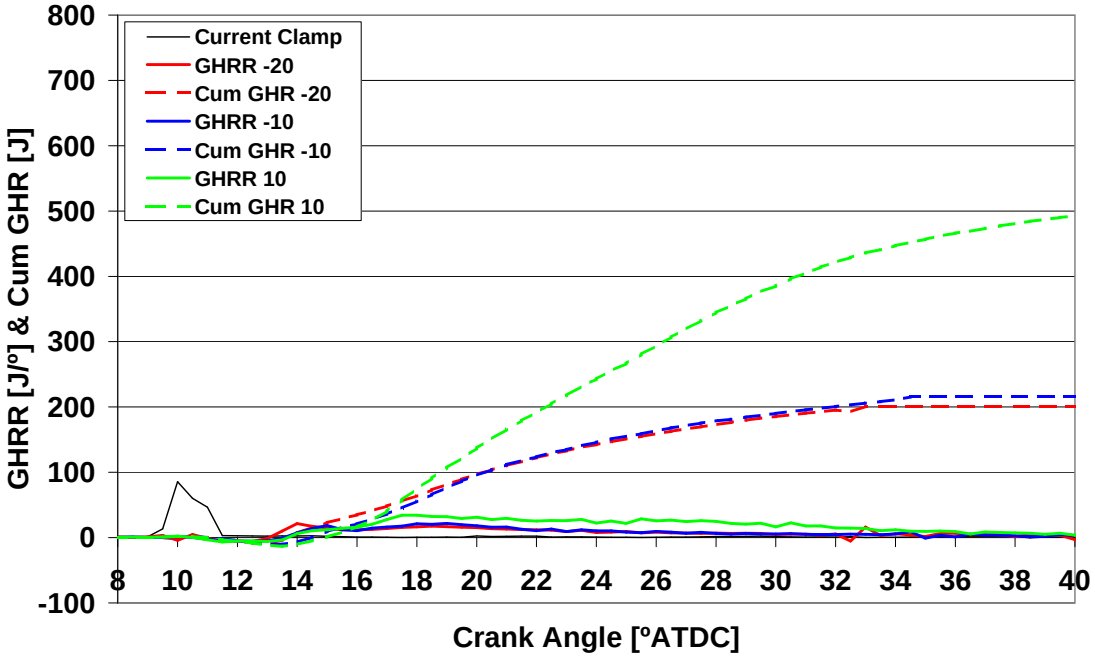

Figure 5.22: Effect of temperature on first cycle Gross Heat Release Rate and Cumulative Gross Heat Release, 30 mm^3/str main timing 10°ATDC, 300 rpm, HCR

Higher temperature equates to higher peak rate of heat release at all temperatures for this fuelling. There is also a shorter burn duration except at the most retarded timings where low compression temperatures result in very poor self sustaining combustion and swifter termination with reduced ambient temperature. There are only small differences in cumulative heat release at the advanced and TDC timings, but the negative effect of reduced temperatures in the retarded case is apparent from the much reduced rates of heat release and cumulative totals. The increase in IMEPg at 10°BTDC, $-20°C$, despite lower cumulative burn, can partially be attributed to the longer burn resulting in more combustion in the optimum region close to TDC without doing negative work against compression which is never fully recovered by expansion. Considering in more detail the heat release rate and pressure traces for each temperature in Figure 5.23 reveals that significantly higher pressure is maintained for the whole power stroke at $-20°C$ due to some low level combustion sustained for many degrees.

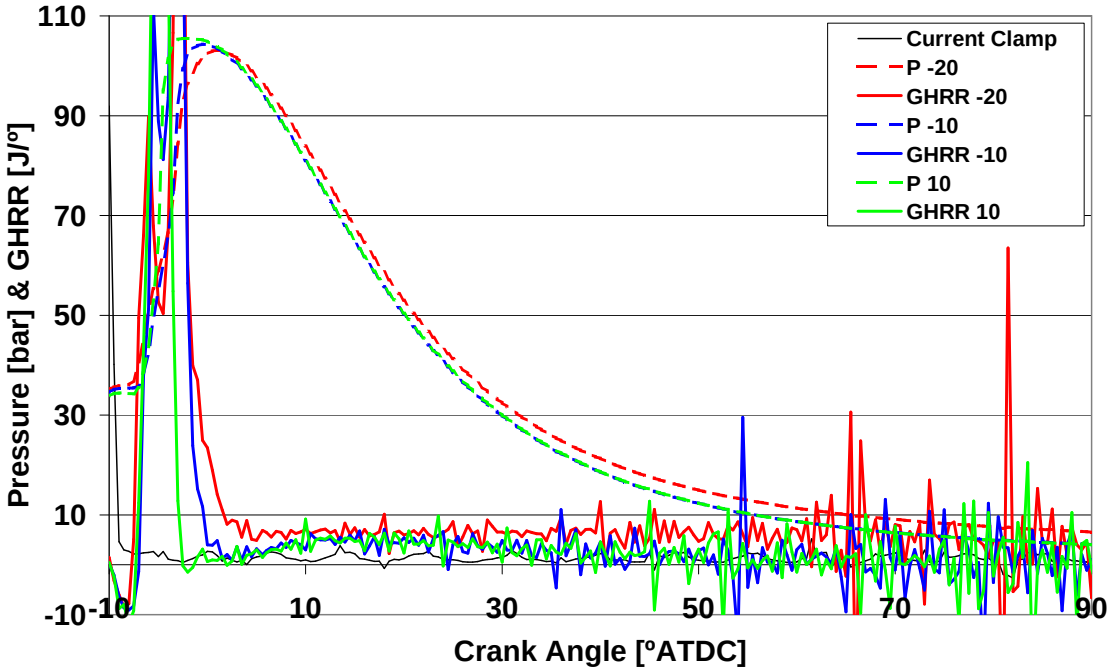

Figure 5.23: Heat release and pressure later in power stroke, 30 mm^3/str main timing 10°BTDC, 300 rpm, HCR

It appears the cumulative heat release calculation cut-off is too aggressive in this case as this low level heat release is ignored. Reduced losses from the lower burn rate around TDC plus this extra combustion results in a first cycle pressure at exhaust valve opening

(EVO) advantage of approximately 2 bar. This difference is too great and of the wrong sign to be attributed to thermal shock. As explained in the literature [90–92], this generally results in a *reduced* pressure and can lead to negative pressure readings. Exposure of the pressure transducer to high temperature combustion causes thermal strain leading to reduced transducer output. The Kistler 6125B piezoelectric sensor was specifically chosen as it has excellent resistance to thermal shock. Further investigation into the process at $-20°C$ involved bulk cylinder gas calculation throughout the first cycles, as depicted in Figure 5.24. Assuming an ideal gas, knowing intake conditions and using $pV = mRT$ allows a reasonable approximation of global average cylinder temperature to be calculated based on pressure transducer readings.

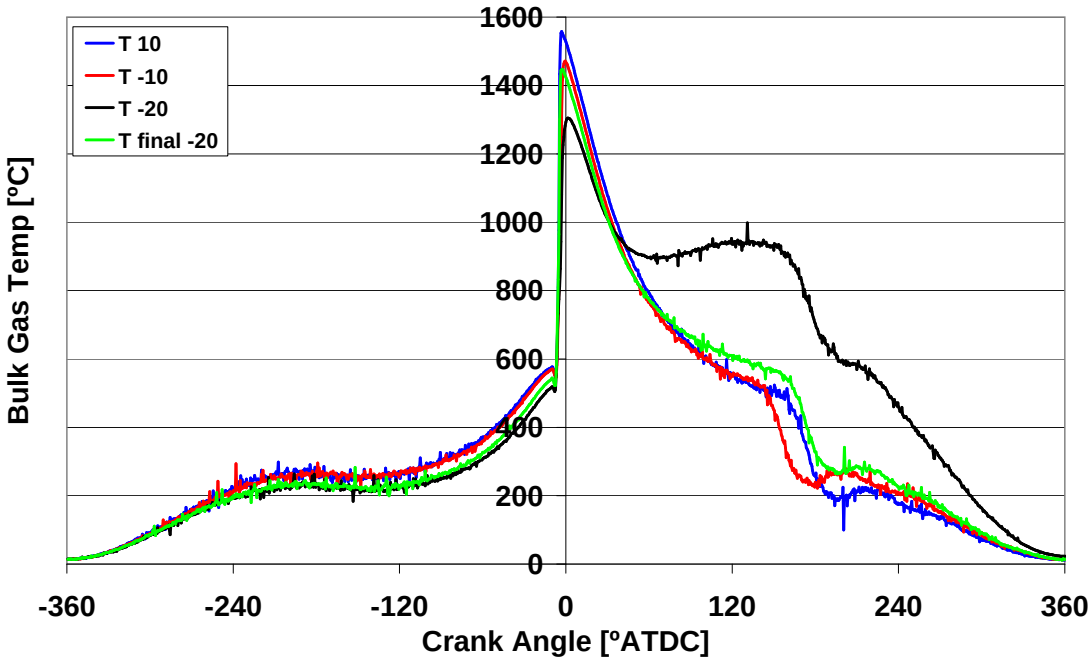

Figure 5.24: First cycle bulk cylinder gas temperature at different ambients, 30 mm^3/str main timing 10°BTDC, 300 rpm, HCR

The bulk gas temperature plots show first temperature rise due to compression before combustion rapidly increases global averages to a peak above $1200°C$ in all cases. Once fuel burn becomes negligible, expansion causes an exponential type decay in gas temperature with crank angle until the EVO at approximately 165°ATDC. This is the case in all but the first cycle for the $-20°C$ case, where temperature levels off at $900°C$ at 65°ATDC. This suggests that there is a second phase of low level combustion which is sufficient to negate

the cooling effects of expansion in this region. Heat release in this part of the stroke is very difficult to pick up due to larger signal to noise ratio and high volume change per crank angle, but as was pointed out before, it is possible to see that the $-20°C$ heat release rate trace is always above those at higher temperatures in Figure 5.23. Secondary ignition at low temperature could be caused by fuel impinging on the cold piston and puddling instead of vaporising during the initial combustion period. High post combustion charge temperature could cause accumulated fuel to evaporate and fumigate until sufficiently rich for secondary autoignition, as temperatures are still in the region of $900°C$ at $\approx 60°$ATDC. Temperature for the final cycle of the $-20°C$ case is also plotted in Figure 5.24, showing that this effect is no longer apparent after multiple firing cycles. This heat addition may cause surface temperatures to increase to those found in the warmer tests where there was no evidence of puddling or secondary ignition. This low rate combustion over the first few cycles may contribute to the reduction in IMEPg from first cycle-to-cycle 5–6 as discussed in section 5.3.1.

This section has shown that a reduction in test temperature increases the maximum IMEPg achievable with high fuelling due to increased oxygen availability and a reduction in the peak rate of heat release, allowing more time for thorough fuel air mixing in the diffusion burn and a longer, more complete burn. This is a favourable result as oil viscosity is highly temperature dependent, so increased work output at low temperature is desirable.

5.5 Varying Number of Injections

The effects of adding further injections is now studied to ascertain if any performance improvement can be obtained, and to identify the physical processes behind any effects encountered.

5.5.1 Pilot Injection

As detailed in the literature review, pilot injection is often employed in the cold start calibration to reduce ignition delay and misfire. A study conducted at The University by Brown et al. [76] found that a pilot injection improved the cold start as long as it was above the minimum fuel level deliverable by FIE and close coupled to the main injection. Based on these findings, a small pilot quantity of 2 mm^3/str injected 5° in advance of the main was used in this injection. Figure 5.25 gives $\overline{IMEP}g_5$ results for the single 60 mm^3/str injection sweep of timings in Figure 5.1 on page 61 compared to pilot plus main injection strategy. A reduced main quantity of 58 mm^3/str was injected at the same time as for the single main to maintain total fuelling.

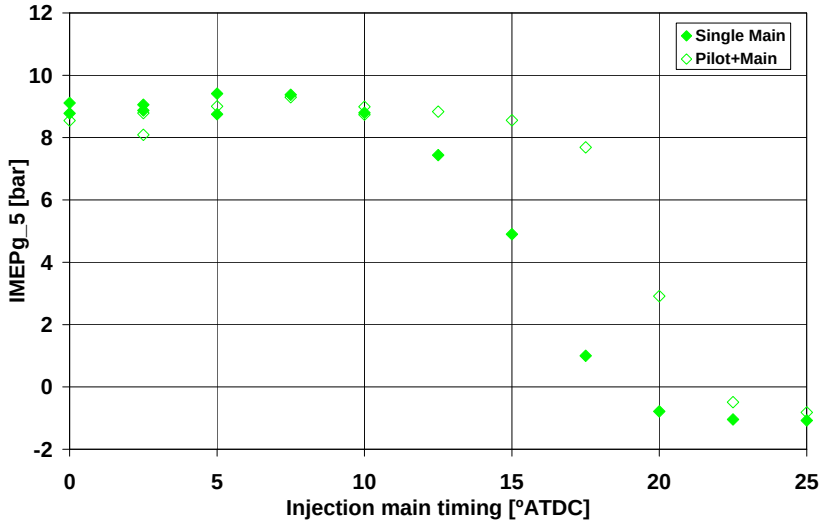

Figure 5.25: Effect of pilot injection on $\overline{IMEP}g_5$, 60 mm^3/str, 300 rpm, $-10°C$, HCR

No increase in peak $\overline{IMEP}g_5$ is apparent at this condition, but there is significant extension of the optimum region of operation. Reasonable $\overline{IMEP}g_5$ of 8 bar is achievable at timings as retarded as 17.5°ATDC where a single main injection experienced much misfire (only two out of five cycles with any significant combustion) and average IMEPg of only 1 bar. This is an important effect as it makes cold start less timing/speed sensitive. There is a rapid transient in a real engine from rest to 200+ rpm cranking speed, to 1000 rpm, ideally within a few cycles — the more robust to dynamic changes the calibration can be the better. The first cycle heat release profiles given in Figures 5.26 and 5.27 compare single and pilot+main

injection strategies at the optimum 5°ATDC and retarded 17.5°ATDC.

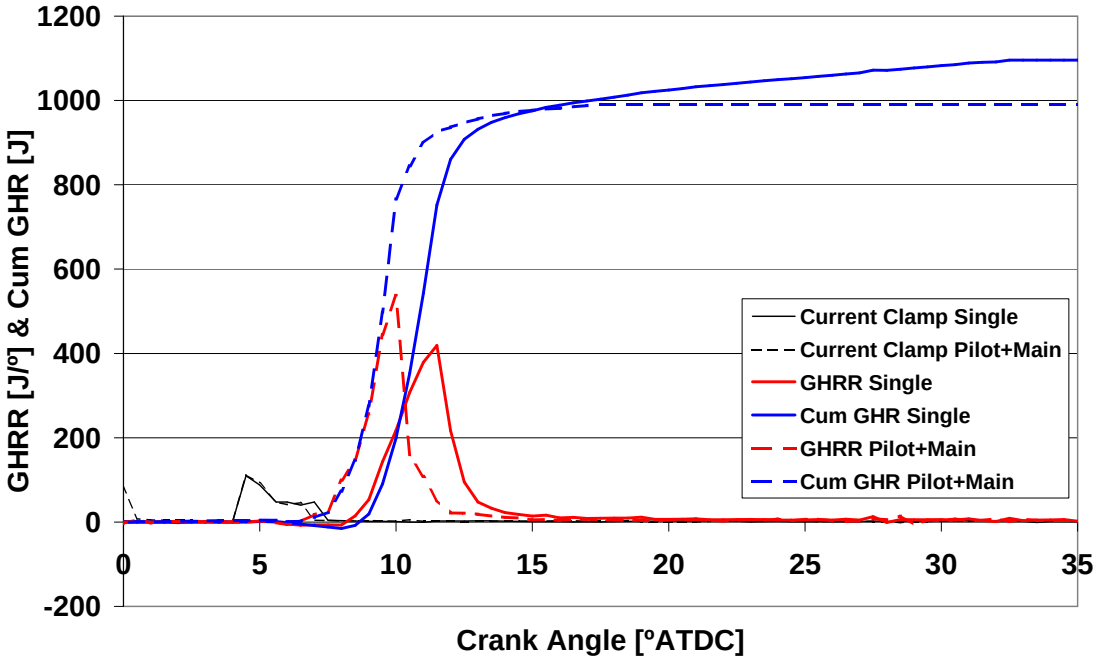

Figure 5.26: Effect of pilot injection on first cycle Gross Heat Release Rate and Cumulative Gross Heat Release, 60 mm^3/str main timing 5°ATDC, 300 rpm, $-10°C$, HCR

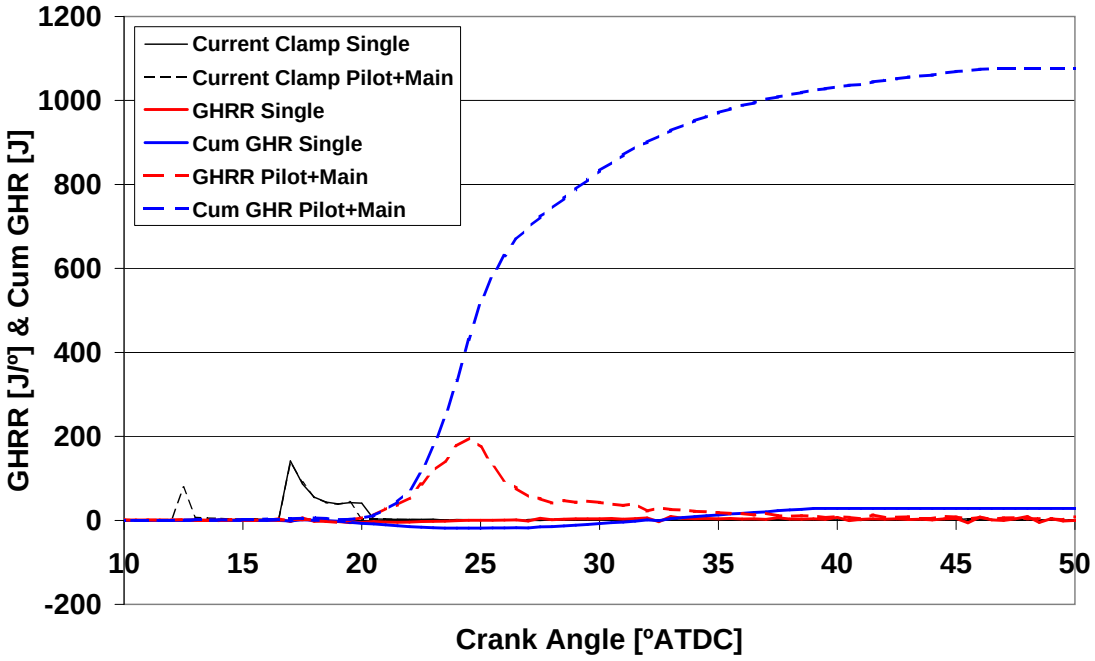

Figure 5.27: Effect of pilot injection on first cycle Gross Heat Release Rate and Cumulative Gross Heat Release, 60 mm^3/str main timing 17.5°ATDC, 300 rpm, $-10°C$, HCR

In the stable 5°ATDC case ignition delay is reduced by approximately 50% with the introduction of a pilot injection. There is no evidence of pilot ignition, which would be difficult to isolate using this low quantity at reduced temperatures on a single cycle basis. It is theorised in the literature [19, 56, 93] that this reduction in ignition delay is caused by cool flame reactions in the fumigated fuel/air mixture. An activated environment is created with some localised heat release and more readily combustible hydrocarbon species. This activated environment promotes ignition of the main injection. Evidence of pilot heat release is visible in Figure 5.28, where all fired cycle heat release data has been averaged and compared to the first and last cycle data.

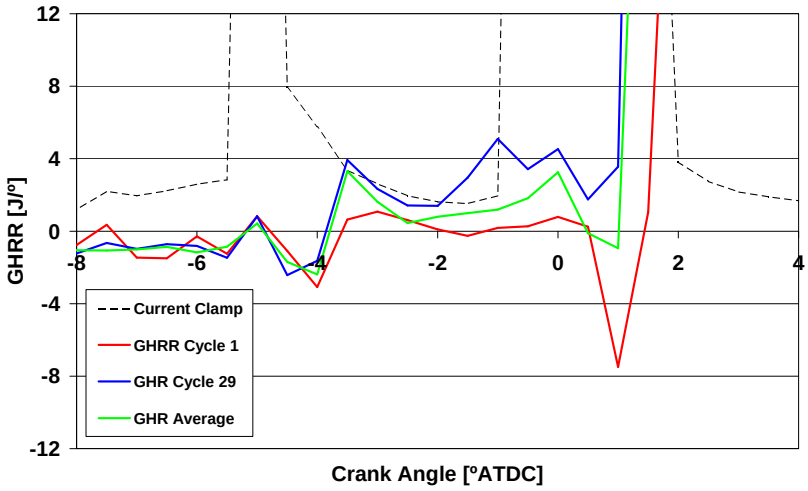

Figure 5.28: Average Gross Heat Release Rate analysis of pilot ignition, 60 mm^3/str main timing TDC, 300 rpm, $-10°C$, HCR

Low level increases in heat release rate before the main are visible, principally from contributions of the later cycles where temperatures have increased. This results in a slightly reduced main ignition delay. Referring back to Figure 5.26, the main combustion for the pilot injection case has a higher peak rate of heat release despite shorter ignition delay. This cannot be explained simply because of the slightly advanced combustion because the peak is above that for a single injection at 2.5°ATDC. This has an earlier start of combustion and is presented in Figure 5.29.

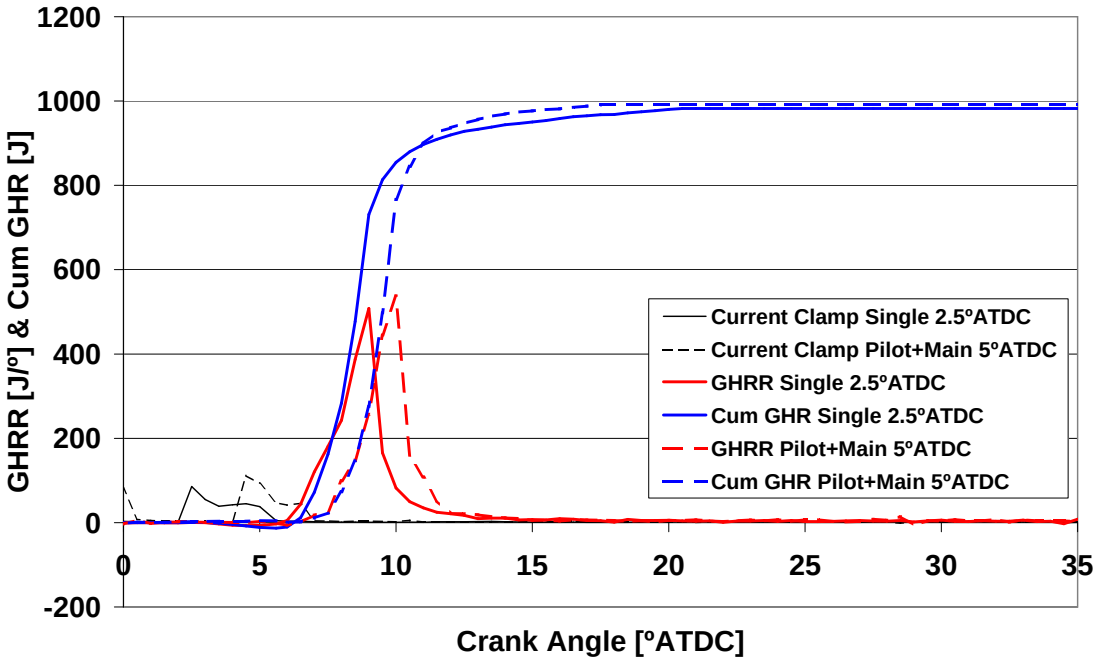

Figure 5.29: Greater first cycle peak Gross Heat Release Rate when utilising a pilot injection despite more retarded combustion and shorted ignition delay, 60 mm^3/str, 300 rpm, $-10°C$, HCR

The 50% reduction in ignition delay with a simultaniously increased premixed combustion spike implies that pilot injection at least doubles the rate of fuel preparation prior to main combustion initiation, despite there being no evidence of pilot combustion in the first cycle. This high rate of heat release leads to a swift termination of combustion at a marginally lower cumulative total to that using a single injection — effectively over advancing the combustion. Whilst improved mixture preparation and greater peak rate of heat release is detrimental close to TDC, it is highly beneficial for retarded injection as shown in Figure 5.27. At 17.5°ATDC, a single injection of 60 mm^3/str is liable to completely misfire. Introducing a pilot results in self sustaining combustion of the main peaking at 200 J/° and excellent cumulative heat release comparable to that with injection close to optimum timings in the region around TDC.

Pilot injection makes cold start less sensitive to injection timing with high fuelling, but there is no improvement in fuel burn or IMEPg obtained at optimum timings. A similar study was conducted using half the fuel at 30 mm^3/str for a broad sweep of timings between 25°BTDC and 25°ATDC. At this lean condition, small gains may be achieved at all sensible

timings by utilising a pilot injection as shown in Figure 5.30.

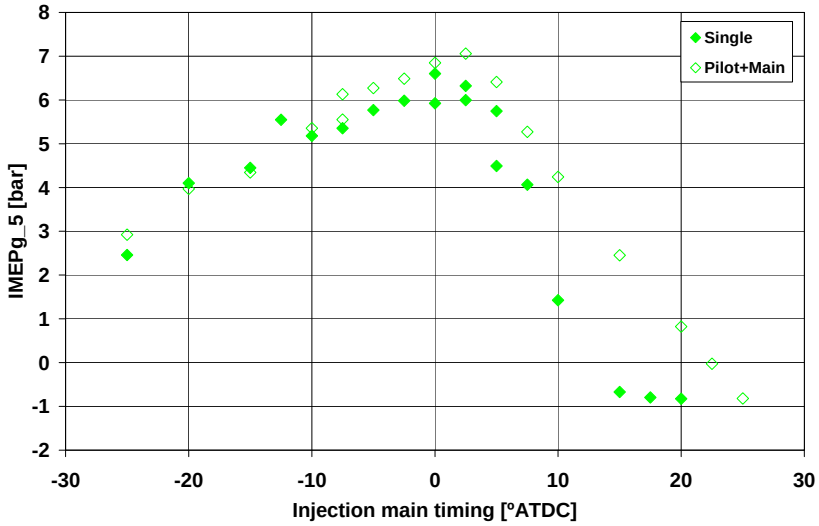

Figure 5.30: Effect of pilot injection on $\overline{IMEPg}_5$, 30 mm^3/str, 300 rpm, $-10°C$, HCR

The lean conditions add instability to the cold start, evident in test-to-test variations at the same timing around the peak at TDC. There is a rapid reduction in $\overline{IMEPg}_5$ after TDC at a greater rate than at 60 mm^3/str. Heat release analysis for advanced 10°BTDC, optimum 2.5°ATDC and retarded 10°ATDC are given in Figures 5.31, 5.32 and 5.33.

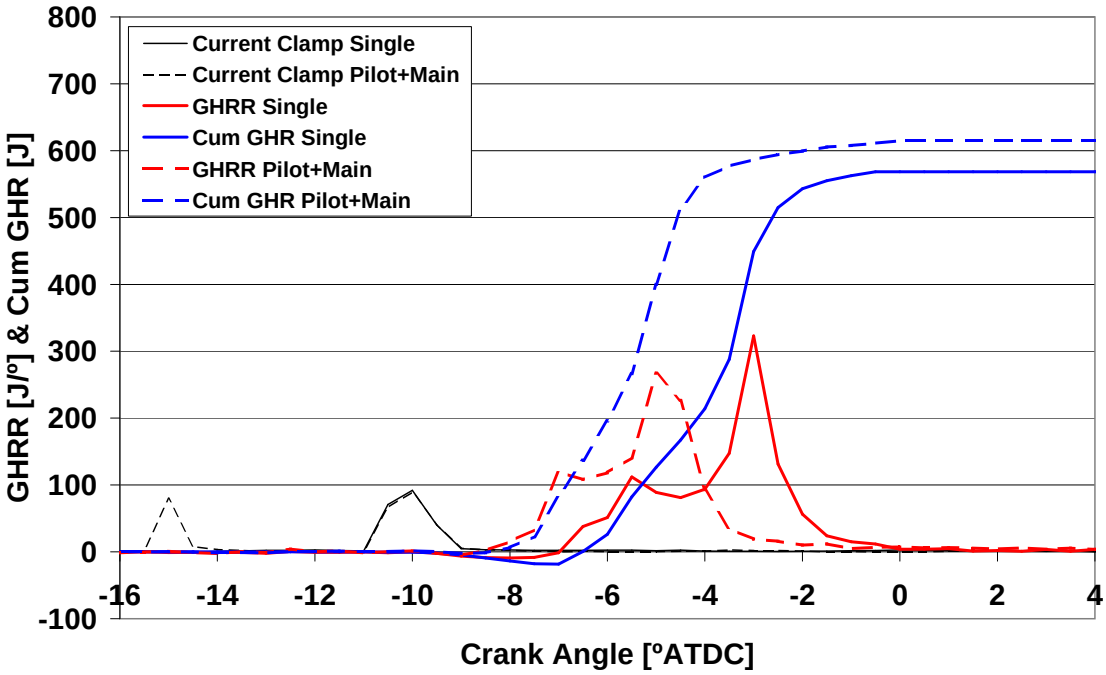

Figure 5.31: Effect of pilot injection on first cycle Gross Heat Release Rate and Cumulative Gross Heat Release, 30 mm^3/str main timing 10°BTDC, 300 rpm, $-10°C$, HCR

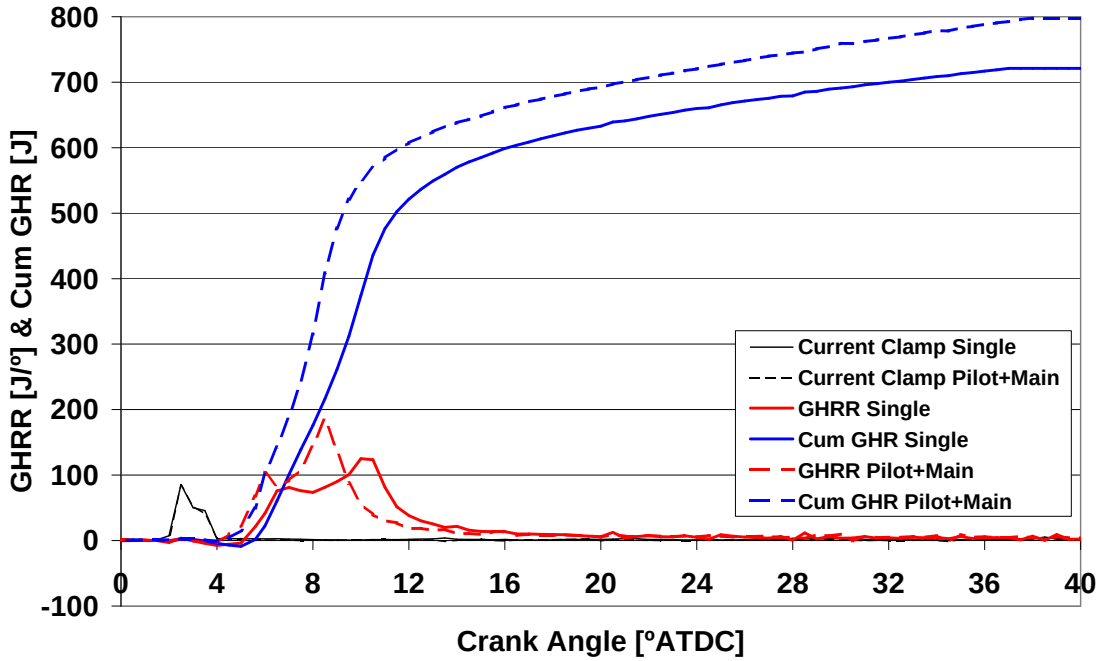

Figure 5.32: Effect of pilot injection on first cycle Gross Heat Release Rate and Cumulative Gross Heat Release, 30 mm^3/str main timing 2.5°ATDC, 300 rpm, $-10°C$, HCR

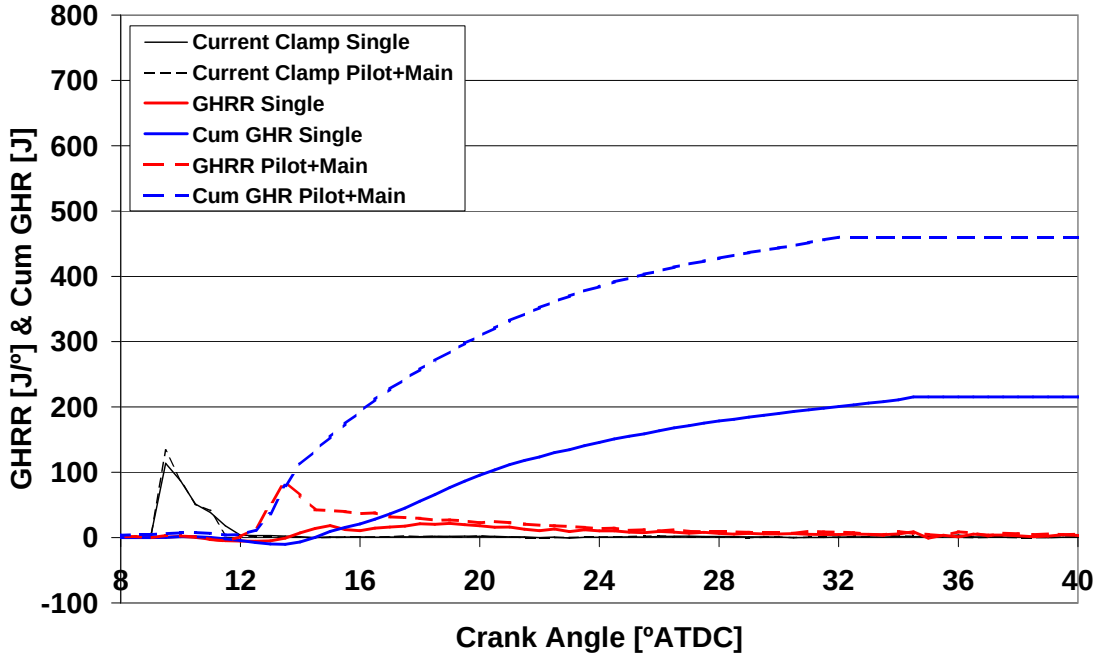

Figure 5.33: Effect of pilot injection on first cycle Gross Heat Release Rate and Cumulative Gross Heat Release, 30 mm^3/str main timing 10°ATDC, 300 rpm, $-10°C$, HCR

Cumulative burn is enhanced at all timings by pilot injection at low fuelling. Again there is a large reduction in ignition delay of the main. An increase in peak rate of heat release is observed in injections close to or in retard of TDC due to better fuel preparation, but peak rate is decreased before TDC, because the reduction in ignition delay advances combustion to a point with lower compression temperatures and pressures. Lean conditions result in poor performance in the retard, but pilot injection, along with the ability for advanced injection timing, frees up a 20° region where $\overline{IMEP}g_5 > 5$ bar is achievable. There is also a small peak $\overline{IMEP}g_5$ gain in the region of 0.5 bar close to TDC and a reduced rate of deterioration in the retard

5.5.2 Twin Pilot Injection

The use of multiple pilots has become possible due to advances in fuel injection equipment in recent years. To assess the impact of multiple pilot on cold start, a study was conducted whereby total fuelling was held constant at 60 mm^3/str, but 10 mm^3/str was split between two pilot injections. The pilot injections were varied between 2 mm^3/str and 8 mm^3/str with the inter-pilot separation varied between 5° and 20°. The second pilot was kept at a fixed 5° before the main. Results for a fixed main timing of 6°ATDC at $-20°C$ are presented in Figure 5.34. $\overline{IMEP}g_5$ results are given for four levels of pilot split (percentage of pilot fuel in first pilot) when holding the separation between pilots constant. For comparison, there are single injection results, still with fixed total quantity when utilising either a 2 or 10 mm^3/str pilot. In the 10° and 20° separation sub-figures the single pilot is injected at the same crank angle as the first of the twin pilots. In the 5° separation case the single pilot is injected at the same time as the second twin pilot because no single pilot data were collected with pilot timing 10° before the main.

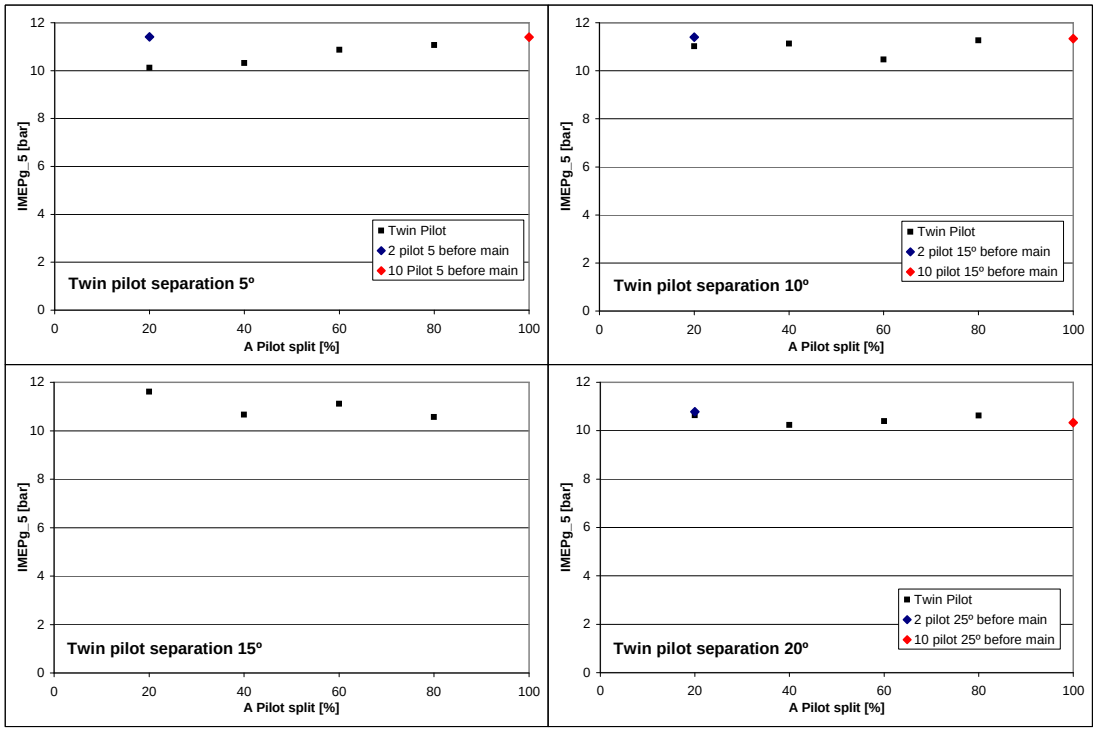

Figure 5.34: Effect of twin pilot fuel split on $\overline{IMEPg}_5$ at different pilot separations, 60 mm^3/str main timing 6°ATDC, 300 rpm, $-20°C$, HCR

There is no IMEPg advantage to using two pilot injections at this optimum main timing. The same or better $\overline{IMEPg}_5$ can be achieved with only one pilot regardless of when that pilot is injected. Twin pilot results suggest that if the two pilots are to be close spaced then the first pilot should be large. If the separation is large, the first pilot should be small. This, combined with the 20° pilot separation data, which shows reduced IMEPg, reinforces earlier studies showing that pilot injections should be close coupled. Average heat release rate results for a 5° pilot separation sweep of pilot splits are given in Figures 5.35 and 5.36. The averages are used because they are able to shed some light on what is happening to the pilots. For comparison, two single pilot examples are given for small and large pilot quantity.

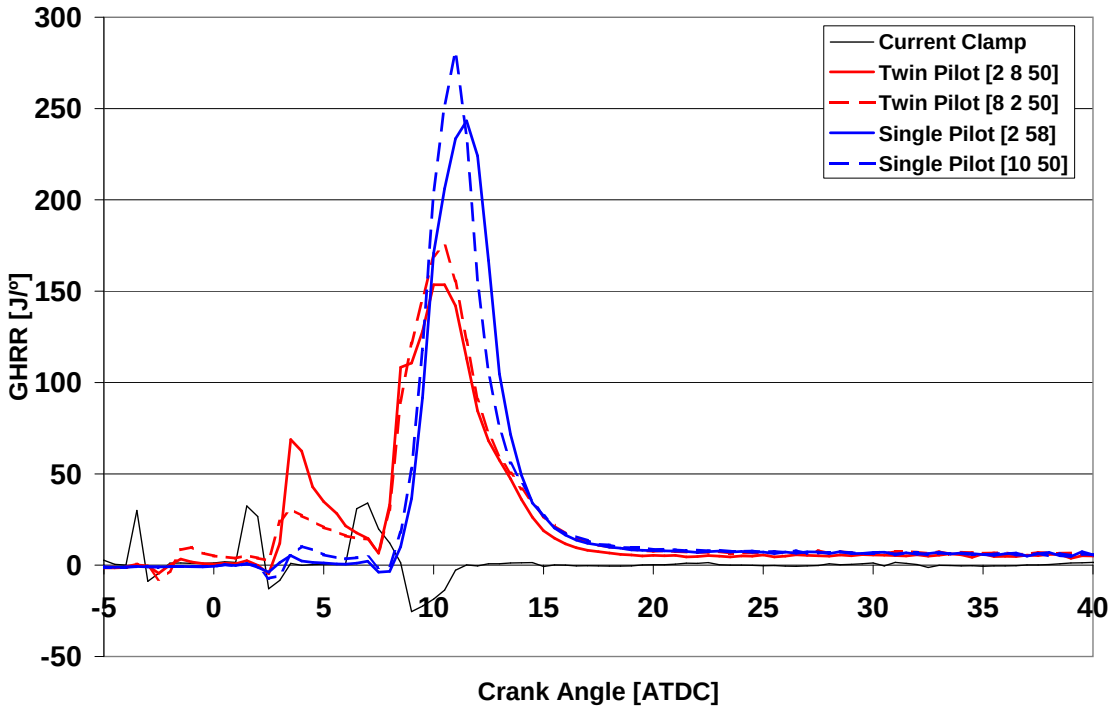

Figure 5.35: Effect of twin pilot fuel split on average cycle Gross Heat Release Rate at 5° pilot separation, 60 mm^3/str main timing 6°ATDC, 300 rpm, $-20°C$, HCR

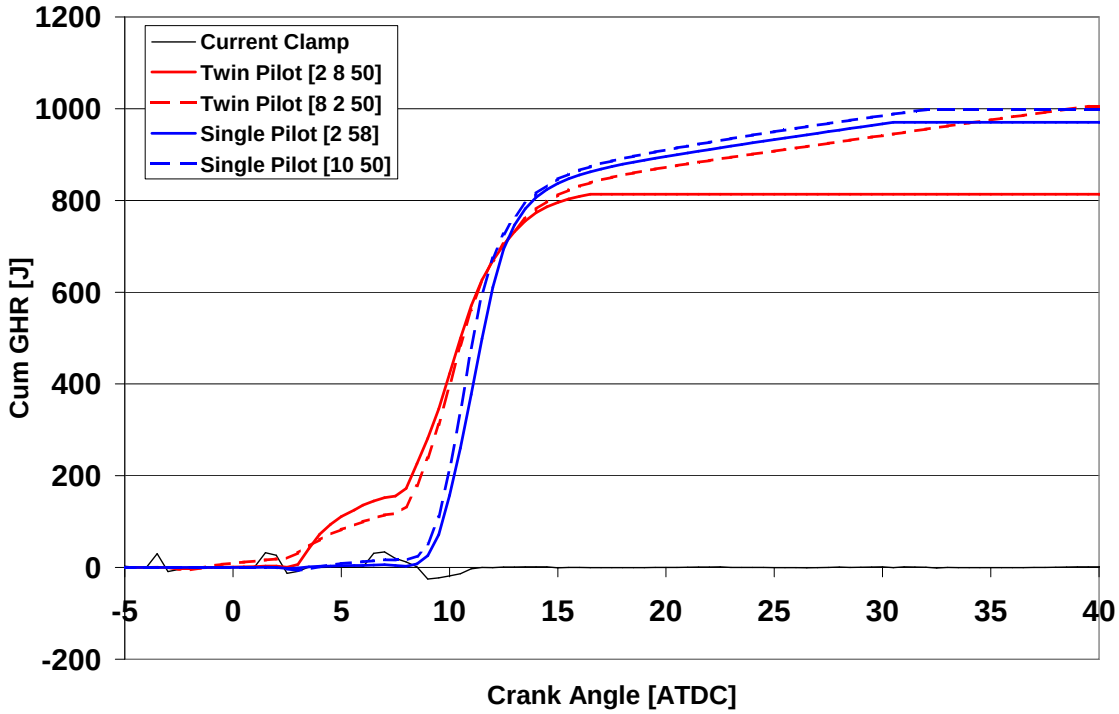

Figure 5.36: Effect of twin pilot fuel split on average cycle Cumulative Gross Heat Release at 5° pilot separation, 60 mm^3/str main timing 6°ATDC, 300 rpm, $-20°C$, HCR

For a small pilot separation, a large first pilot results in autoignition and relatively strong second pilot combustion considering the 2 mm^3/str quantity. The injection of more fuel close to TDC causes stronger heat release and more complete combustion of the initial pilot charge. There is then a long main combustion period extending to around 40°ATDC. In the small first pilot case, more of the pilot fuel is burnt before main injection, but this appears to be detrimental to combustion duration and overall combustion efficiency, resulting in nearly 200 J less heat release from the average cycle. Single pilot results show similar cumulative heat release to the large first pilot case which results in similar IMEPg. Heat release from the single pilot, even at 10 mm^3/str is very low comparative to twin pilots of the same size, again showing the importance of fumigating and cold flame reactions in later combustion. Single pilot has a longer ignition delay due to lower temperatures with the reduction in pilot heat release, but a stronger combustion, as the global equivalence ratio is higher when well mixed unburnt fuel is already present in the cylinder before main combustion. In this optimal main timing case, it appears that twin pilots are not beneficial because combustion phasing is already at the best trade-off between maximum fuel burn and conversion efficiency with minimum losses.

The data presented in Figure 5.37 compares twin pilot operation for identical main timing for two pilot quantity splits at a larger 15° pilot separation. In one case, the majority of fuel is in the first pilot, in the other case the majority of fuel is in the second pilot. IMEPg for the first five injected cycles is plotted in the insert.

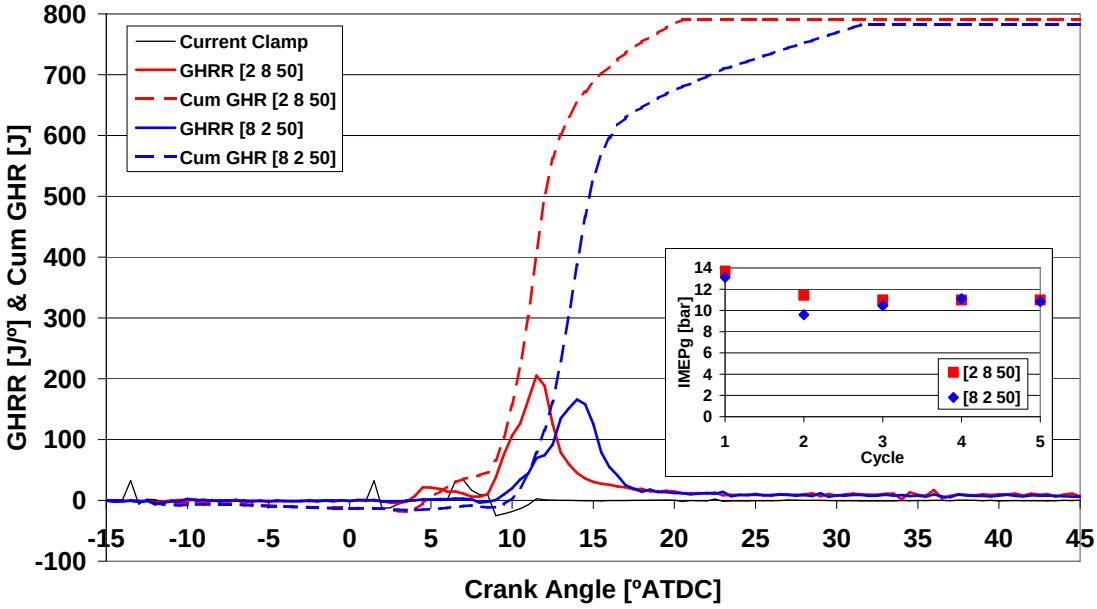

Figure 5.37: Effect of twin pilot fuel split on second cycle Gross Heat Release Rate and Cumulative Gross Heat Release at 15° pilot separation, 60 mm^3/str main timing 6°ATDC, 300 rpm, $-20°C$, HCR. Insert: First 5 cycle IMEPg comparison.

In this case the average IMEPg of all cycles is very similar, but there is a lower result in the first three cycles for the large first pilot. The worst performance drop is seen on the second cycle, so the heat release data are shown for this cycle to see why a large first pilot split is detrimental. As the first pilot is injected very early, it does not appear to burn, even at 8 mm^3/str. Therefore there is no rise in-cylinder temperature and pressure (a small drop will have occurred due to evaporation). When the second pilot is injected close to peak compression, the 2 mm^3/str quantity does not appear to be enough to cause autoignition and burn the initial pilot which should have fumigated throughout the chamber. The 8 mm^3/str however does combust with a short ignition delay and is still burning as the main is injected, resulting in well phased heat release. The other heat release profile has a much longer ignition delay. Whilst it appears to burn a similar amount of fuel, the lower rate of heat release at later phasing means the in-cylinder pressure during the power stroke is always lower and therefore thermal efficiency is reduced.

Early heat release and advanced main combustion are the key factor effects when utilising a twin pilot strategy close to optimum main injection timing. It is of interest to see if twin pilot could extend the region of useful engine operation as single pilot was found to do

against single main injection. Figure 5.38 repeats the previous sweep of varying pilot splits and separations for a retarded 16°ATDC main injection case. Data were not collected at this timing for single pilot injection, but the results from the earlier investigation covered in Figure 5.25 are plotted.

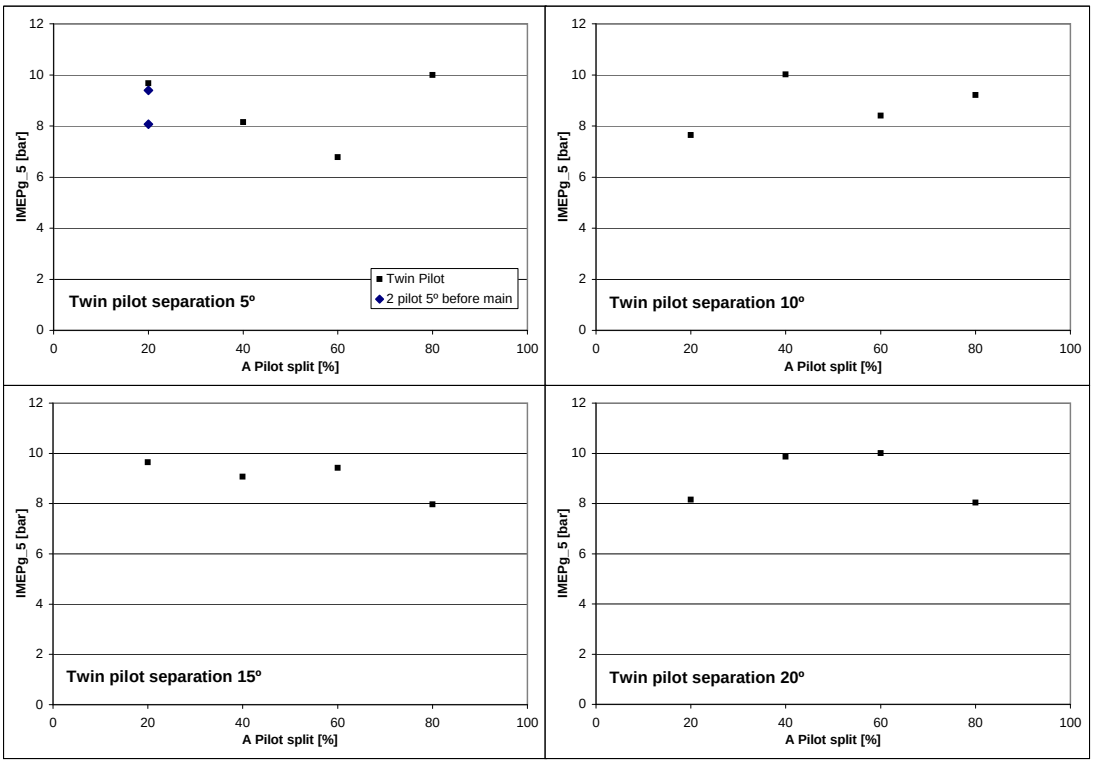

Figure 5.38: Effect of twin pilot fuel split on $\overline{IMEPg}_5$ at different pilot separations, 60 mm^3/str main timing 16°ATDC, 300 rpm, $-20°C$, HCR

The first point to highlight is that there is some reduction in IMEPg due to the combustion phasing, but there are no notable trends with pilot factors, indicating the increased variability at this timing. There is nothing to suggest that there are significant gains to be had from twin pilot operation — some results are higher, some lower with no discernible pattern. Figure 5.39 explains any advantage that a twin pilot may offer at these retarded timings when utilising twin pilot injections around TDC.

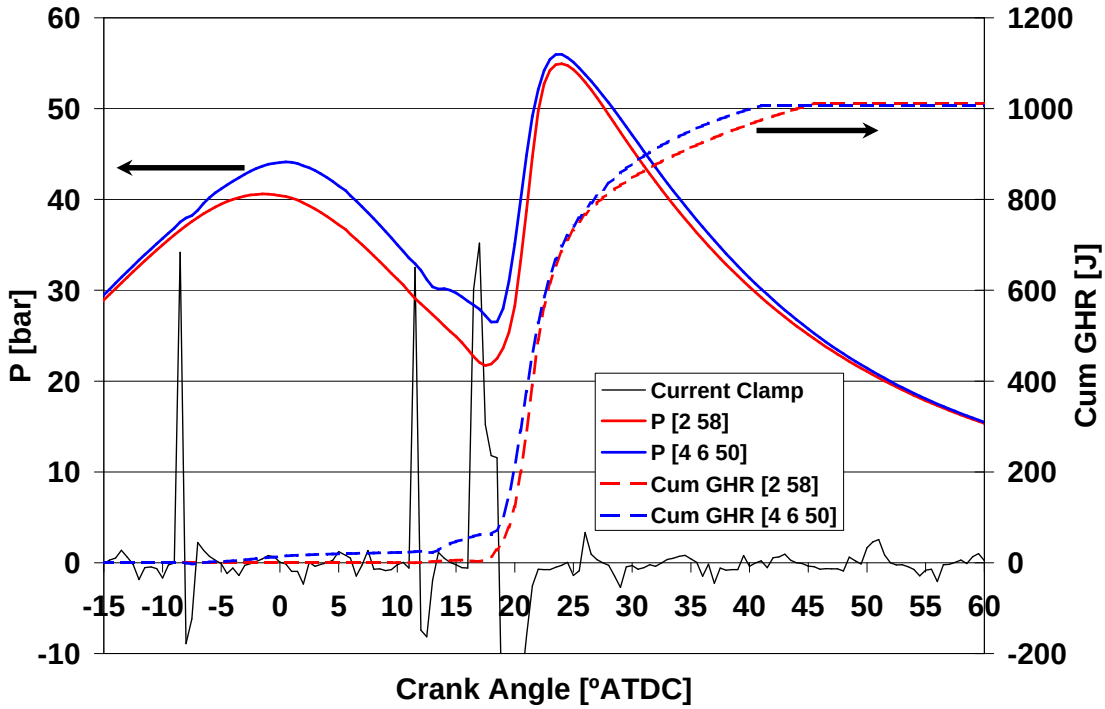

Figure 5.39: Effect of twin pilot fuel injection with large pilot separation for retarded main timing on average cycle Pressure and Cumulative Gross Heat Release, 60 mm^3/str main timing 16°ATDC, 300 rpm, $-20°C$, HCR

By considering the average pressure on the power stroke it can be seen that small heat release close to TDC results in a significant pressure rise before main injection. There is very little difference in total fuel burn as the pressure traces overlap again later in the stroke, but the small increase in IMEPg is a direct result of pilot combustion with significant injection before TDC. However, when the same pilot separations are maintained and main injection advanced, the pilots are no longer injected into good conditions for combustion and are not beneficial. Single pilot injection was found to expand the region of operation with little requirement for fine tuning, whereas twin pilot operation does not appear to offer any significant advantages. Modern FIE is sophisticated enough to accurately inject fuel for optimum phasing. Twin pilot injection cannot recoup lost thermal efficiency if fuel is injected in a retarded position — that can only be done by advancing main injection — in which case there is no need for twin pilot as single pilot is at least as good in a reasonably wide window.

Summarising, single pilot injection was found to increase the region where high work output

may be achieved by significantly increasing the rate of fuel preparation, reducing ignition delay by 50%. There was also a less steep reduction in work output at retarded timings. No further benefit was observed by adding a second pilot injection across a range of pilot to pilot separation or quantity split.

5.6 Varying Engine Speed

High IMEPg is possible at cold starts down to $-20°C$. This facilitates a swift acceleration to idle speed where the target is to hold speed against high initial friction and varying ancillary demands. As was noted in the literature review, there are concerns about difficulties encountered when developing a robust diesel cold idle strategy at greatly reduced temperatures. The addition of reduced compression temperatures associated with low compression ratio is likely to exacerbate the problem. The following section considers operational behaviour observed at high compression ratio for later comparison at low compression to characterise the differences. The effects of various injection strategies on operating performance are categorised and the mechanisms explained.

5.6.1 Importance of Pilot Injection at Cold Idle

Various tests were conducted with and without pilot injection at higher engine speed to assess the impact on cold idle performance. Pilot injection was found to be crucial to achieving any reliable combustion at increased engine speed. As an example of this, the cycle resolved IMEPg of 1000 rpm cold idle tests conducted at 10, 0, -10 and $-20°C$, both with and without pilot injection are plotted in Figure 5.40. Total fuel quantity was increased with decreasing test temperature to mimic higher target load from increased friction. In the single main case the entire quantity was injected at 1.5°BTDC. In the pilot+main case, 2 mm^3/str was removed from the main and injected 13° in advance.

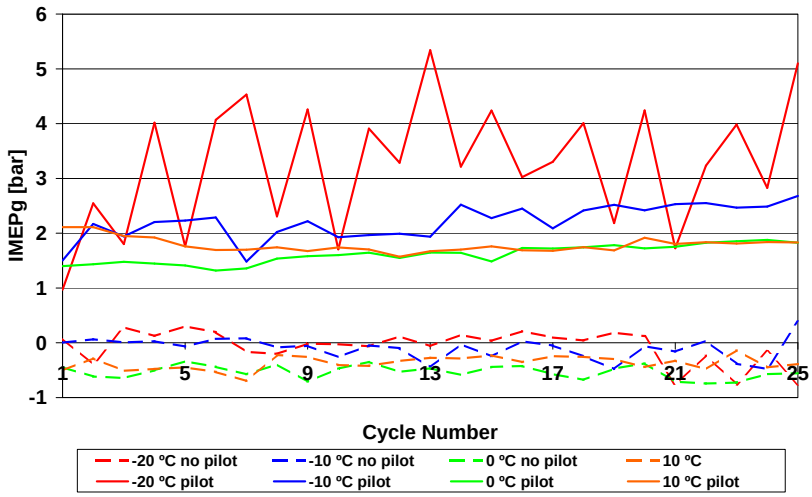

Figure 5.40: IMEPg effect of running with and without pilot injection at four test temperatures. Total fuel quantity constant for each test temperature at 8 mm^3/str for 10 and $0°C$, 10 mm^3/str at $-10°C$, 17 mm^3/str at $-20°C$, main timing 1.5°BTDC, 1000 rpm, HCR

Relatively stable output was found using a pilot injection at 0 and $10°C$. Some degradation was experienced at $-10°C$ and significant fluctuation occurred at $-20°C$. When no pilot was used, there was a dramatic reduction in IMEPg at all test temperatures. Gross heat release rate profiles are presented for the $-10°C$ case in Figure 5.41. Profiles are given for the best and worst IMEPg cycle as well as the average cycle, both with and without pilot injection.

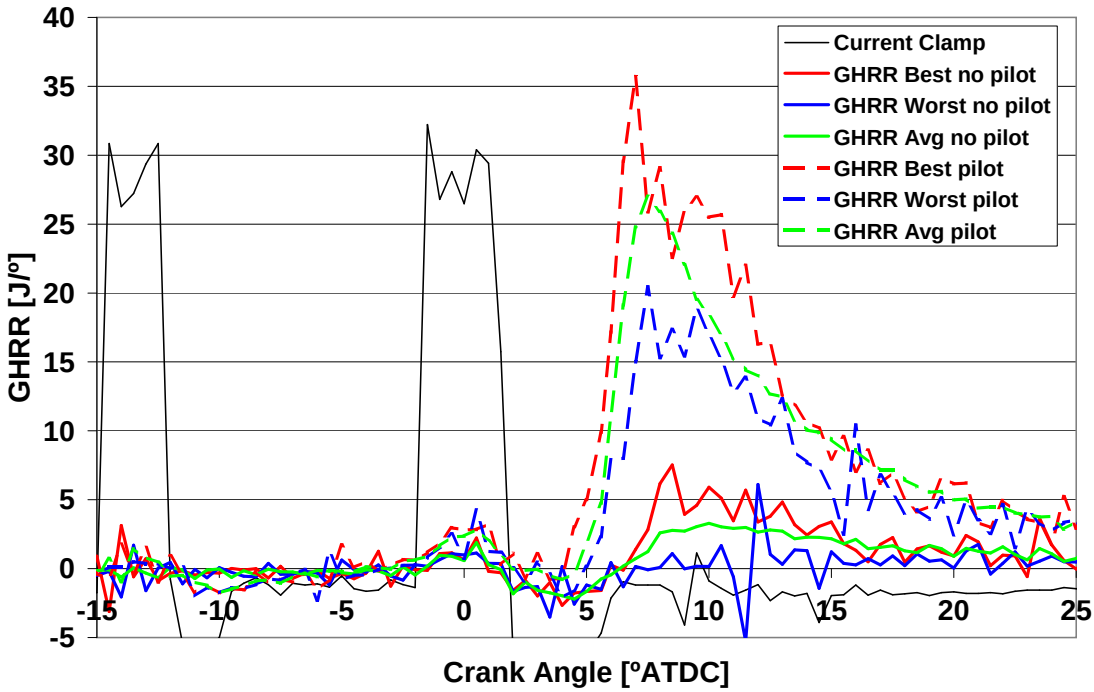

Figure 5.41: Effect of pilot addition on variations in Gross Heat Release Rate through a test, 10 mm^3/str main timing 1.5°BTDC, 1000 rpm, $-10°C$, HCR

Without pilot there was unstable low level combustion with a minimum of 8° ignition delay. Some cycles were very close to misfire, none exceeded maximum GHRR of 8 J/°. With pilot injection there was evidence of pilot ignition on best and average cycles with minor heat release rate increase close to TDC. The pilot reduced ignition delay by approximately 4°, increased peak rate of heat release above 35 J/° and promoted significant combustion for a duration of nearly 20°. Whilst there was still some variation, pilot addition is clearly crucial to cold idle operation.

5.6.2 Effect of Engine Speed on IMEPg

Cold idle speed is typically a little over 1000 rpm depending on temperature and load demands. The effects of varying engine speed in the range 600–1500 rpm on three key performance indices is illustrates in Figure 5.42. As detailed in Chapter 4, $\overline{IMEP}g_{10}$ is the average work output of the first ten injected cycles divided by swept volume. A 10 cycle average is used instead of 5 due to potential for large variability and as idle is closer to

steady-state than the rapid acceleration desired around cranking. The standard deviation of IMEPg ($\mathrm{StD_{IMEPg}}$) is calculated based on all fired cycles in bar and the coefficient of variation ($\mathrm{CoV_{IMEPg}}$) is given as the percentage value of the ratio $\mathrm{StD_{IMEPg}}/\overline{IMEPg}_{10}$. In these tests the main injection timing is held at 7.5°BTDC and three quantities are tested to compare different load cases. A 2 $\mathrm{mm^3}$/str pilot is injected with variable timing before the main to ensure there is always a 5° dwell time between pilot end of injection and main start of injection as injection duration extends in the crank domain with speed. If this separation is reduced there is insufficient dwell for full injector closure, and main injection quantity can deviate from the desired value. Tests were performed at the worst case $-20°C$ temperature.

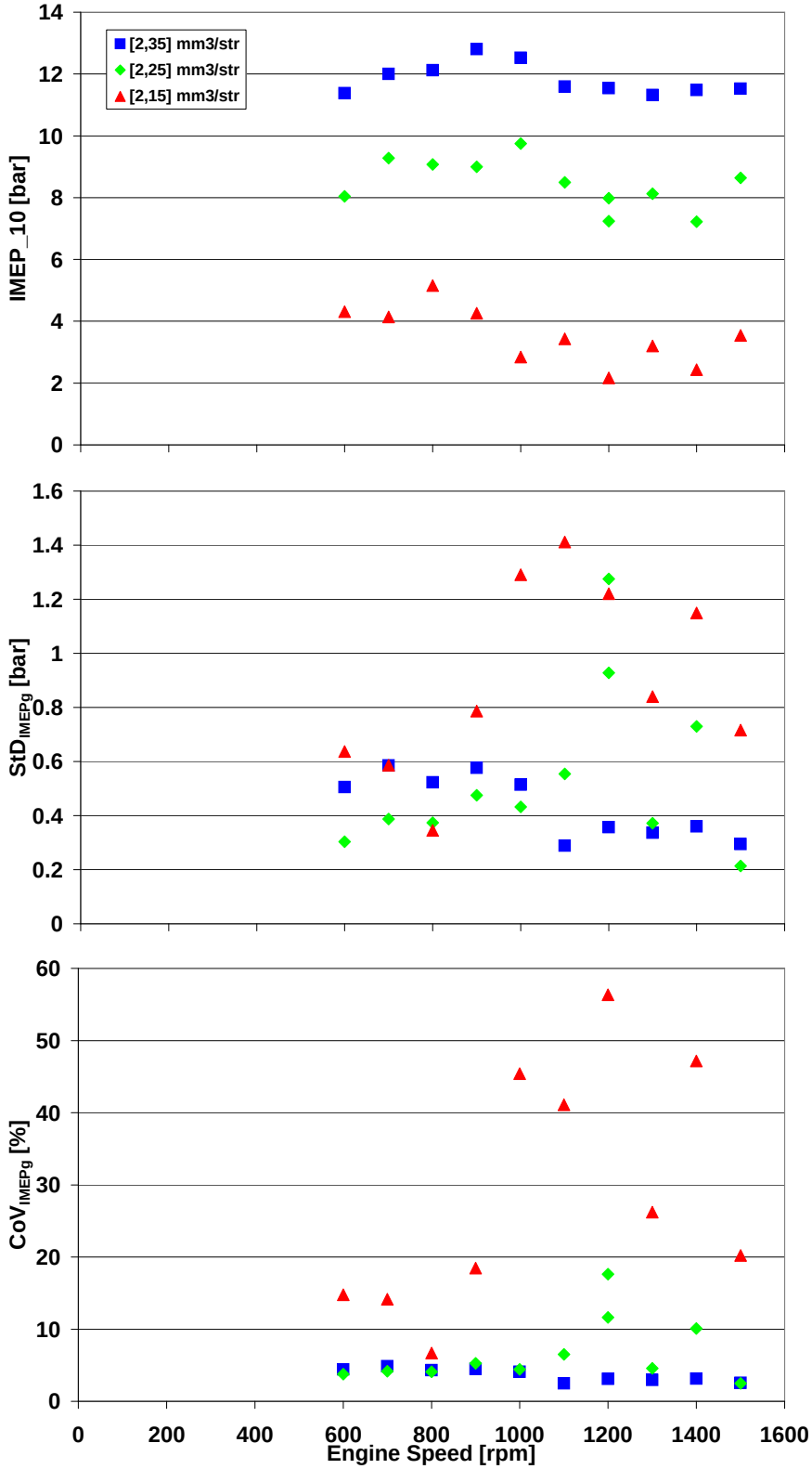

Figure 5.42: Effect of engine speed on idle performance (Average Indicated Mean Effective Pressure over first 10 injected cycles, Standard Deviation of IMEPg over 25 cycles and Coefficient of Variation of IMEPg over 25 cycles), main timing 7.5°BTDC, $-20°C$, HCR

IMEPg results show that for a given fuelling, engine speed has a small, non-linear impact on work output. It appears that there is an initial increasing period from around 600–900 rpm, followed by a gradual reduction towards the higher speeds. Figures 5.43 and 5.44 shown on the following page plot heat release data for the same set of tests, one in the crank angle domain, one in the time domain. They are presented together to aid comparison. First cycle gross heat release rate and cumulative heat release for four engine speeds in the range 600–1500 rpm are presented in Figure 5.43. Ignition delay lengthens in the crank domain with engine speed as would be expected and, in general, premixed combustion and rate of heat release diminishes. Considered in the time domain in Figure 5.44, maximum rate of heat release in terms of Watts actually increases with engine speed, at least up to 1200 rpm. This, in conjunction with reduced absolute ignition delay, suggests that higher temperatures and pressures due to lower time for loss promote better fuel preparation and swifter combustion. Interestingly the increase in IMEPg between 600 and 900 rpm can be explained by greater fuel burn, but 1200 rpm burns the same amount as 900 with a significantly lower IMEPg. 1500 rpm burns more again for a similar $\overline{IMEPg}_{10}$ at 1200 rpm. To explain the underlying causes for this trend, indicateed combustion (n_c), thermal (n_t) and fuel conversion (n_f) efficiencies are plotted for all speeds at this fuelling in Figure 5.45. Maximum pressure on the final motored cycle is also plotted.

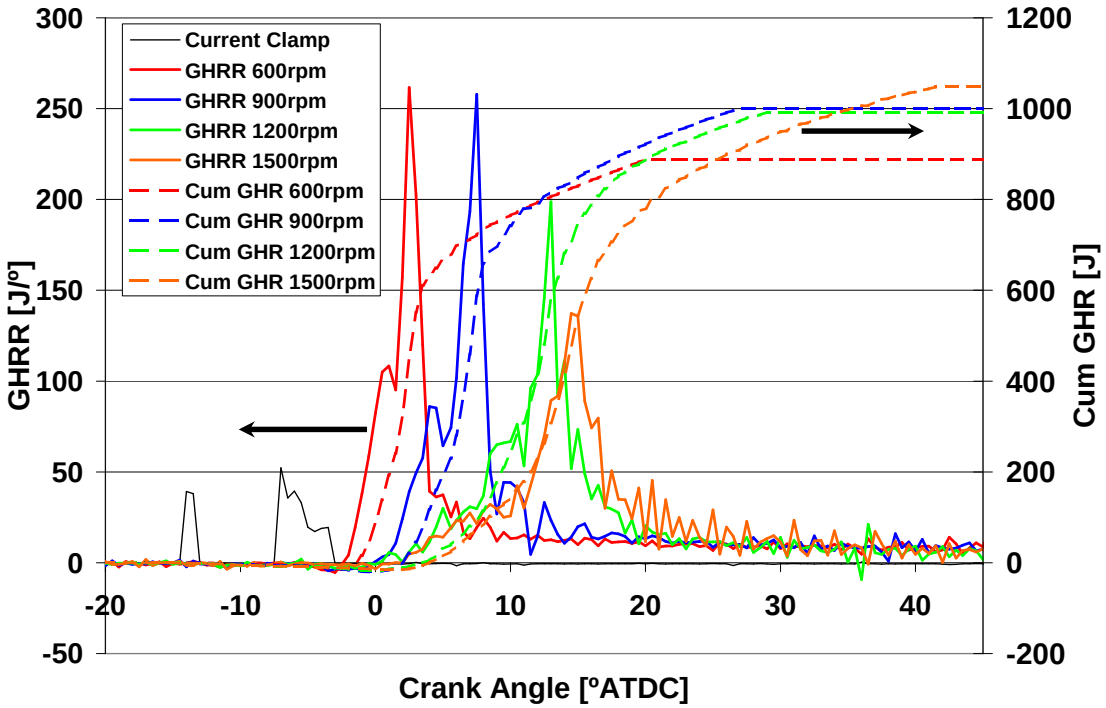

Figure 5.43: Effect of engine speed on first cycle Gross Heat Release Rate and Cumulative Gross Heat Release, [2,35] mm^3/str main timing 7.5°BTDC, $-20°C$, HCR

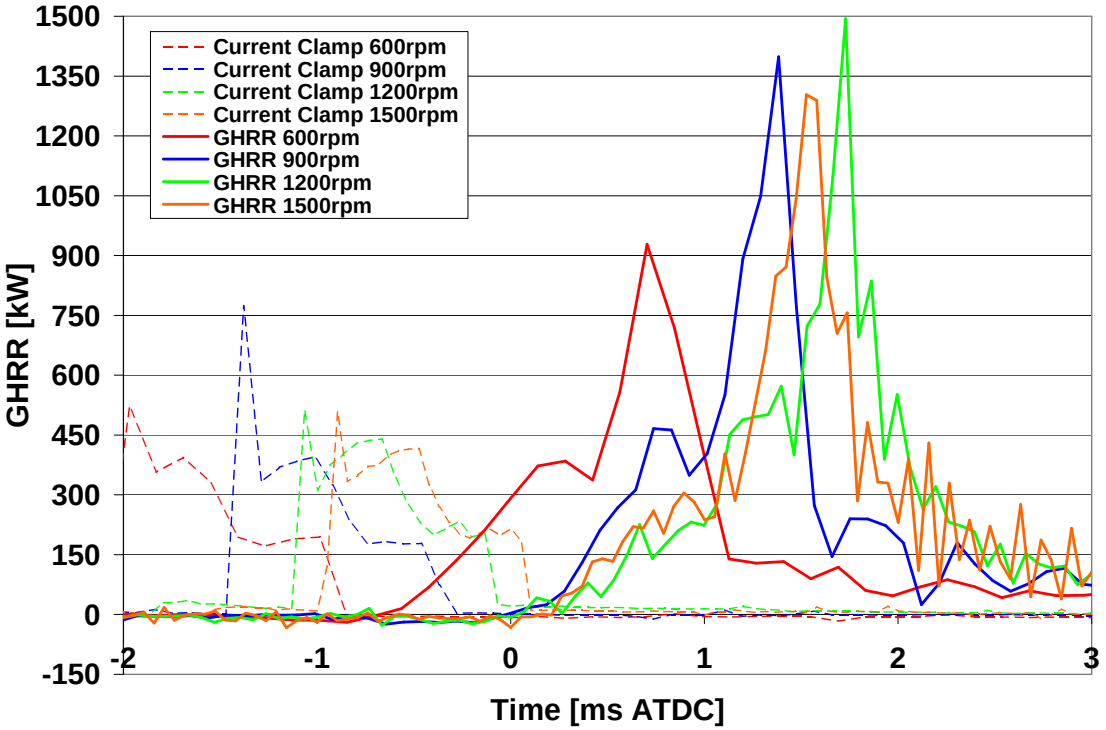

Figure 5.44: Figure 5.43 expressed in the time domain with kW GHRR against ms after TDC, [2,35] mm^3/str main timing 7.5°BTDC, $-20°C$, HCR

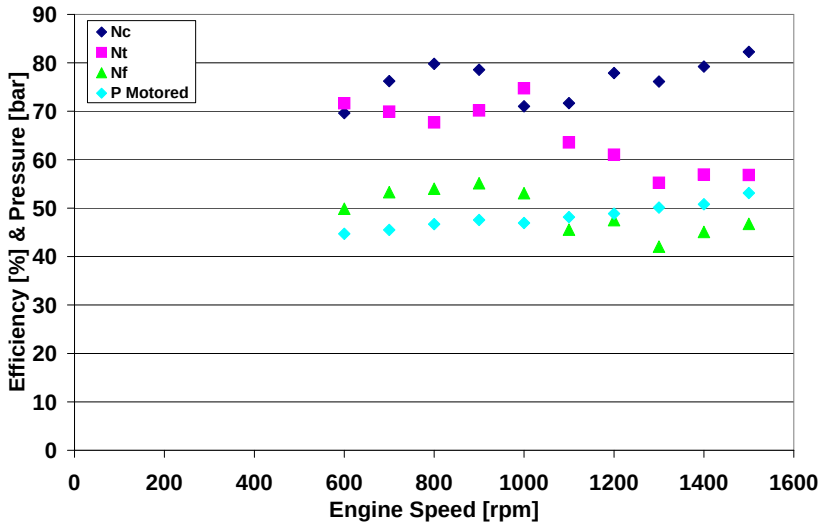

Figure 5.45: Effect of engine speed on first cycle indicated combustion, thermal and fuel conversion efficiencies and final motored cycle peak pressure, [2,35] mm^3/str main timing 7.5°BTDC, $-20°C$, HCR

Up to approximately 1000 rpm the dominant factor in total fuel conversion efficiency is increasing fuel burn with speed. After this point the thermal conversion efficiency drops off markedly which reduces overall efficiency despite the generally increasing trend for combustion efficiency. There is a good link between combustion efficiency and peak cylinder pressure in the final motored cycle for the higher speeds. This increases with engine speed due to lower losses, both to blowby and heat transfer, apart from in the 1000 rpm region where there is likely a form of flip point caused by variations in the way the ring pack is dynamically sealing the combustion chamber. The increase in pressure leads to greater temperature rise, and therefore better fuel preparation allowing greater fuel burn up to around $\approx 82\%$ at 1500 rpm. Values greater than 99% are targeted for fully warm operation [23, 87], but this is a reasonable figure considering the cold conditions.

Referring back to Figure 5.42, there is a non-linear reduction in $\overline{IMEP}g_{10}$ with variations in fuelling. There is a larger reduction when decreasing main injection from 25 to 15 mm^3/str than 35 to 25 mm^3/str. Heat release analysis is presented for the medium 900 rpm case in Figure 5.46. Table 5.2 details the various conversion efficiencies at the three fuellings.

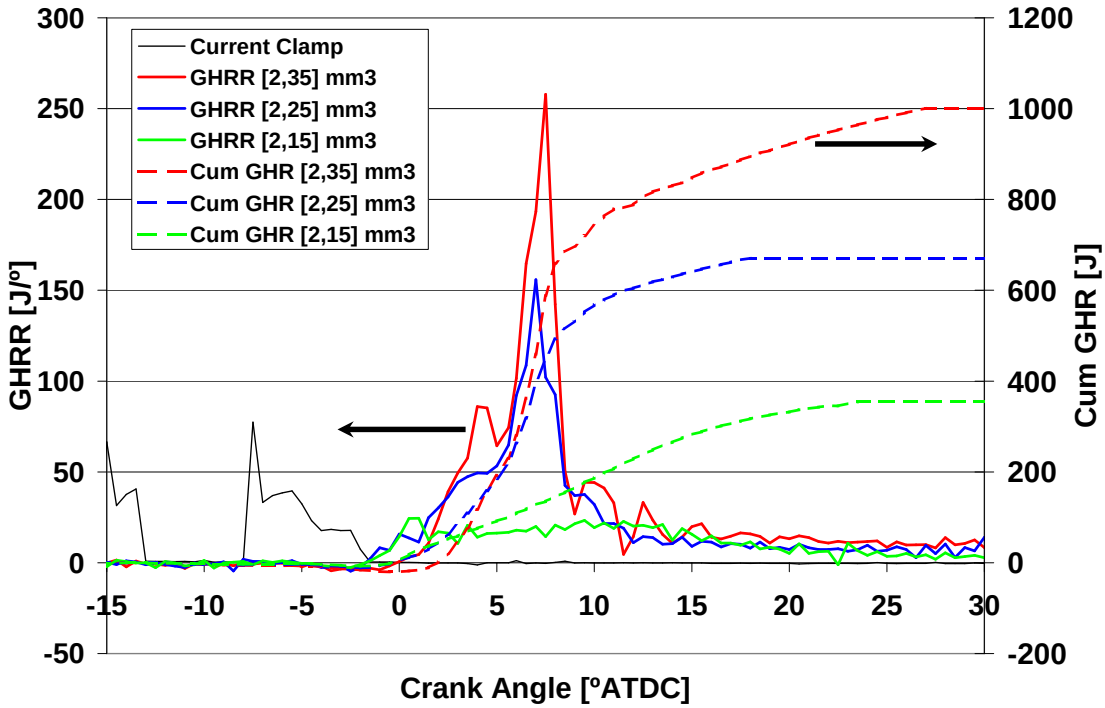

Figure 5.46: Effect of fuel quantity on first cycle Gross Heat Release Rate and Cumulative Gross Heat Release, main timing 7.5°BTDC, 900 rpm, $-20°C$, HCR

Fuelling [mm^3/str]	$\mathbf{n}_c$ [%]	$\mathbf{n}_t$ [%]	$\mathbf{n}_f$ [%]
37	78.6	70.2	55.1
27	72.2	76.5	55.2
17	60.5	61.3	37.1

Table 5.2: Combustion, Thermal and Fuel Conversion efficiencies of cold idle when varying total fuelling, main timing 7.5°BTDC, 900 rpm, $-20°C$, HCR

The information presented in both the above figure and table makes it clear that the low fuelling both burns substantially less fuel relative to the total quantity supplied and utilises this fuel less well. The low fuel quantity results in a lean mixture and very low rates of heat release throughout the combustion process which never gets above 25 J/°, unlike the others, with distinct peaks at 156 and 258 J/°. These low rates lead to combustion termination by the time 60% of the fuel has been burnt. The lack of high heat release close to TDC and long burn reduce thermal efficiency. This is further skewed by the fact that some of the heat release must be used to counter losses (0.3–0.5 bar motored) before contributing to positive IMEPg. Increased fuelling leads to higher peak rates of heat release which further benefit fuel preparation and diffusion burn. Higher peak heat release rate and accompanying

cylinder pressure found for the 37 mm^3/str case likely increased losses which resulted in the slightly reduced thermal conversion efficency.

5.6.3 Effect of Engine Speed on Coefficient of Variation of IMEPg

Work output must be maintained with a minimum deviation to maintain stable idle speed with no surging, misfire or other effects which would be detrimental to consumer perception. As described in Chapter 4, standard deviation of IMEPg is used as a measure of idle stability. The ratio of this to the IMEPg produced is the Coefficient of Variation and under fully warm operating conditions this would be expected to be below 2–3% [78–80]. Some deterioration of this is inevitable, and would be acceptable to consumers in cold climates. For the purposes of this investigation, $\mathrm{CoV_{IMEPg}} < 10\%$ is targeted as acceptable, with 5% being desirable. Shayler et al. [53] found that for a sump oil temperature of $-20°C$ engine friction plus ancillary demand was between 4.5 and 6 bar FMEP when comparing four different engines at 1000 rpm, a typical cold idle speed. This falls midway between $\overline{IMEPg}_{10}$ found when comparing the results with a main quantity of 15 and 25 mm^3/str. The low fuel quantity is a particularly poor test whereas the medium quantity has a high IMEPg and stability result. To assess the effects of speed on stability, the following two figures, 5.47 and 5.48 plot the heat release rates of the best and worst IMEPg cycles, as well as the average cycle, at 600 rpm and 1000 rpm for each fuelling.

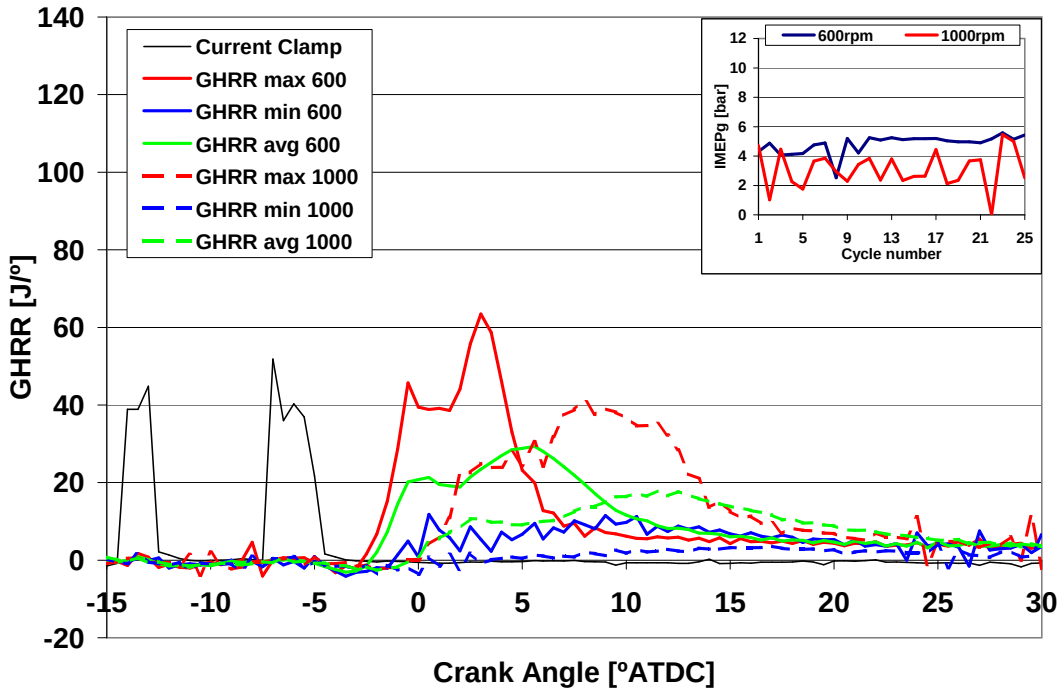

Figure 5.47: Effect of engine speed on variations in Gross Heat Release Rate through a test, [2,15] mm^3/str main timing 7.5°BTDC, $-20°C$, HCR. CoV_{IMEPg} 600 rpm=14.8% CoV_{IMEPg} 1000 rpm=45.4%. Insert: IMEPg

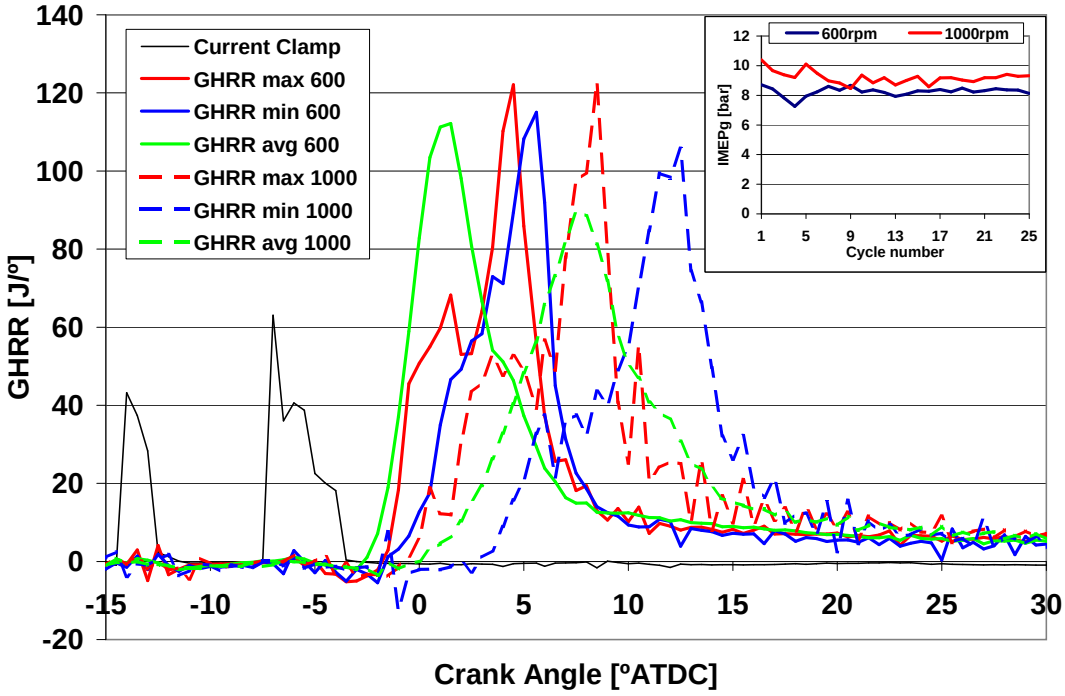

Figure 5.48: Effect of engine speed on variations in Gross Heat Release Rate through a test, [2,25] mm^3/str main timing 7.5°BTDC, $-20°C$, HCR. CoV_{IMEPg} 600 rpm=3.8% CoV_{IMEPg} 1000 rpm=4.4%. Insert: IMEPg

In the low fuelling case (Figure 5.47) there is instability and very low rates of heat release, even at low speed. There are large differences between maximum, minimum and average heat release rates. When speed is increased the ignition delay extends in the crank angle domain, heat release rates are even more variable, down to very near misfire. The general pattern of the maximum IMEPg cycle heat release is similar in both cases taking into account higher engine speed and therefore resulting in lower GHRR in the crank domain. This results in nearly equal cumulative heat release and IMEPg for this cycle. On average, however, there is insufficient combustion intensity for comparable performance. Average combustion efficiency for both speeds is 49%, but there is poor thermal efficiency of 54% at high speed compared to 84% at 600 rpm.

In the 27 mm^3/str fuelling case (Figure 5.48) it can be seen that engine speed has comparably little overall effect on combustion, even though ignition delay and therefore phasing is different. Peak heat release rates are similar for all cycles in both tests and average heat release rate traces are comparable to best in both cases. The high speed case results in longer combustion duration in the crank domain, but as the GHRR is similar, there is actually a greater combustion efficiency (81 vs. 73% average) for similar thermal efficiency (61 vs. 60%). It appears that at high fuelling, the increased temperatures caused by high engine speed enable a greater proportion of fuel to be suitably prepared for combustion whilst maintaining thermal efficiency. At low fuelling, combustion is optimally phased at 600 rpm, and the additional compression temperature at high speed is insufficient to promote high rates of heat release required for reasonable self sustaining combustion after the extended ignition delay.

As phasing is crucial for stable combustion, a sweep of injection timings was performed to ascertain if desirable stability could be achieved by modifying start of combustion with start of injection. The results are given in Figure 5.49.

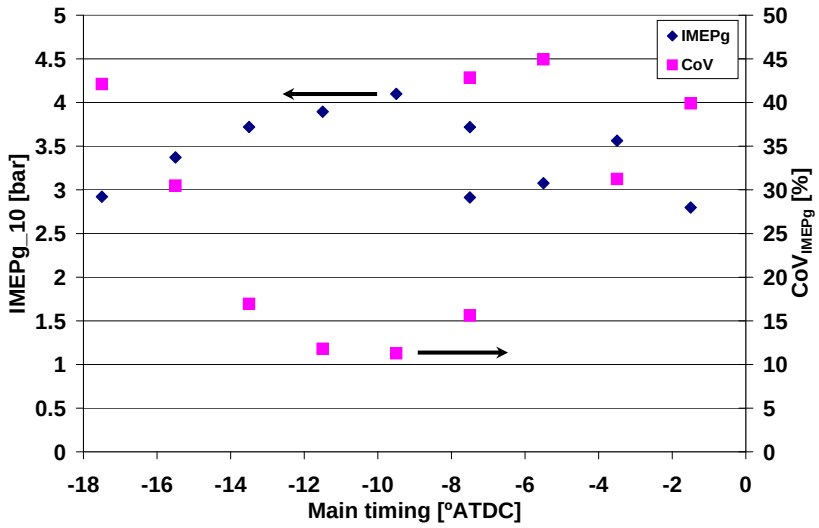

Figure 5.49: Effect of injection timing on $\overline{IMEPg}_{10}$ and $\mathrm{CoV}_{\mathrm{IMEPg}}$, [2,15] mm^3/str, 1000 rpm, $-20°C$, HCR

Initially, a high stability result was found at the previous timing of $\approx$ 8°BTDC with $\mathrm{CoV}_{\mathrm{IMEPg}}$ improving from $\approx$ 40% to $\approx$ 15%. A repeat test resulted in a return to the old stability as graphed. When comparing all three tests at this condition, the average heat release profiles are very similar as depicted in Figure 5.50. The test is on the borderline of stability where minor variations in external factors may have an influence, or one poor cycle is likely to lead to poor performance of subsequent cycles. The insert shows similar deviations in IMEPg for repeats 1 and 3 with a much more stable result for 2.

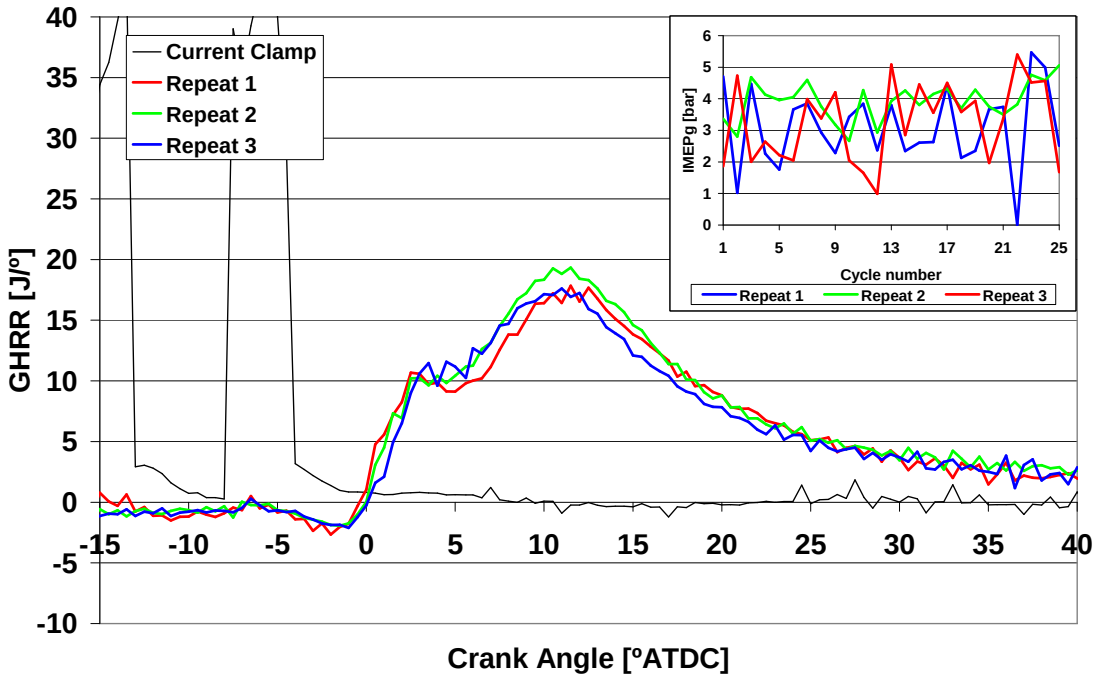

Figure 5.50: Three repeats of a point showing poor test-to-test repeatability of unstable tests despite similar average Gross Heat Release Rate, [2,15] mm^3/str main timing 7.5°BTDC, $-20°C$, HCR. Insert: IMEPg

Analysing Figure 5.49 further, it is clear that the optimal timing in terms of both IMEPg and CoV_{IMEPg} is between around 14°BTDC and 8°BTDC. Outside of these timings there is increased variation and corresponding drop in average $\overline{IMEPg}_{10}$. Figure 5.51 compares optimum heat release with advanced and retarded injection timing heat release averages which result in similar poor performance to see how they differ. For the average cycle, the early injection has poor fuel burn but good thermal efficiency compared to the reverse for the retarded timing. The optimum timing has far superior combustion efficiency mated to good thermal efficiency.

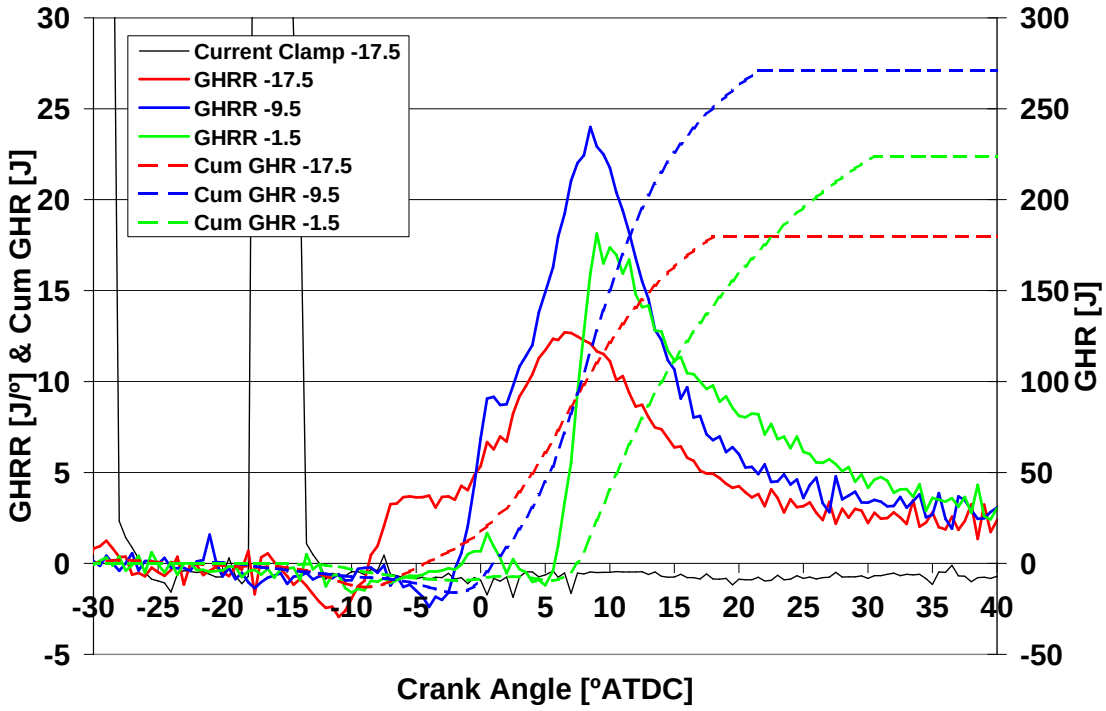

Figure 5.51: Effect of injection timing on average cycle Gross Heat Release Rate and Cumulative Gross Heat Release, [2,15] mm^3/str, 1000 rpm, $-20°C$, HCR. $\text{CoV}_{\text{IMEPg}}$ $-17.5°$=42.1% $\text{CoV}_{\text{IMEPg}}$ $-9.5°$=11.3% $\text{CoV}_{\text{IMEPg}}$ $-1.5°$=39.9%

To summarise the findings at increased engine speed so far — pilot injection has been found to be crucial to achieve some reasonable level of idle combustion stability at cold temperatures, but cycle-to-cycle stability is poor with pilot at the required IMEPg for $-20°C$. There is a very narrow range of injection timings for a given speed where good combustion phasing with reasonable combustion efficiency allows the appropriate work output with $\text{CoV}_{\text{IMEPg}}$ approaching the desired $< 10\%$.

5.6.4 Effect of Multiple Injection on Cold Idle

The utility of a second, further advanced pilot injection at cold idle was investigated by repeating the timing sweep performed previously at 1000 rpm. Total fuel quantity was kept at 17 mm^3/str, but 2 mm^3/str was removed from the 15 mm^3/str main and injected 8° in advance of the original pilot. $\overline{IMEPg}_{10}$ and stability results are presented in Figure 5.52.

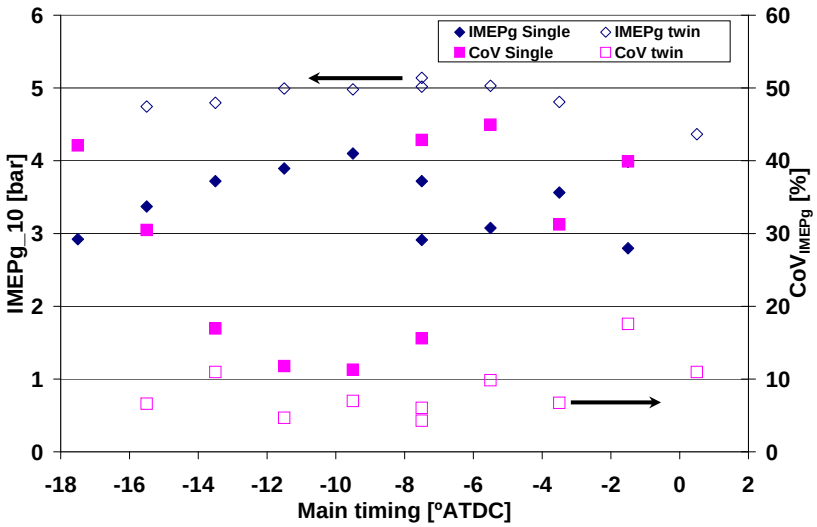

Figure 5.52: Benefit of twin pilot operation on cold idle indicated mean effective pressure and combustion stability, [2,15] mm^3/str vs. [2,2,13] mm^3/str, 1000 rpm, $-20°C$, HCR

The extra pilot increases average IMEPg whilst reducing CoV_{IMEPg} to acceptable levels across much of the timing sweep, with a shallower drop-off in performance. This result was not found at 300 rpm cold start speeds, therefore a different mechanism must be in operation in these lean, higher speed tests. Figure 5.53 compares best, worst and average GHRR, then cumulative GHR for the best case single pilot at 9.5°BTDC against the same main timing utilising twin pilot.

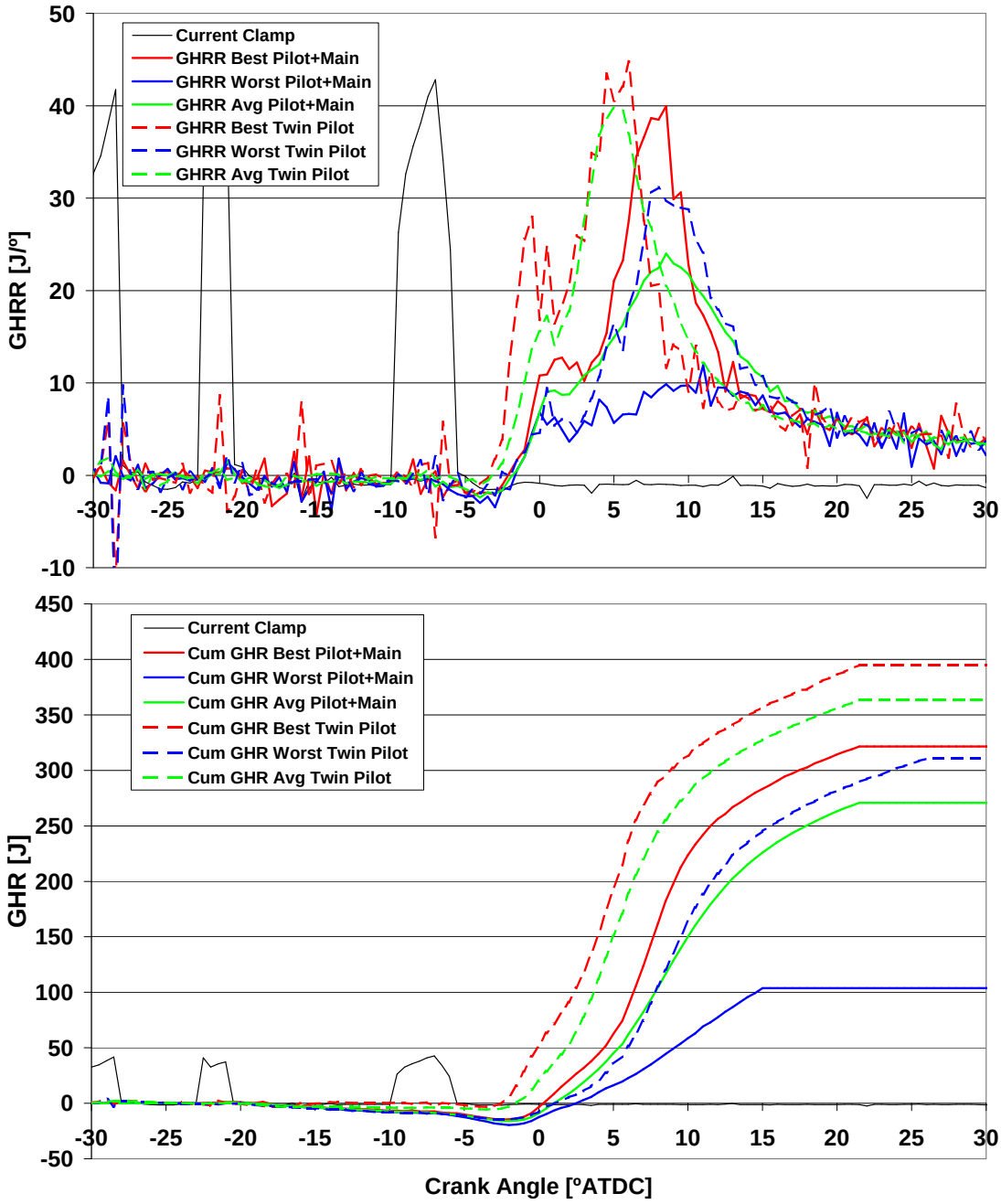

Figure 5.53: Gross Heat release analysis comparing cold idle cycles utilising a single or twin pilot strategy, main timing 9.5°BTDC, 1000 rpm, $-20°C$, HCR. CoV_{IMEPg} [2,15] mm^3/str=11.3% CoV_{IMEPg} [2,2,13] mm^3/str=7.0%

Evaporation is evident for the pilot plus main case in the continuing negative cumulative heat release until main combustion. In the twin pilot case for best and average cycles, there is some positive heat release countering evaporation and holding the cumulative total close

to zero until combustion of the main. The result of this is reduced ignition delay and a higher initial peak rate of heat release. The average heat release rate for the twin pilot is very similar to the best cycle, whilst there is a much greater difference in the single pilot case, where poor cycles impact the average trace. The most crucial difference is in the worst cycle heat release rate. Of great interest is that for both injection strategies, the ignition delay and first few degrees of heat release up to approximately TDC are virtually identical. It is only at this point where the twin pilot strategy has a second, much stronger phase of combustion, resulting in a cumulative burn $\frac{3}{4}$ the magnitude found in the best cycle as opposed to $\frac{1}{4}$ with single pilot, despite no evidence of pilot ignition. This added combustion results in the worst cycle for twin pilot being comparable to the best cycle for single pilot.

As this combustion occurs significantly after ignition it is theorised that there is some fundamental difference in the way fuel is distributed within the cylinder at this stage due to the multiple injection. In the single pilot case it is possible the flame front reaches an area where the local equivalence ratio is no longer sufficient for self sustaining combustion and therefore retreats into low level diffusion burn instead of being able to fully combust the rich mixture. In the multiple pilot case more of the fuel is entrained in the air before the smaller main injection is introduced, providing further combustible regions. This is investigated in a later section.

5.6.4.1 Twin pilot Cold Idle optimisation

An investigation was performed to test the potential for further improvement by varying fuel quantity in the pilot splits. Four repeats were conducted for combinations (multiples of 2 mm^3/str) of twin pilot operation removing 2 mm^3/str at a time from the main down to a final main quantity of 7 mm^3/str. Main timing was fixed at the medium stability 7.5°BTDC timing. Effects on $\overline{IMEP}g_{10}$ and $\mathrm{CoV_{IMEPg}}$ are shown in Figure 5.54. Results are ordered from left to right in groups of increasing total pilot quantity, staggered around the total pilot value on the x axis. Each pilot quantity group is sub-ordered with respect to first pilot quantity.

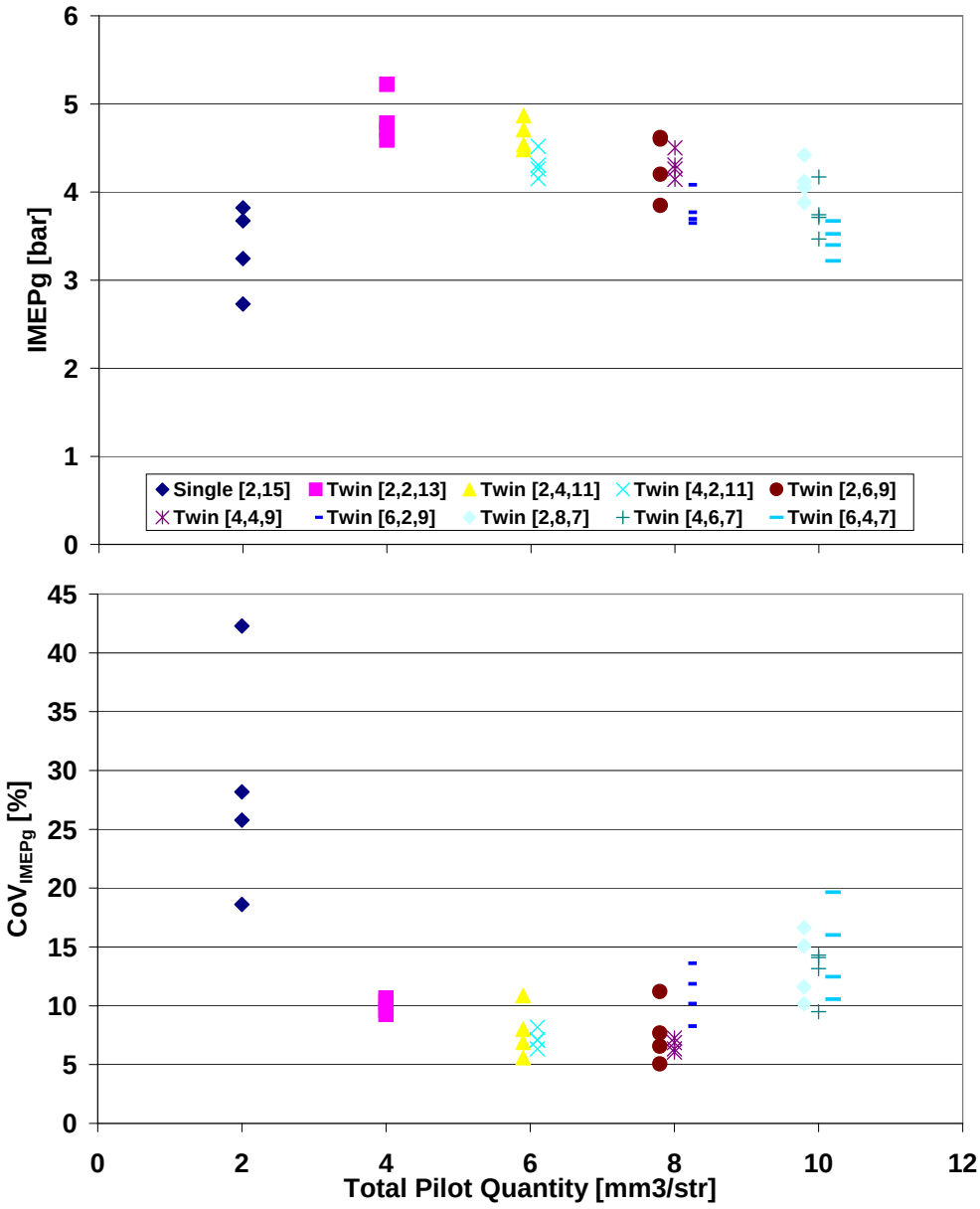

Figure 5.54: Effect of various twin pilot splits on cold idle performance, total quantity 17 mm^3/str main timing 7.5°BTDC, 1000 rpm, $-20°C$, HCR. Staggering around integer values of pilot quantity is to aid clarity — not indicative of varying inputs

In terms of work output there is a clear trend of reducing IMEPg with increasing pilot quantity. Combined with the general trend within the same pilot quantities of small first pilot→higher IMEPg this is further evidence of the sacrificial nature of pilot injection. Despite reducing work output, CoV_{IMEPg} can be lowered by using any combination of twin pilots up to two pilots of 4 mm^3/str followed by a main of 9 mm^3/str ([4,4,9] mm^3/str).

In terms of test-to-test variability, the [4,2,11] mm^3/str and [4,4,9] mm^3/str appear to be the most reliable, with all 4 repeats falling in a very narrow range whilst still producing up to 4.5 bar. A small increase in main quantity would be expected to increase IMEPg to a potentially slightly higher target IMEPg whilst slightly reducing CoV_{IMEPg}, as load assists stability. There is a large potential for variability with single pilot injection as previously seen. Figure 5.55 compares the best, worst and average gross heat release performance of a typical [2,2,13] mm^3/str twin pilot case with that of a [4,4,9] mm^3/str.

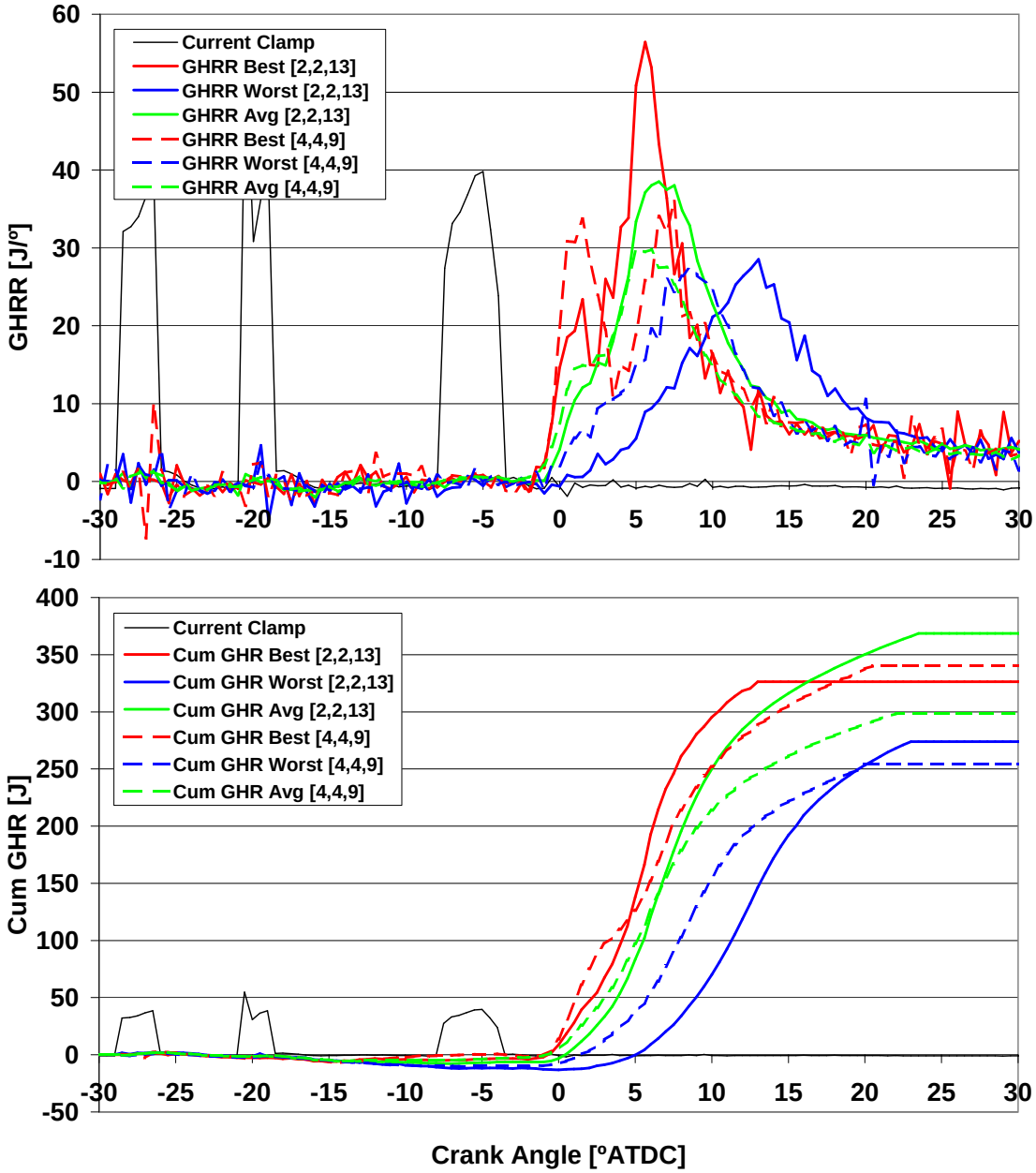

Figure 5.55: Effect of small vs. large twin pilots on Gross Heat Release at cold idle, main timing 7.5°BTDC, 1000 rpm, $-20°C$, HCR. $\text{CoV}_{\text{IMEPg}}$ [2,2,13] mm^3/str= 9.6% $\text{CoV}_{\text{IMEPg}}$ [4,4,9] mm^3/str= 6.9%

Larger pilots lead to low levels of heat release before main injection, but reduced overall combustion. Ignition delay of the main is much more stable in the [4,4,9] mm^3/str case. There is effectively no variation, even for poor cycles where the [2,2,13] mm^3/str case lags by around 3°. The result is minimum difference between the highest IMEPg cycles and the lowest — all being close to the average, resulting in 6.9% $\text{CoV}_{\text{IMEPg}}$.

5.6.4.2 Cold Idle operation with further pilot injections

Optimisation of twin pilot quantities has been used to obtain desirable CoV_{IMEPg} results. A more simple solution of additional pilot injections was attempted by removing a further 2 mm^3/str from the main and injecting it 8° before the previous first pilot. Timing sweeps were conducted as before. A degree of test-to-test repeatability has been experienced, and therefore Figure 5.56 compares $\overline{IMEPg_{10}}$ and stability for twin pilot and triple pilot tests conducted on two different days.

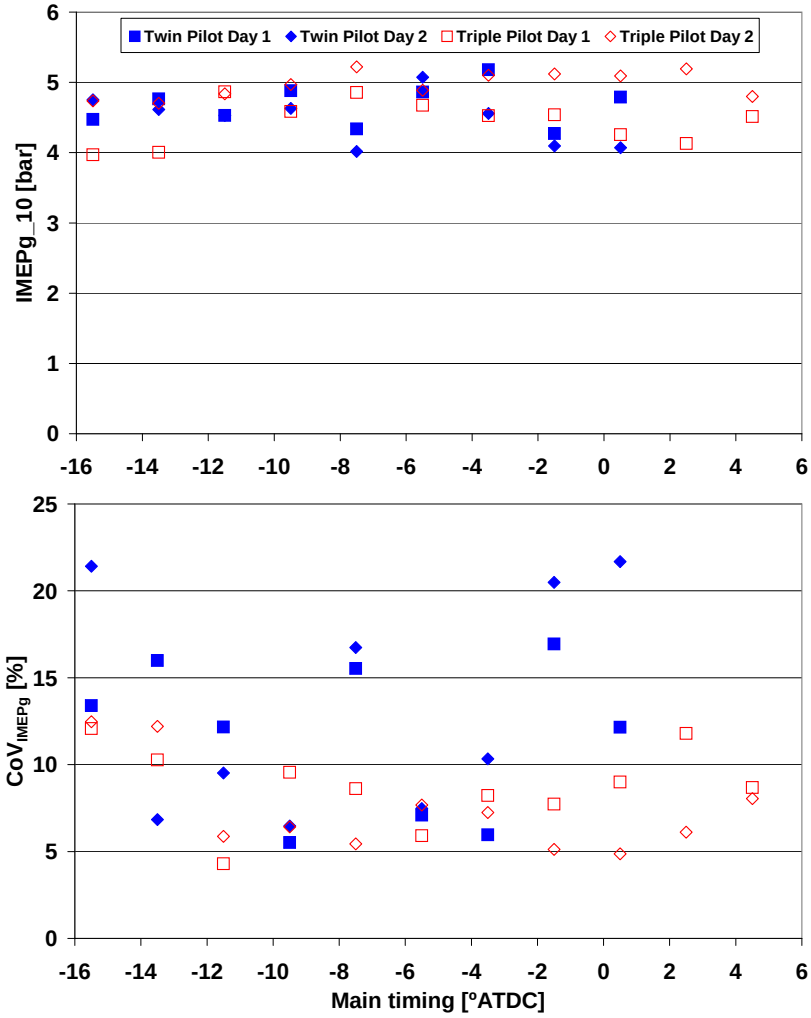

Figure 5.56: Utility of triple pilot injection at cold idle, [2,2,13] mm^3/strvs. [2,2,2,11] mm^3/str, 1000 rpm, $-20°C$, HCR

Again with twin pilot injection there is noticeable CoV_{IMEPg} variation in results both within

these two days of testing and previous findings at a given timing. This emphasises how unstable cold idle operation is at these low temperatures with realistic load demands. Whilst there is no further gain in peak IMEPg with the additional injection, there is the possibility of obtaining this level of work output across a broader range of timings, and the CoV_{IMEPg} is almost universally better, even when extending injection timing slightly past TDC. Twin pilot operation becomes unstable by this point, whilst it is likely some greater heat release or mixing in triple pilot operation extends the region where reliable combustion is obtained. Considering a retarded timing of 1.5°BTDC on day one, twin pilot $CoV_{IMEPg} \approx 17\%$ whilst triple $\approx 7\%$. This represents the best case twin pilot vs. the worst case triple. Heat release information is presented in Figure 5.57.

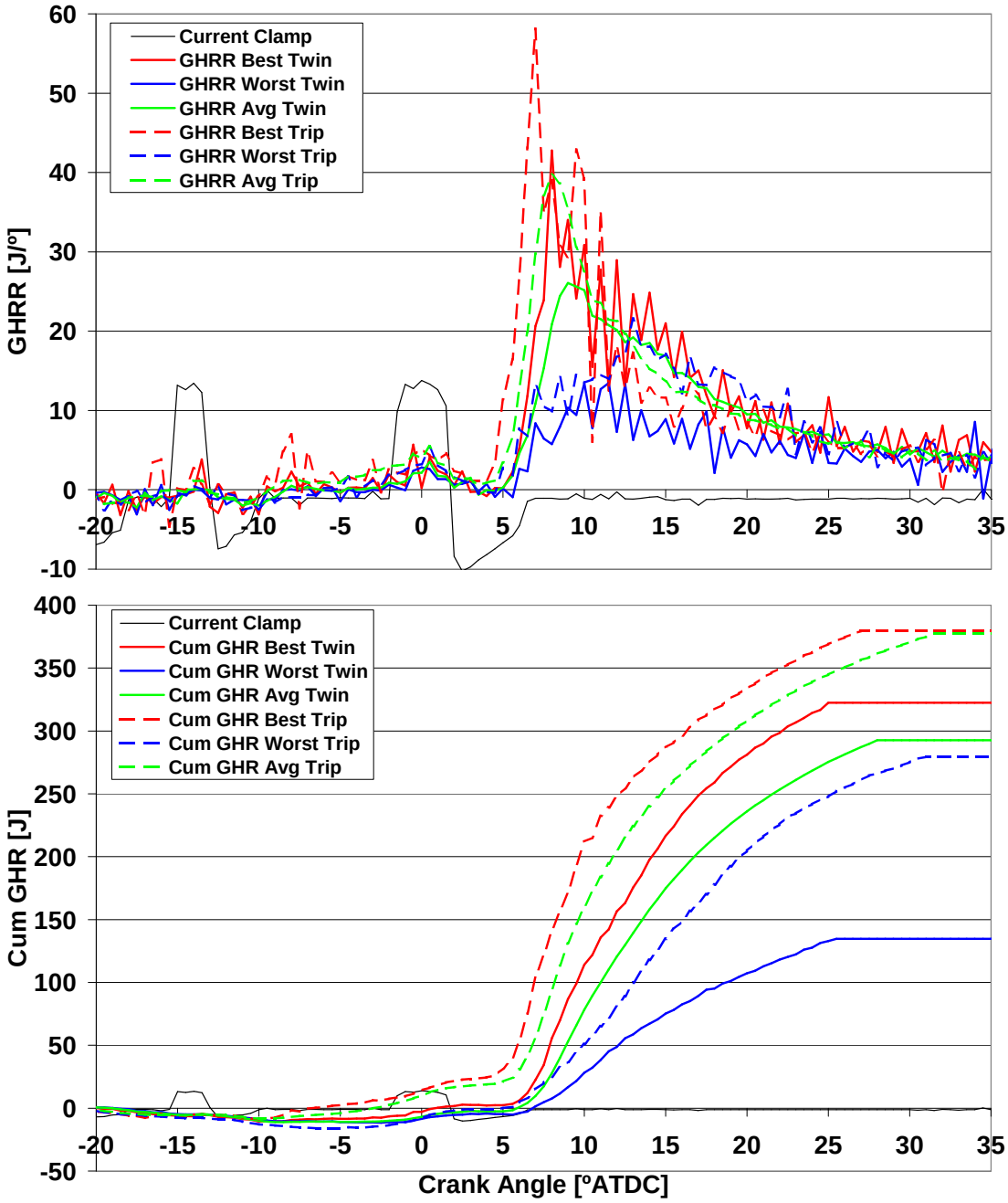

Figure 5.57: Twin pilot vs. Triple pilot Gross Heat Release at cold idle, main timing 1.5°BTDC, 1000 rpm, $-20°C$, HCR. $\text{CoV}_{\text{IMEPg}}$ [2,2,13] mm^3/str=16.9% $\text{CoV}_{\text{IMEPg}}$[2,2,2,11] mm^3/str=7.7%

In the best and average cases there is extra pilot heat release at triple pilot with an accompanying reduction in ignition delay and increase in peak rate of heat release. Again, the important difference occurs for the poor cycles. Similar heat release is observed for the first few degrees until the point where the twin pilot case begins to burn out, whilst the

triple has a second renewed phase of combustion as seen when moving from single pilot to twin. The benefit of twin pilot is both in stability and better fuel preparation resulting in higher cumulative burn and IMEPg. The benefit of triple pilot is not greater fuel burn when optimum timing is used, but a boost in combustion when otherwise there would be a poor cycle as well as greater burn at non-optimum timings. This further extends the region of acceptable operation. Figure 5.58 compares performance by adding a further pilot to make a quad pilot injection strategy.

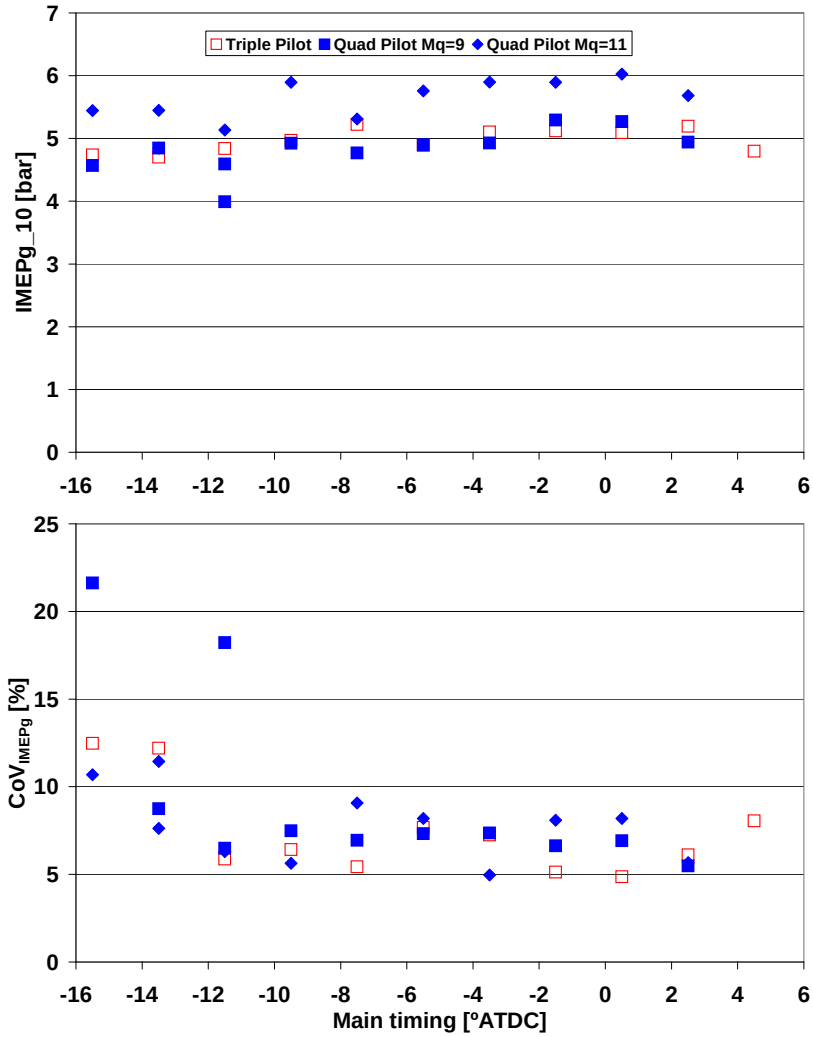

Figure 5.58: Limited utility of quad pilot injection at cold idle, [2,2,2,11] mm^3/str vs. [2,2,2,2,9] mm^3/str vs. [2,2,2,2,11] mm^3/str, 1000 rpm, $-20°C$, HCR

Utilising a 4^{th} pilot injection confers no further advantage to idle operation. In fact the reduction of the main quantity leads to the re-introduction of poor cycles that were not

evident using triple pilot at advanced timings. This effect is detailed in Figure 5.59 which illustrates heat release data for the 11.5°BTDC case.

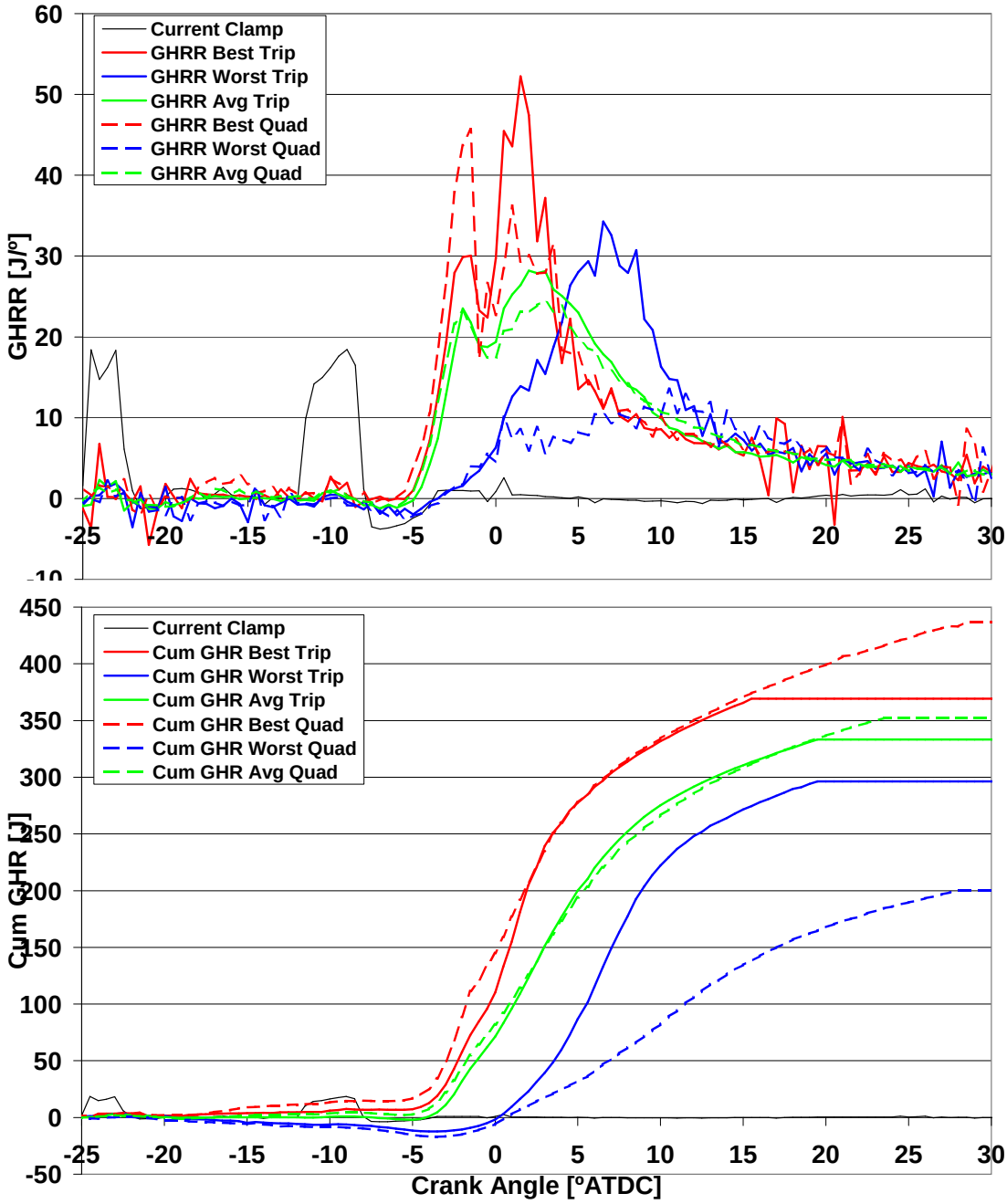

Figure 5.59: Triple pilot vs. Quad pilot Gross Heat Release at cold idle, main timing 11.5°BTDC, 1000 rpm, $-20°C$, HCR. CoV_{IMEPg} [2,2,2,11] mm^3/str=5.9% CoV_{IMEPg} [2,2,2,2,9] mm^3/str=18.2%

In general the quad pilot has slightly greater pilot heat release as may be expected, again resulting in higher initial peak rates of heat release. In all but the poor cycles the heat

release rate trace is very similar to utilising a triple pilot. Poor mid-combustion heat release rate makes poor cycles for quad pilot operation worse than triple. The main quantity is now possibly too small for thorough mixing and promotion of self sustaining combustion on all cycles. This results in the worst cycle cumulative heat release being reduced by approximately 50% for quad pilot. It appears that triple pilot cumulative heat release calculation is clipped a little early at these conditions, resulting in slightly lower total than quad. Quad pilot tends to have a more gradual reduction in the diffusion burn phase whereas the triple pilot slows faster before stabilising back to the quad pilot levels just after the cutoff time. Whilst the calculation is not perfect at this condition it has proved difficult to develop an algorithm which performs well across the wide range of speeds and loads encountered. Using the same criteria for all tests at least allows general comparison without too many variables obscuring any overall trends.

With reference to Figure 5.58, re-introducing 2 mm^3/str to the main quantity both increases IMEPg by an average of 0.75 bar and reduces CoV_{IMEPg} to acceptable levels in the poor tests. Quad pilot injection with the initial fuel quantity yields the same IMEPg at good timings as triple pilot. Even IMEPg for good cycles in poor tests is approximately the same. This implies that the fuel injected very early in the cycle is not lost to wall wetting and so not taking any part in combustion, but that the reduced main quantity is detrimental to combustion stability.

5.6.4.3 Multiple pilot injection at a variety of test speeds

To check applicability of results at other speeds, a sweep was performed in the range 600–1500 rpm with fixed injection timing of 8.5°BTDC. Figure 5.60 graphs $\overline{IMEPg}_{10}$ and CoV_{IMEPg} results for one to four pilot injections with fixed total fuelling of 17 mm^3/str.

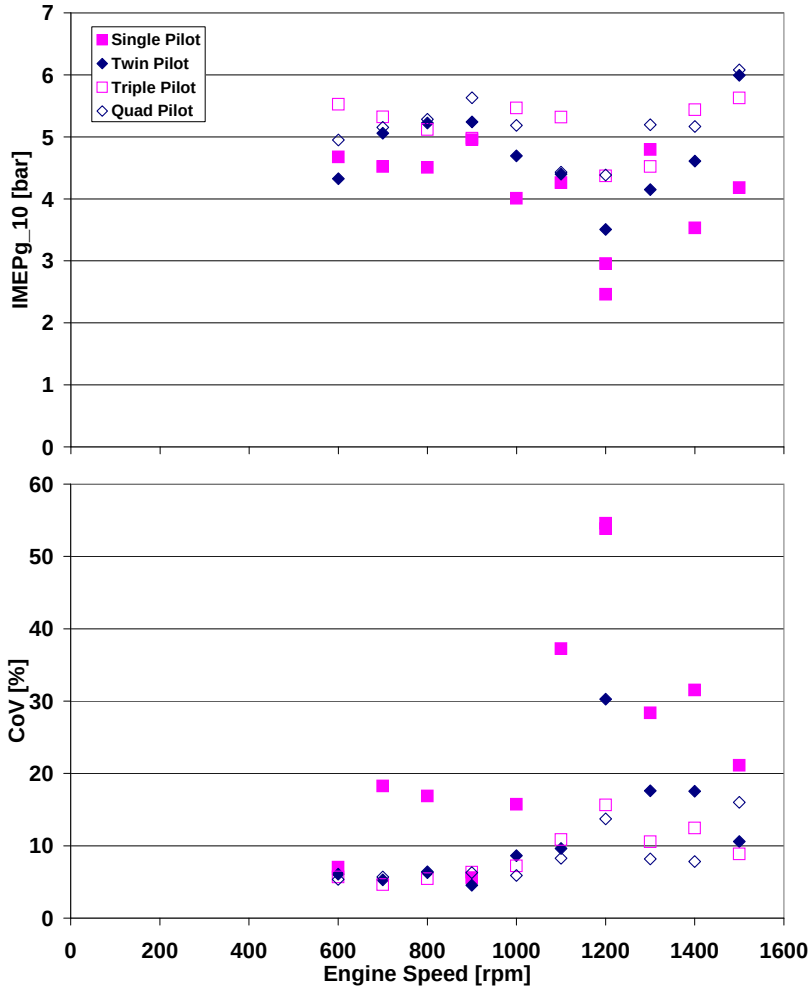

Figure 5.60: The effect of multiple injections across a range of engine speeds, total quantity 17 mm^3/str main timing 8.5°BTDC, $-20°C$, HCR

This set of data reveals that single pilot injection is only suitable at the lowest engine speed, but up to 1000 rpm any multiple pilot strategy yields acceptable stability and work output. At greater speeds, stability suffers for all cases, but triple and quad pilot are the least susceptible. Triple pilot yields the most repeatedly high $\overline{IMEP}g_{10}$ and is generally the, or very close to the, most stable.

5.6.4.4 Multiple pilot injection at a variety of test temperatures

Multiple pilot injection is beneficial at the worst case $-20°C$. Results for a sweep of injection timings at this and higher test temperatures up to $10°C$ are presented in Figure 5.61 for

single and twin pilot injection strategies. Note the $\mathrm{CoV_{IMEPg}}$ scale is 0–20% for the three higher temperatures, but rises to 0–50% for the $-20°C$ case, indicating how stability rapidly reduces as temperature approaches extreme values despite increased fuel quantity for higher target IMEPg to combat cold oil friction.

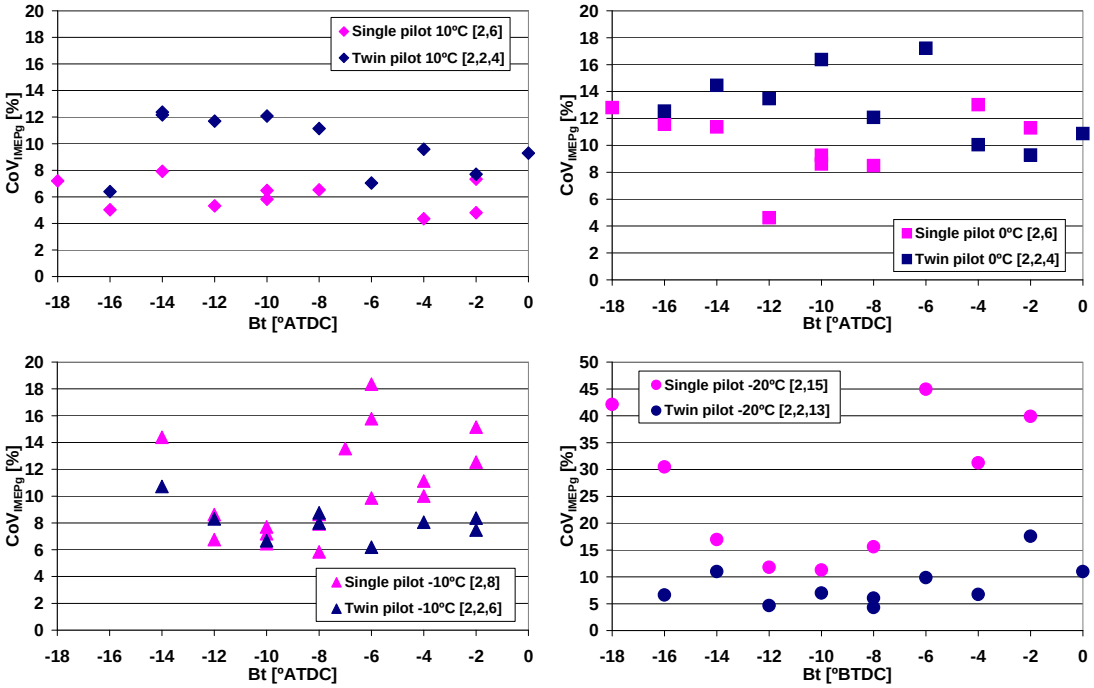

Figure 5.61: Single vs. twin pilot injection utility at various cold idle temperatures, 1000 rpm, HCR. Target IMEPg 2 bar @ $10°C$ and $0°C$, 3 bar @ $-10°C$, 5 bar @ $-20°C$

As previously discussed, there is a significant advantage to twin pilot injection at the lowest temperature, but this is not the case at higher temperatures. There is some improvement in $\mathrm{CoV_{IMEPg}}$ at $-10°C$, but twin pilot is detrimental at 0 and $-10°C$, likely due to the small main quantities required for low ($\approx$ 2 bar) IMEPg target. There is no requirement for further pilot injection at raised start temperatures as single pilot delivers reasonable $\mathrm{CoV_{IMEPg}}$ without need for optimisation despite low load.

Summarising the findings of multiple pilot studies at cold idle, it is possible to obtain highly desirable improvements in both indicated work output and cycle-to-cycle variability with the introduction of multiple pilots. Some level of pilot combustion further assists fuel preparation and increases initial rate of heat release. There is less variation of ignition delay at optimum timings and a second phase of increasing combustion at non-optimum timings

for poor cycles which was not observed with single pilot, suggesting improved mixing. Triple pilot is robust to changes in timing and engine speed at $-20°C$, twin pilot is sufficient at $-10°C$, single pilot is suitable at higher temperatures.

5.7 Computational Validation of Mixture Distribution

Without optical access it is impossible to categorically conclude that the mixture distribution is better in the multiple pilot cases. Conclusions are inferred primarily from heat release information. Computational fluid dynamics (CFD) is commonly used in automotive studies to model in-cylinder processes and analyse the effects of altered parameters without having to perform specialised detailed testing. CFD was not in the initial remit for this investigation, but the problems at idle and the good results found utilising multiple pilots generated interest in a brief study. Results presented in this section are derived from the work of other researchers at the University, no credit is taken for any development. The work is presented only as validation of theory and for further discussion.

A KIVA-3v Release 2 model for the Ford Puma combustion system had previously been developed within the University, principally by Ng [94], to run the code on a PC equipped with Linux. A thorough description of KIVA and the submodels used to accurately predict processes within an internal combustion engine would require several chapters. Ng provides a thorough documentation of this in his thesis, as well as validation of the KIVA model with experimental pressure traces, both motored and fired. Selected results were also published with Shayler [95], giving a more concise overview.

In summary, the piston in cylinder was modelled using a 60° mesh taking advantage of rotational symmetry about the the vertical, centrally mounted 6 hole injector as depicted in Figure 5.62. A 28,389 cell mesh with typical grid size of 1.11 by 1.44 mm by 2° was found to give grid independent solutions, where further reduction in grid size resulted in insignificant change in model prediction. Modification of various coefficients in the sub-models resulted in a good agreement with experimental data collected from the single cylinder rig.

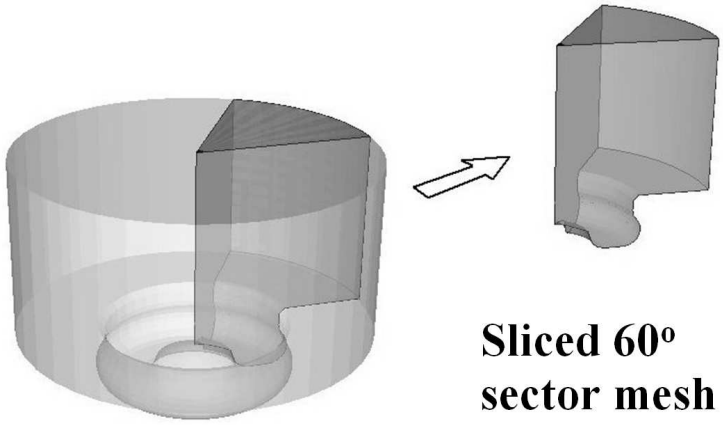

Figure 5.62: Mesh of combustion chamber showing 60° sector where modelling takes place

Calculation was initiated at inlet valve closing where initial conditions are specified from experimental data. For this study, the number of injections was varied from 1–4, but total fuel quantity kept constant at 17 mm^3/str as in experimental investigations at $-20°C$. Start of main injection was fixed at 11°BTDC, and calculation of fuel distribution was terminated at 20°ATDC. In experimental work, the start of main combustion was generally found to be around 5°BTDC. Figure 5.59 is an example of experimental data collected at this condition. Table 5.3 details the timings and quantities of the various injections in each case.

	Far Pilot		**Mid Pilot**		**Close Pilot**		**Main**	
	Timing [°ATDC]	Quantity [mm3/str]	Timing [°ATDC]	Quantity [mm3/str]	Timing [°ATDC]	Quantity	Timing [mm3/str]	Quantity [°ATDC]
Case 1	-	-	-	-	-	-	-11	17
Case 2	-	-	-	-	-24	2	-11	15
Case 3	-	-	-33	2	-24	2	-11	13
Case 4	-43	2	-33	2	-24	2	-11	11

Table 5.3: Matrix of four injection strategies modelled by KIVA 3V

Results from KIVA were post-processed with the EnSight visualisation tool. This allowed both 2D clip plane and 3D surface representations to be produced. An example of both outputs is given in Figure 5.63.

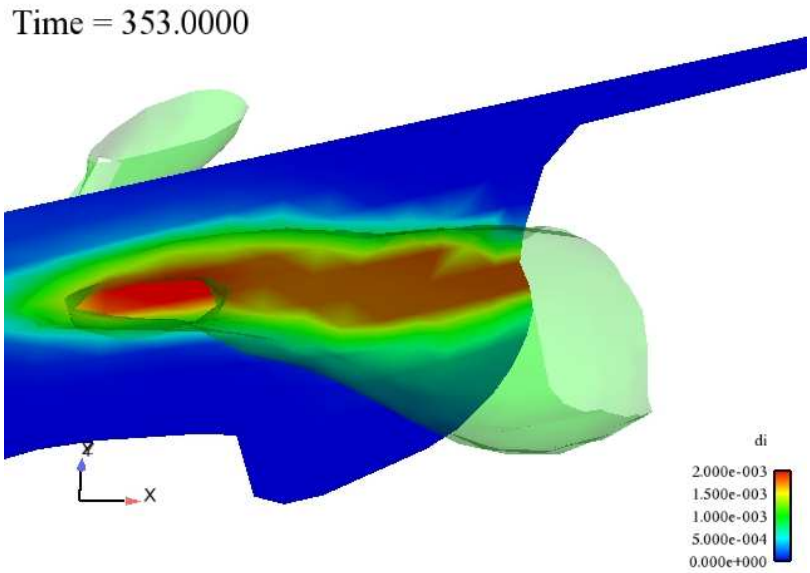

Figure 5.63: Example of fuel distribution on a clip plane for a single injection and the 3D isosurface representing fuel vapour concentration above a set value for a 60° section of the chamber

This example is of a clip plane of one symmetrical 60° section of the combustion chamber at 5°BTDC through the axis of one injector nozzle in blue. The fuel vapour mass fraction distribution on the plane is depicted by a colour map with a colourbar legend. A translucent green isosurface indicates the 3D region within the cylinder where a fuel vapour mass fraction in excess of the middle value in the colourbar exists. This is intended to be indicative of the boundary of rich fuel/air mixture. As shown on the clip plane, outside of the green area the fuel concentration rapidly reduces through the light blue region before leaning out entirely. This distribution mimics the model for diesel combustion proposed by Flynn et al. [96], developed by analysing results from several laser sheet imaging diagnostics investigations.

The purpose of this CFD investigation was to observe fuel distribution through the cylinder and not to model combustion. All reactions were disabled, meaning neither cool flame reactions or combustion could occur. There was also no glow plug providing a combustion initiation source or heat addition to the spray. Combined with cold intake and surface conditions, this resulted in the majority of fuel remaining in the liquid phase and adhering to the walls in calculations. There was very little vaporisation as the jet crossed the combustion chamber, so calculated values of diesel vapour concentration are very low. As a brief

check that fuel distribution was representative of likely areas for combustion, one simulation was performed where reactions were promoted by reducing the temperature at which they commence in KIVA. Local temperature for the combustion case is depicted above local diesel vapour mass fraction in the no combustion case around 5° after injection in Figure 5.64. Local temperature rise is evident in similar areas to those which have a higher fuel distribution, indicating the first stages of autoignition as seen experimentally at this timing.

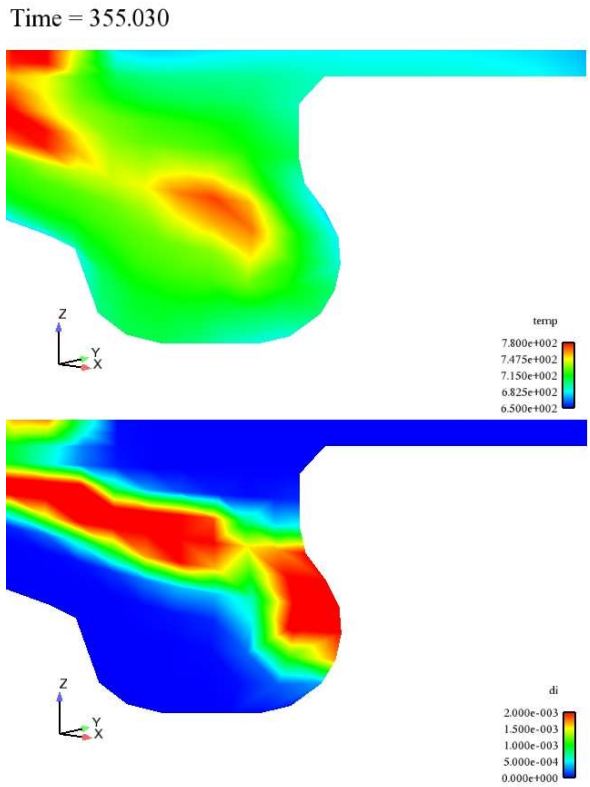

Figure 5.64: Clip plane through one injector nozzle approximately 5° after injection showing local heat release with combustion enabled above local diesel fuel vapour concentration with combustion disabled for the same timing

A full piston 3D visualisation of the fuel vapour isosurface for a single injection is depicted at four crank angle steps in Figure 5.65. It is possible to see that the fuel rapidly crosses the bowl volume and impacts the bowl wall before the jet spreads out, increasingly becoming bent in the direction of swirl.

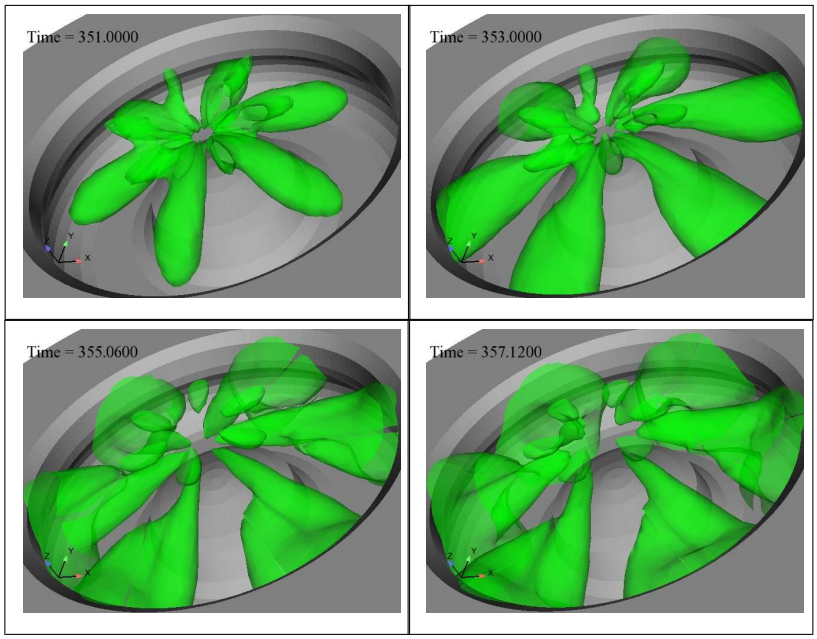

Figure 5.65: Example of 3D visualisation of fuel spray at 2° crank angle steps for the full cylinder

The next four figures occupy pages 131–134. Introduction and discussion of these figures precedes them.

Plots of fuel distribution on the clip plane through the centre of one injector nozzle, at three timings preceding experimental start of combustion for each of the injection strategies, no pilot through triple pilot, are presented in Figure 5.66. Figure 5.67 illustrates the top down view of fuel concentration isosurfaces for the same timings. Significantly greater fuel distribution is achieved by injecting just one pilot compared to no pilot. A further pilot increases the surface area of the vapour cloud to a greater extent which should assist fuel/air mixing for a more complete burn. There is less improvement apparent in triple pilot until considering the top down view, where fuel appears well distributed by the first timestep. Some fuel is always exposed to the glow plug tip, where combustion initiation is expected, from a very early timing — allowing both heat input and more chance of a repeatable start of combustion. The full bowl with no lean regions should ensure that combustion can propagate uninhibited. Any sectors which do not ignite with the initial phase of heat release can be expected to burn as combustion spreads across the chamber. These findings agree with experimental conclusions derived from heat release information that better fuel/air mixing is the principle reason why multiple pilots assist stability of cold idle.

Further CFD work was completed where pilots were injected with no main to observe distribution of pilot fuel. Pilot combustion was apparent from heat release data with multiple pilots in experimental work. Areas where pilot fuel is distributed prior to main injection should be representative of regions where combustion may occur, with higher temperatures and more volatile hydrocarbon species. Differences in fuel distribution were even more pronounced, as illustrated in Figures 5.68 and 5.69. In the single pilot case the small fuel quantity did not distribute through the bowl, whilst the early pilots and larger overall fuel quantity of triple pilot result in much of the bowl being filled with fuel by the first timestep, 2° after main injection. This excellent pilot fuel distribution again indicates that some fuel is always exposed to the glow plug in the crucial period close to TDC and that the main injection is into an area where conditions are primed for combustion.

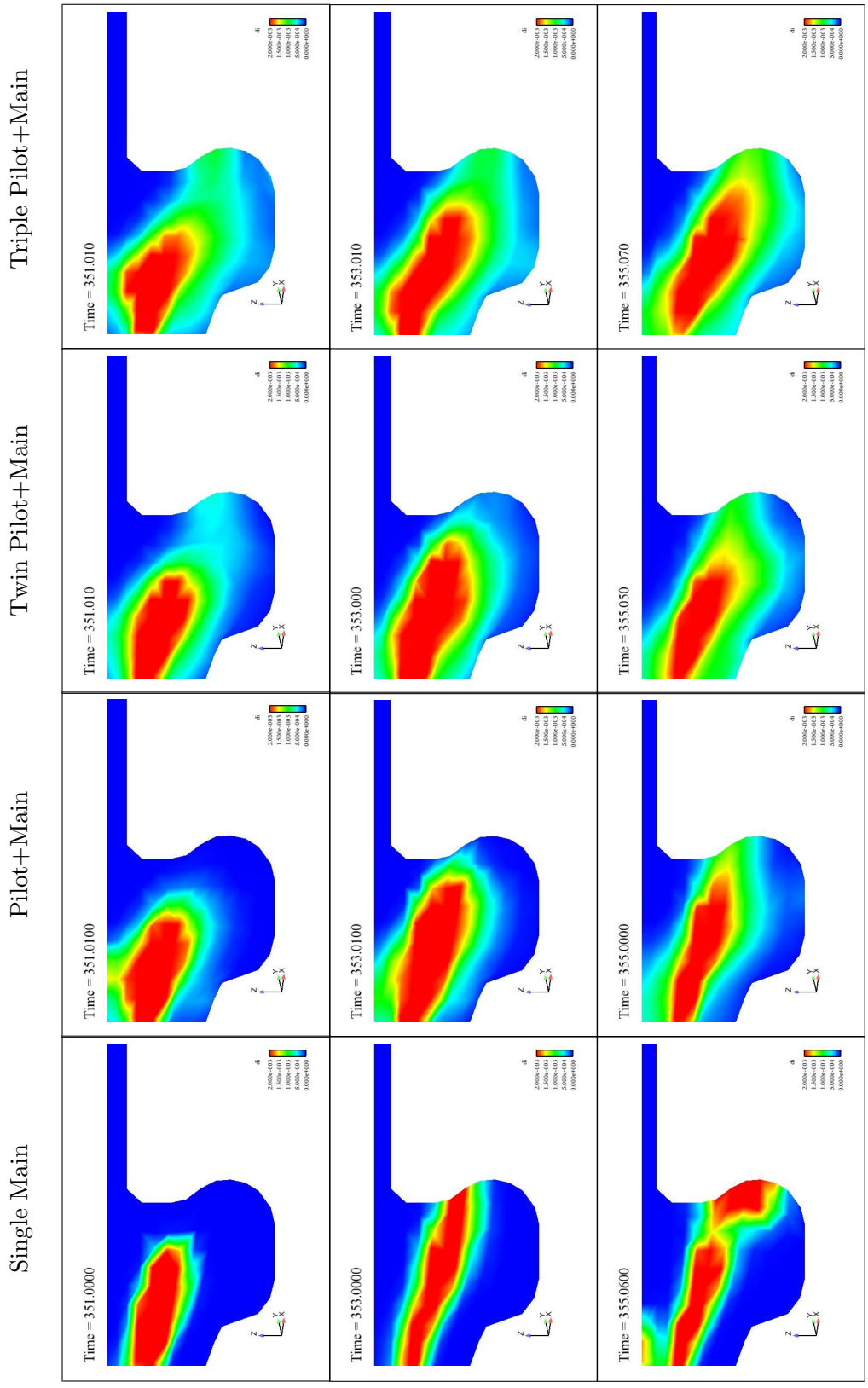

Figure 5.66: Fuel vapour concentration on the clip plane through an injector nozzle for the 4 injection cases at 9°BTDC, 7°BTDC and 5°BTDC

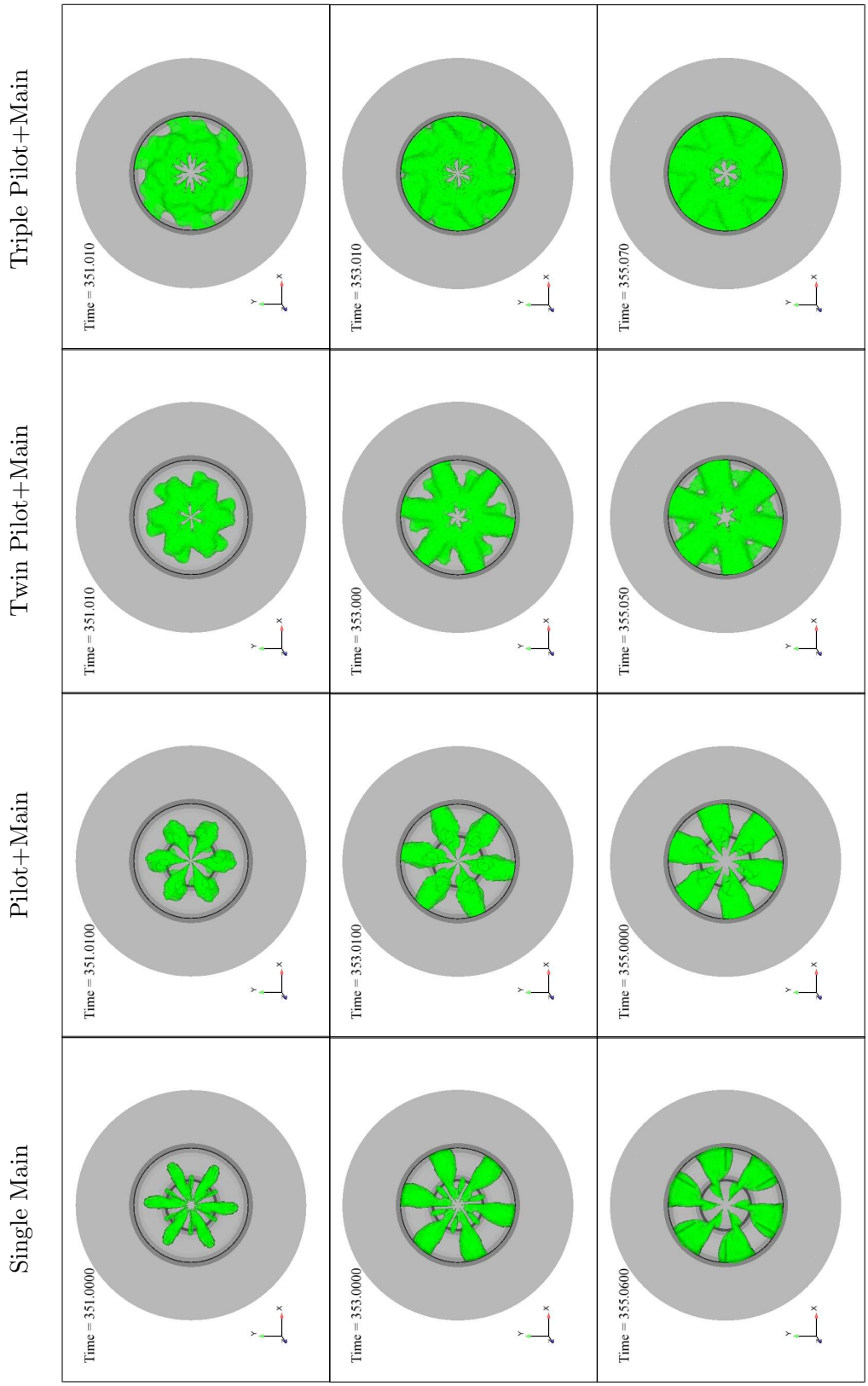

Figure 5.67: Representative fuel vapour concentration isosurfaces for the 4 injection cases at 9°BTDC, 7°BTDC and 5°BTDC

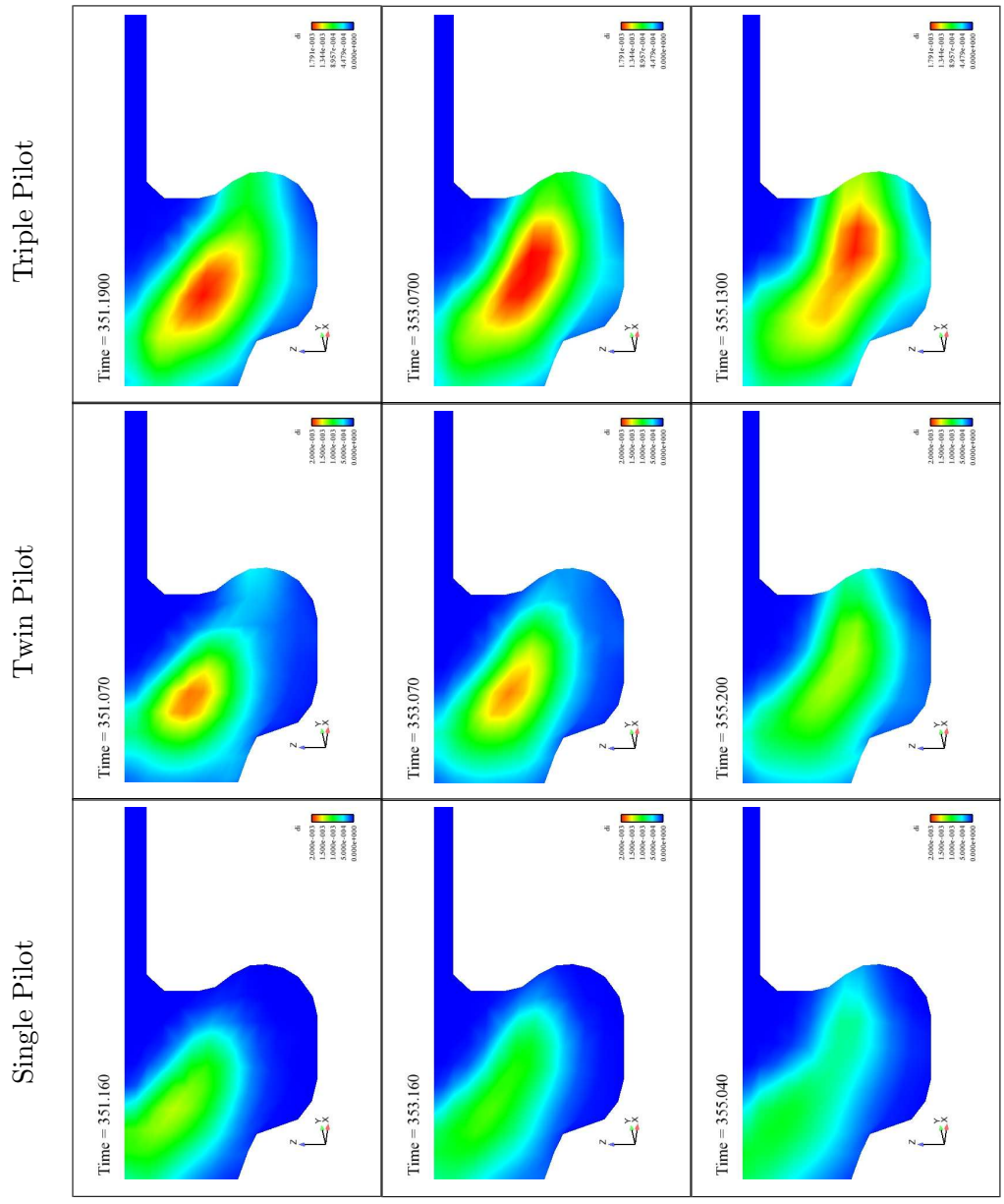

Figure 5.68: Fuel vapour concentration on the clip plane through an injector nozzle for the 3 pilot only injection cases at 9°BTDC, 7°BTDC and 5°BTDC

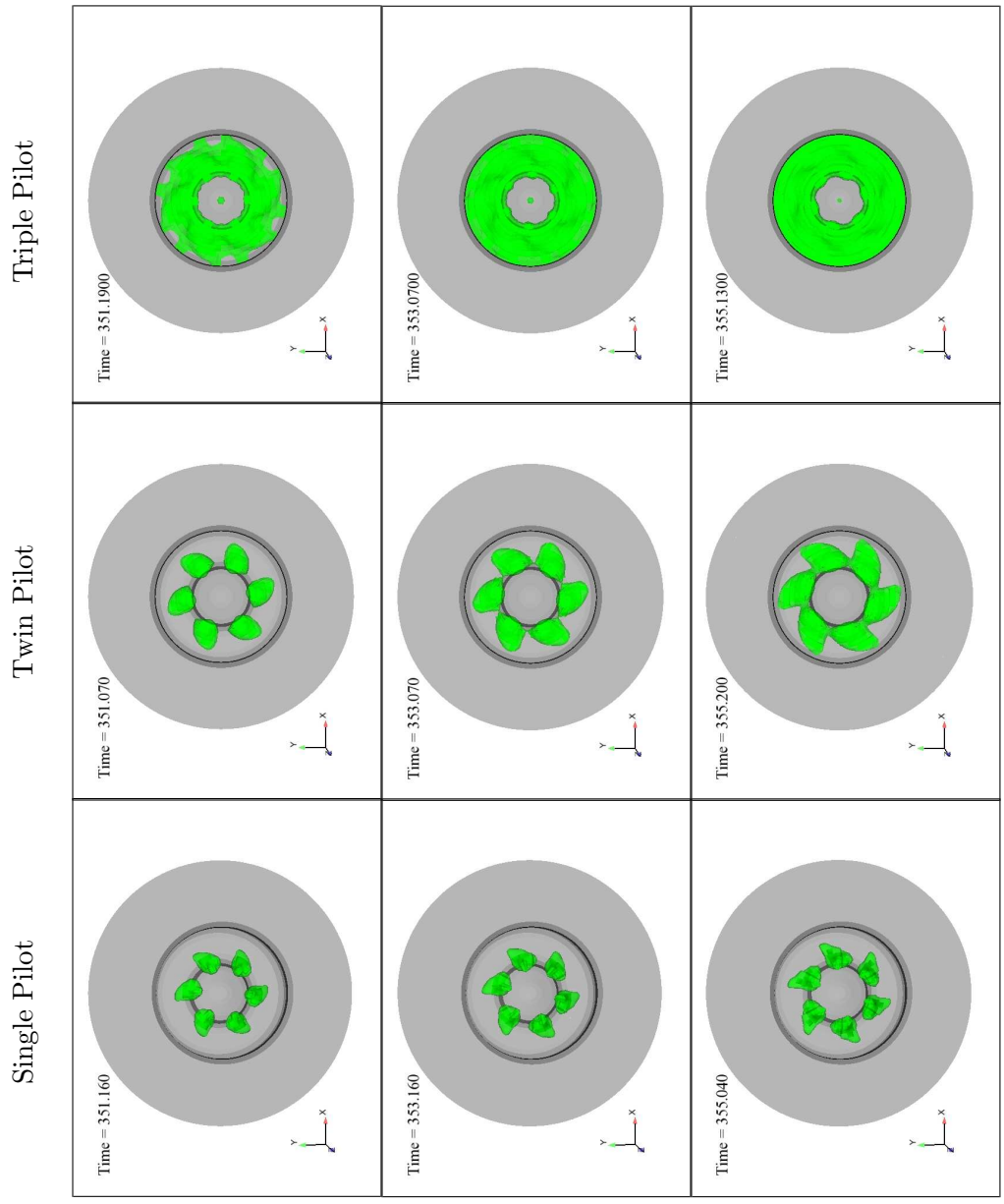

Figure 5.69: Representative fuel vapour concentration isosurfaces for the 3 pilot only injection cases at 9°BTDC, 7°BTDC and 5°BTDC

As a check to ensure the same benefit of mixture distribution cannot be achieved with a single large pilot injected far in advance, a further set of computational experiments were run. There was also a single main injection of the full 17 mm^3/str at the earliest pilot timing of 43°BTDC. Two single pilot plus main tests were processed by KIVA, where first 4 mm^3/str then 6 mm^3/str was used as a pilot at 43°BTDC, followed by the remainder of the 17 mm^3/str at the standard 11°BTDC. Figures 5.70 and 5.71 present the clip plane and isosurface distributions at 19°, 9° and 5°BTDC.

Early injection of a single main results in much of the fuel missing the bowl and flowing into the squish area. Not only is this distant from the glow plug, but there is a large surface area to volume ratio which would result in heat transfer to the cold piston and head with liquid fuel being deposited on the surfaces. A better mixture distribution is obtained with the 4 mm^3/str pilot where fuel just avoids entering the squish region, but in the top down view there is still some degree of stratification into sectors corresponding to each injector. Again, the early fuel injection gives more time for liquid fuel to be deposited on surfaces before compression temperature reaches a maximum. With the 6 mm^3/str pilot, there is faster injection of a larger early quantity and some of the pilot is again trapped in the squish region, resulting in poor distribution in the isosurface plots even around time of expected combustion.

The multiple pilot strategies with appropriate timings allow the main to be injected into an environment which already has ideal conditions for combustion, and may already be experiencing low level combustion, increasing pressure and temperature. Small, well spaced pilots allow fuel vapour to be carried by air motion around the whole bowl without being lost to the squish region. The small fuel quantity reduces speed of injection and therefore there is more time for evaporation before settling on the cold walls, and less liquid fuel remains by this time.

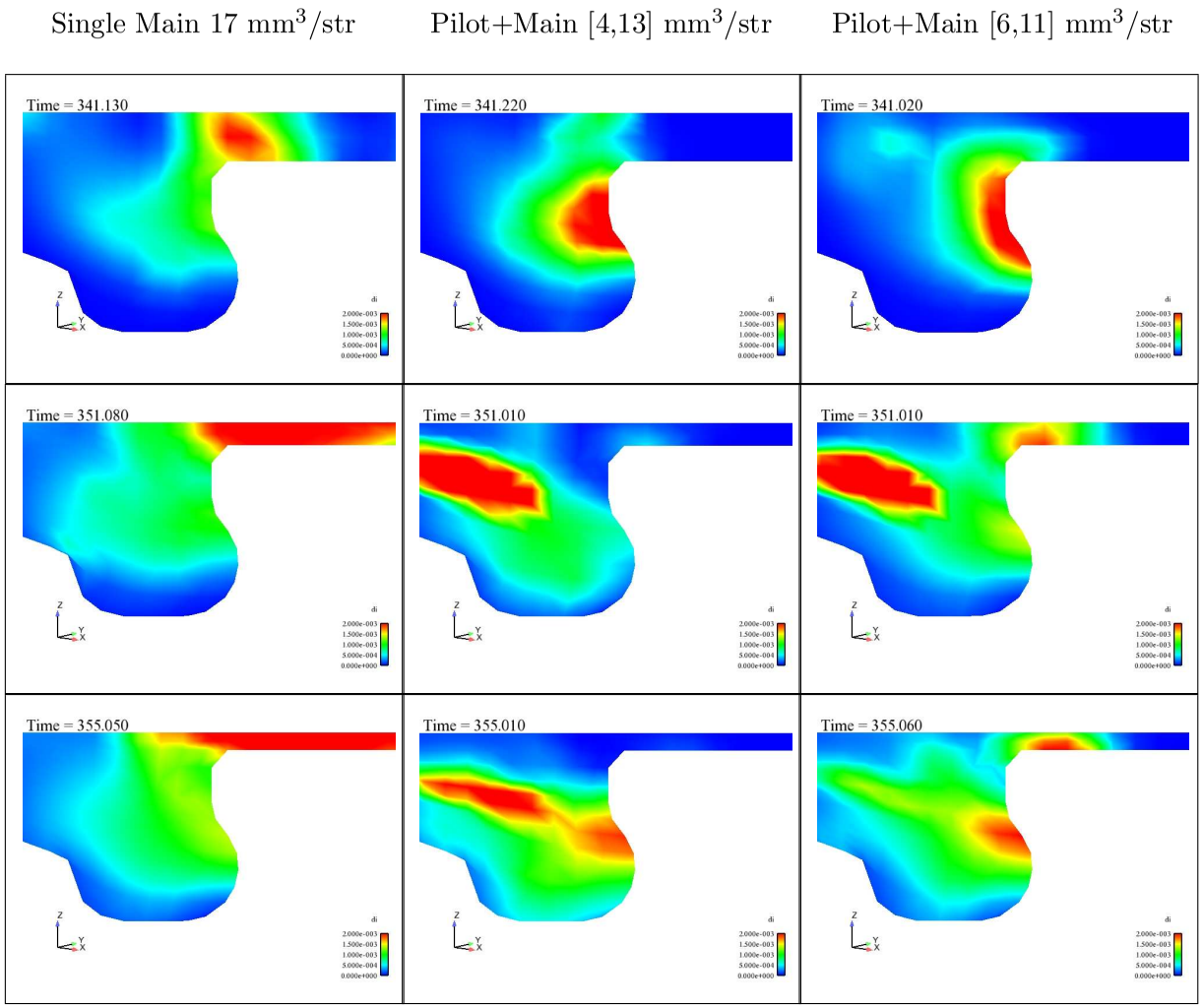

Figure 5.70: Fuel vapour concentration on the clip plane through an injector nozzle for an advanced main injection and two advanced pilot plus standard timing main injection cases at 19°BTDC, 9°BTDC and 5°BTDC

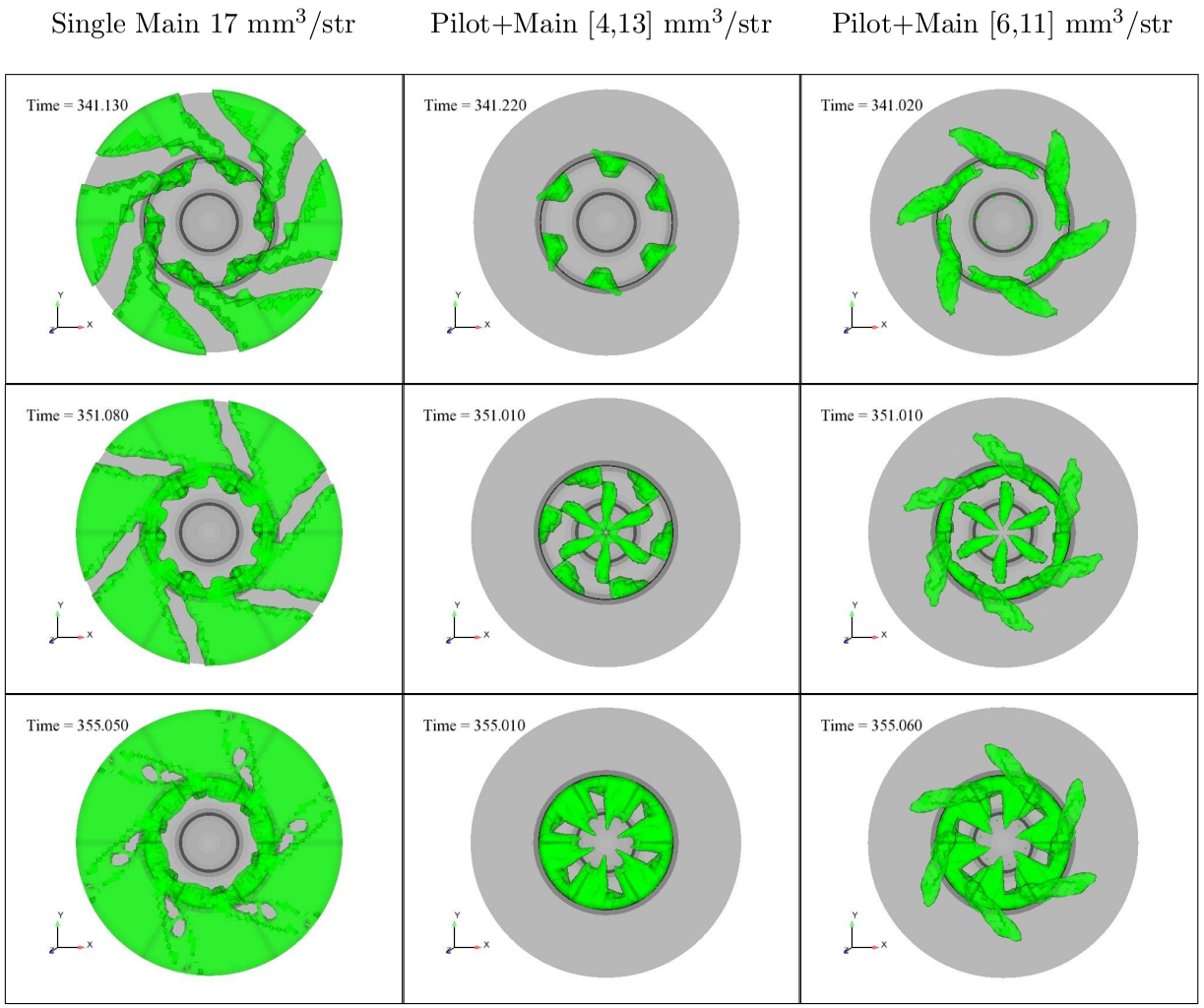

Figure 5.71: representative fuel vapour concentration isosurfaces for an advanced main injection and two advanced pilot plus standard timing main injection cases at 19°BTDC, 9°BTDC and 5°BTDC

5.8 Summary

Various aspects of cold start operation have been investigated at 18.4:1 compression ratio. Baseline performance measures have been identified for direct comparison at 15.4:1.

Conditions representative of initial cold start just above cranking speed were approximated by a motored start at 300 rpm with injection enabled once steady-state had been reached. Factor effects of injection timing, number of injections and injection quantity were investigated. It was found that high IMEPg was possible at all test temperatures, providing that appropriate injection timing was selected. Increasing test temperature led to lower peak work output as intake air density decreased, reducing oxygen availability. Higher peak rates of heat release also reduced mixing time during the diffusion burn phase. These two effects combined, leading to incomplete combustion.

Peak $\overline{IMEP}g_5$ of ≈ 10.5 bar was achievable at $-20°C$ utilising a single main injection just after TDC. The range of optimum injection timings was extended with an additional small pilot injection before the main. This small injection increased fuel preparation with low level localised heat release creating an activated environment of high volatility hydrocarbon species in which to inject the main, reducing ignition delay by approximately 50%. Optimum fuel quantity was ≈ 60 mm^3/str. Above this level there is greater heat loss due to fuel evaporation and no increase in cumulative heat release, as mixtures are already excessively rich. Lower fuelling first introduces variability as the mixture approaches stoichiometry in these low temperature conditions, and then work output reduces as the mixture leans out further.

Operation at typical cold idle speed with fuelling controlled so that load would approximately match engine friction and ancillary demand introduced unacceptable variability into results, especially at $-20°C$. A pilot injection was crucial to obtain any reliable combustion. Even with a pilot there was only a very narrow range of injection timings where $\mathrm{CoV}_{\mathrm{IMEPg}}$ approached the acceptable target of 10% and there was much test-to-test variability. This was due to decreased residence times at sufficient pressures and temperatures

to ensure repeatable ignition delay and combustion intensity of the moderate quantity of fuel injected.

Multiple pilot injection resulted in a great improvement of idle $\mathrm{CoV_{IMEPg}}$ at $-20°C$, from an absolute best of 11% with low repeatability at one combination of inputs to $< 10\%$ at range of timings and engine speeds. This was achievable either with a quantity optimised twin pilot strategy or a simple triple pilot with no need for optimisation. In both cases additional pilots promoted early combustion, increasing initial GHRR from the main, promoting further fuel preparation and less heat release profile variability. If there was poor initial heat release, multiple pilots promoted a second increasing phase of combustion shortly after start of combustion. This minimised any reduction in IMEPg for that cycle, supressing variability. This was attributed to greater homogenity of well prepared fuel throughout the cylinder. In the single pilot case, the rich fuel jet may not have enough readily available fuel to continue self sustained combustion on a poor cycle. If this occurs in a multiple pilot case, combustion of the mixture in the rest of the cylinder continues, increasing time for mixture preparation of the remaining main injection. In this way the desired 5% $\mathrm{CoV_{IMEPg}}$ target could be achieved with appropriate injection timings or pilot quantities.

The homogeneous mixture distribution theory was validated by a CFD investigation. Single main injection resulted in a spoke of rich fuel radially from each injector nozzle at the time of combustion initiation. This left areas of un-utilised oxygen in the gaps. Triple pilot injection promoted a more homogeneous fuel distribution by the time of the main injection. This should enable good combustion propagation with no interruption from exceptionally lean areas. Variability previously introduced by diffusion burns of rich fuel jets in discrete portions of the cylinder should be reduced.

Chapter 6

Effects of Reducing Compression Ratio

6.1 Introduction

This chapter will compare cold start performance of the single cylinder engine at a low compression ratio of 15.4:1 (LCR) with that found using the production 18.4:1 (High Compression Ratio, HCR). Differences identified are investigated and explained. Techniques which may be utilised to improve performance have been identified.

The compression ratio of the research engine was reduced by using a piston with enlarged bowl volume. The primary effects of reducing the compression ratio on compression pressure and temperature are considered, along with any expected changes in losses as a result of low compression. Sweeps of injection timings at 300 rpm were repeated as before, varying test temperature both with and without a pilot. Heat release information is used to determine how compression ratio affects the way in which fuel is burnt at cold conditions. Cold idle performance is also analysed to highlight the effects of compression ratio on this regime of engine operation. Multiple pilot utilised at HCR is tested at LCR when aiming for high quality cold idle.

6.2 Method for Reducing Compression Ratio

It was decided to reduce the compression ratio of the test engine from the current 18.4:1 to a target of around 15.5:1 to investigate cold start performance. It is important to have the minimum impact on other operating parameters when making such changes. An increase in piston bowl volume was considered to be the most straightforward way of doing this whilst keeping the most variables fixed. A new piston was machined with the same bowl geometry, but to a larger scale (Homothetic transformation). The reduction in compression ratio could have been achieved with a shorter connecting rod, but this would have also decreased swept volume as well as increased squish area, leading to reduced turbulence from squish induced flows [97].

Previous bowl volume was 21.783 cc for a total clearance volume of 28.56 cc. Increasing bowl volume to 27.93 cc resulted in a total clearance volume of 34.70 cc, for a compression ratio of 15.4:1. This is a 28% increase in bowl volume, but as all other dimensions are maintained it was considered that this was the lowest impact method for reduction of compression ratio. The lower squish to bowl volume ratio will reduce swirl, but this is unlikely to be significant at low engine speeds considered here. The magnitude of bowl radius increase is in the region of 10%, or 2 mm, therefore other changes such as fuel impingement should be small.

6.3 Primary Effects of Compression Ratio

A reduction in compression ratio leads to theoretical lower energy input to the working gas during compression. As a simple estimation, $p_1 v_1^\gamma = p_2 v_2^\gamma$ may be used to calculate the adiabatic lossless pressure at TDC knowing initial conditions and the compression ratio. For a fixed γ of 1.4 for air and 1 bar intake pressure, TDC pressure for 18.4:1 $\approx$ 59 bar and 15:4 is $\approx$ 46 bar. Using $W = \int p\,dV$ with half crank angle steps in pressure and volume calculation results in an energy input to the cylinder charge of $\approx$ 295 J at HCR and $\approx$ 268 J at LCR, a 9% reduction. This effect is quantified for the real engine using experimental data in the following section. Models used to estimate losses to heat tranfer and blowby

will also be exercised at both compression ratios.

Figure 6.1 plots part of the compression/expansion process for the last motored cycle of two $-20°C$ 300 rpm cold start tests, one using the HCR piston, the other the LCR. These specific results were chosen because although there is some test-to-test variability in compression pressure, they are representative of the the majority of the results obtained, the losses are typical of those experienced at these conditions.

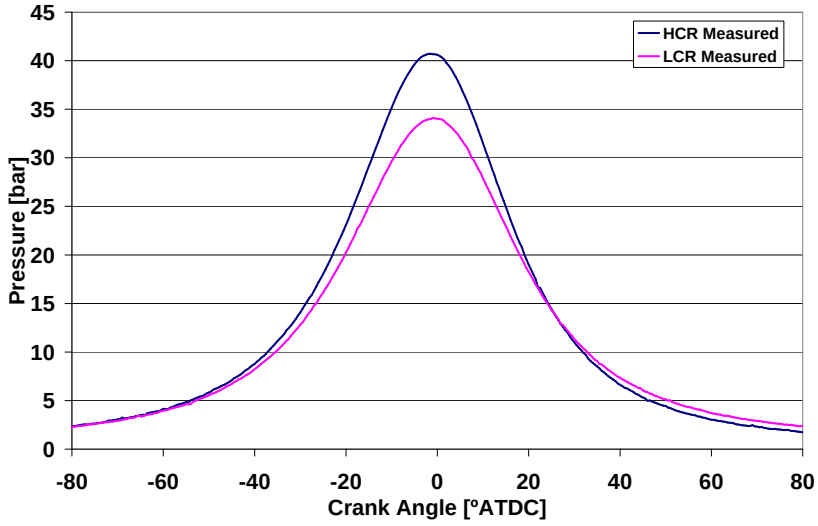

Figure 6.1: Motored pressure traces for high and low compression ratio, $-20°C$, 300 rpm

There is a large reduction in peak pressure from that found using the simple no loss, fixed γ calculation: 31% at HCR and 26% at LCR. In reality, the reduction in compression ratio at 300 rpm caused a peak compression pressure drop from 40.7 to 34.1 bar. Possibly the most significant difference is the crossing over of the pressure traces at approximately 25°ATDC, after which LCR pressure is always higher than HCR. This is a motored trace with no energy input from fuel and therefore this is attributed to heat transfer and blowby losses. Before the exhaust valve opens, LCR pressure $\approx$ 1.15 bar, whereas HCR pressure $\approx$ 0.85 bar.

Equation 6.1 is the mass form of the Ideal Gas Law, where R is the specific gas constant for dry air, 287.1 J/kgK. At this point in the study mass loss to blowby is ignored. Knowing values for volume and pressure during the cycle allows Figure 6.2 to be plotted, the bulk

gas temperature for both compression ratios throughout the cycle.

$$T = \frac{pV}{Rm} \tag{6.1}$$

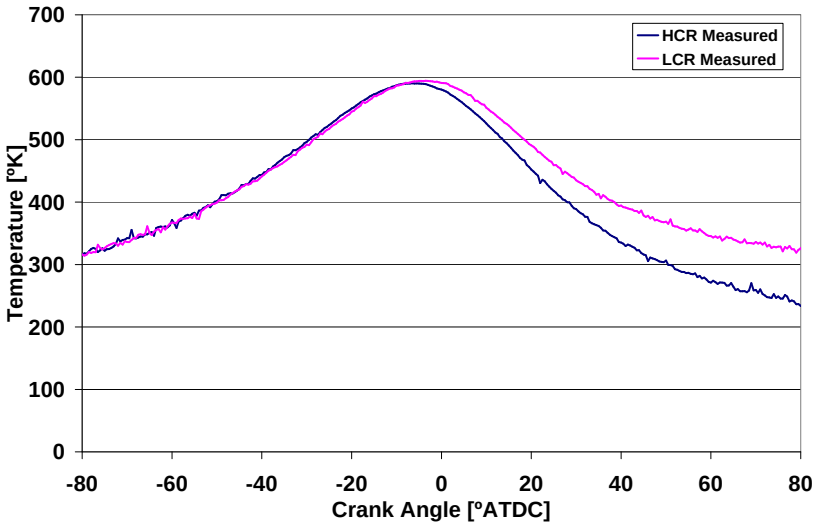

Figure 6.2: Motored bulk gas temperature traces for high and low compression ratio, $-20°C$, 300 rpm

Despite the increased pressure of HCR, there is no increase in peak cylinder temperature using the Ideal Gas Law with no blowby, as well as significantly higher temperature for the whole expansion stroke. This is explained by considering the ratio of p and V at TDC in both cases. If the ratio of HCR to LCR peak pressure is not greater than the ratio of LCR to HCR volume, 1.214, cylinder temperature is actually increased for the Ideal Gas calculation for a given mass at lower levels of compression due to differing losses. In this case the pressure ratio is 40.7/34.1=1.19. This, along with higher LCR pressure during the expansion stroke, implies losses at HCR are significantly greater than at LCR for an engine speed of 300 rpm. The pressure ratio and peak compression pressures through the speed range 300–1500 rpm are presented in Figure 6.3. Results are plotted for the average of two data points at each speed to reduce the impact of test-to-test variability. A pressure ratio above the dotted line indicates theoretical higher peak compression temperature at HCR with no mass loss.

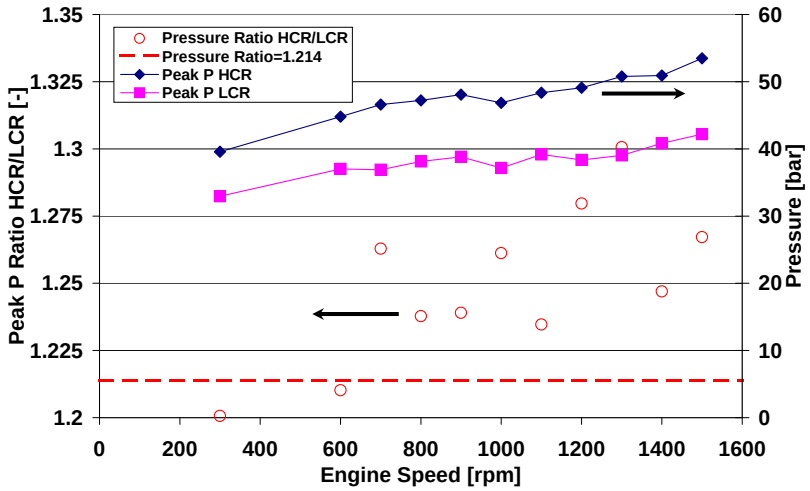

Figure 6.3: Effect of engine speed on motored peak pressure and pressure ratios HCR/LCR $-20°C$

The peak pressure readings have some scatter around a linear fit, resulting in significant variation of pressure ratio. The trend is an increasing pressure ratio with speed. At all speeds over 600 rpm the value is larger than 1.214. Above this speed HCR continues to improve its pressure ratio against LCR, suggesting that low speed operation introduces excessive losses — exacerbated by increased cylinder pressure at HCR. The effect of engine speed and compression ratio on heat transfer using the Hohenberg correlation given previously in Equation 4.15 on page 54 is illustrated in Figure 6.4. Cumulative heat transfer is calculated from BDC to TDC of the compression stroke using pressure data from the final motored cycle. This is effectively the total heat energy lost from the charge during compression.

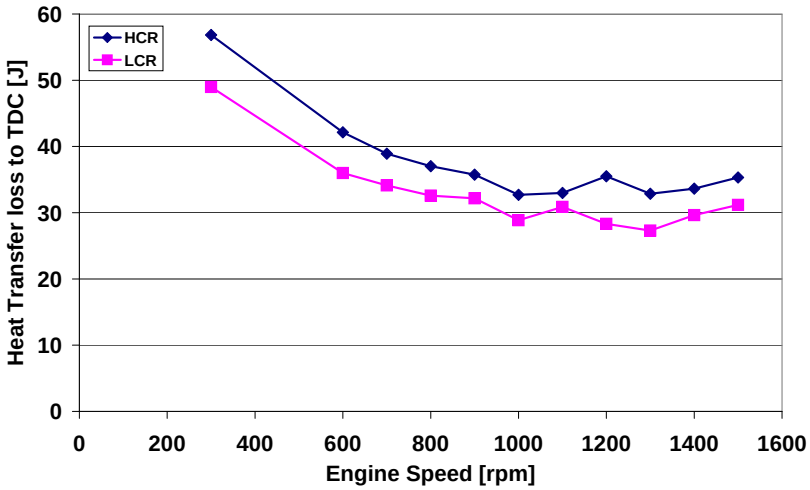

Figure 6.4: Effect of engine speed on heat transfer calculated using the Hohenberg correlation for the compression stroke of the final motored cycle for both compression ratios, $-20°C$

Total heat transfer increases rapidly as speed reduces to 300 rpm. LCR exhibits reduced heat transfer losses as expected due to lower pressures, and the exponential nature further reduces relative total loss between compression ratios at 300 rpm. LCR heat transfer is approximately 14% lower than HCR. Dividing total heat transfer by the time it takes to perform the compression stroke results in Figure 6.5, the average rate of heat transfer during the compression stroke against engine speed. As seen, this is approximately linear. The exponential nature of Figure 6.4 is due to the exponentially longer time for losses to occur for each 100 rpm decrement of engine speed as speed decreases, not due to a less than proportionate reduction in heat transfer rate as speed decreases.

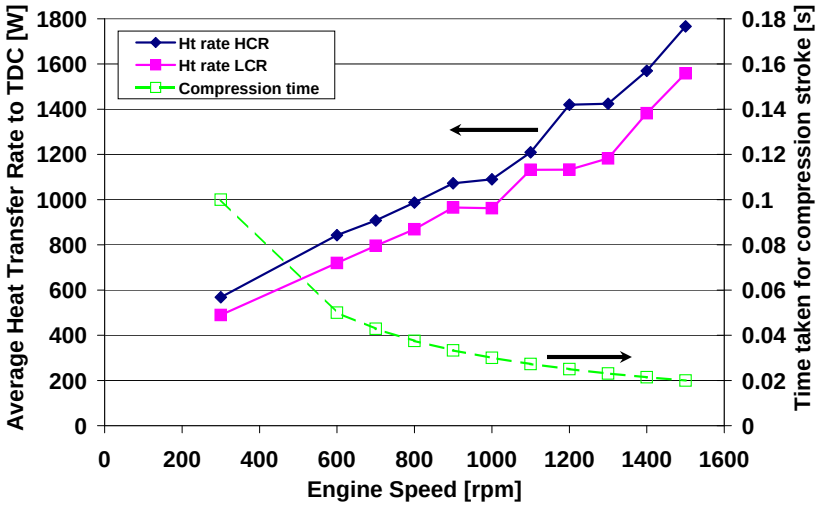

Figure 6.5: Effect of engine speed on heat transfer rate calculated using the Hohenberg correlation for the compression stroke of the final motored cycle for both compression ratios, $-20°C$

Blowby losses (both mass fraction and energy within the escaping gas) calculated by the flow through an orifice model presented in Equation 4.16 are graphed in Figure 6.6 for the same data used when considering heat transfer.

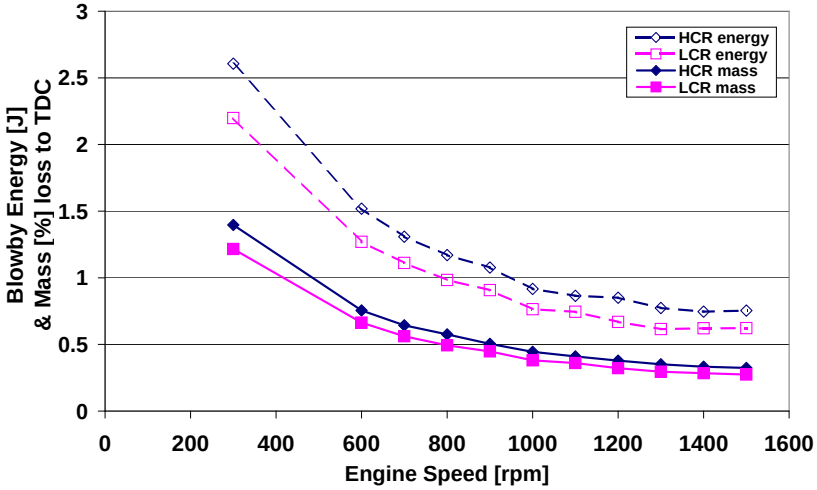

Figure 6.6: Effect of engine speed on energy loss and mass loss due to blowby calculated assuming flow through an orifice for the compression stroke of the final motored cycle for both compression ratios, $-20°C$

Calculated blowby losses are very low for this motored compression process, less than 1.5% of the mass is lost by TDC at 300 rpm. Cheng [86] performed motored tests of a multi-cylinder engine at 300 rpm, $-20°C$, and found blowby to be nearly 10%. The engine was a DI diesel from the same manufacturer as the single cylinder unit, but two generations earlier with slightly higher compression ratio. Losses were judged to be excessive, so new piston

rings were utilised with smaller end gaps. Blowby was approximately halved to 5% mass loss per cycle at 300 rpm. As such, a reduced compression ratio and further development on this engine suggests that the blowby model may provide reasonable results, at least under motored conditions. As the model is only generally used to adjust net heat release rate to gross heat release rate and calculated energy loss to blowby is negligable compared to heat transfer, it is considered to be acceptable for the purposes of this investigation. The same rapid increase in blowby is observed as engine speed reduces, and again high compression ratio is at a disadvantage due to higher compression pressures.

Blowby may be measured directly with a flow meter connected to the crankcase on a multi-cylinder engine, but for single cylinder applications this is not accurate, as any blowby flow is masked by large pulsations of crankcase breathing as the single piston displaces 500 cc of air per stroke. In a multi-cylinder engine this is generally not such a problem because for each cylinder descending there will be another on the equivalent upwards stroke. Despite this, an AVL 405 blowby meter was connected to the crankcase and the signal was integrated over each engine cycle in an attempt to remove the flows of air in and out associated with piston motion, leaving only blowby gas. Output from the blowby meter over a typical 300 rpm cycle is given in Appendix Figure d.

The blowby remainder for the entire final motored cycle is graphed at a variety of engine speeds for both HCR and LCR operation in Figure 6.7. 10 repeats were performed at the lowest speed for each compression ratio. There is added uncertainty in results in the range 600–900 rpm as volume flow rate from the crankcase was high enough to exceed the measurement capability of the blowby meter, saturating output at 10 V. Below 600 rpm, the flow speed was low enough to avoid saturation, above 900 rpm, compressibility of air led to insufficient time for flow rate build up, lowering peak rate below saturation.

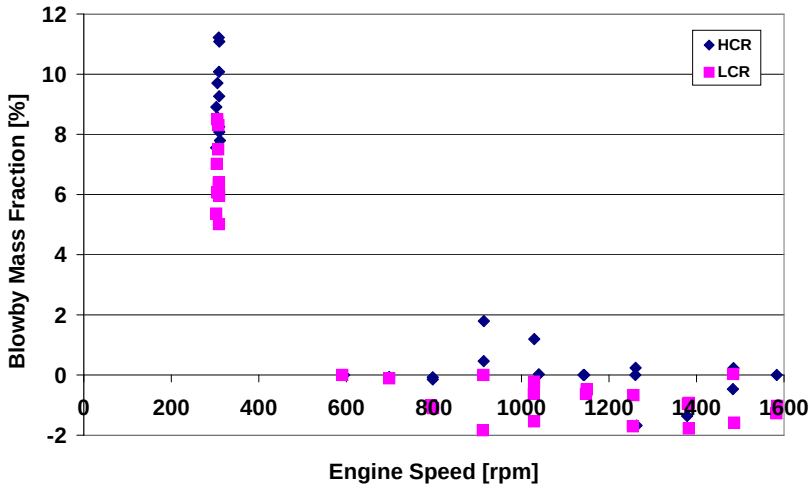

Figure 6.7: Effect of engine speed on blowby mass fraction measured using AVL blowby meter for the final motored cycle for both compression ratios, $-20°C$

Clearly the measurements are not very reliable, but still point to significantly increased losses to blowby at 300 rpm. At all other speeds the measurement varies around the zero blowby level. The spread at 300 rpm is 7.5–11.2% at HCR, average 9.4%. At LCR this drops to a spread of 5.0–8.5% with an average of 6.5%, a 30% reduction from HCR. As no other changes were implemented in the method of blowby gas measurement between the compression ratios, this effect can be considered a real one. Despite the inaccuracy of the measurement technique there is a measurable decrease in low speed blowby when reducing compression ratio from 18.4 to 15.4. The 30% average figure for HCR to LCR blowby reduction indicates that there is a more substantial reducion in blowby between HCR and LCR than in heat transfer, where only 14% reduction was calculated using the Hohenberg correlation. Again a 14% reduction was calculated using the differential pressure flow through an oriface blowby calculation, so it appers blowby may be more significantly different between the two compression ratios than differential pressure would suggest. Combined with theroetical reductions in heat transfer, this helps to explain why there is a higher calculated pressure later in the power stroke for LCR as was seen in Figure 6.1. The lower temperatures after TDC calculated using the Ideal Gas Law seen for 300 rpm operation in this cycle are also likely to be a true effect. Ideal Gas Law temperature will increase due to mass loss, but the mass loss difference between HCR and LCR is unlikely to be significant enough in the motored case to impact the overall trend of higher temperatures due to lower

losses.

In summary, the primary effects of the reduction in compression ratio are a reduction in peak compression pressure of ≈ 17% at 300 rpm, increasing to ≈ 21% at 1500 rpm. The smaller relative pressure reduction at low speed is due to rapidly increasing time for losses (which are exacerbated by higher pressures and temperatures at HCR) to occur as engine speed reduces.

6.4 Cold Start Comparisons

Section 5.2 onwards presented baseline results obtained at HCR, first targeting high IMEPg at 300 rpm cold start, then stable work output at higher engine speeds representative of cold idle. The results at HCR represent desirable operational characteristics to be achieved at the reduced compression ratio of 15.4:1. With particular reference to Figures 5.17 and 5.25, Figure 6.8 repeats the injection timing sweep for a single main injection at 300 rpm LCR at the three test temperatures, Figure 6.9 details the pilot plus main case.

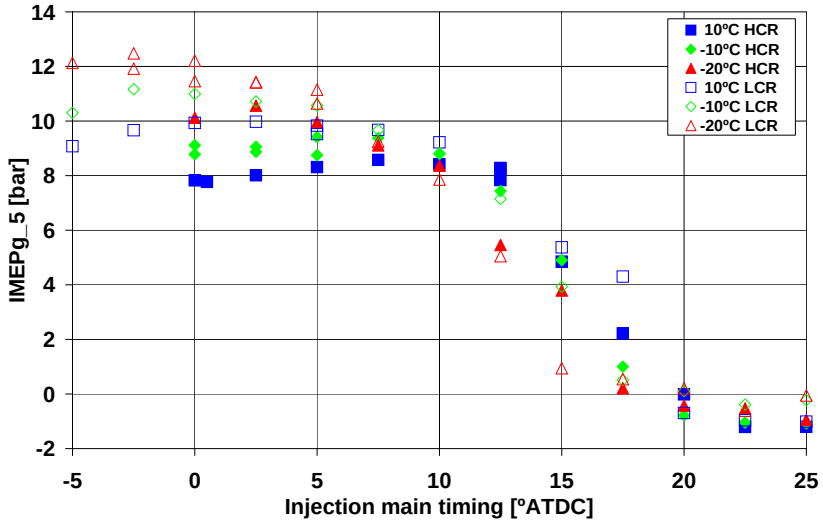

Figure 6.8: Effect of main timing on $\overline{IMEPg}_5$, HCR vs. LCR, 60 mm^3/str single injection, 300 rpm

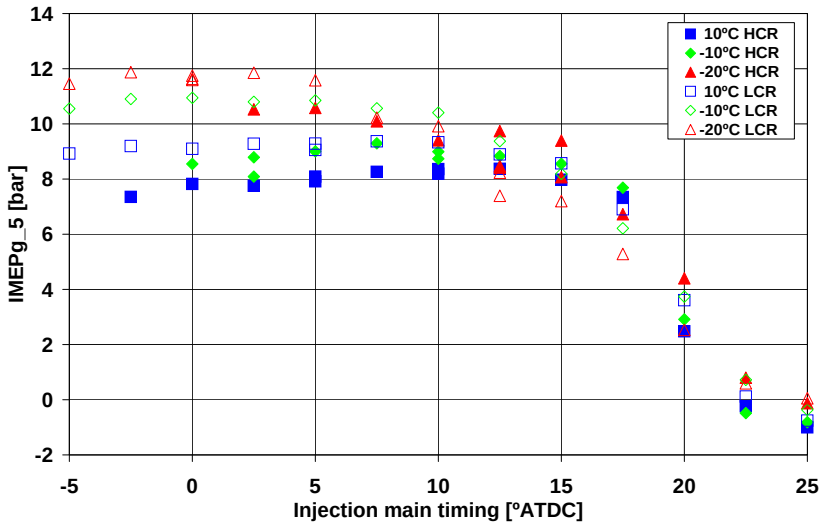

Figure 6.9: Effect of main timing on $\overline{IMEP}g_5$, HCR vs. LCR, [2,58] mm^3/str pilot+main injection, 300 rpm

The variations of $\overline{IMEP}g_5$ with injection timing and the sensitivity to test temperature are similar for both compression ratios. The most significant difference is that the peak $\overline{IMEP}g_5$ achievable is higher by approximately 2 bar for each test temperature at LCR. $\overline{IMEP}g_5$ of just over 12 bar was found with single injection just in advance of TDC, a region where operation was not possible at HCR due to peak cylinder pressures above 120 bar. The advantage of LCR does not appear to be this capability to advance further as HCR peak IMEPg is found slightly in retard of TDC. The other main finding is that low compression ratio performs less well at moderately retarded timings for the two negative test temperatures, with a faster drop-off in $\overline{IMEP}g_5$. The introduction of a pilot injection has the same small effect at high and low compression ratios. There is a minor reduction in maximum IMEPg at LCR where there was very little difference at HCR, but the region of high work output is extended significantly into the retard. Performance degradation for LCR at the most retarded timings is not as complete as at HCR. This is further evidence of reduced losses at LCR resulting in higher temperatures after TDC as was illustrated in Figure 6.2. Figures 6.10 and 6.11 compare performance with and without pilot injection at the lower fuel quantity of 30 mm^3/str. The equivalent Figures for HCR only are 5.19 and 5.30.

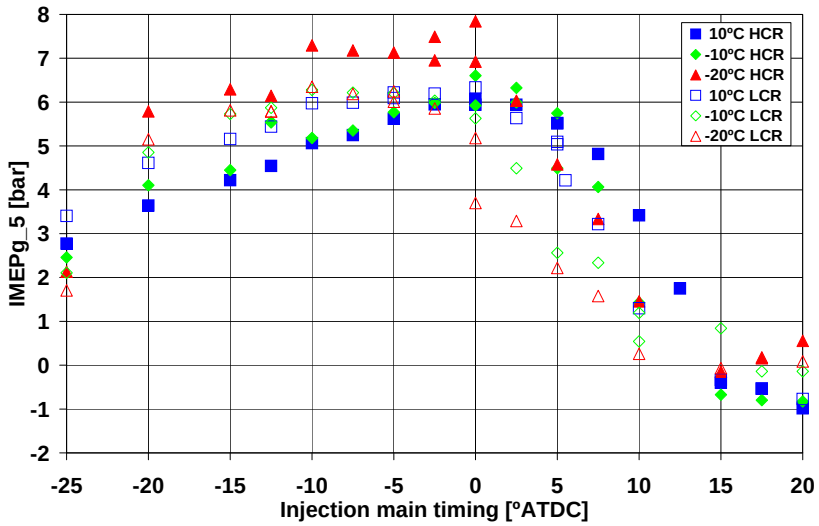

Figure 6.10: Effect of main timing on $\overline{IMEPg}_5$, HCR vs. LCR, 30 mm^3/str single injection, 300 rpm

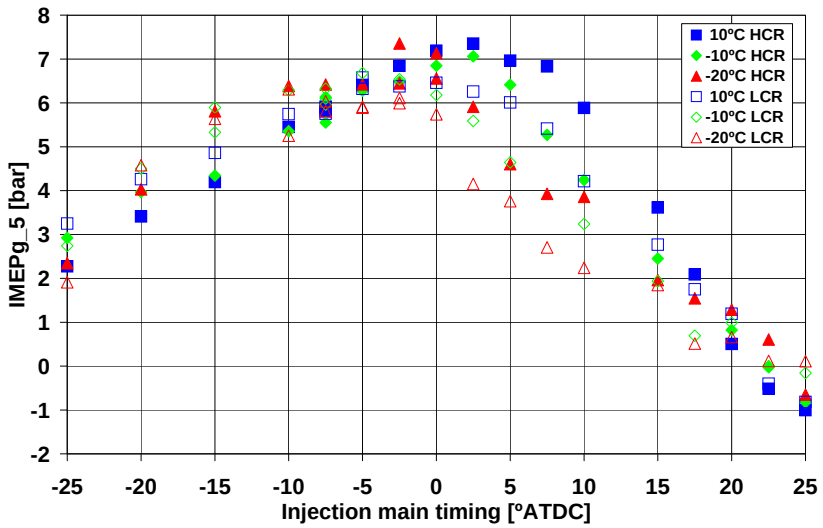

Figure 6.11: Effect of main timing on $\overline{IMEPg}_5$, HCR vs. LCR, [2,28] mm^3/str pilot+main injection, 300 rpm

In both cases, HCR has a slight advantage over LCR and again performs better at retarded timings until the latest injections, with advanced performance subject to some variation with test temperature. Pilot injection stabilises performance over a slightly wider range of acceptable injection timings, but does not close the gap between LCR and HCR performance. This better performance at HCR with low fuelling is more in line with what would be expected in the ideal case. Higher temperatures and pressures would be expected to benefit cold start, resulting in more thorough fuel preparation and greater combustion efficiency, whilst the larger expansion ratio should be capable of extracting more work from

the combustion gasses.

To investigate the reasons behind these differences between high and low compression ratio, heat release analysis is now presented. The relationship between peak rate of heat release and the cumulative total released by combustion is shown in Figure 6.12 for the HCR case and Figure 6.13 for LCR.

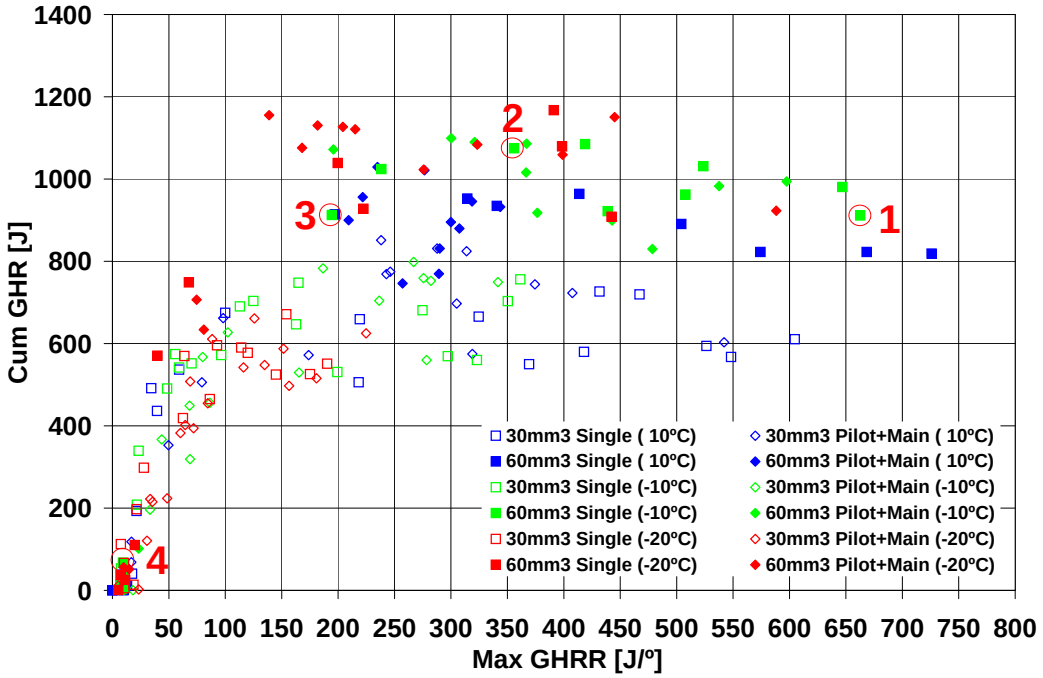

Figure 6.12: Maximum Gross Heat Release Rate vs. Cumulative Gross Heart Release for all collected data during 300 rpm timing sweeps, HCR

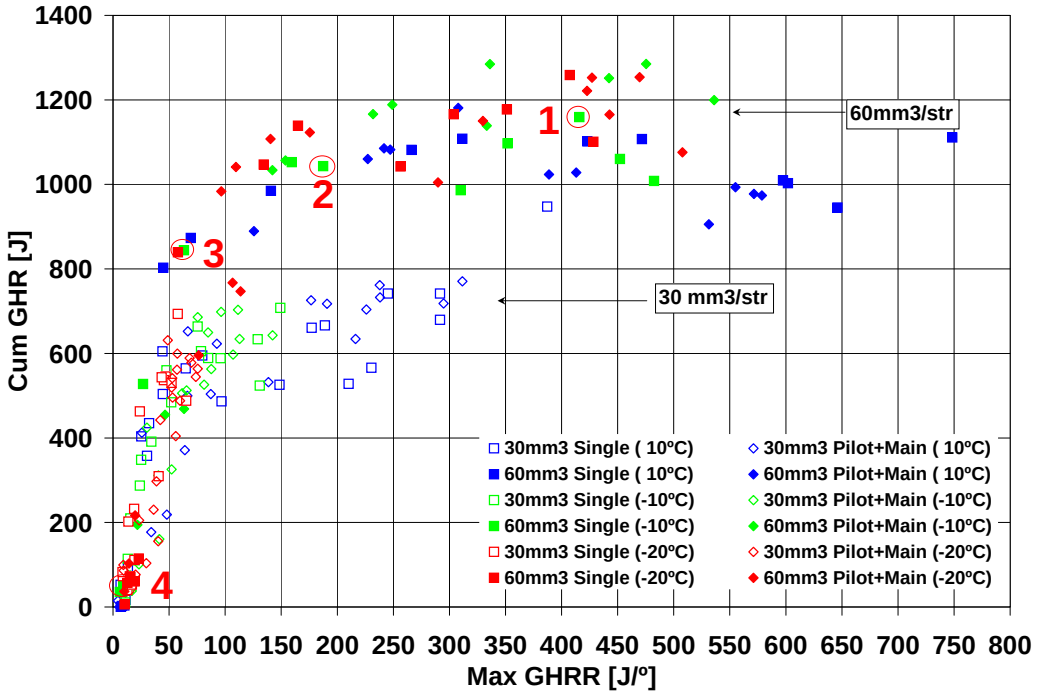

Figure 6.13: Maximum Gross Heat Release Rate vs. Cumulative Gross Heart Release for all collected data during 300 rpm timing sweeps, LCR

There is a clear correlation between low maximum rates of heat release and a low cumulative total for poor burning cycles which have a maximum rate less than about 50 J/°. The increase in cumulative total is of the order of 10 J per 1 J/° increase in maximum rate. Therefore, in weak burning cycles, the rate of heat release plays an important role in sustaining combustion. However, the cumulative totals level off and become almost independent of the maximum rate of heat release once this exceeds values of 100–200 J/°. By implication, for a given fuel quantity injected there are a range of heat release patterns burning the same fraction of the fuel. In the high compression ratio case there is no clear separation of the results for the two fuelling levels examined. At LCR, the separation into two bands of data is obvious, with 60 mm^3/str releasing significantly greater energy at all timings as long as max GHRR > 150 J/°. At the highest rates of heat release over 500 J/° there is some reduction in maximum achievable cumulative burn. This is further evidence of advanced injection, particularly at warmer test temperatures, promoting excessive peak rates of heat release which are detrimental to combustion duration as they terminate before fuel/air mixing is complete.

The conditions giving rise to four points marked on each of Figures 6.12 and 6.13 have been examined in more depth. All the points represent first firing cycles for the single injection strategy of 60 mm^3/str at $-10°C$. The high and low compression ratio cases are paired to have the same injection timings. Details are summarised in Table 6.1. The heat release profiles are given in Figures 6.14–6.17.

Point	Timing [°ATDC]	CR	Peak GHRR [J/°]	Cumulative GHR [J]	IMEPg [bar]
1	0	HCR	662	908	10.06
		LCR	416	1151	12.71
2	7.5	HCR	356	1074	10.28
		LCR	187	1040	10.34
3	12.5	HCR	194	909	8.54
		LCR	63.4	840	7.38
4	17.5	HCR	9	58	-0.56
		LCR	9	49	-0.70

Table 6.1: Comparison of data for high and low compression cases covering 4 single injection timings at a fixed quantity of 60 mm^3/str 300 rpm, $-10°C$

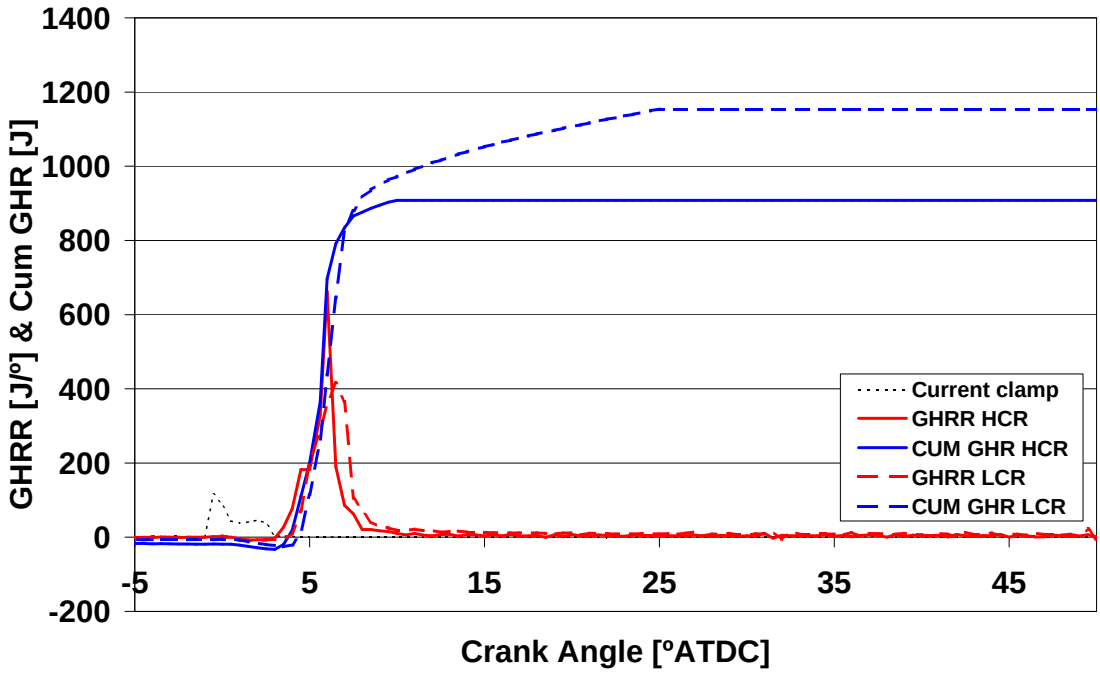

Figure 6.14: Point 1 — First cycle Gross Heat Release Rate and Cumulative Gross Heat Release, HCR vs. LCR, single injection, 60 mm^3/str TDC, 300 rpm, $-10°C$

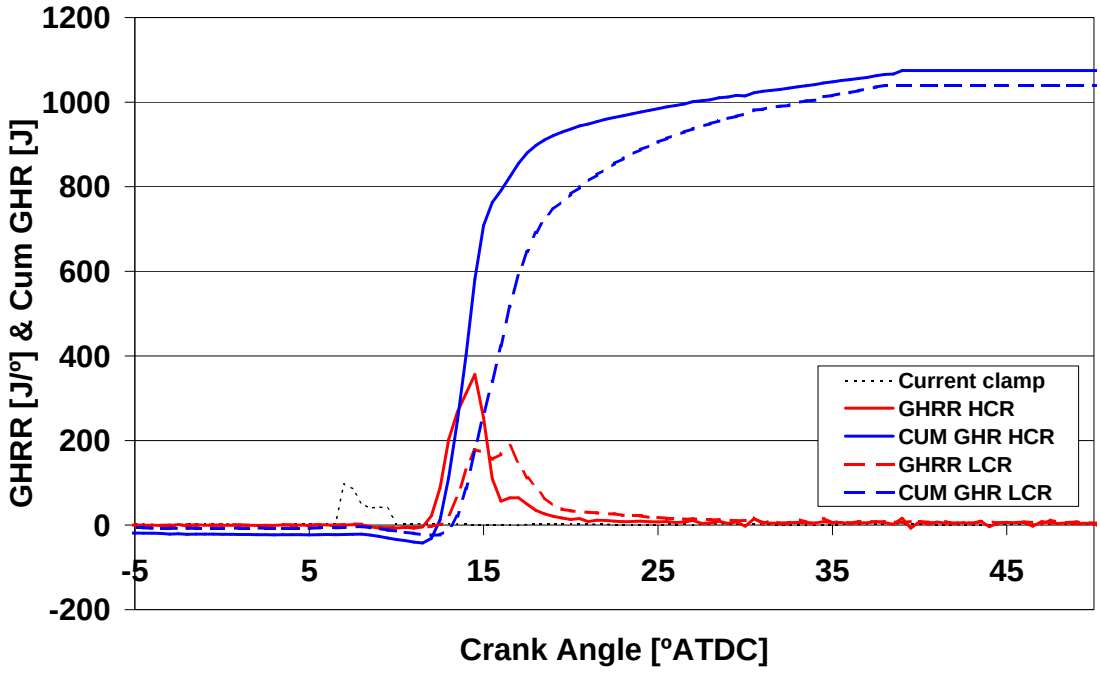

Figure 6.15: Point 2 — First cycle Gross Heat Release Rate and Cumulative Gross Heat Release, HCR vs. LCR, single injection, 60 mm^3/str 7.5°ATDC, 300 rpm, $-10°C$

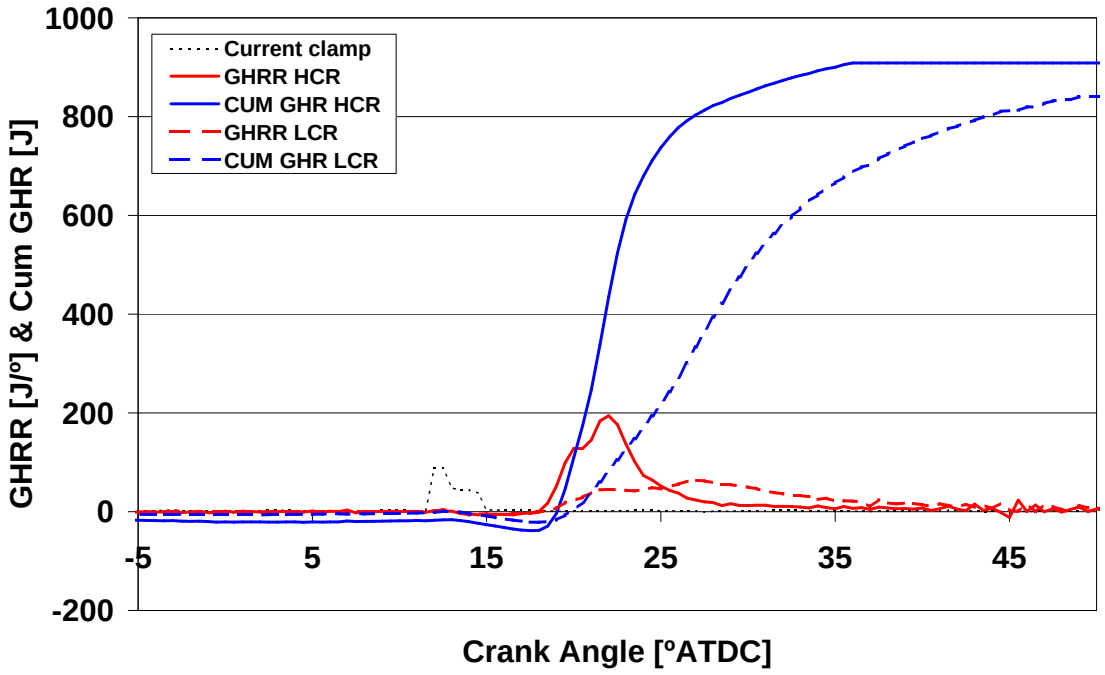

Figure 6.16: Point 3 — First cycle Gross Heat Release Rate and Cumulative Gross Heat Release, HCR vs. LCR, single injection, 60 mm^3/str 12.5°ATDC, 300 rpm, $-10°C$

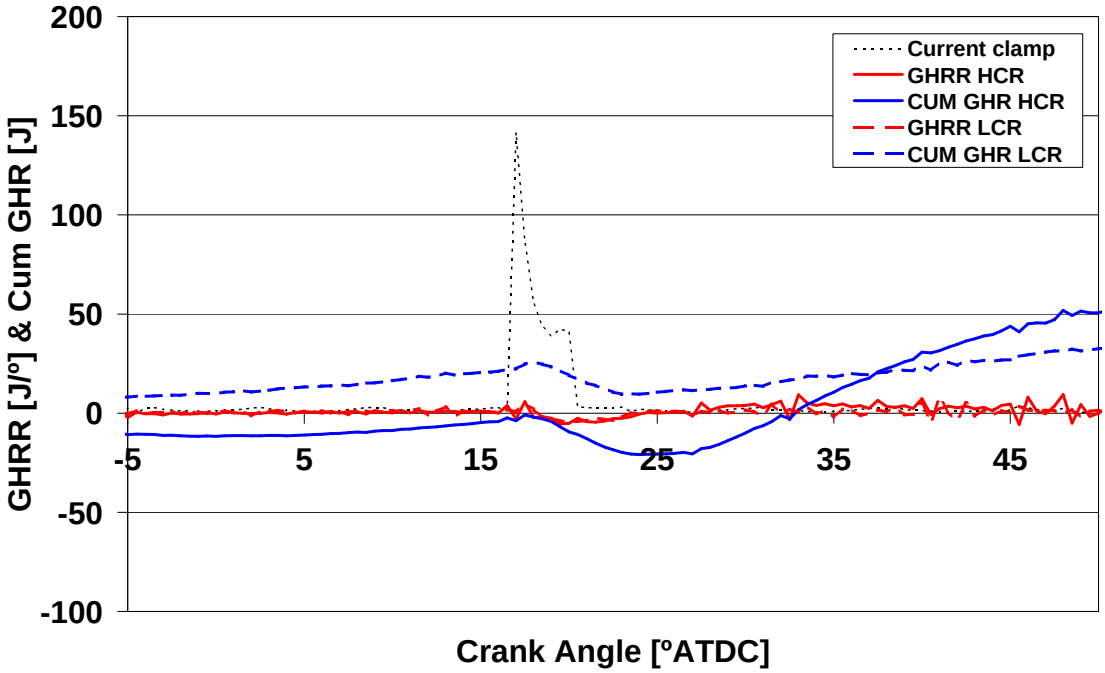

Figure 6.17: Point 4 — First cycle Gross Heat Release Rate and Cumulative Gross Heat Release, HCR vs. LCR, single injection, 60 mm^3/str 17.5°ATDC, 300 rpm, $-10°C$

For points 1–3, the peak rate of heat release is higher for the HCR case. Injection is too retarded in point 4 for any significant combustion. For the HCR case relative to the corresponding LCR value, the cumulative heat release is lower for point 1, and higher for points 2–4. The IMEPg values are dictated by the cumulative heat release in these cases and follow the same pattern of being lower for point 1 and higher for the other combusting points. The high peak rate of heat release for HCR point 1 brings about early termination of combustion, possibly due to insufficient mixture preparation time. The effect of retarding injection timing, from TDC for point 1 to 17.5°ATDC for point 4, on combustion phasing appears to be less important than its effect on cumulative heat release. For point 1, heat release continues longer for the LCR case, accounting for almost all the positive difference in the cumulative totals. For the more retarded timings, LCR shows the disadvantage of relatively low rates of early heat release which persist well into the expansion stroke. Points 1 and 2 show a slight extension of ignition delay from the reduction in compression ratio in the order of 0.5–1°, despite theoretically similar compression temperatures. This is further evidence of the temperature independent pressure effect on mixture preparation as found in the literature [33, 98].

The effect of adding a pilot injection prior to the main injection for points 1 and 3, timings just in advance and retard of the optimum is depicted in Figures 6.18 and 6.19.

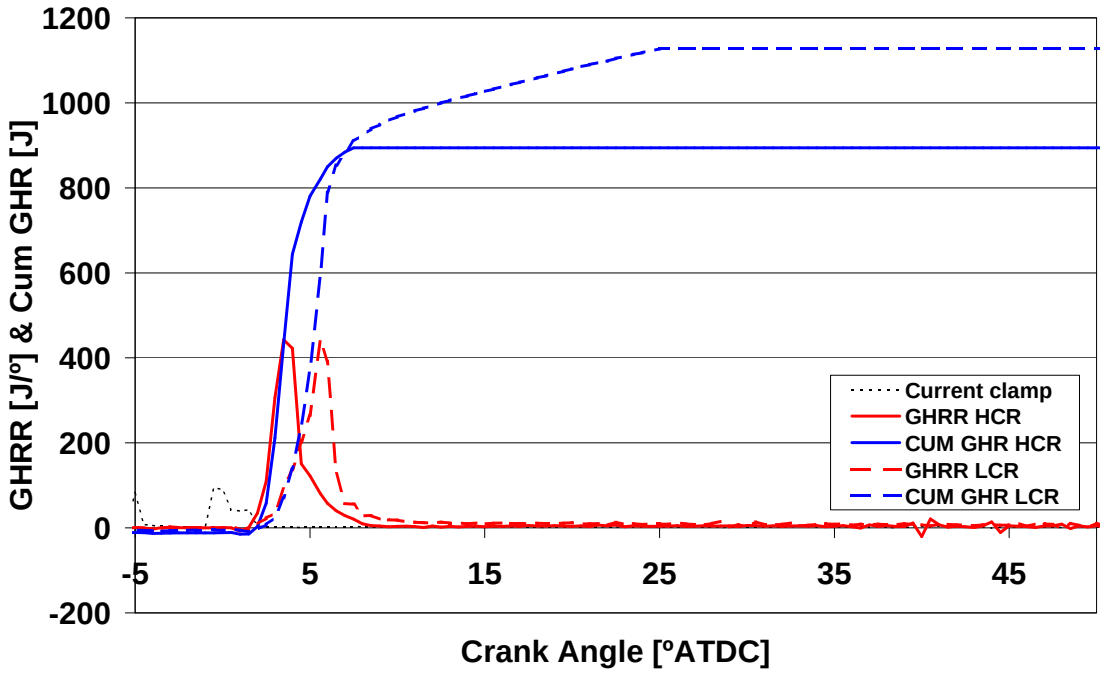

Figure 6.18: Point 1 — First cycle Gross Heat Release Rate and Cumulative Gross Heat Release, HCR vs. LCR, pilot+main injection, [2,58] mm^3/str TDC, 300 rpm, $-10°C$

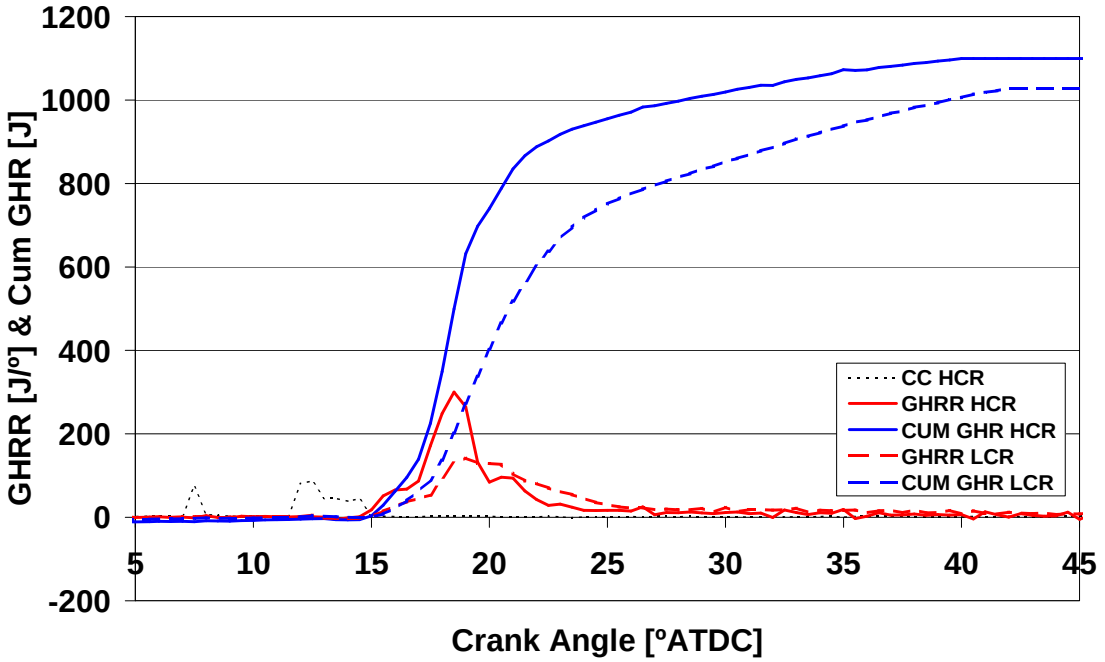

Figure 6.19: Point 3 — First cycle Gross Heat Release Rate and Cumulative Gross Heat Release, HCR vs. LCR, pilot+main injection, [2,58] mm^3/str 12.5°ATDC, 300 rpm, $-10°C$

The addition approximately halved the ignition delay of the main to 2.5° at point 1. This resulted in a reduced premixed combustion spike for TDC injection in the HCR case, but made little difference at LCR. The total fuel burnt was similar to single main injection, again showing problems with complete mixing for HCR, with further reduced ignition delay resulting in combustion close to TDC. For the retarded case, pilot injection substantially raised cumulative heat release, by around 200 J for both compression ratios compared to when fuel was delivered in a single injection. The total fuel burn is only 20% less for LCR when compared to TDC and actually 10% better than HCR achieved at TDC. This can all be linked with cool flame reactions of the pilot creating an activated environment in which to inject the main.

The heat release results of a pilot plus main 30 mm^3/str injection strategy are presented in Figures 6.20–6.22. These cover advanced, TDC and retarded injection timings respectively, at a temperature of $-10°C$. Peak and cumulative heat release, as well as IMEPg values for the low and high compression ratio cases are compared in Table 6.2.

Point	Timing [°ATDC]	CR	Peak GHRR [J/°]	Cumulative GHR [J]	IMEPg [bar]
a	-15	HCR	165	523	4.75
		LCR	81	522	6.72
b	0	HCR	238	850	7.79
		LCR	191	715	6.47
c	15	HCR	68	339	2.69
		LCR	41	158	1.79

Table 6.2: Comparison of data for high and low compression cases covering 3 pilot+main main injection timings at a fixed total quantity of 30 mm^3/str and $-10°C$, 300 rpm

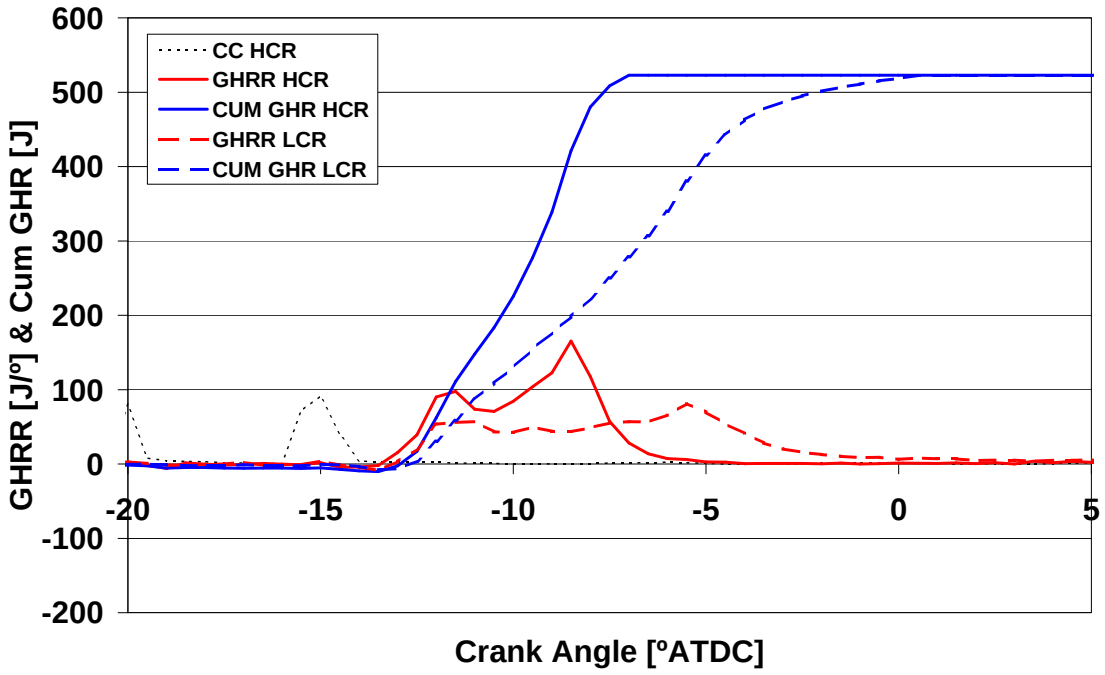

Figure 6.20: Point a — First cycle Gross Heat Release Rate and Cumulative Gross Heat Release, HCR vs. LCR, pilot+main injection, [2,28] mm^3/str 15°BTDC, 300 rpm, $-10°C$

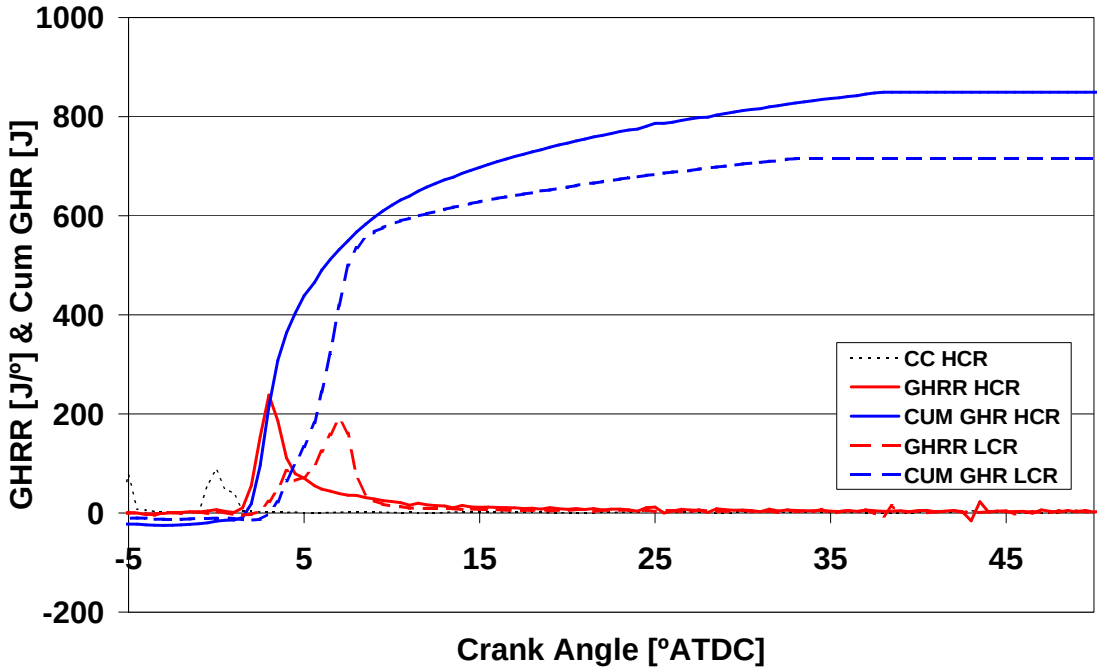

Figure 6.21: Point b — First cycle Gross Heat Release Rate and Cumulative Gross Heat Release, HCR vs. LCR, pilot+main injection, [2,28] mm^3/str TDC, 300 rpm, $-10°C$

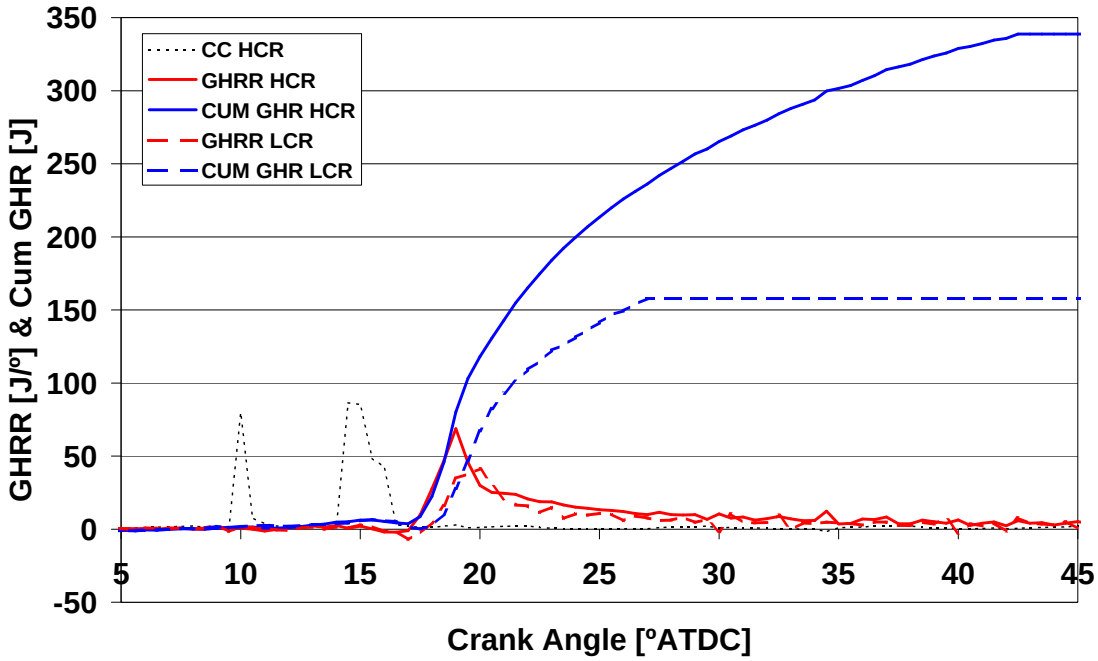

Figure 6.22: Point c — First cycle Gross Heat Release Rate and Cumulative Gross Heat Release, HCR vs. LCR, pilot+main injection, [2,28] mm^3/str 15°ATDC, 300 rpm, $-10°C$

In general, the results are similar to those at the high fuelling with any fall in IMEPg becoming more pronounced. As indicated by the results for point a, it was possible to inject well in advance of TDC in the low fuelling case, but the heat release and IMEPg data show that this is not an optimum strategy. The peak heat release is reduced and combustion duration is much longer with a second peak occurring as cylinder temperatures increase towards TDC. Using the same timing in the HCR case results in the same cumulative heat release as for LCR, but the IMEPg is much reduced, indicating that losses to heat transfer and blowby were higher during the compression stroke. At the low fuel injection quantity, a higher peak rate of heat release and greater cumulative total are achieved at the higher compression ratio at timings just in advance of and after TDC.

Better fuel preparation and more complete combustion are achieved where $\phi < 1$. However, when $\phi >1$ at the 60 mm^3/str fuelling and timing is optimised, higher $\overline{IMEPg_5}$ values are achieved at the lower compression ratio. The reason becomes clear when IMEPg contributions for each crank angle in the cycle are compared. The motored cycle before injection is considered in Figure 6.23.

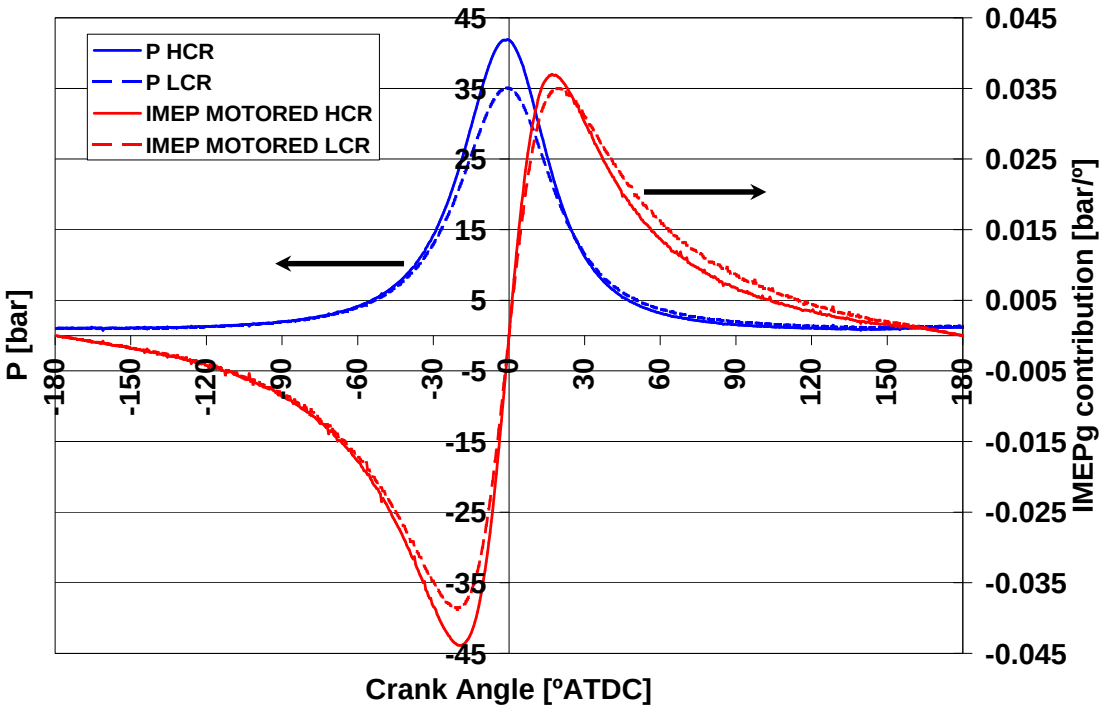

Figure 6.23: Comparison between crank angle resolved IMEPg contributions at HCR and LCR for the final motored cycle, 300 rpm , $-10°C$

It is clear that the extra work input required to compress the air from LCR to HCR conditions is not recouped in the expansion stroke. As this is a motored cycle with no heat input from combustion, this may only be attributed to losses as discussed at the beginning of this chapter. Even simply considering the peak IMEPg contribution values before and after TDC, the 0.0054 bar/° extra indicated work input required for compression at 18°BTDC HCR only results in 0.0020 bar/° more work obtained in the same period after TDC. IMEPg contributions from LCR quickly become greater than HCR for the whole power stroke. The IMEPg contributions for the first injected cycle in a TDC single 60 mm^3/str injection at $-10°C$ is plotted in Figure 6.24. The heat release for this case was given in Figure 6.14.

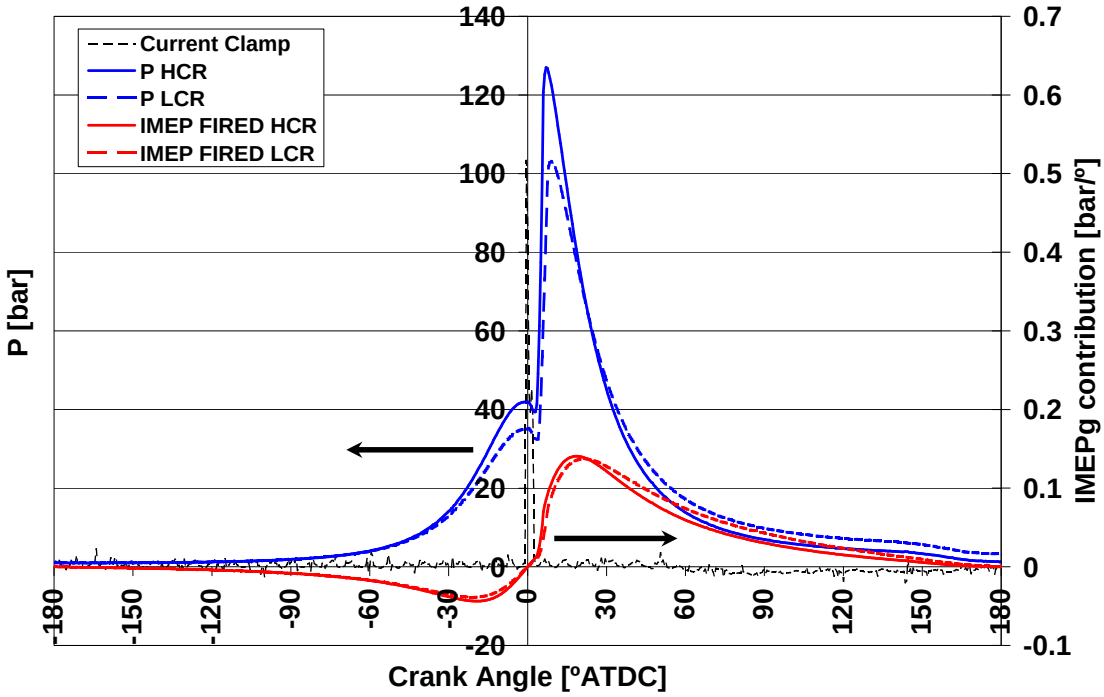

Figure 6.24: Comparison between crank angle resolved IMEPg contributions at HCR and LCR for the first fired cycle, TDC single injection 60 mm^3/str, 300 rpm , $-10°C$

The faster rate of burn for HCR leads to an earlier increase in cylinder pressure to a higher peak and a greater initial IMEPg contribution until the lines cross over at 21°ATDC. The running IMEPg difference between HCR and LCR for both motored and fired cycles is plotted in Figure 6.25.

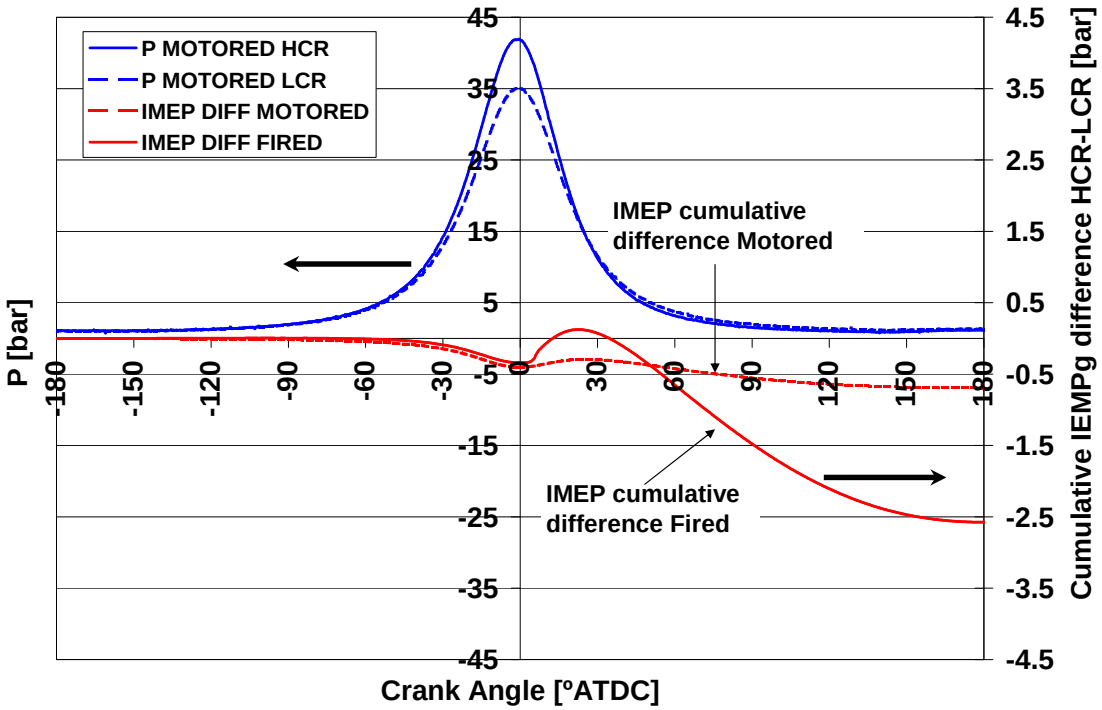

Figure 6.25: Comparison between crank angle resolved running IMEPg difference at HCR and LCR for the last motored and first fired cycles, TDC single injection 60 mm^3/str, 300 rpm , $-10°C$

In the motored case LCR achieves a cumulative IMEPg advantage of 0.47 bar over HCR. The difference for the first fired cycle is a more significant 2.65 bar improvement for the LCR cycle, the majority of which is gained in the middle of the power stroke, after combustion termination. Analysis of Figures 6.26 and 6.27 help to explain this. The cumulative heat release is plotted against IMEPg for the first cycles of all tests in this investigation, first at HCR then LCR.

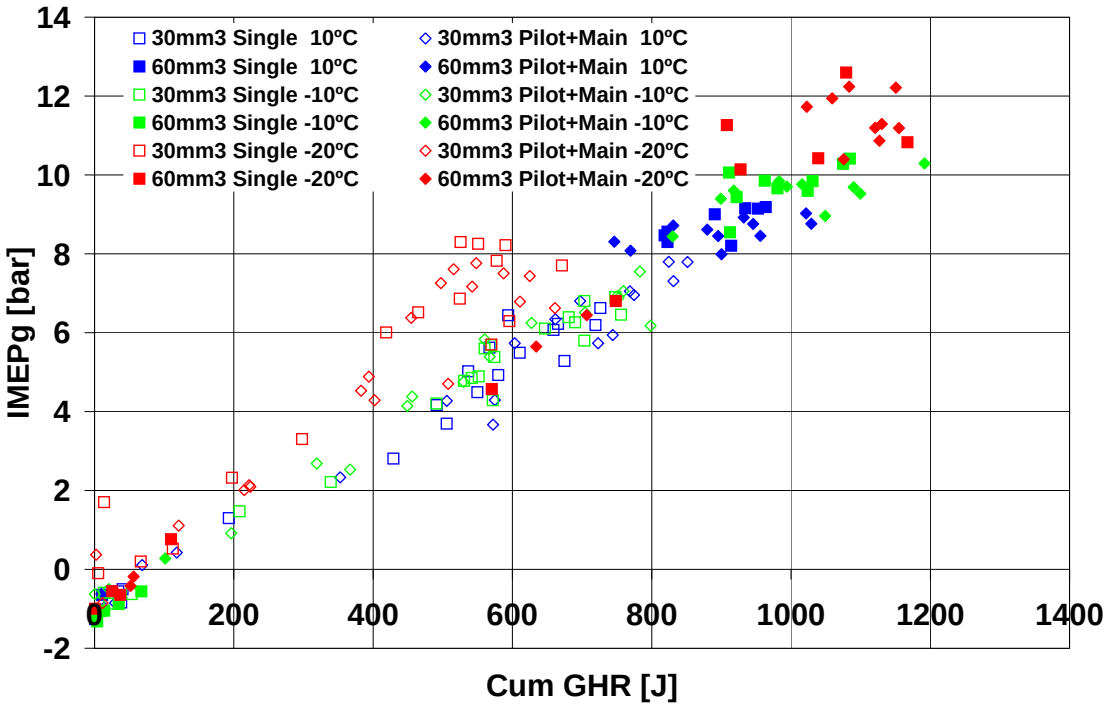

Figure 6.26: Comparison between first cycle IMEPg and first cycle cumulative heat release for all gathered data at HCR

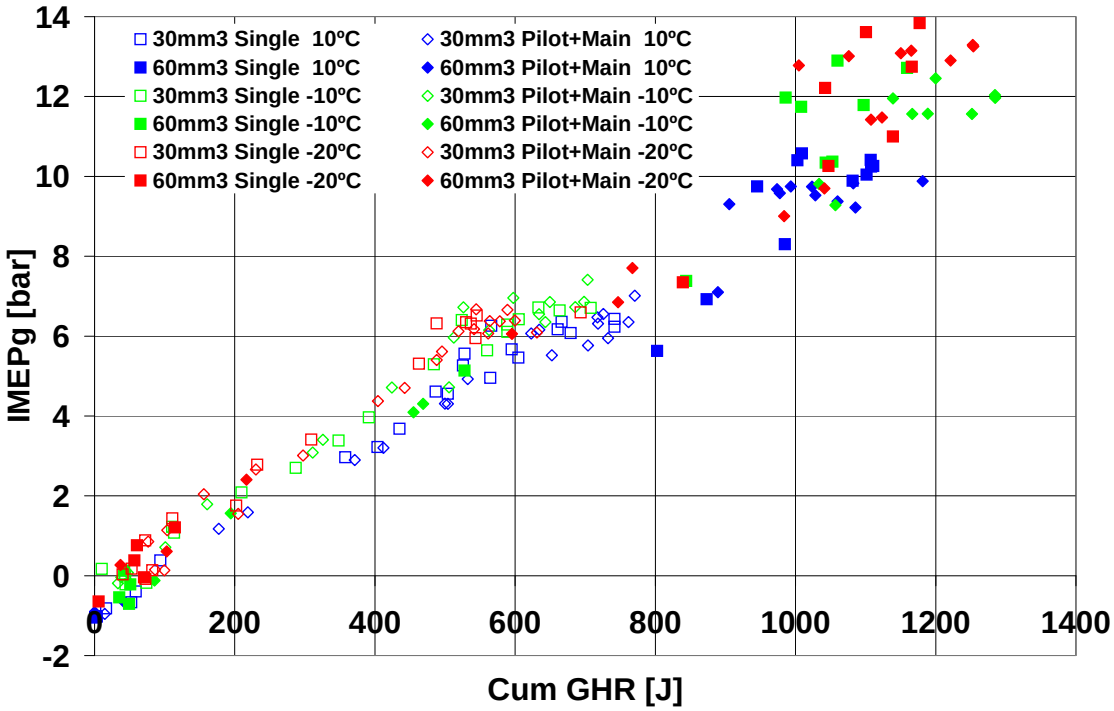

Figure 6.27: Comparison between first cycle IMEPg and first cycle cumulative heat release for all gathered data at LCR

In both the above figures, there is a relationship in which approximately 100 J of heat release results in 1 bar IMEPg. Slightly less heat release is required at LCR than HCR per bar IMEPg, again showing the higher thermal efficiency from reduced losses. At peak work output, LCR both releases more energy from the fuel and better converts this to work, resulting in the significant peak IMEPg advantage found at LCR. At low fuelling there is better fuel preparation at HCR due to higher pressures. This results in greater combustion efficiency, mitigating the lower thermal efficiency. For the case shown in Figures 6.14 and 6.24, the cumulative heat release for the LCR case is approximately 250 J more than the value for HCR, principally because of the extended duration of late, low-level heat release. The higher cumulative total translates into a 2.65 bar higher IMEPg value.

Higher heat transfer and blowby combine with lower cumulative fuel burn at HCR to cause the crossing over of the pressure traces evident in Figure 6.24. The lower total fuel burn in the HCR case is likely a result of a combination of high rates of heat release that bring an early end to combustion before available oxygen has thoroughly mixed with the fuel and lower total oxygen availability due to blowby in this heavily rich environment. Slightly retarded injection timings with lower rates of heat release and longer burns see no increase in IMEPg or cumulative burn. This suggests that blowby may be a greater problem than the low calculated motored losses would suggest. Blowby losses on a typical motored cycle calculated using flow through an orifice were approximately 3%. Cheng [86] found that effective ring gap area had to be increased for fired tests. In some cases, a doubling of ring gap area was required to match modelled blowby with higher cylinder pressures resulting in 4–5 times greater measured blowby (up to 50% mass fraction) at initial start. A strong link was found with high blowby and early termination of combustion, and therefore it is possible that short combustion durations at HCR are partially caused by reduced oxygen availability that stems from increased blowby. Both blowby and heat transfer are exacerbated by higher in-cylinder pressures in the high fuelling cases. In the low fuelling cases it is clear that the advantage of HCR is better combustion of the lean mixture. This outweighs the greater losses of HCR by boosting cylinder pressure high enough over LCR to avoid the crossover seen in high fuelling tests.

The strong relationship between IMEPg and cumulative heat release holds regardless of injection timing, quantity, compression ratio or number of injections per cycle. IMEPg depends more on burning the fuel than phasing — it appears injection timing is crucial not to optimally phase combustion with TDC, but because if the fuel is injected into a region with insufficient temperature and oxygen density it will not combust as fully and/or may penetrate to the bowl and walls where it cannot burn. Similarly, in HCR high fuelling, if the combustion is phased too close to TDC the rate of heat release is too high, resulting in early end of combustion linked to insufficient mixing duration and high pressure blowby drawing away oxygen. The importance of injection timing for fuel combustion is highlighted in Figures 6.28 and 6.29, where combustion efficiency and thermal efficiency are compared for the sweep of injection timings at LCR. Whilst combustion efficiency can rapidly drop to zero after TDC, especially at reduced fuelling, thermal efficiency remains over 40% for most of the data gathered.

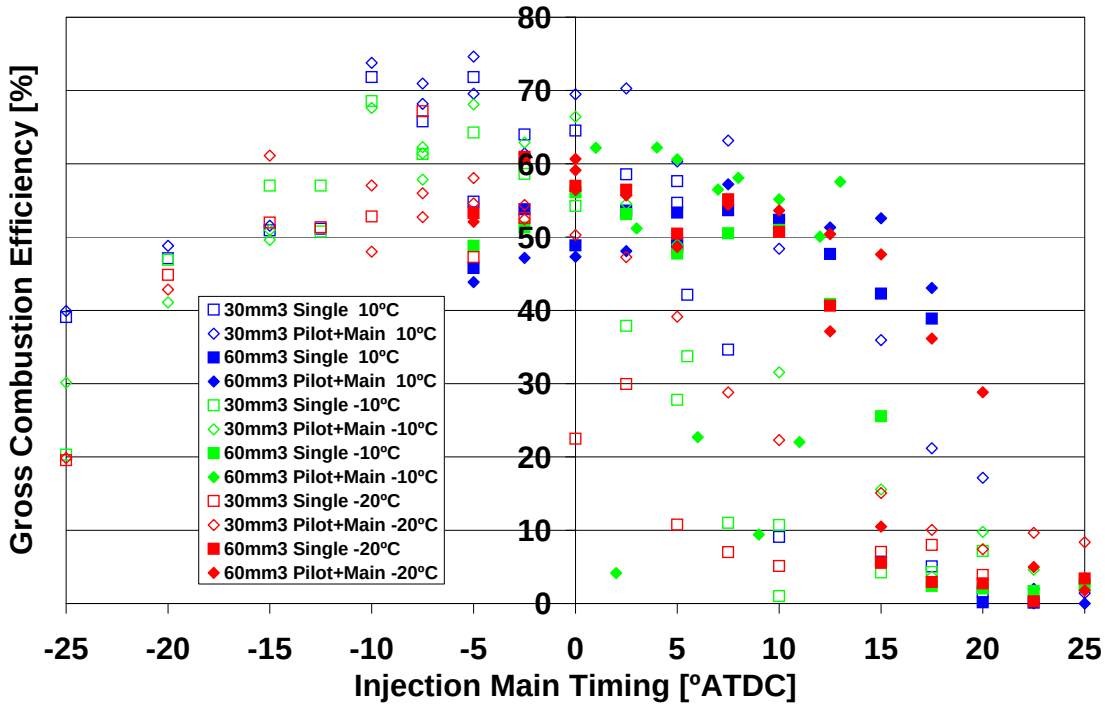

Figure 6.28: Indicated combustion efficiency across a sweep of injection timings for all data collected at LCR

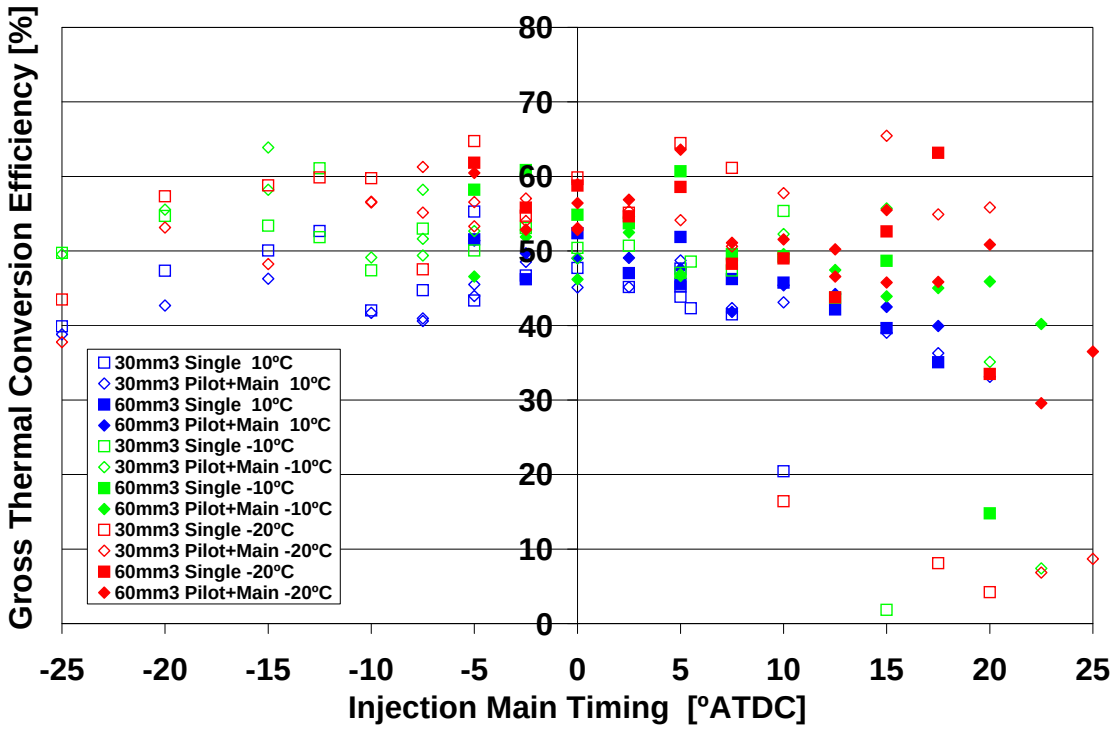

Figure 6.29: Indicated thermal conversion efficiency across a sweep of injection timings for all data collected at LCR

6.5 The Effect of Reducing Temperature on LCR Cold Start

Parallels with effects at high vs. low compression ratio were found when considering heat release analysis of LCR whilst varying test temperature. Figures 6.30 and 6.31 plot the heat releases for the first fired cycle with a single injection (60 mm^3/str then 30 mm^3/str) at TDC, LCR at the three temperature levels.

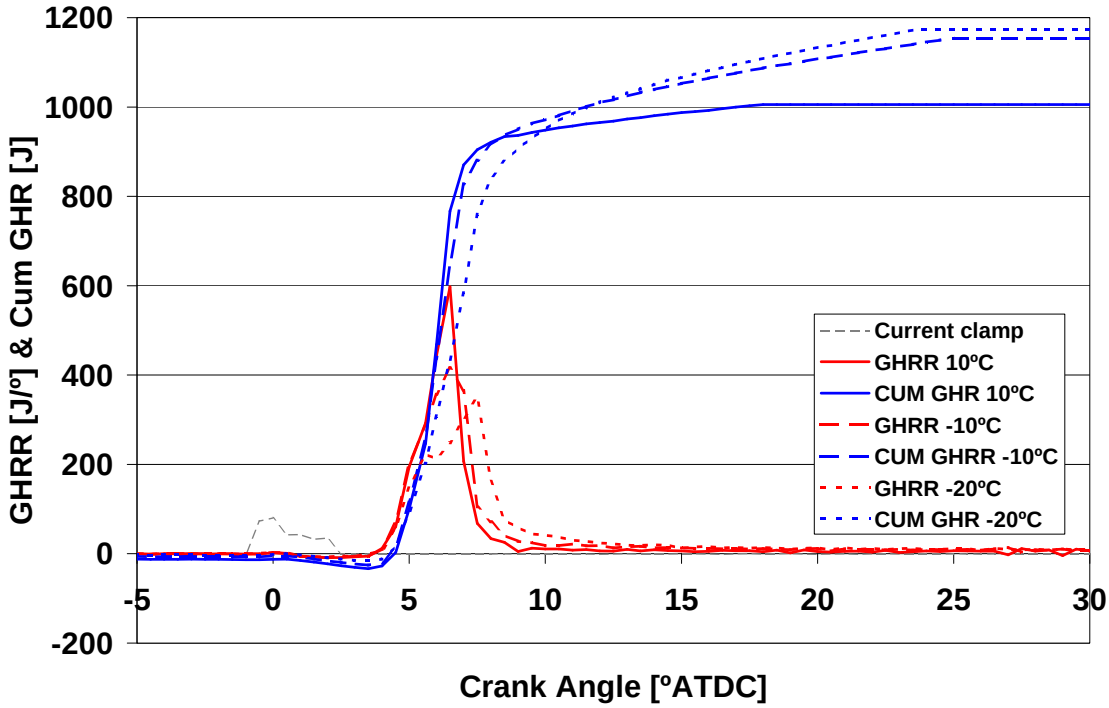

Figure 6.30: Effect of varying ambient temperature on heat release, TDC single injection 60 mm^3/str, 300 rpm, LCR

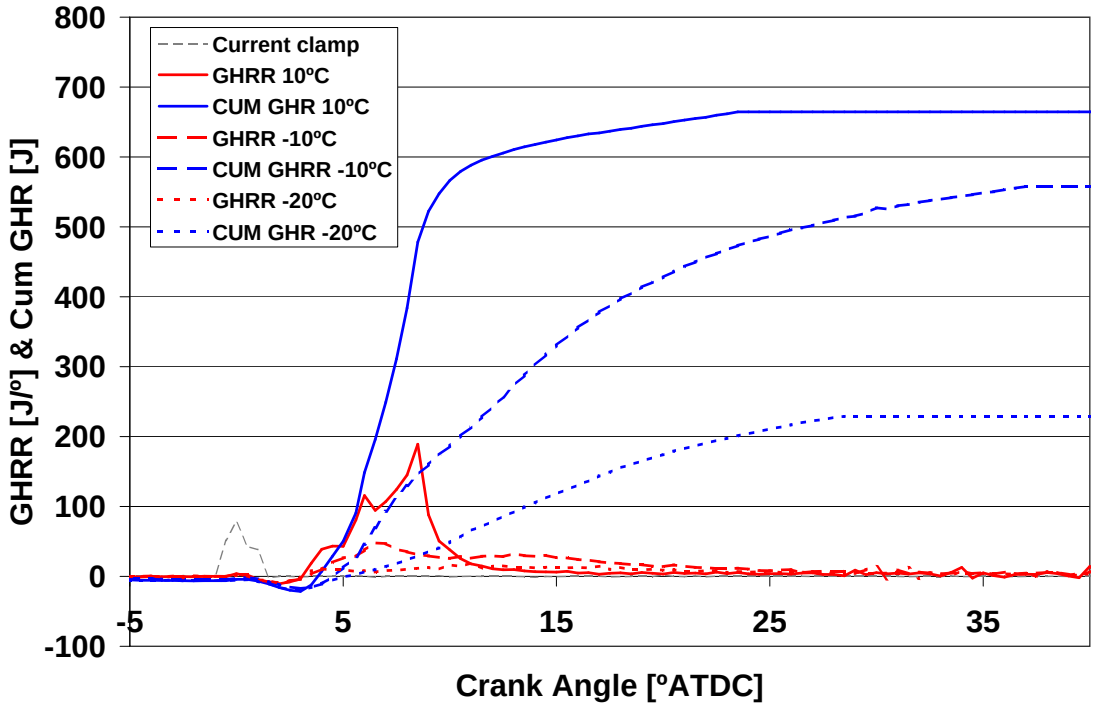

Figure 6.31: Effect of varying ambient temperature on heat release, TDC single injection 30 mm^3/str, 300 rpm, LCR

In the high fuelling case the ignition delays are identical and the rate of heat release continues to accelerate to the peak of combustion at $10°C$, whilst the rate of acceleration slows after combustion initiation at $-10°C$, reaches a lower peak, but has a longer duration and a greater cumulative burn. At $-20°C$ this trend continues with a second distinct increasing phase of combustion followed by a prolonged diffusion burn. In the low fuelling case the effects are more significant — all of the heat releases are quite faltering at this unstable condition, but the positive ambient temperature has the clear advantage. Both negative ambients have very low peak rates of heat release and diffusion burns over 25° in duration, with the $-20°C$ case approaching misfire. The effects of reducing ambient temperature are analogous to those of reducing compression ratio. For $\phi > 1$ higher cumulative burn is achieved at low temperatures due to lower peak rates of heat release with longer, more complete burn periods. For $\phi < 1$, higher temperatures have the advantage promoting better fuel preparation and more rapid, complete burn. As intake air temperature is decreased, its density increases giving more oxygen availability. Again this is analogous to reduction in compression ratio as lower cylinder pressures may lead to reduced blowby and greater

trapped mass and oxygen availability.

To summarise findings for 300 rpm operation at LCR, very similar trends have been found to those at HCR. Higher maximum work output is achievable due to reduced losses and reduced peak rates of heat release which allow longer, more complete diffusion burns, but this also leads to more severe reduction in IMEPg as timing is retarded.

6.6 Cold Idle Comparisons

High work output at 300 rpm should ensure a fast run-up to idle speed operation at LCR. The much reduced losses at LCR were found to diminish with speed such that, above 600 rpm, motored cylinder pressure at HCR was sufficiently higher than LCR to ensure that calculated gas temperatures were higher as expected. Due to the lower fuellings required for idle operation and the significantly worse fuel preparation expected at LCR idle speed, there are doubts about idle stability. Acceptable operation was achievable at $-20°C$ HCR only by use of multiple pilot injection. With reference to Figure 5.42, Figure 6.32 repeats a sweep of engine speeds performed at HCR $-20°C$ with fixed injection timing to directly compare $\overline{IMEPg}_{10}$ and $\mathrm{CoV}_{\mathrm{IMEPg}}$. Results for 15 mm^3/str LCR are not plotted because no significant repeatable combustion was found at this condition and therefore $\mathrm{CoV}_{\mathrm{IMEPg}}$ values could be very high.

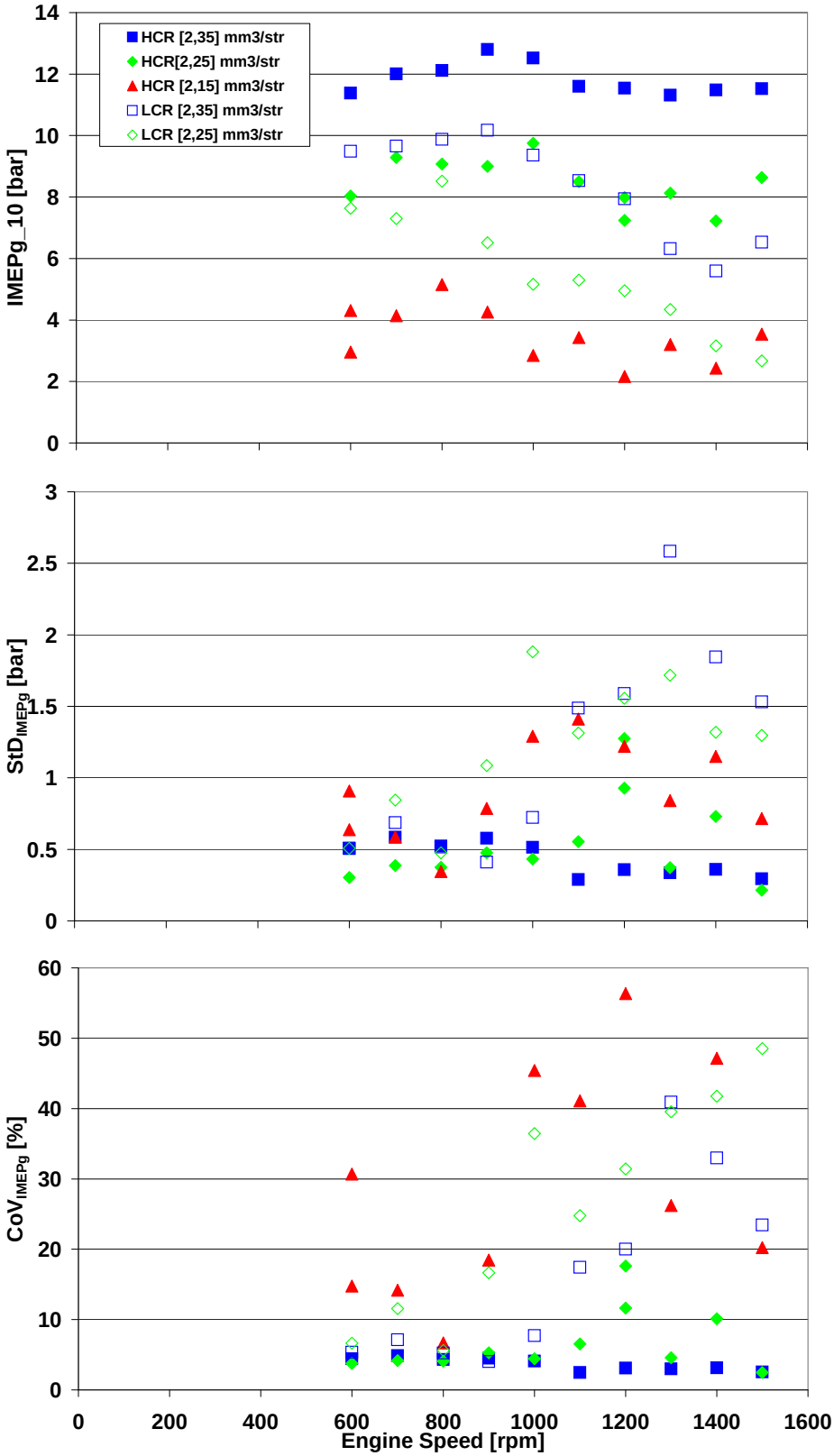

Figure 6.32: Comparison of cold idle behaviour varying engine speed for HCR and LCR, main timing 7.5°BTDC, $-20°C$

At each fuelling HCR performs better in terms of both IMEPg and stability. $\overline{IMEPg}_{10}$ and stability decrease markedly with increasing engine speed at LCR. This effect is much less significant at HCR which provides strong evidence that mixture preparation suffers at LCR because residence time at high temperature and pressure decreases at higher speed. Comparable results are achieved when considering 15 mm^3/str HCR with 25 mm^3/str LCR and similarly 25 mm^3/str HCR with 35 mm^3/str LCR. At typical cold idle speeds LCR work output using 15 mm^3/str is too low to defeat friction as well as unacceptably unstable. To interpret the difference between HCR and LCR, the cycle resolved IMEPg and heat release characteristics of an identical injection strategy have been analysed in Figure 6.33. In both cases the main quantity was 25 mm^3/str and a typical cold idle speed of 1100 rpm was chosen. This quantity delivers acceptable performance at most speeds for HCR, but not at any speed above 600 rpm for LCR.

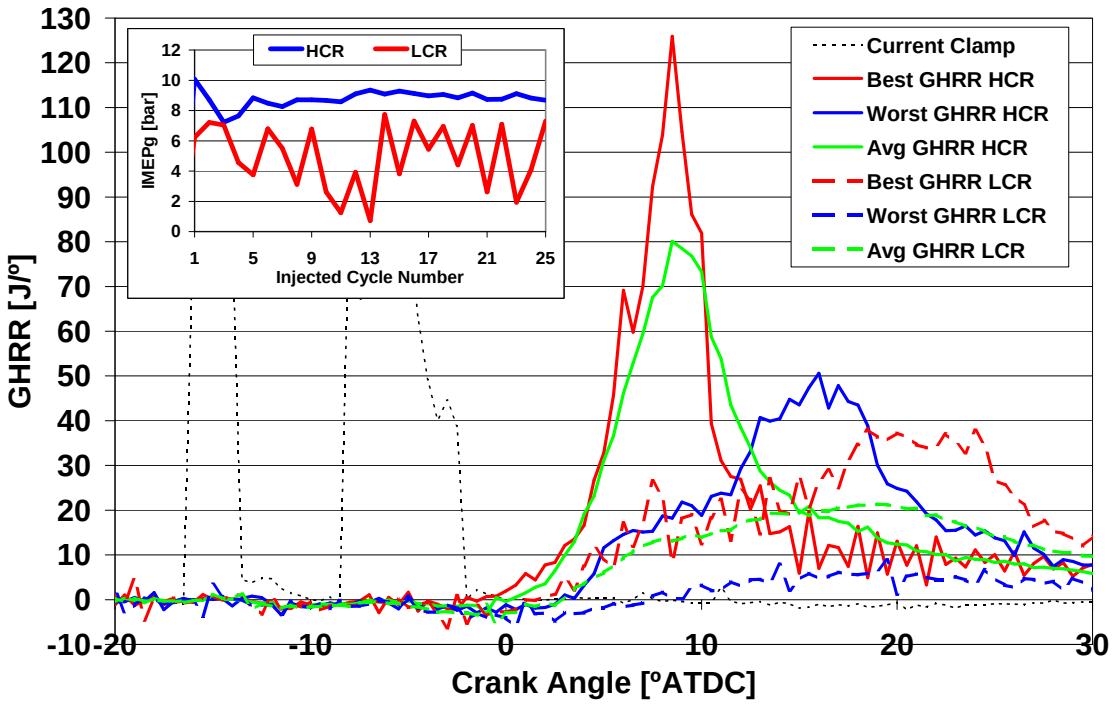

Figure 6.33: Comparison of maximum, minimum and average heat release profiles at high and low compression ratio, main timing 7.5°BTDC [2,25] mm^3/str, $-20°C$, 1100 rpm. $\text{CoV}_{\text{IMEPg}}$ HCR=6.5% $\text{CoV}_{\text{IMEPg}}$ LCR=24.8%

The cycle-to-cycle variations in IMEPg show that the LCR case is relatively unstable. The standard deviation is 1.31 bar compared to 0.55 bar for the HCR results. The LCR case does not reach stable operation within 25 cycles. The heat release profiles are lower and

more extended for the LCR case, with much greater difference between the average and the best. The lowest HCR heat release profile is similar to that of the best for the LCR. The early parts of the heat release variations are very similar, but the peak occurs earlier for the HCR case, reflecting the effect of higher pressures and temperatures and reducing the influence of variations in phasing on IMEPg. The picture this presents is similar to that for combustion and work output for low fuelling at 300 rpm, cold start conditions (see Figures 6.20–6.22) where combustion is also stronger for the HCR case. The similar effects of lowering either compression ratio or test temperature for low fuel injection conditions can be seen with reference to Figure 6.31; both are associated with lower rates and more extended durations of heat release giving lower cumulative totals.

Figure 6.34 illustrates the responses to a small sweep of main injection timing at 1100 rpm to ensure the poor results were not due to inappropriate injection timing. This study was performed at the less extreme $-10°C$, but there are still no points of acceptable $\mathrm{CoV_{IMEPg}}$.

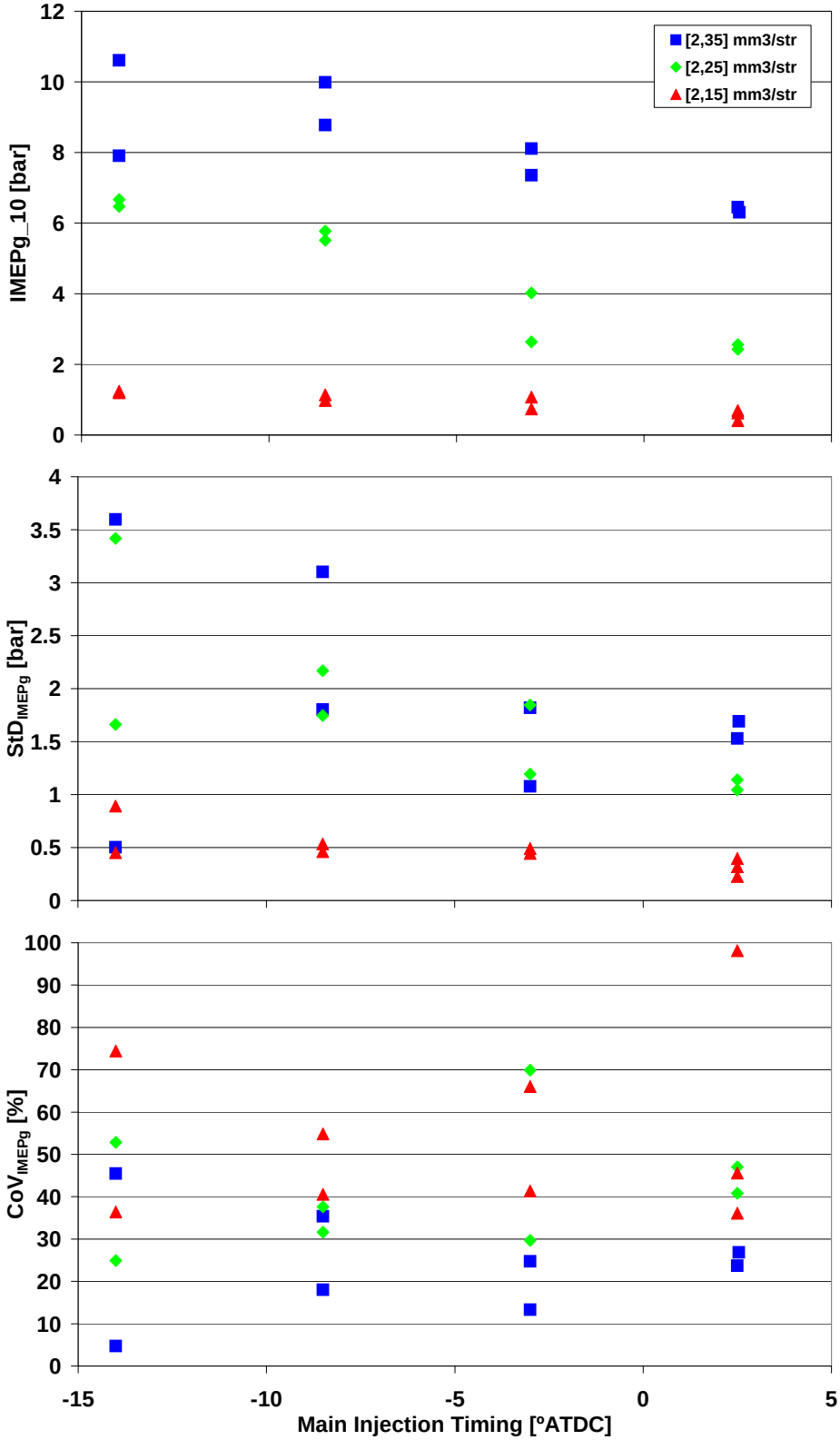

Figure 6.34: Comparison of cold idle behaviour varying injection timing, 1100 rpm, [2,25] mm^3/str, $-10°C$, LCR

Higher IMEPg is produced at the more advanced timings, but this is offset by a degradation in standard deviation, as multiple misfires have a greater effect at the high load. Repeat testing shows that there is great potential for variability, even at the same test point at the advanced timing.

Heat release analysis of the medium fuel quantity at the most advanced and retarded injection timings is given in Figures 6.35 and 6.36. In each case both repeats are plotted along with their IMEPg variation through the 25 injected cycles.

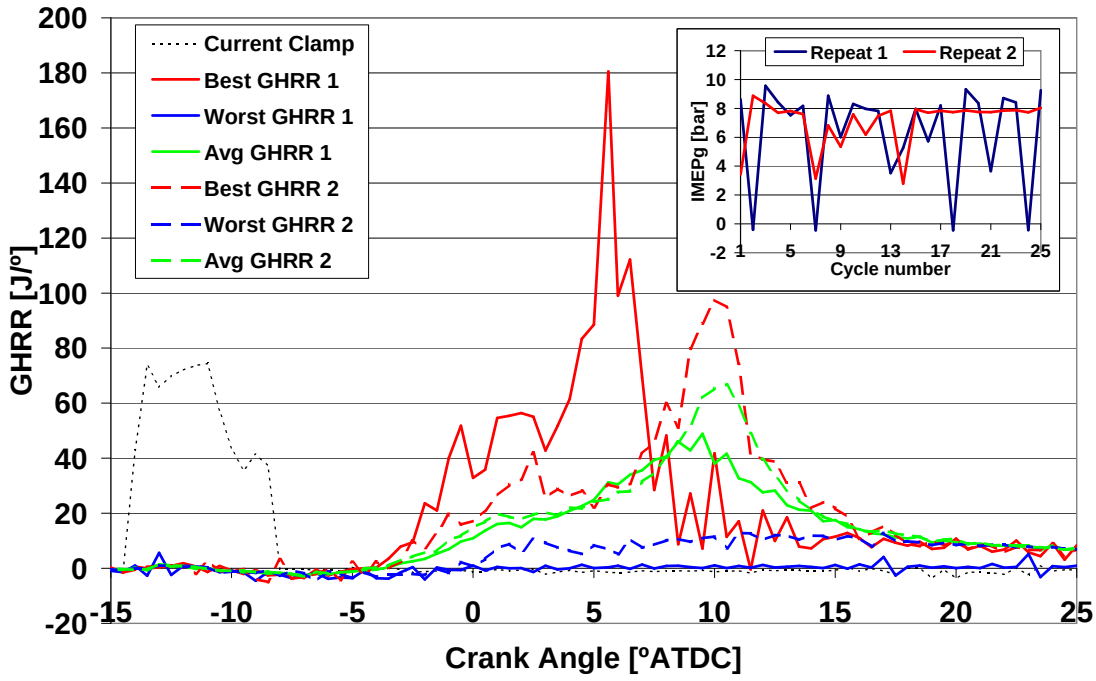

Figure 6.35: Comparison of maximum, minimum and average heat release profiles for two repeats, main timing 14°BTDC [2,25] mm^3/str, $-10°C$, 1100 rpm, LCR. CoV_{IMEPg} 1=54.8% CoV_{IMEPg} 2=24.9%

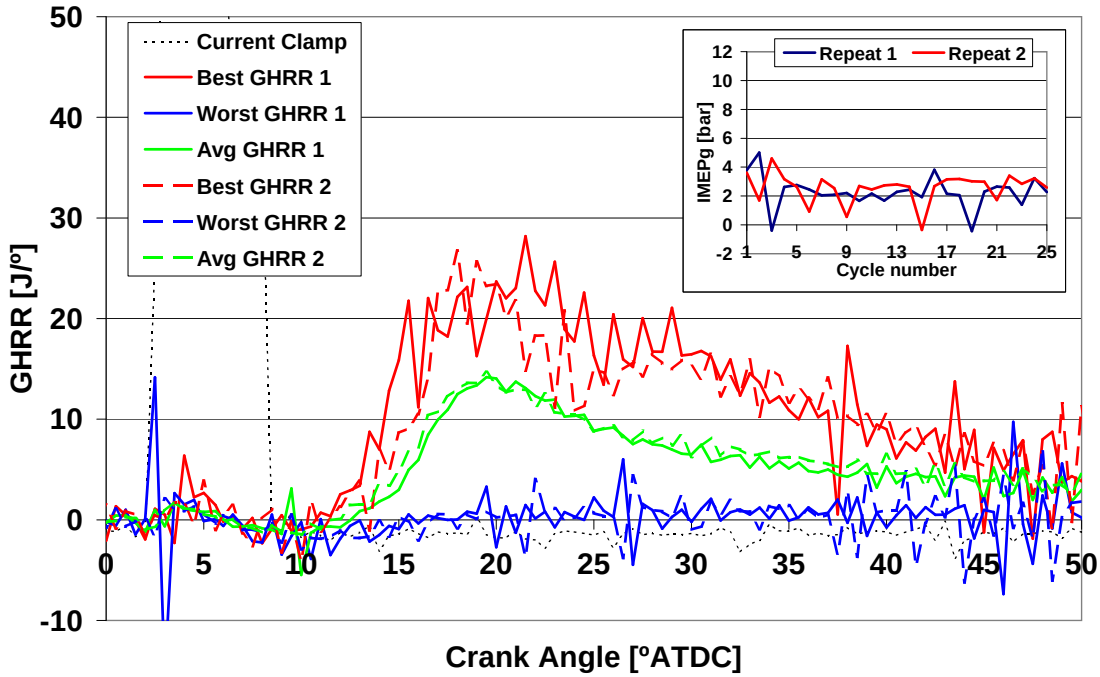

Figure 6.36: Comparison of maximum, minimum and average heat release profiles for two repeats, main timing 2.5°ATDC [2,25] mm^3/str, $-10°C$, 1100 rpm, LCR. CoV_{IMEPg} 1=47.0% CoV_{IMEPg} 2=40.8%

There is a great variability in both shape and completion of heat release profiles, especially at the advanced injection timing, where the two repeats produce significantly altered traces. With reference to Figure 5.49, a sweep of injection timings at HCR with both reduced fuelling and lower $-20°C$ temperature, a drop in $\overline{IMEPg}_{10}$ from around 4–3 bar is experienced over a similar range of injection timings. Here, the drop is 6–2 bar with 25 mm^3/str, indicating just how poor the conditions are for combustion.

In summary, at higher speeds representative of cold idle, the reduced fuel preparation rates of LCR become severely detrimental to both combustion efficiency and combustion stability. Performance reduces with increasing engine speed in a way not seen at HCR. Significant extra fuel is required for similar work output to HCR and cycle-to-cycle variability, as well as test to rest repeatability is severely deteriorated to the point that no acceptable CoV_{IMEPg} results were obtained at appropriate load for $-20°C$ operation.

6.7 Multiple Pilot Injection at LCR

At high compression ratio it was found that a twin pilot fuel injection strategy could stabilise combustion, increasing average IMEPg and reducing $\mathrm{StD}_{\mathrm{IMEPg}}$. Some work was carried out at LCR to assess any positive effect of twin pilot operation at cold idle. Due to the various demands for testing time and the order in which tests were carried out, there are no detailed sweeps of injection timing or engine speed available at LCR to directly compare to HCR, but conclusions can still be drawn as detailed.

Figure 6.37 compares $\overline{IMEP}g_{10}$ and $\mathrm{CoV}_{\mathrm{IMEPg}}$ for 1000 rpm operation at $-10°C$. This data were not gathered in a pre-defined sweep, injection quantities and pilot splits were modified in an attempt to achieve 2 bar $\overline{IMEP}g_{10}$ with acceptable $\mathrm{CoV}_{\mathrm{IMEPg}}$. Main injection timing is fixed at 5.5°BTDC.

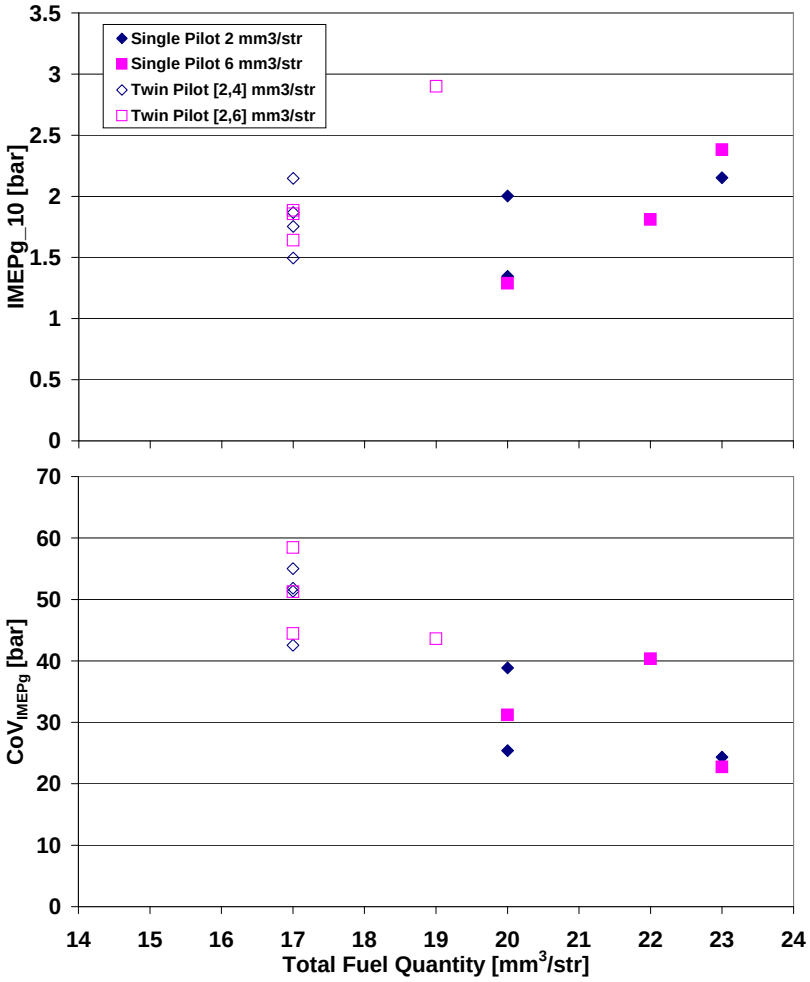

Figure 6.37: Comparison of cold idle behaviour varying pilot strategy, main timing 5.5°BTDC, 1000 rpm, $-10°C$, LCR

It was impossible to achieve $\mathrm{CoV_{IMEPg}} < 20\%$, twice the desired target. Twin pilot operation could not perform as well as single pilot, even when using a larger main quantity to increase work output. No results were found with $\mathrm{CoV_{IMEPg}} < 40\%$. Near identical $\overline{IMEPg}_{10}$ was achieved either utilising a twin pilot strategy of [2,4,11] $\mathrm{mm^3}$/str or single pilot of [2,21] $\mathrm{mm^3}$/str. Figure 6.38 illustrates how variability is derived from an increased spread of possible cycle resolved IMEPg values.

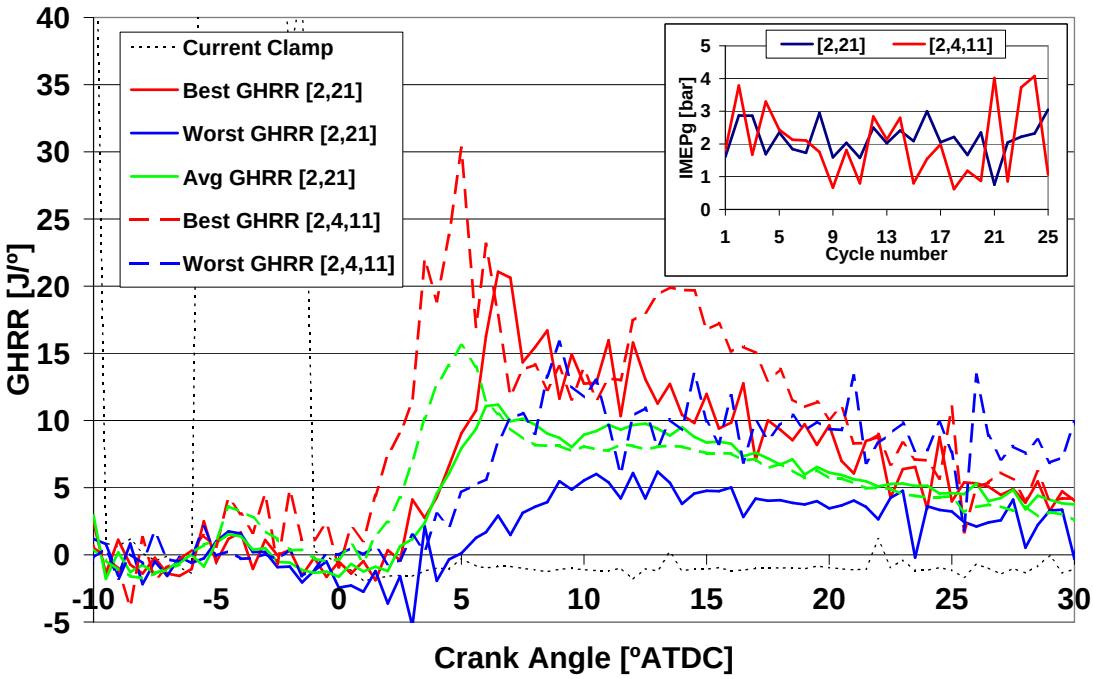

Figure 6.38: Comparison of maximum, minimum and average heat release profiles for single and twin pilot injection strategies both producing ≈ 2.15 bar $\overline{IMEPg}_{10}$, main timing 5.5°ATDC, $-10°C$, 1000 rpm, LCR. CoV_{IMEPg} [2,21] mm^3/str=24.4% CoV_{IMEPg} [2,4,11] mm^3/str=51.3%

In the single pilot case the best cycle IMEPg is just over 3 bar with the worst at 0.75 bar. The range 0.6–4 bar was recorded in the twin pilot strategy. There is evidence of second pilot combustion resulting in reduced and less variable ignition delay for twin pilot, generally leading to a higher peak rate of heat release and slightly shorter combustion duration. As was experienced at HCR multiple pilot, greater combustion efficiency is possible due to increased mixing, resulting in a second phase of accelerating heat release rate. This mechanism was used to boost poor cycles up to target IMEPg at HCR. It is only evident on the best cycles at LCR, in this case cycles 2, 21, 23 and 24. All other cycles display the same GHRR progression as found for single pilot operation. It appears that the same mixing phenomenon encountered at HCR is occurring at LCR, but that the temperatures and pressures of LCR are too low to take advantage of the improved mixing in all but the best cycles with significant early combustion. This, combined with reduced main quantity, leads to a wider spread of possible IMEPg and therefore a reduction in stability.

These findings were confirmed with further testing at higher load and 1400 rpm without

reducing fuelling for twin pilot operation. A total quantity of 27 mm^3/str was injected as either a pilot+main [2,25] mm^3/str or a twin pilot of [2,5,20] mm^3/str. These results are plotted in Figure 6.39.

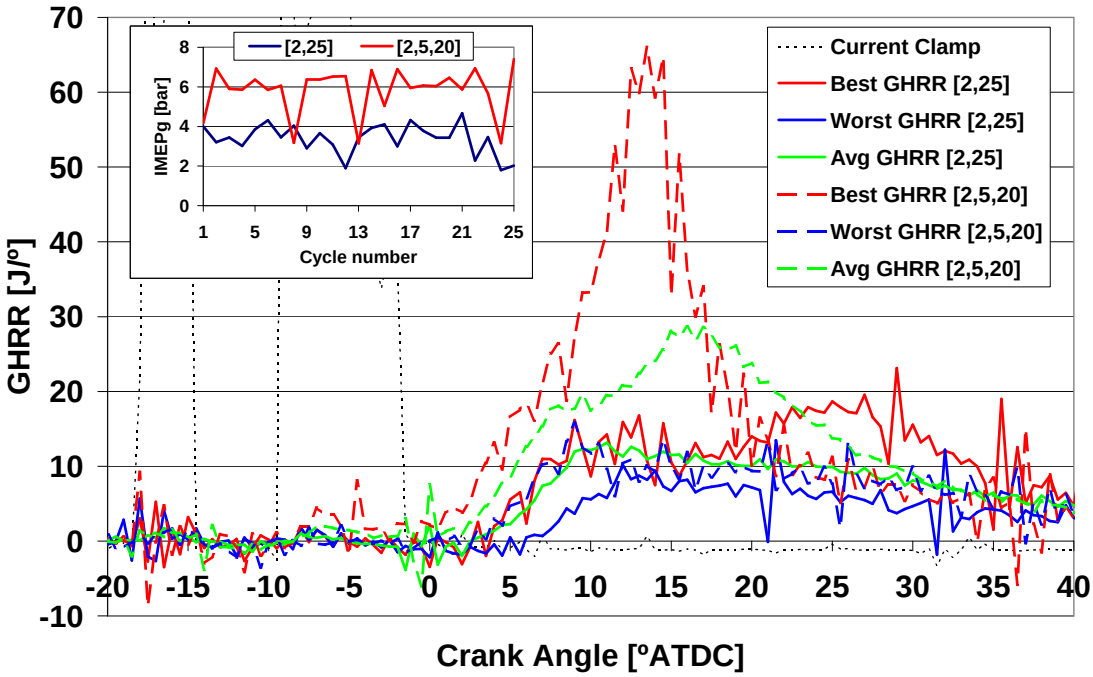

Figure 6.39: Comparison of maximum, minimum and average heat release profiles for single and twin pilot injection strategies, main timing 5.5°ATDC, $-10°C$, 1400 rpm, LCR. CoV_{IMEPg} [2,25]=20.1% CoV_{IMEPg} [2,5,20]=20.5%

The insert depicts how a poor cycle for twin pilot results in a reduction of IMEPg to levels seen at single pilot operation. Heat release rate traces reveal again that there is a decrease in ignition delay when using a second pilot injection and the potential for much greater rates of heat release. Both the best and average cycle traces for twin pilot show a second accelerating phase of combustion in the heat release rate data. Long combustion duration resulting in extended mixing in the best single pilot case also leads to this second rising phase of combustion, but it is less intense due to the retarded location. The average heat release rate profile for single pilot is very similar to worst case twin pilot, indicating that the early injection was not sufficiently prepared to assist combustion in this cycle.

Twin pilot operation is detrimental to LCR cold idle stability as it can boost combustion efficiency and IMEPg above that found at single pilot, but this cannot be guaranteed on

all cycles, therefore there is a greater spread of possible work output. Triple pilot was not investigated at LCR due to this, and due to the order of testing, the benefits at HCR had not yet been discovered. The instability of twin pilot at the lower loads required suggests that further pilot injection would be even more detrimental as fuel is removed from the main quantity to maintain the desired load, but it is still an important future work topic that may be addressed.

6.8 Summary

The single cylinder engine was reduced in compression ratio from 18.4:1 to 15.4:1 by replacing the piston with one of the same geometry, but with a proportionally larger bowl volume. At low engine speed < 600 rpm there were significantly reduced losses at low compression ratio when compared to those at high compression ratio. Lower cylinder pressures at LCR result in reduced losses to heat transfer and blowby. At low speeds these losses become rapidly worse due to extended time for heat transfer and mass loss, therefore any differences between the ratios are amplified. Theoretically, the reduced losses result in bulk gas temperatures being higher at LCR below 600 rpm in key phases of the cycle. Increased losses to blowby under fired conditions may also lead to greater oxygen availability at LCR.

Initial cold start, investigated with 300 rpm speed controlled tests, revealed that trends found at HCR are repeated at LCR. Higher peak $\overline{IMEPg_5}$ may be achieved at LCR by approximately 2 bar if appropriate injection timing is utilised. This is due to reduced losses combined with reduced peak rates of heat release facilitating extended combustion duration and lower blowby, both allowing more thorough fuel utilisation. Degradation of work output for retarded injection timings is faster at LCR due to lower cylinder pressure, reducing mixture preparation. A strong relationship was found for all tests where each 100 J of gross heat release led to 1 bar increase in IMEPg. Indicated combustion efficiency could quickly drop to zero after TDC, whereas indicated thermal efficiency was generally above 40%.

Any instability or poor combustion efficiency is worsened by a reduction in compression ratio. This was especially evident at increased engine speed where idle combustion stability was investigated. Previously stable points at HCR were found to be unstable at LCR, particularly at speeds and loads representative of cold idle. Approximately 10 mm^3/str more fuel was required at LCR to give comparable work output due to poor fuel preparation causing low rates of heat release and reduced combustion efficiency. These effects are compounded with any additional increase in speed to an extent not seen at HCR as residence times at sufficient pressure and temperature for mixture preparation and combustion propagation are reduced. LCR cold idle is not robust to changes in injection timing which had lower impact at HCR.

Multiple pilot injection at cold idle, used to good effect at HCR, was unable to stabilise the poor performance at LCR. Borderline cylinder temperature and pressure conditions for mixture preparation at LCR resulted in unpredictable behaviour. The early pilot injection could either have no effect on combustion or give pilot ignition, stronger initial heat release and/or a second phase of increasing combustion as seen at HCR with higher IMEPg. Poor cycles were not eliminated, resulting in a greater spread of possible work output and worse idle stability.

Chapter 7

The effects of Glow Plug operation

7.1 Introduction

All previous results have simulated a period of pre-glow before engine cranking as utilised in typical cold starts. The glow plug was enabled at full battery voltage prior to cranking to ensure operation at surface temperatures in the $800°C$ region. The work presented in this chapter aims to quantify the importance of the glow plug in terms of its impact on work output and stability in cold environments.

Firstly, operation with no power supply to the glow plug is considered to determine how critical the glow plug is at a range of typical cold start temperatures, both at 300 rpm and cold idle speed. Certain experiments were performed at HCR that were not possible at LCR due to hardware limitations, but the range of experiments allows conclusions to be drawn. Investigations utilising a new type of ceramic glow plug, capable of very high tip temperatures above $1200°C$ are reported. This is primarily focussed on the utility of high glow plug temperature to stabilise poor cold idle quality found at reduced compression ratio. A brief study of glow plug tip protrusion quantifies the importance of correct spatial location in successful design for cold start.

7.2 Impact of Glow Plug Operation on Cold Start

To demonstrate the value and influence of the glow plug on initial cold start performance, tests were repeated at previously stable 300 rpm or idle speed conditions, both with and without power supply to the plug. Temperature dependence of 300 rpm cold start glow plug operation is revealed in Figures 7.1 and 7.2. A stable pilot+main [2,58] mm^3/str strategy was repeated at high compression ratio, 10°C, then the colder −10°C. Heat release rate profiles are given for the highest and lowest IMEPg cycle as well as the average, both with and without glow plug operation.

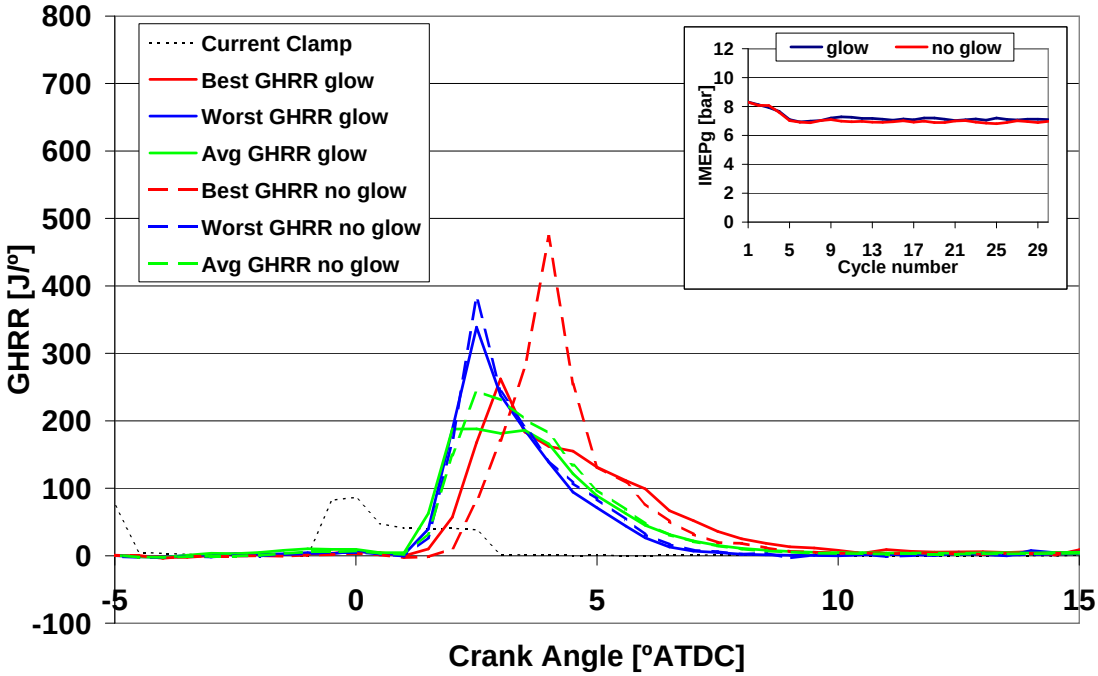

Figure 7.1: Comparison of maximum, minimum and average heat release profiles for operation with and without glow plug power, [2,58] mm^3/str main timing 0.5°BTDC, 10°C, 300 rpm, HCR

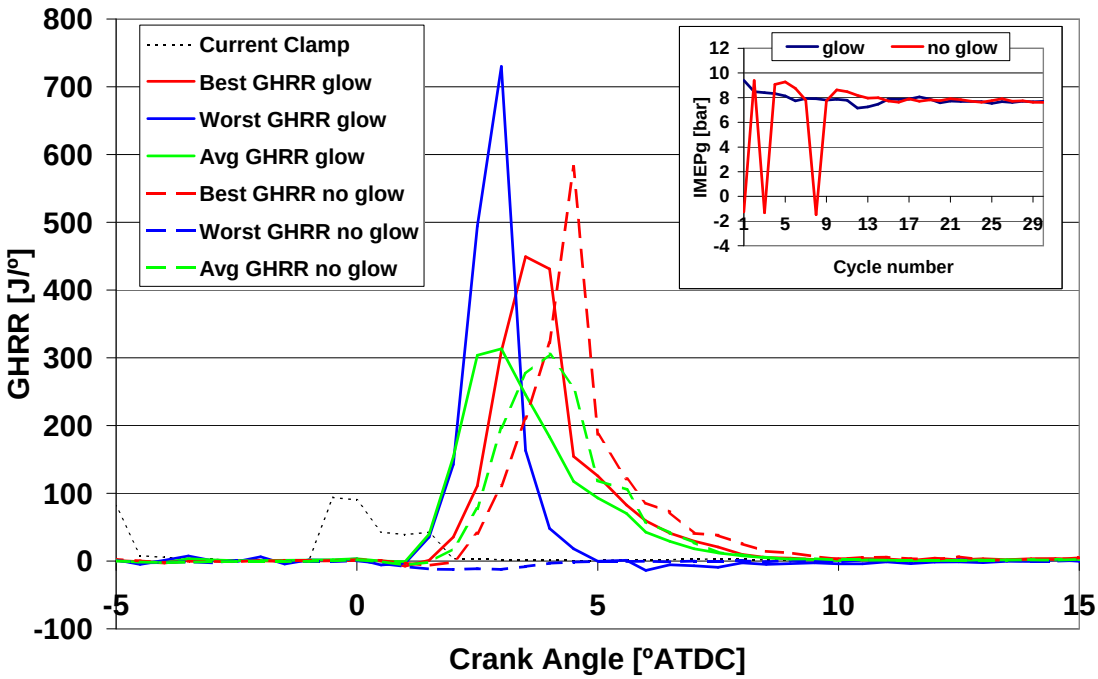

Figure 7.2: Comparison of maximum, minimum and average heat release profiles for operation with and without glow plug power, [2,58] mm^3/str main timing 0.5°BTDC, $-10°C$, 300 rpm, HCR

At the positive ambient, near identical IMEPg is achieved in all 30 injected cycles as shown by the insert in Figure 7.1, with IMEPg for each cycle nearly overlaying on the trace. The heat release traces are also nearly identical apart from a slight extension in ignition delay of between 0.5 and 1° for the first few cycles as shown in the dashed red profile. This extended mixing time resulted in a higher premixed peak. A reduction in test temperature to $-10°C$ in Figure 7.2 resulted in misfire on the first, third and eighth injected cycles when the glow plug was disabled. There was a significant extension of ignition delay evident in both the best and average cycle, extending to infinite ignition — misfire. Clearly, at $-10°C$ glow plug operation is important for stable combustion, even at high compression ratio.

At low compression ratio the glow plug becomes crucial. A high stability, pilot+split main point, used as a cleaning test, was repeated at $-10°C$ with and without power supply to the glow plug. The results are plotted in Figure 7.3

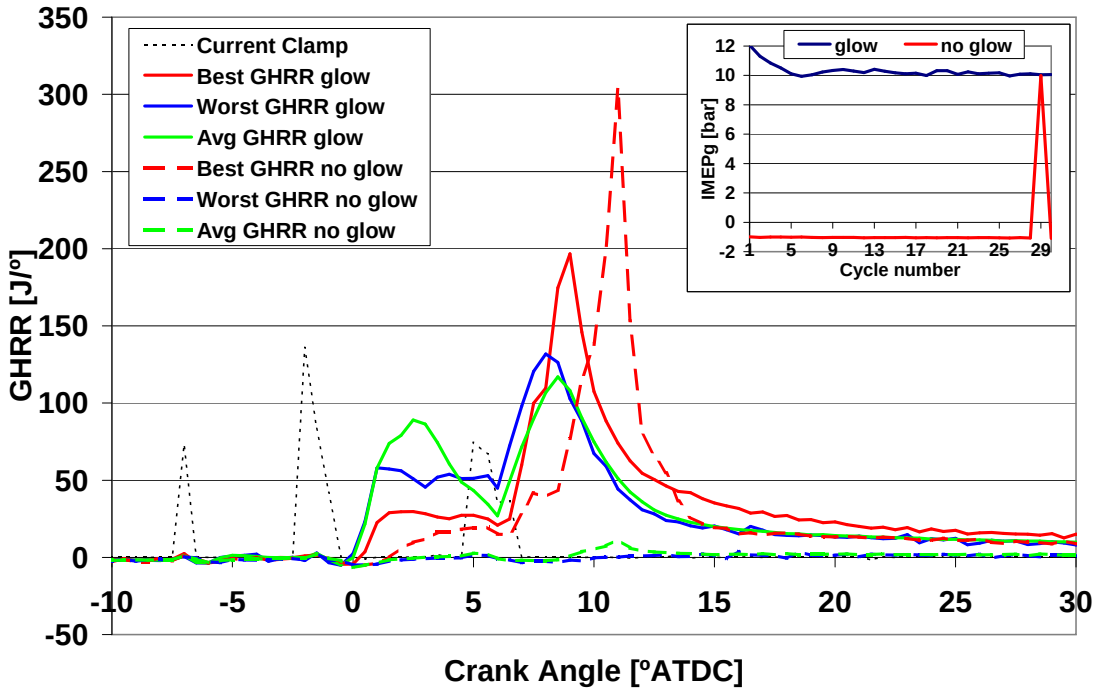

Figure 7.3: Comparison of maximum, minimum and average heat release profiles for operation with and without glow plug power, [2,20,35] mm^3/str main timing 0.5°BTDC, $-10°C$, 300 rpm, LCR

In the IMEPg insert there is only one fired cycle in 30 when the glow plug was deactivated (red line). Consistent > 10 bar operation was achieved with the glow plug (blue line). Unburnt liquid fuel accumulation in the no glow plug case resulted in a 1 bar increase in peak compression pressure between first injected cycle and the cycle before combustion. Residual fuel effectively increased the compression ratio, whilst multiple compression cycles added heat to the chamber until conditions were suitable for a firing cycle. The gross heat release traces reveal that combustion was reliable with glow plug operation—worst cycle heat release comparable to average. 29 misfires from 30 injections results in almost no average heat release without glow plug and a 1.5° extension of ignition delay for the only combusting cycle.

The importance of glow plug operation at reduced temperatures for idle stability at the relatively stable HCR is illustrated in Figure 7.4. Single pilot+main and twin pilot tests with main timings around TDC were repeated with and without glow plug power. Total fuelling was 17 mm^3/str for $-20°C$ decreasing to 8 mm^3/str for the $10°C$ case to mimic reduced friction load demand as detailed previously.

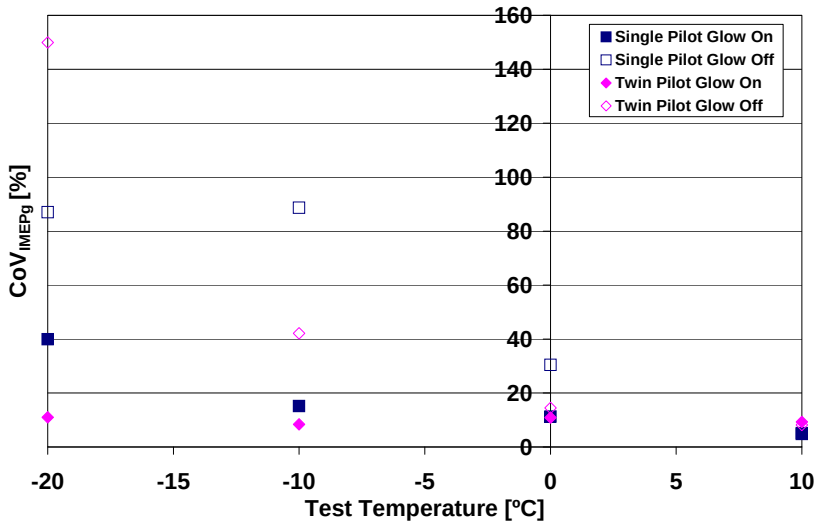

Figure 7.4: $\mathrm{CoV_{IMEPg}}$ of idle operation with and without glow plug for pilot+main and twin pilot+main, main timing $\approx$ TDC, total fuelling $-20°C$=17 mm^3/str, $-10°C$=10 mm^3/str, $0°C$=8 mm^3/str, $10°C$=8 mm^3/str, 1000 rpm, HCR

Above $0°C$ there is no significant advantage to powering the glow plug in terms of $\mathrm{CoV_{IMEPg}}$. As temperature decreases, previously stable tests were greatly destabilised. Twin pilot operation could not compensate for poor idle stability due to no glow plug operation. Heat release analysis for the twin pilot case at $-20°C$ is given in Figure 7.5.

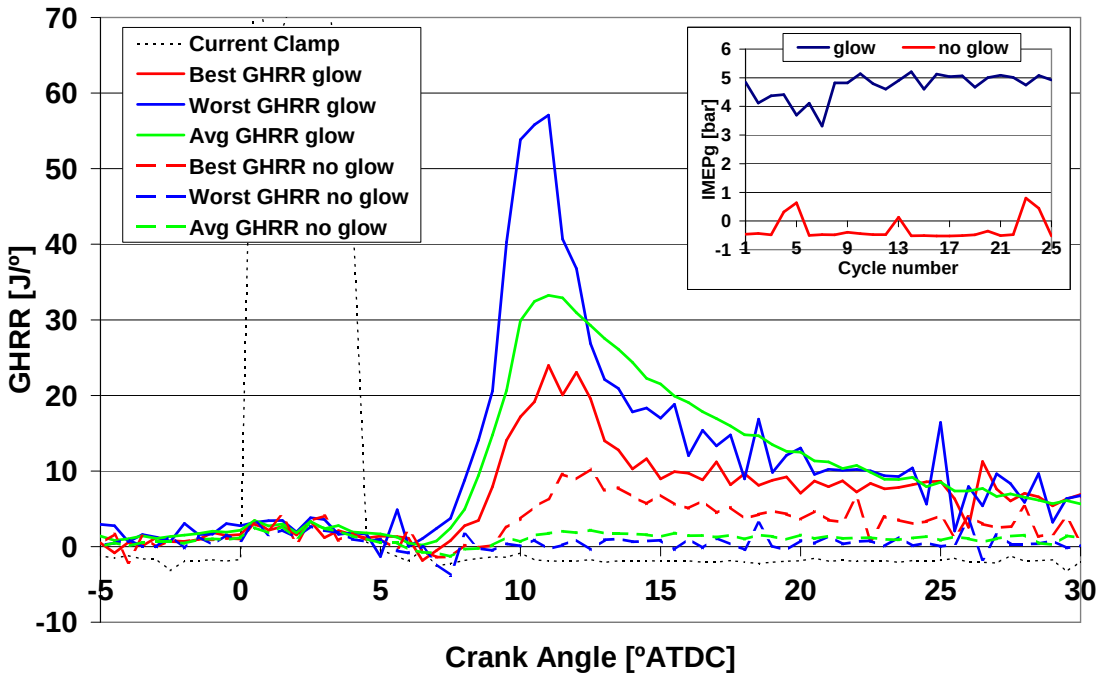

Figure 7.5: Comparison of maximum, minimum and average heat release profiles for operation with and without glow plug power, [2,2,13] mm^3/str main timing 0.5°BTDC, $-10°C$, 300 rpm, LCR

The IMEPg insert shows that the cause of instability is almost complete misfire, resulting in very low work output, with several small positive work output cycles. Close to TDC there is always some combustion of the twin pilot quantity, resulting in the poor cycles having a raised IMEPg of approximately 0.1 bar above pure motoring. This small heat release does not result in reliable combustion of the main without further assistance from the glow plug.

In summary, glow plug operation is crucial to cold start at temperatures below $0°C$, although it appears to have little impact above this temperature. Indications are that the glow plug is especially critical at LCR. Multiple pilot at HCR cold idle cannot make up for poor performance introduced by deactivating the glow plug.

7.3 The Effect of Varying Glow Plug Temperature

Current generation engines typically make use of glow plugs with a steel casing and two internal electrical coils, one for heating and one for temperature regulation. Voltage supply

from the battery enables this design to achieve a tip temperature of over $850°C$ in approximately five seconds. These are referred to hereafter as standard steel glow plugs. Difficulties in achieving acceptable cold idle operation at low compression ratio led to the acquisition of a new type of prototype glow plug where a single heating coil is encased in a ceramic material. Reduced thermal inertia, more localised heating, high temperature capable ceramic materials and accurate control of voltage supply allow temperatures in excess of $1200°C$ to be reached within 2 s. The prototype ceramic glow plug had an S-type thermocouple embedded in the tip to allow internal temperature to be monitored. Typical readings during the course of a 300 rpm test with target glow plug temperature before first injection around $1150°C$ are given in Figure 7.6. Data for a similar test conducted with a standard steel glow plug supplied battery voltage are given for comparison. Temperature data were acquired using a K-type thermocouple channelled down the glow plug shaft, braised and crimped to the glowing tip. In this case the thermocouple reports surface temperature and is more susceptible to direct heating from exposure to combustion. Maximum recorded temperature is clipped at $\approx 977°C$, as voltage input to dSPACE from the thermocouple amplifier exceeds the peak 10 V input.

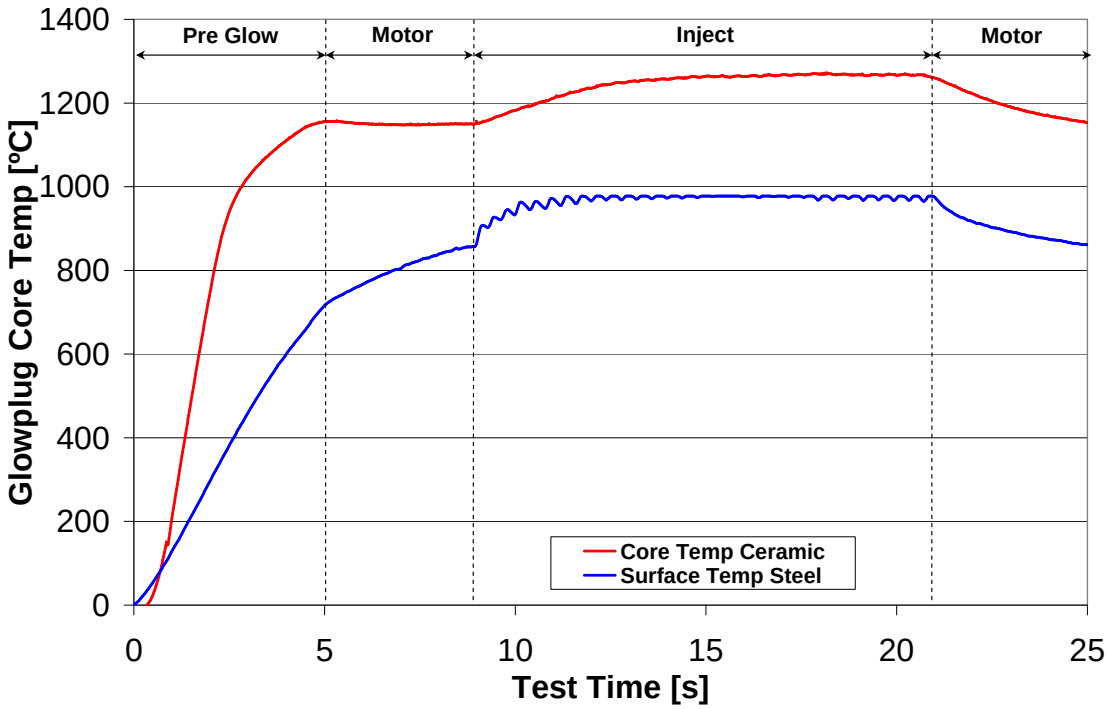

Figure 7.6: Typical 300 rpm cold start ceramic glow plug core temperature and standard steel glow plug surface temperature

7.3.1 Effect of Glow Plug Temperature on 300 rpm Cold Start

To assess the importance of glow plug temperature on 300 rpm operation, different voltages were applied to the ceramic plug before performing previously stable high IMEPg tests, both with and without pilot, at $-10°C$. The data were collected at low compression ratio and are presented in Figure 7.7.

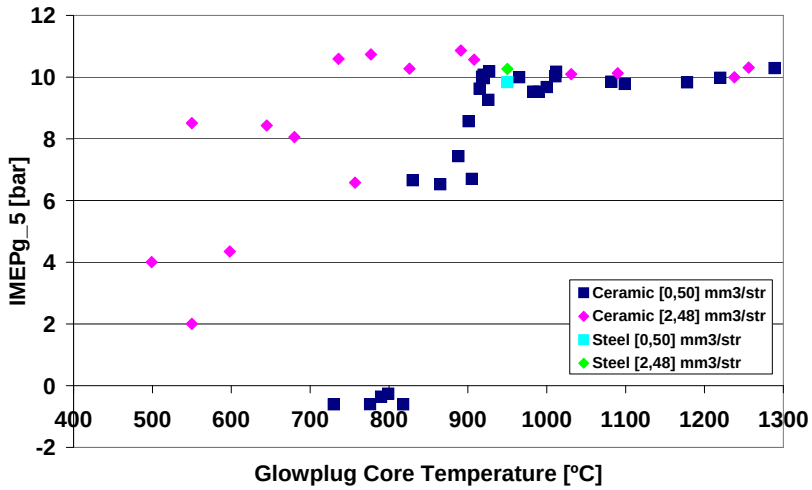

Figure 7.7: Average indicated mean effective pressure variation with ceramic glow plug core temperature at injection for a single main and a pilot+main injection with total fuel quantity 50 mm^3/str, main timing TDC, $-10°C$, 300 rpm, LCR

High and repeatable IMEPg was achieved at core temperatures above $\approx 900°C$ using a single main injection. The introduction of a pilot reduces this by approximately $100°C$. $\overline{IMEP}g_5$ does not improve beyond 10 bar with further increase in temperature, the level achieved with steel plugs for the same tests. Steady-state ceramic glow plug internal temperature is approximately $100°C$ above surface temperature as depicted in Appendix Figure e. Due to this, steel glow plug test data are plotted at a supposed internal temperature of $950°C$. There were no directly comparable data available for steel plugs at $-20°C$ LCR, but the ceramic results are given in Figure 7.8.

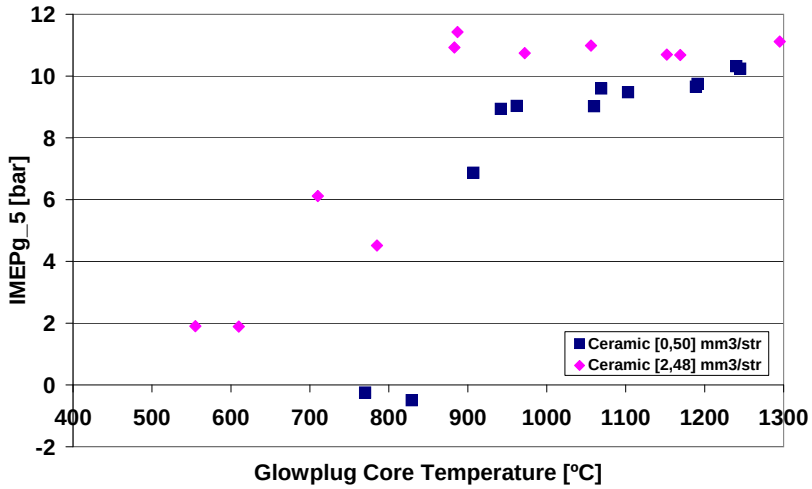

Figure 7.8: Average indicated mean effective pressure variation with ceramic glow plug core temperature at injection for a single main and a pilot+main injection with total fuel quantity 50 mm^3/str, main timing TDC, $-20°C$, 300 rpm, LCR

In this case a core temperature of $900°C$ is sufficient for pilot+main operation, but a single main injection is on the borderline of instability at this temperature. Temperatures below $900°C$ resulted in misfiring cycles that reduced average IMEPg. Above $900°C$, combustion efficiency increased until the hottest tests, where it approached the levels found utilising pilot+main.

Ignition delay at the two test temperatures for the more variable single injection case are given in Figures 7.9 and 7.10. A zero value for ignition delay does not imply instant combustion, but total misfire.

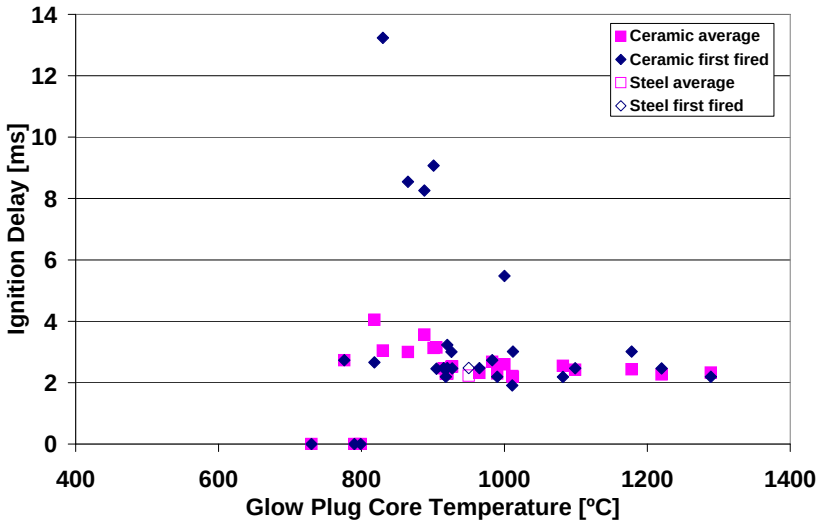

Figure 7.9: Ignition delay variation with ceramic glow plug core temperature at injection for a single main injection, [0,50] mm^3/str, 50 mm^3/str, main timing TDC, $-10°C$, 300 rpm, LCR

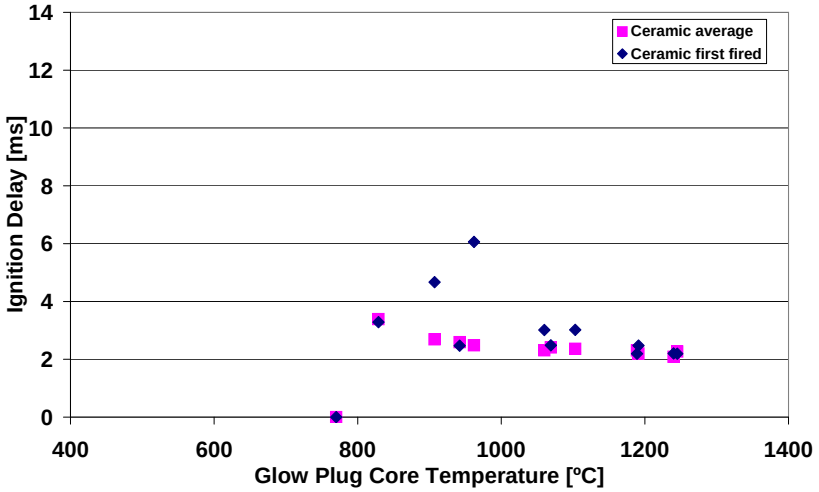

Figure 7.10: Ignition delay variation with ceramic glow plug core temperature at injection for a single main injection, [0,50] mm^3/str, main timing TDC, $-20°C$, 300 rpm, LCR

Glow plug temperature has a small but noticeable effect on ignition delay, both for the first combusting cycle and the average. At the borderline of stability around $800°C$, where the first cycle may misfire or have an extended ignition delay, the average ignition delay for combusting cycles was approximately 4 ms at both test temperatures. Increasing glow plug temperature resulted in an approximately 50% reduction in ignition delay. Most of this reduction was achieved in the first 100–$150°C$ increase as poor stability cycles were eliminated. Less data were gathered at $-20°C$ in the borderline conditions between 800 and $900°C$ where first cycle ignition delay could vary greatly, therefore the deviation of first

cycle to average is shown to be less in the $-20°C$ case.

Heat release rate data for the average cycle for three ceramic glow plug tests at low, steel-like, and high temperatures is compared to steel glow plug data for a single injection at $-10°C$ in Figure 7.11. Results for similar ceramic temperatures at $-20°C$ are given in Figure 7.12.

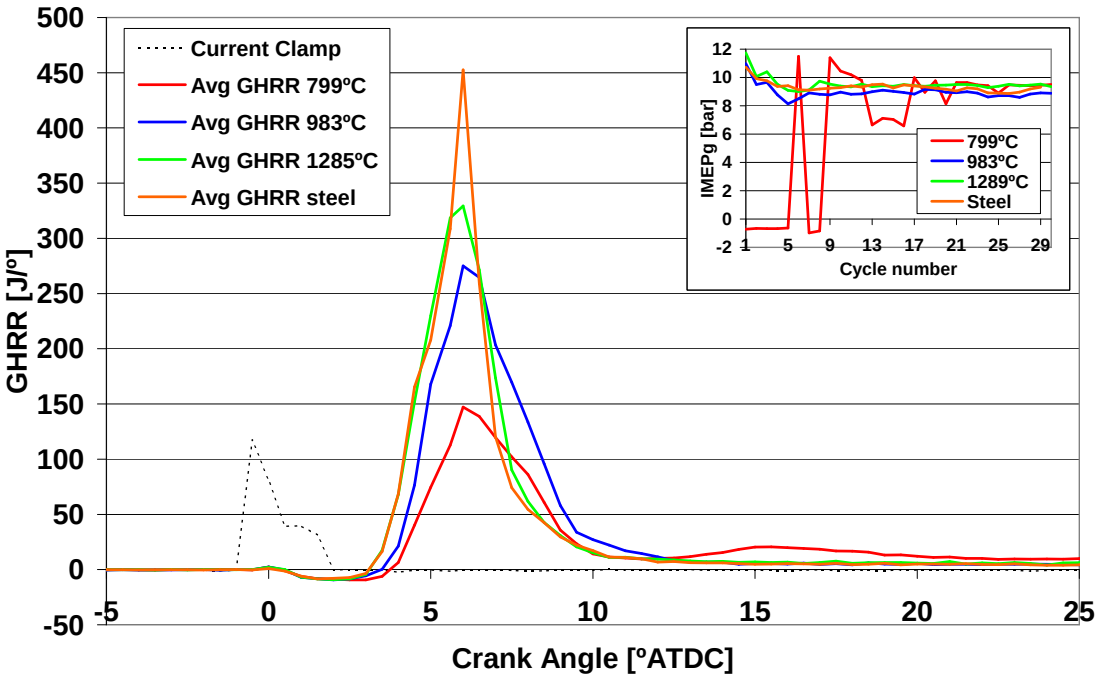

Figure 7.11: Average heat release rate variation with ceramic glow plug core temperature at injection for a single main injection, [0,50] mm^3/str, main timing TDC, $-10°C$, 300 rpm, LCR

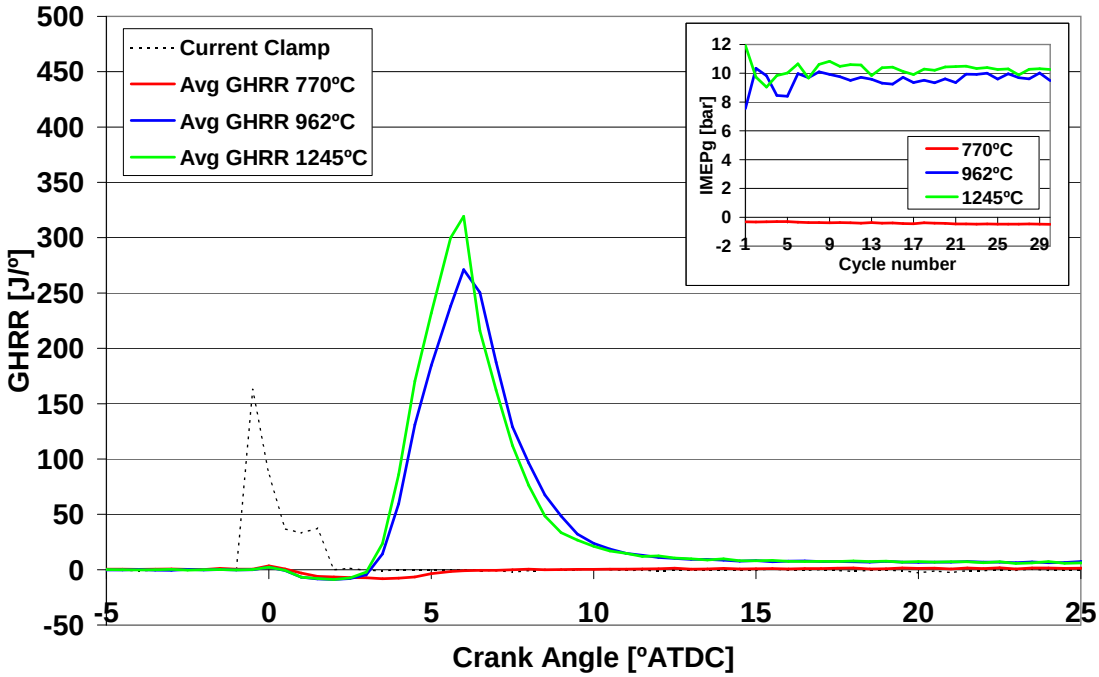

Figure 7.12: Average heat release rate variation with ceramic glow plug core temperature at injection for a single main injection, [0,50] mm^3/str, main timing TDC, $-20°C$, 300 rpm, LCR

There was little variation in IMEPg and the way fuel was burnt once over the critical glow plug temperature for reliable combustion. Higher temperatures resulted in increased peak GHRR after a reduced ignition delay at both test temperatures. At $-20°C$ combustion is marginally more complete with better phasing resulting in higher IMEPg at high glow temperatures. Comparing steel glow plug performance at $-10°C$ to the mid-temperature ceramic plug test reveals similar performance and ignition delay. GHRR increased at the same rate until $\approx 6°$ATDC when combustion began to reduce for the ceramic plug whilst continuing to an approximately 100 J/° higher peak rate using a steel plug. As the surface temperatures at steady-state of the two plugs are expected to be similar, it is likely that the increased thermal inertia and larger surface area of the steel plug resulted in greater fuel preparation with more heat input to the spray, possibly over a greater volume of fuel as it passes close to the glowing tip. Steady-state power delivery ($P = IV$) for the ceramic plug is approximately 30 W for this tip temperature compared to over 100 W for the steel plug. This may account for the greater total premixed burn.

7.3.2 Effect of Glow Plug Temperature on Cold Idle

Steel glow plugs were sufficient for stable 300 rpm operation at both compression ratios, and multiple pilot injection could be used to stabilise HCR idle combustion, but no solution was found for poor LCR idle stability. At $-10°C$ it was very difficult to obtain any reasonable stability, even when targeting higher loads than the $\approx$ 3 bar required to maintain idle speed at these ambient temperatures. At $-20°C$ the best stability that could be achieved for the $\approx$ 5 bar target was in the 20–30% region with poor repeatability. High temperature ceramic glow plugs were proposed as a possible solution to poor idle stability. Whilst the total heat input to the fuel is likely less, as ceramic plugs use less power, the temperature is greater and the heat more focused on the protruding tip. If the glow plug is operating primarily as a combustion initiator, it is hoped that this higher temperature will produce stronger and more reliable initial combustion around the tip which may aid combustion stabilty. An initial test revealed there was merit in further investigation. A pilot+main injection strategy of [2,30] mm^3/str was injected with the main just before, approximately on and just after TDC. $\text{CoV}_{\text{IMEPg}}$ results are given for a variety of glow plug temperatures in Figure 7.13.

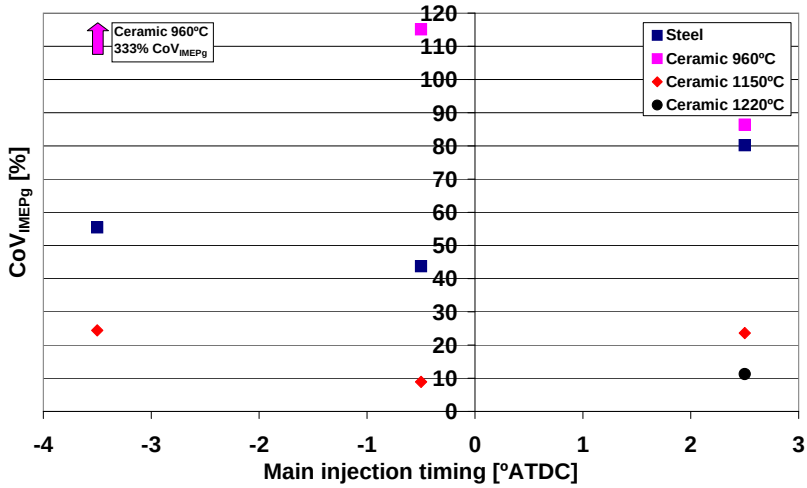

Figure 7.13: $\text{CoV}_{\text{IMEPg}}$ variation with ceramic glow plug core temperature at injection and main injection timing for a pilot+main injection, [2,30] mm^3/str,$-10°C$, 1200 rpm, LCR

Approximately $960°C$ glow plug core temperature at first injection gave variable, but generally poorer, performance than the standard steel plug. Increasing this to $1150°C$ gave

better results at all timings. A further increase to 1220°C at the least stable, retarded condition resulted in a $> 50\%$ improvement in $\mathrm{CoV_{IMEPg}}$ from the previous best. Average heat release rate analysis for these test temperatures at this most retarded injection timing is given in Figure 7.14.

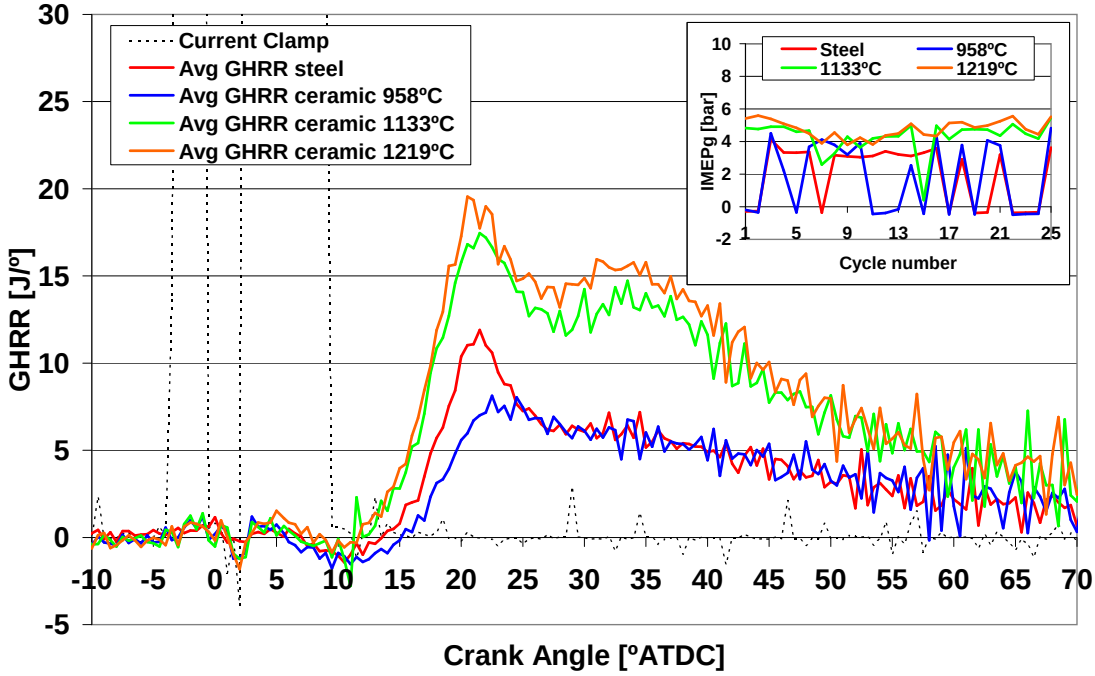

Figure 7.14: Average gross heat release rate variation for a steel glow plug vs. ceramic at a selection of core temperatures at first injection, [2,30] $\mathrm{mm^3/str}$, main timing 2.5°ATDC, $-10°C$, 1200 rpm, LCR

As glow plug temperature increased, average ignition delay reduced and peak heat release rate increased, despite reduced preparation time. This implies that there is significantly more heat input to the charge resulting in a greater proportion of the fuel being well prepared for the premixed burn portion of combustion. After the premixed burn, heat release rate is maintained above that of lower temperatures as self sustained combustion continues, boosted by a second phase of rising heat release rate combustion as was found with multiple pilot injection at high compression ratio in Section 5.6.4. The conclusion at HCR was that multiple pilots lead to better mixture distribution throughout the cylinder with low level pilot heat release freeing more volatile species which are more combustible in these unstable conditions. Higher initial heat release rate, complete suppression of misfire, increased work output, much reduced $\mathrm{CoV_{IMEPg}}$ and evidence of a second increasing phase of combustion suggest that high glow plug temperatures assist continued mixture preparation

after ignition as well as combustion initiation.

Maximum, minimum and average cycle heat release rates for the highest temperature ceramic test are compared to those utilising a steel plug in Figure 7.15.

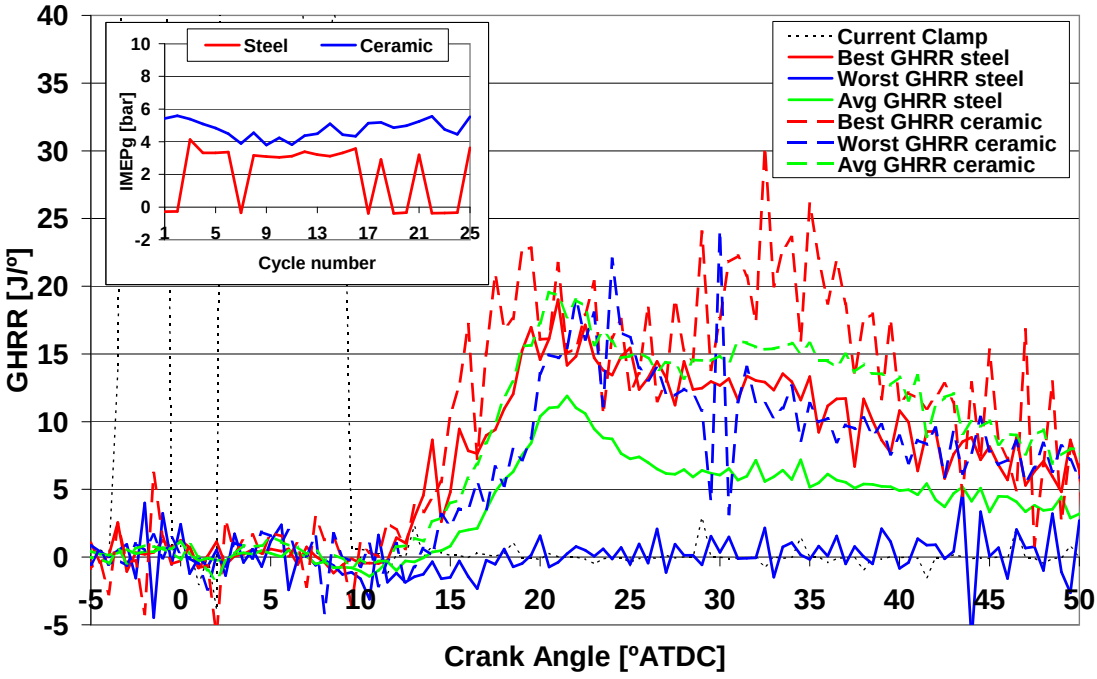

Figure 7.15: Maximum, minimum and average heat release rate variation for a steel glow plug vs. ceramic core temperature at first injection of 1219°C, [2,30] mm^3/str, main timing 2.5°ATDC, −10°C, 1200 rpm, LCR

Ignition delay and heat release rate variation between best, worst and average IMEPg cycles are minimised by high temperature operation when compared to data for steel glow plug operation. Similar peak rates of heat release are reached for the best and worst cycle using the ceramic glow plug, whilst total misfire is possible using steel plugs. Variation in IMEPg for the ceramic plug over the first few cycles is caused by the less intense second phase of combustion, shown by the dashed blue line. This lack of secondary combustion may be due to convective cooling of the glow plug surface caused by air motion as seen in Figure 7.16.

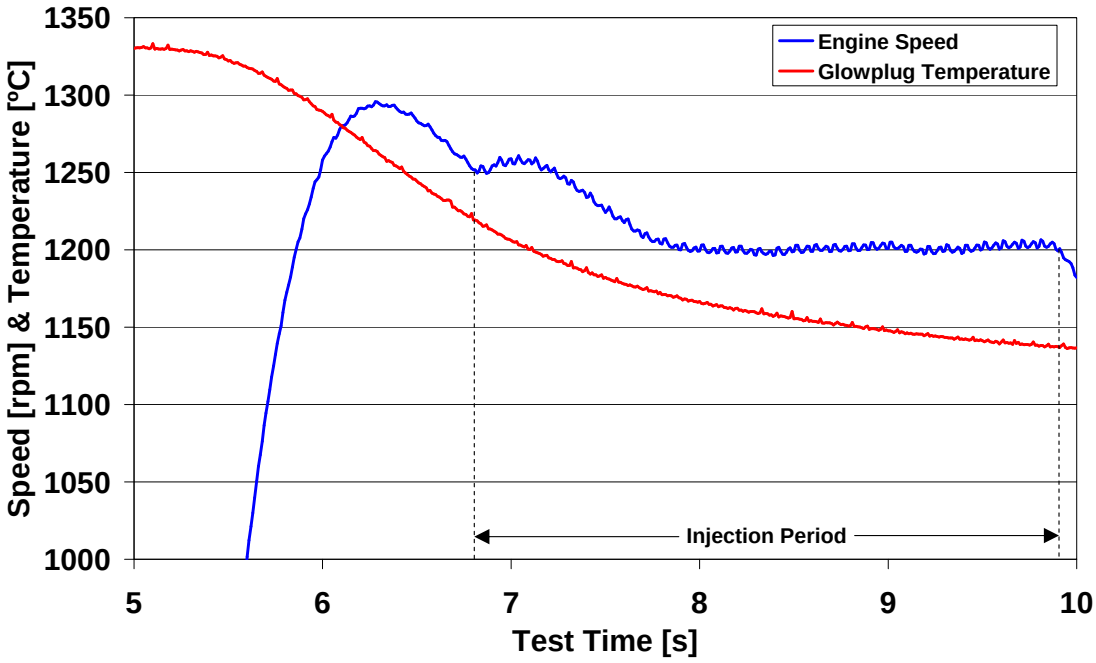

Figure 7.16: Ceramic glow plug core temperature and engine speed during motoring period and injection portion of test, temperature at first injection 1219°C, [2,30] mm^3/str, main timing 2.5°ATDC, −10°C, 1200 rpm, LCR

At these high engine speeds there is a slight overshoot of speed which is not entirely remedied before first injection. With constant voltage supply the core temperature drops by over 100°C from steady-state during the motoring period (≈ 2 s) until injection commences, then continues to reduce during the test. Surface temperature would be significantly lower than core because it is directly cooled by convection. The ceramic plug has low thermal inertia (a design feature for reduced pre-glow), but without variable power supply it is unable to maintain temperature at high engine speed. Reducing IMEPg over the first few cycles, caused by poor secondary increasing phase of combustion, indicates that it takes several cycles for heat addition to mitigate the effects of convective cooling lowering glow plug temperature.

A more focused investigation was performed at the less stable −20°C targeting an appropriate friction loading of 5 bar for firing cycles. A sweep of tests at 800 rpm with core temperature at injection between 800 and 1200°C were completed with fixed injection of [2,25] mm^3/str, main timing TDC. $\overline{IMEPg}_{10}$, $\mathrm{StD}_{\mathrm{IMEPg}}$ and $\mathrm{CoV}_{\mathrm{IMEPg}}$ performance are plotted in Figure 7.17. Steel plugs gave very poor performance at typical ≈ 1000 rpm

engine speed for $-20°C$, and therefore tests were performed at the more stable 800 rpm where there is more time for mixing and fuel preparation. Four repeats of the point using a standard steel glow plug are plotted at the supposed $950°C$ internal temperature level on the x axis.

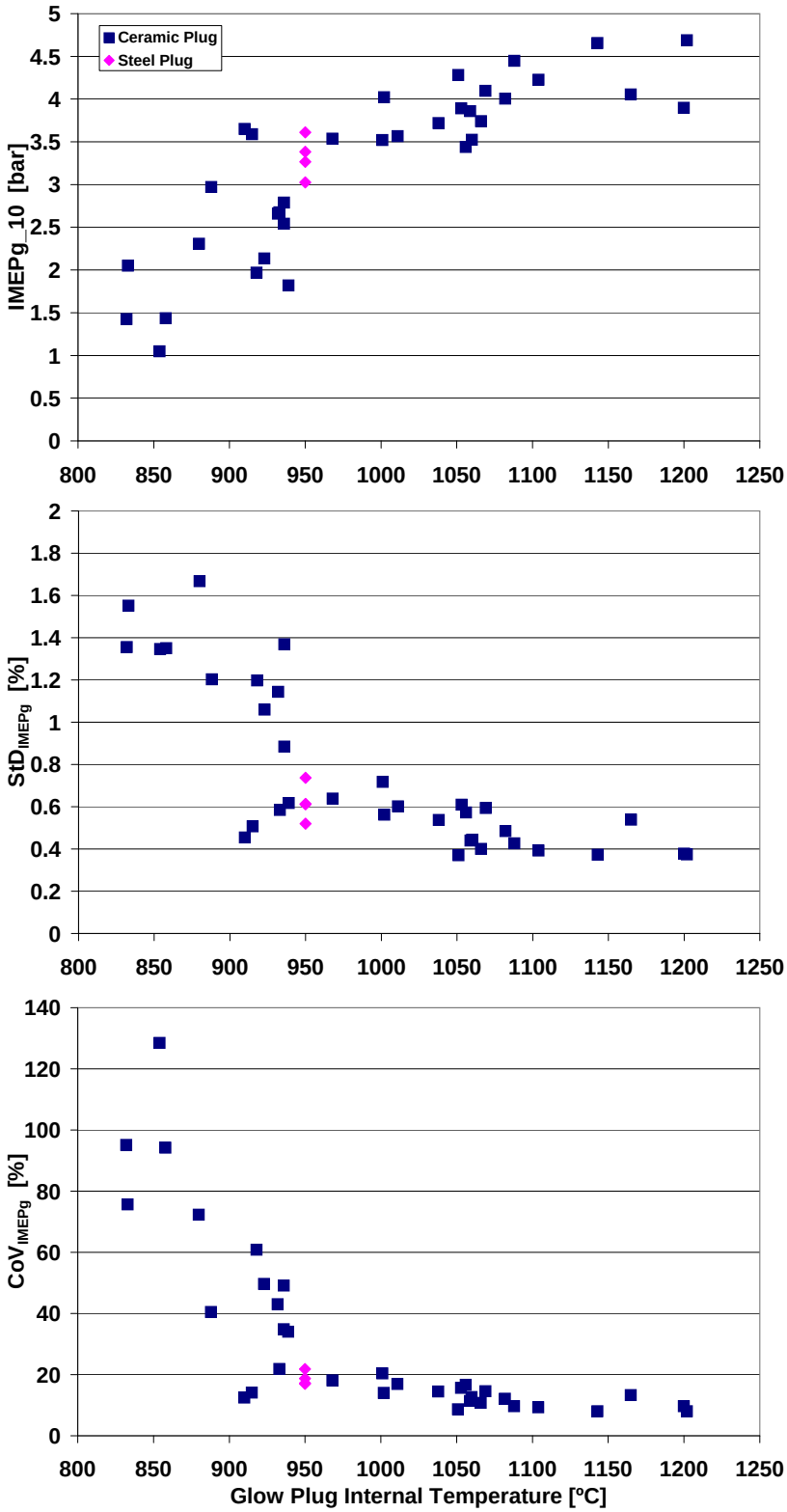

Figure 7.17: Idle performance of a single pilot+main injection strategy varying ceramic glow plug core temperature at injection, [2,25] mm^3/str, main timing TDC, $-20°C$, 800 rpm, LCR

Approximately equivalent performance was obtained in terms of work output and stability with the steel glow plug and ceramic plug at just over $950°C$, but performance was subject to much test-to-test variation at this level. Increasing ceramic temperature above this level led to improved work output and $\mathrm{StD}_{\mathrm{IMEPg}}$ simultaneously until approximately $1100°C$. Above this temperature there were small gains in work output, approaching the desired average value of 5 bar IMEPg, but absolute stability remained constant at approximately 0.4 bar, resulting in $\mathrm{CoV}_{\mathrm{IMEPg}} < 10\%$ target. As temperature was decreased from $950°C$, average work output reduced markedly and there was onset of total failure of combustion below $900°C$. The poor perfomance utilising a steel glow plug is related to the proximity of its operating temperature to this critical stability limit.

Heat release data given in Figure 7.18 compare the most stable steel test to the ceramic results found at a core temperature of $968°C$.

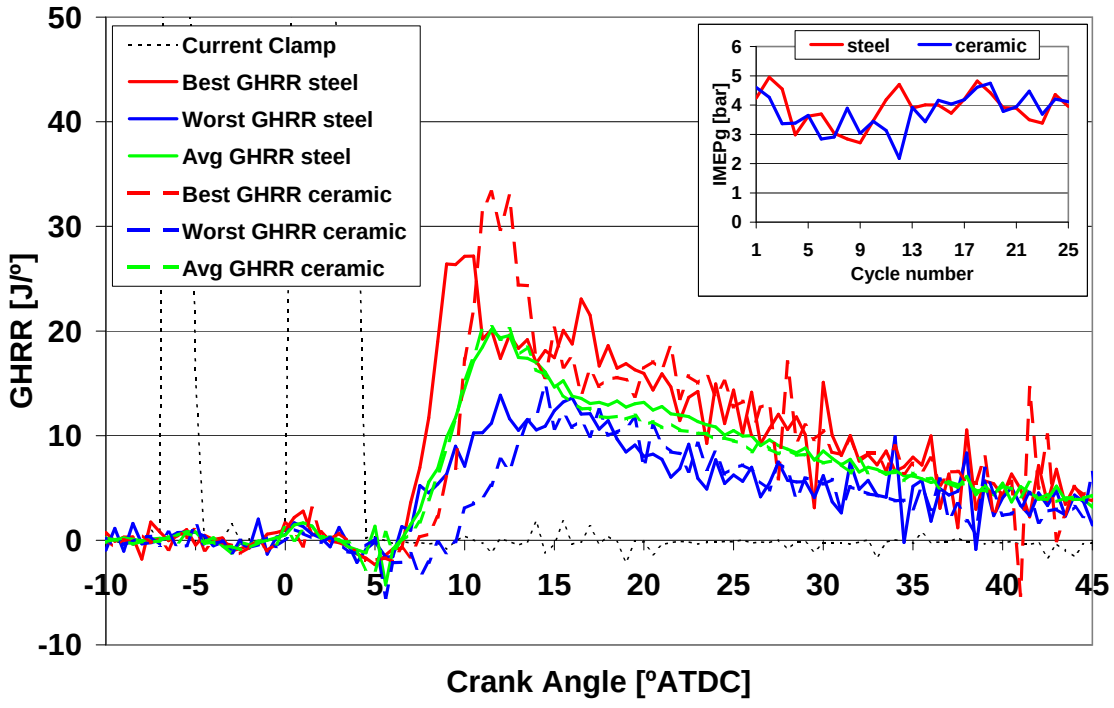

Figure 7.18: Maximum, minimum and average heat release rate variation — steel glow plug vs. ceramic core temp at first injection $968°C$, [2,25] mm^3/str, main timing TDC, $-20°C$, 800 rpm, LCR

Similar combustion occurred for the two different plugs at these levels. Average performance was marginally better for the steel with an improved diffusion burn. It is also subject to less variation in ignition delay, witnessed by the worst cycle plot. The benefits obtained by

an increase in ceramic plug temperature to 1202°C are illustrated in Figure 7.19.

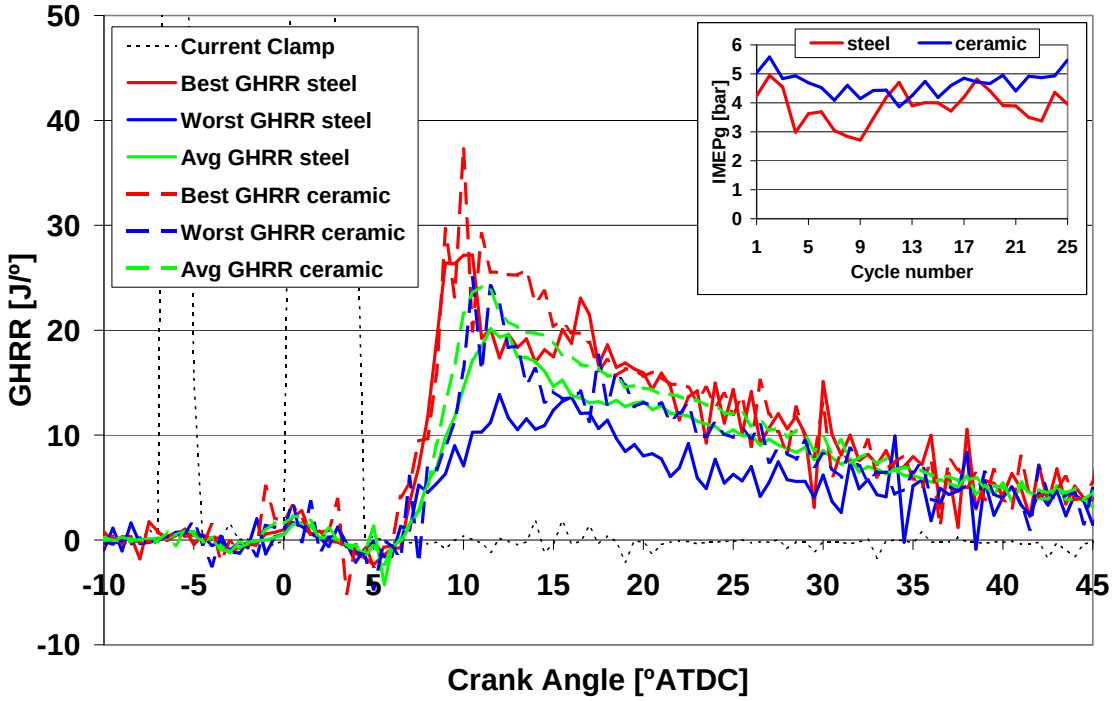

Figure 7.19: Maximum, minimum and average heat release rate variation — steel glow plug vs. ceramic core temp at first injection 1202°C, [2,25] mm^3/str, main timing TDC, −20°C, 800 rpm, LCR

Heat release rate variation was much reduced with peak, average and minimum IMEPg cycle heat release rate traces measurably higher for the ceramic plug than the steel case. Again a second phase of combustion is evident in the ceramic worst cycle which is not observed for the worst steel case, reducing the spread of work output. A dual benefit of increasing initial rate of heat release and stabilisation of poor cycles with a secondary period of increasing burn was found utilising multiple pilots at HCR. This has been recreated at LCR with high temperature ceramic glow plugs, enabling good quality cold idle combustion stability to be achieved at low ambient temperature.

Summarising the effect of glow plug temperature on cold start, once above a critical internal temperature in the region of 950°C, there is little improvement in peak 300 rpm work output, but there is some stabilising of ignition delay and an increase in peak rate of heat release. At idle speeds, increased glow plug temperature has the potential to greatly improve cold idle operation with significantly more repeatable heat release profiles, boosting GHRR of poor cycles and reducing $\mathrm{CoV}_{\mathrm{IMEPg}}$ to the target 10% above ≈ 1100°C.

7.4 The Effect of Glow Plug Protrusion on Idle Stability

Glow plug location is very important for cold start performance. Good start quality may be obtained with fuel impinging directly on the plug [50], but this can lead to increases in soot emissions for normal running, as liquid fuel adheres to the plug once deactivated. Carefully designed spray/bowl interactions would also be ruined by direct spray impingement. As a result, the glow plug is generally located so that liquid spray narrowly misses it during cold start. As engine speed rises, swirl becomes more prominent, carrying liquid fuel away from the glow plug.

At high compression ratio, reasonable idle speed performance was obtained without the need for high temperature glow plugs. Even a single pilot+main could return near to target stability with appropriate timings. It was noted that the ceramic glow plug had a smaller glowing tip than standard. Measured vertical protrusion was 0.35 mm less and the diameter of the tip was 3.3 mm vs. 4.5 mm for the steel. The reduced glowing area lowers pre-glow time and enables higher surface temperature to be reached. Providing the relative angular location of glow plug to spray must stay the same, it is important to ascertain whether changes in protrusion could have an effect on performance when specifying new hardware.

To assess the impact of changes on protrusion, a range of washers were manufactured which locate on the conical sealing face at the base of the steel glow plug shank. An example is shown in Figure 7.20. As the glow plug enters the head at an angle, these washers vary maximum vertical protrusion into the combustion chamber as given in Table 7.1.

Figure 7.20: 2.5 mm glow plug spacing washer

Washer Size (mm)	Protrusion (mm)
No Washer	4.7
0.5	4.39
1	4.07
1.5	3.76
2	3.44
2.5	3.13

Table 7.1: Maximum vertical protrusion of glow plug with each washer size

Four repeats were performed at the more stable HCR using each washer at the same 800 rpm test point previously used at LCR to study the effect of glow plug temperature in figures 7.17–7.19. $\overline{IMEPg}_{10}$ and $\mathrm{CoV}_{\mathrm{IMEPg}}$ for these tests are given in Figure 7.21.

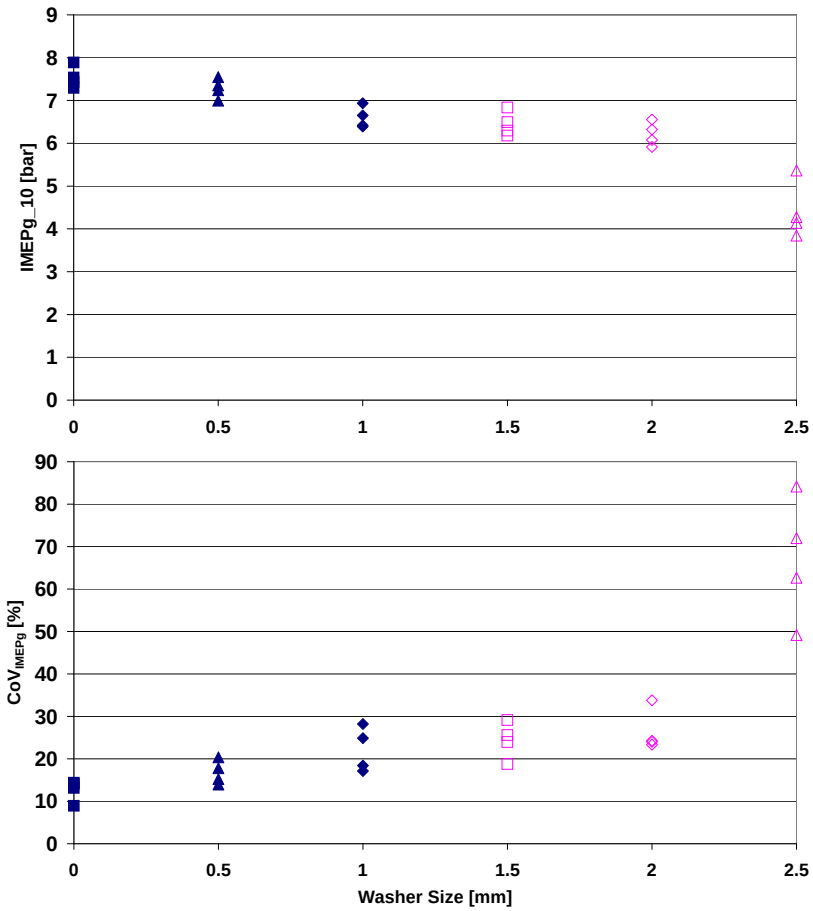

Figure 7.21: Idle performance of a single pilot+main injection strategy for each glow plug washer, [2,25] mm^3/str, main timing TDC, $-20°C$, 800 rpm, HCR

Repeatability of results was well within ±0.5 bar for all washers except the largest 2.5 mm washer, where glow plug protrusion was approximately $\frac{3}{4}$ standard. Larger washers decrease $\overline{IMEPg}_{10}$ and increase $\mathrm{CoV}_{\mathrm{IMEPg}}$. The spread of values was high and therefore the correlation is not strong enough to draw a line, but mean $\overline{IMEPg}_{10}$ reduced by 1.31 bar (17.5%) and mean $\mathrm{CoV}_{\mathrm{IMEPg}}$ increased by nearly 14% absolute, more than doubling instability by withdrawing the glow plug just 1.25 mm vertically and 1.56 mm radially outwards. The minimum, maximum and average cycle rates of heat release for a typical test with standard glow plug protrusion are compared to a 1.5 mm test with performance in the middle of the range in Figure 7.22. Figure 7.23 reveals further degredation by comparing 1.5 mm to a typical 2.5 mm washer run.

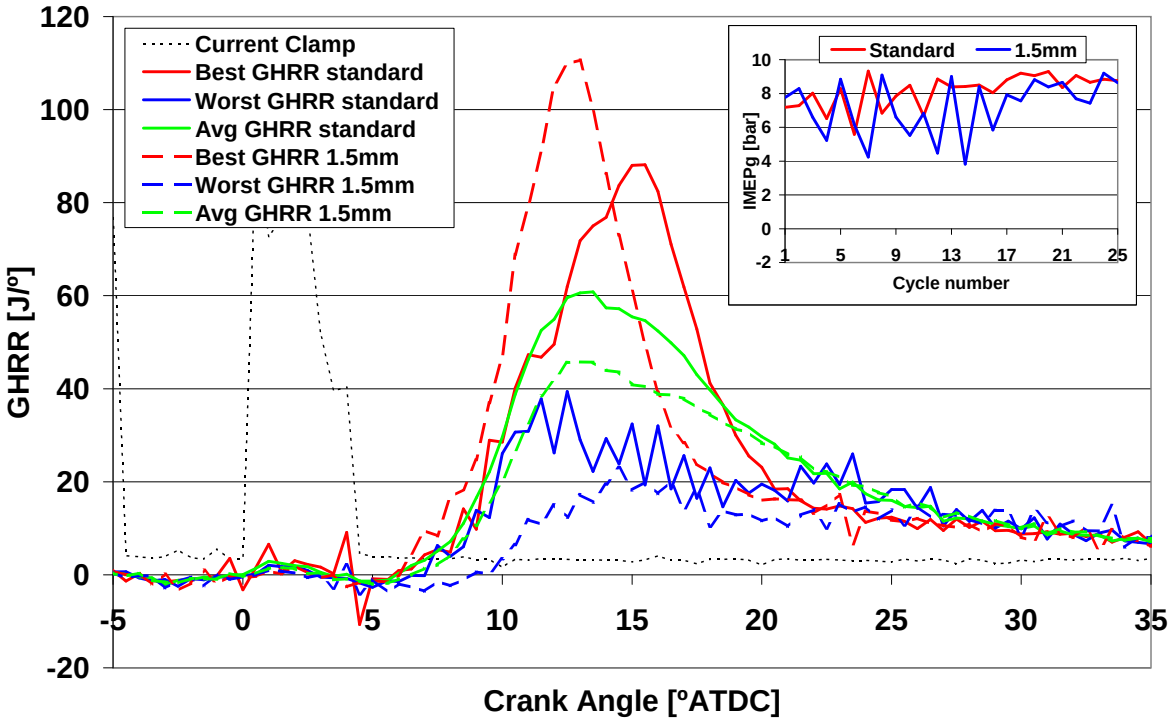

Figure 7.22: Maximum, minimum and average heat release rate variation — standard glow plug vs. plug with 1.5 mm washer, [2,25] mm^3/str, main timing TDC, $-20°C$, 800 rpm, HCR

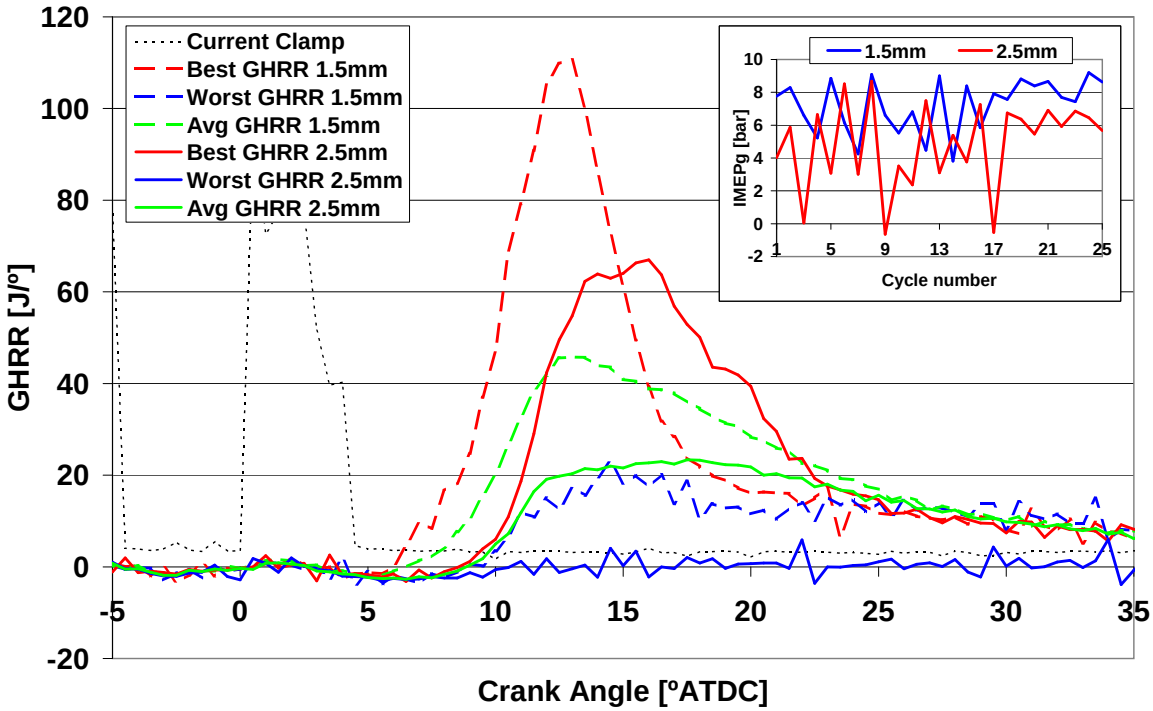

Figure 7.23: Maximum, minimum and average heat release rate variation — plug with 1.5 mm washer vs. 2.5 mm washer, [2,25] mm^3/str, main timing TDC, $-20°C$, 800 rpm, HCR

As the glow plug was withdrawn there was an extension in average ignition delay along with heat release rate. Higher IMEPg variability using a 1.5 mm washer was further degraded and included three misfiring cycles with a 2.5 mm washer. Reduced spray/glow plug interaction and lower overall glowing length providing heat input to the passing spray reduced direct evaporation and the intensity of combustion initiation at the plug.

Parallels exist with results found when reducing glow plug temperature from stable points in the region of $1050°C$. Small decreases in temperature initially decreased peak rate of heat release with some cycle-to-cycle work output variability penalty. Below $950°C$ there was a rapid reduction in stability, increased ignition delay and onset of misfire. Clearly glow plug protrusion has a similarly significant effect on cold idle combustion stability when making changes of tenths of a millimetre. Further gains could be expected with greater than standard protrusion, although this could have a detrimental impact on operation at fully warm conditions. The results presented here suggest that changes in the design of the reduced diameter and protrusion ceramic glow plug could improve stability, or that the

same stability could be achieved with lower surface temperature.

7.5 Summary

Investigations were conducted to determine the role and importance of the glow plug for combustion at cold start. Results indicate that glow plug operation is critical to cold start at both high and low compression ratio, but especially at LCR. At HCR there was negligible impact on 300 rpm operation at $10°C$, but a reduction in temperature to $-10°C$ resulted in onset of misfire for a previously stable injection strategy and extension of ignition delay. Low compression ratio operation with glow plug deactivated at $-10°C$ resulted in near total misfire. Increasing engine speed to idle revealed much the same results. At the more stable high compression ratio there was no need for glow plug operation at $10°C$, but poor stability with multiple misfire was obtained at negative ambient temperatures for previously stable test points. Multiple pilot injection was unable to compensate for this, revealing that the pilot strategy is only capable of improving performance provided suitable conditions for ignition are generated by the glow plug.

High temperature ceramic glow plugs were found to be unnecessary for low speed operation at 300 rpm. Performance was no better than when full battery voltage was supplied to the steel glow plug for operation at nominal $850°C$ tip temperature. No improvement was gained by increasing ceramic core temperature over $950°C$ provided a suitable injection strategy for high IMEPg output was selected at either $-10°C$ or $-20°C$. When a slightly less stable single main injection was used, $950°C$ was suitable for stable combustion at $-10°C$, slightly higher core temperature must be achieved for total stability at $-20°C$.

Poor stability at low compression ratio cold idle can be greatly improved with the use of high temperature ceramic glow plugs. Whilst $950°C$ was sufficient for 300 rpm cold start, it was not suitable for higher engine speeds. As core temperature was increased, ignition delay reduced and peak rate of heat release was increased. At the highest temperatures there was evidence of a secondary phase of rising combustion after initial heat release for poor

cycles. As a result of this, IMEPg continued to increase at higher glow plug temperatures as a greater proportion of the fuel was combusted. Above $1100°C$ $\mathrm{CoV_{IMEPg}}$ was within target stability, generally below 10%, compared to steel glow plugs at approximately 20%. Incremental work output gains were achieved at even higher temperatures, but absolute stability remained similar.

Significant degradation was found when withdrawing the glow plug radially from the combustion chamber. A 25% reduction in protrusion doubled cycle-to-cycle variability in IMEPg. Above this withdrawl, greater degredation was found. Larger variability in ignition delay, lower average peak GHRR and cumulative burn indicate that the withdrawl reduces heat input to the spray, eventually leading to complete failure to ignite. It is crucial that any new glow plug design utilising smaller glowing surfaces takes this into account, as small changes in protrusion can be detrimental.

Chapter 8

Discussion, Future Work and Conclusions

8.1 Introduction

The work presented in this thesis was undertaken to better understand the impact on cold operation of a reduction in compression ratio for a direct injection, common rail diesel engine. Whilst this area is very topical, the literature review revealed that published work in the specific field is currently scarce. The single cylinder motored experiments were developed to give a good approximation of actual engine operation with good control over operating conditions which would not have been possible on a multiple cylinder rig or on-vehicle. Low heat input and direct cooling by circulating chilled coolant allowed a high rate of data collection. It is hoped much has been added to the work in the field. This section aims to discuss the key findings of the thesis in the context of their applicability to real-world cold start. If there are apparent limitations in the findings, alternative methods will be proposed for future consideration. Similarly, if the current investigation is deemed to need further depth, future experiments and areas for investigation are proposed. Finally, the key findings of the thesis are listed.

8.2 Discussion of Key Findings

8.2.1 General Validity of Test Procedure

30 cycles of combustion were required for each test point, followed by a further 30 cycles for a cleaning point, then two minutes of motoring. Direct cooling with circulating coolant and this low total heat input for a test allowed approximately 20 test points per day. The test was only designed to be representative of engine conditions at cold start. The direct internal conductive cooling and heat transport with coolant flow results in a non-linear temperature profile within the engine compared to that which would be found for a true cold start after prolonged soak in cold conditions. This may be better replicated by external refrigeration of an entire test cell [37, 99, 100], or a sealed, insulated environmental chamber around the test rig [20, 21, 86]. This provides more realistic cold start replication with a more consistent temperature throughout the engine. Cooling of the entire environment draws heat out of the engine by convection. This method was not chosen for the study presented here as significant dwell periods are required to cool the engine from the outside in. Typically, a test is set up the evening before experimentation and the equipment is left to soak overnight. In this way, one test may be completed in the morning, with the possibility of a second in the evening on each day of testing. This did not fit the requirements for the broad sweeps and investigative work contained both within this thesis and for work completed for sponsors. The direct cooling allowed swift progress in any given area. As such it is felt much has been added to the knowledge base which would not have been possible with indirect cooling.

8.2.2 Low Speed Findings

A reduction in compression ratio leads to a reduction in work input to the cylinder charge during the compression stroke. Losses at HCR were higher than those at LCR due to higher cylinder pressures. There was significant non-linearity with engine speed — losses increased exponentially at 300 rpm. As such the difference in losses between HCR and LCR also increased. When calculated using the Hohenberg correlation, the difference in heat transfer

losses at 300 rpm under motored conditions was approximately 14%. A similar difference existed when calculating blowby based on differential pressure. Direct blowby measurement was challenging on the single cylinder rig, resulting in much variability. The average result however confirmed the speed dependency, with no measurable blowby at 600–1500 rpm under motored conditions, but a sharp increase at 300 rpm with LCR 30% lower than HCR. This implies blowby may be more of a problem at HCR than the differential pressure would suggest. The blowby mass fraction values were in the range 5–11% under motored conditions. This is the approximate range of values previously found by Cheng [86] under similar conditions. Ideal Gas Law calculations showed bulk gas compression temperature to be approximately the same as in the high compression ratio case near to TDC at 300 rpm despite significantly reduced pressure. LCR temperature was then higher for the whole expansion stroke. Therefore it is likely that higher peak rate of heat release for HCR is mainly due to the temperature independent pressure effect of fuel preparation as discussed in the literature [33, 98]. Speeds above 600 rpm result in LCR compression temperature lower than HCR, as would originally have been expected.

Peak indicated mean effective pressure was found to increase by approximately 2 bar when reducing temperature from $10°C$ to $-20°C$. This was attributed primarily to increased oxygen availability with more dense intake air. A longer, more complete diffusion burn was also possible due to lower temperatures slowing fuel preparation, avoiding an excessively high premixed spike. Peak combustion pressures and temperatures were lower, which should also reduce losses to heat transfer and blowby. This behaviour is favourable as reduced temperatures increase oil viscosity, increasing frictional resistance. The extra work output as temperatures are reduced at least partially offsets this increase.

The increased low speed peak IMEPg found at low compression ratio ($\approx$ 2 bar at all temperatures) is highly desirable as it should ensure a swift run-up to idle speed against high engine friction at reduced temperature in real cold start. This is the first stage in successful cold start, therefore it is likely that this phase will be accomplished faster at LCR than HCR. Increased work output was achieved with lower peak cylinder pressures and rates of pressure rise, offering knock-on benefits for durability and noise respectively. If absolute

peak IMEPg is not required, LCR offers scope to produce target output with even lower pressure operation.

At 300 rpm pilot injection was utilised at both compression ratios to extend the region of high work output, making the strategy more robust to changes in timing or speed. Peak rate of heat release was increased despite a 50% reduction in ignition delay, indicative of how effective cool flame reactions were in assisting fuel preparation. This is of particular importance at LCR due to the faster deterioration of work output as timing is retarded when compared to HCR. It is likely that pilot injection will be more critical for cold starts in a real engine at reduced speed. Starter motor cranking speed is typically in the region of 250 rpm at $20°C$ cold start. This was found to degrade to $\approx$ 150 rpm at $-25°C$ by Pacaud [50]. The dynamometer was unable to accurately hold the engine at low speeds without significant fluctuation during dynamic changes of loading in compression and expansion, especially during combustion. 300 rpm was chosen as the best compromise between low speed operation representative of cold cranking and speed stability. Pacaud found that increasing cranking speed from 140 rpm to 190 rpm reduced start delay dramatically from 30 s to 5 s. This is related to the exponentially longer time for losses to occur at lower engine speeds, reducing pressures and temperatures. The literature reveals that there is much variation in the low speed loss behaviour of engines, but that exponential loss does occur at reduced speeds. Zahdeh et al. [52] showed that a reduction in speed from 350 to 275 rpm caused a compression temperature and pressure drop from 570 to $430°C$ and 45 to 34.5 bar respectively. Gonzalez et al. [34] found a less extreme drop for a numerical study between 300 and 100 rpm of 390 to $360°C$ and 31 to 27.5 bar. Clearly the results are highly engine design dependent, but there is much to gain from focused development of low speed sealing behaviour.

8.2.3 Idle Speed Findings

The most challenging aspect of cold start raised in these studies occurred at elevated engine speed of approximately 1000 rpm whilst delivering load representative of engine friction

to maintain idle speed. At positive ambients this was not a difficulty, but conventional strategies failed to reliably meet a $< 10\%$ $\mathrm{CoV_{IMEPg}}$ target at points below $0°C$. This was especially difficult at $-20°C$ and unachieveable at LCR. Decreased residence times at sufficient temperatures and pressures for reliable ignition and thorough mixture preparation resulted in variable ignition delay and heat release rate profiles with resulting IMEPg fluctuations cycle-to-cycle.

At high compression ratio a solution was proposed whereby multiple pilot operation allowed acceptable behaviour over a range of injection timings and engine speeds. Optimised pilot quantity twin pilot operation resulted in major performance benefits, but the same effect could be achieved with a simple triple pilot with no need for optimisation. Heat release analysis revealed that there were fewer poor cycles with multiple pilot operation. Poor cycles result from extended ignition delay and/or low initial rate of heat release due to the inherently unstable conditions. Low temperatures and pressures combine with high engine speeds leaving insufficient mixture preparation time. These poor initial combustion characteristics were still present in the multiple pilot cases, but a few degrees after start of combustion, a secondary period of accelerating rate of heat release combustion was observed. This was not present when a single pilot was used. The extra phase of combustion was attributed to better fuel/air mixing with the early injections creating an homogeneous ignitable mixture throughout the cylinder. In the single pilot case this mixture is not present, and therefore when poor combustion initiation occurs, all readily combustible fuel is used up and the flame quenches in excessively lean areas before further mixing can occur. The extra combustion from utilising multiple pilots results in greater combustion efficiency, and therefore lower deviation of IMEPg. Robust work output at idle speed with lower deviations in combustion phasing and intensity should lead to better control of idle speed, increasing consumer comfort and perception of high quality cold idle.

These conclusions were supported by a KIVA-3v computational fluid dynamics investigation showing that triple pilot injection resulted in a well mixed fuel distribution throughout the bowl at the time where start of combustion was found experimentally. This was not the case in single pilot, even when introducing a large, far advanced pilot injection. In this case

fuel was found to escape into the squish region distant from the glow plug with increased time for liquid fuel to condense on the cold chamber surfaces. Small, well placed pilots allow fuel to be distributed around the bowl by air motion with minimum time for liquid fuel to adhere to the walls and therefore there is always vapour near to the glow plug during the crucial near-TDC period. When the main is injected, there is an activated environment where some low level reactions are occurring, releasing energy and volatile hydrocarbon species.

At the cold idle, LCR was at a significant disadvantage to HCR, especially at $-20°C$. Approximately 10 mm^3/str more fuel was required at LCR to generate the same IMEPg as HCR. For example, a 35 mm^3/str main injection at LCR could produce approximately 9 bar $\overline{IMEPg}_{10}$ at 1000 rpm. At HCR, a 25 mm^3/str main injection was sufficient for this $\overline{IMEPg}_{10}$. Lower pressures and temperatures resulted in further reduced mixing and more cycle-to-cycle variability at target loads. Multiple pilot injection was not able to stabilise LCR cold idle operation as at HCR. Secondary combustion was found on some cycles, boosting their IMEPg but not on others, therefore variability was actually increased. Lower energy cylinder conditions at LCR will reduce cool flame reactions, resulting in less volatile hydrocarbon species available for combustion from early pilot injection. As such the chance of secondary combustion is reduced compared to that at HCR.

LCR cold idle may be stabilised with increased glow plug temperature. Ceramic glow plugs used in this investigation produced acceptable work output at cold start 300 rpm conditions provided internal temperature was greater than $900°C$. At $-20°C$ cold idle, temperatures above approximately $1100°C$ were required for acceptable $< 10\%$ $\mathrm{CoV_{IMEPg}}$. Further minor improvements could be made with higher temperatures. This is partially due to higher convective heat transfer away from the glow plug surface with air motion due to engine speed. Heat release analysis revealed that there were higher burning rates for the duration of combustion and increased secondary combustion at higher glow plug temperatures. This may be a result of secondary ignition of fuel impinging on the glow plug or better fuel preparation resulting from greater heat input from the tip.

The power consumption of the ceramic plug at high temperature was typically 50% lower

than the steel plug, but heat was more focused on the glowing tip. As such it seems unlikely that significantly more energy is being transferred to the fuel than in the steel glow plug case. The smaller glowing tip at a higher temperature results in significantly better cold idle stability. As such the glow plug appears to perform a dual role as combustion initiator and fuel preparation aid. Ignition delay was significantly less variable with high tip temperatures, reducing CoV_{IMEPg} with phasing differences. Peak rate of heat release and total fuel burn were also more repeatable and higher, despite probable lower total heat input to the charge. It may be more important to ensure the small stream of fuel which passes close to or impinges upon the glowing tip is very well prepared by a small, high temperature heat source than a larger volume of fuel being partially prepared by a larger, cooler source. The results of the glow plug protrusion test revealed large degredation in performance for small protrusion changes, clearly placement and total glowing area are still crucial at a given temperatue and must be considered very carefully in any future design which utilises low tip area glow plugs.

8.2.4 The Place of Cold Start in General Engine Development

This investigation was initiated because there were concerns related to the trend for light duty diesel engines moving towards lower compression ratios. Deficiencies found at cold start, especially at idle speeds, are a direct but unavoidable side effect of this trend. The majority of engine development takes place at fully warm conditions or at less extreme temperatures typical of daily cold start in the UK. The focus is generally on emissions reduction to meet increasingly strict legislation or a reduction in fuel consumption to improve a vehicle's green credentials. Cold start at significantly reduced temperatures is a secondary, but crucial target for engine development. Once acceptable behaviour is guaranteed under normal operating conditions, it is up to the developer to find a way to make the engine start when temperatures are significantly reduced and to obtain acceptable running in the warm-up phase.

Emissions were not recorded during the course of this investigation. It was not a consid-

eration for the industrial sponsors. There are currently no European guidelines or limits for diesel emissions at starts lower than the standard test cycle, which is performed at $25°C$ [101]. Cold start regulation for SI engines of CO and HC at a test temperature of $-7°C$ came into effect in 2002 [102]. It is proposed that a NO_x test at $-7°C$ will be introduced for CI engines during the Euro V/VI period. A requirement for any NO_x after-treatment to be functioning at acceptable efficiency after 400 seconds and that EGR control functions at this low temperature [103] may also be introduced. Therefore it seems unlikely that emissions at lower temperatures will become part of the standard test for the foreseeable future (Euro VI proposed introduction April 2013). Throughout much of Europe this is inconsequential as temperatures rarely dip significantly below freezing and combustion rapidly warms the engine resulting in only a small transient time at the lowest temperatures. Where low temperature cold start is a regular occurrence, emissions are significantly higher than during steady state temperature, principally due to poor fuel preparation and incomplete combustion. It is likely that a reduction in compression ratio will increase these problems. For example, as mentioned above, LCR typically required 10 mm^3/str more fuel injection than HCR to achieve the same IMEPg utilising a single pilot at cold idle. As the total heat release is similar in the two cases, this extra fuel will be expelled as products of incomplete combustion.

It is unlikely that other design trends and technological improvements will have a negative effect on the cold start regime. For example, the pilot injection techniques investigated for cold start improvements are increasingly used for emissions control. Fuel distribution and mixture preparation before, during and after combustion may be altered with pilot, split main and post injections. Better mixing results in reduced over-rich areas which are detrimental to complete combustion — the consequence being lower soot, hydrocarbon and carbon monoxide emissions. Post injection may be used to further oxidise soot and CO [104, 105] and is a requirement for the regeneration of current diesel particulate filters. The studies presented here indicate that similar processes apply at cold start. Outside of very narrow windows, pilot injection/injections improved fuel preparation, resulting in greater combustion efficiency. Using relatively rich mixtures, where much of the fuel is not expected to burn, would inevitably result in high HC, soot and CO levels. Any increase in fuel burn

would be expected to reduce these incomplete combustion products. Similar results were found at low compression ratio when utilising high temperature ceramic plugs. Greater rates of heat release resulted in improved work output. As claimed by the manufacturers for their current production range of high temperature plugs [49], reduced HC and PM emissions would be expected.

Combustion system design is an area not considered in this work. It has the potential to produce side-effects at cold start when optimised for warm running. There is evidence in the literature to show that there may be a fuel consumption benefit moving to a more quiescent design. Heat transfer correlations generally include an air motion term which would reduce with low swirl. More complex models developed by Payri et al. [106] based on two engines with different swirl numbers confirm this. Lower swirl numbers led to lower convective heat transfer, reducing the heat transfer coefficient and therefore total calculated heat loss. Experimental studies by Mori et al. [107] and Espey et al. [108] have shown that quiescent operation allows combustion to occur throughout the cylinder, whilst swirl has the effect of constraining combustion to the bowl region. In this study, LCR losses were found to be significantly lower than HCR. It is possible that further reduction of losses offered by a more quiescent design may increase in-cylinder pressures and temperatures in the crucial period after fuel injection and during early combustion. This would benefit fuel preparation provided suitable fuel mixing could be achieved.

Quiescent design would reduce fuel/air mixing, and therefore the fuel injection events must rectify this. Multiple pilot injections were found to assist idle stability at HCR, and therefore it is possible that three or four pilot injections could ensure better fuel distribution, but low swirl would reduce the effectiveness. Advanced hardware, considered in the literature for running under normal conditions, may also impact on cold start. A group-hole injector was investigated by Park and Reitz [109], where 8 pairs of 75 μm holes were arranged around the injector. The top 8 holes were targeted to utilise the air in the squish region. The bottom set were aimed to utilise air in the bowl. Smaller holes required an increased 1500 bar rail pressure. Better oxygen utilisation at stoichiometric operation than the standard 8 hole injector resulted in $\approx 16\%$ improvement in specific fuel consumption. Higher rail pressures

up to 3000 bar were investigated by Zhang [110], which further reduced droplet diameter. Lower droplet size increases surface area to volume ratio, therefore oxygen utilisation and rate of evaporation should improve. It was found that excessive spray penetration could be mitigated with microhole nozzles.

It is possible that group-hole nozzles with $< 75\mu$m holes at ultra-high injection pressures, in conjunction with reduced losses from quiescent operation, may allow improved premixed fuel preparation to the extent that it becomes self sustaining. This was not possible at LCR cold idle without high temperature glow plugs. Port deactivation or the use of a swirl flap would allow quiescence to be altered to ascertain the effects of air motion on idle stability, both with or without advanced injector designs.

8.3 Future Work

More accurate replication of the cold start regime is possible with thorough cold soaks in a temperature controlled environment allowing convective cooling than with direct cooling of circulated coolant. Therefore the most general recommendation for future work would be a more targeted application of findings performed under these cold soak conditions. Utilising strategies which produced benefits in this work under cold soak conditions would validate their real world applicability. The next step would be to implement them in a full vehicle application and test their validity in cold environments. The following three steps represent the envisaged path to implementing the findings in a real vehicle, the first of which is summarised in this piece of work

- High test rate direct cooling single cylinder broad study.
- Low test rate single and/or multi-cylinder cold soak targeted validation.
- Full vehicle real world testing proof of concept.

Several additional areas of research could improve insight into the the cold start region and feasibility of reduced compression ratio. The following recommendations may benefit future investigations:

- Better understanding of how heat transfer varies when compression ratio is lowered at cold start could be obtained by using direct measurement of compression and wall temperatures to calculate heat transfer. Fast response thermocouples of the type used by Lee et al. [90] would enable these measurements to be taken. The single cylinder rig made direct blowby measurement very challenging, and could be improved with multi-cylinder experimentation, or the implementation of an extra dummy cylinder which is perfectly out of phase to eliminate the large in-out flow of air from the crankcase.

- Conclusions about mixture preparation drawn within this work are primarily inferred from heat release rate progressions and computer modelling. An optically accessible engine with high speed imaging would enable combustion initiation and propagation to be observed for the different injection strategies. The role of the glow plug would also be clarified by observing the location of combustion initiation and whether this is a discrete event or a continuous combustion for some period of the heat release.

- No testing was performed at LCR with high temperature glow plugs and multiple pilot injection. Additional benefit from high temperatures may move this strategy into the stable region. Low voltage metallic glow plugs operating in the region of $1050°C$, in conjunction with multiple pilots, may prove to be a low incremental cost path to good quality cold idle at low compression ratio.

- A practical test with feedback from a panel of human test subjects similar to that presented by Martino et al. [67] would provide good data on how the different idle strategies perform in terms of cycle-to-cycle IMEPg deviation, engine speed and acceleration variation and consumer perception of overall idle quality in a real multi-cylinder application. The developments suggested in this work could be quantified from a consumer perception point of view, which is arguably as important as statistical data derived from data acquisition.

- Combustion system design and fuel injection equipment are areas not tackled in this work. It would be of use to quantify any potential benefits from designs which reduce heat transfer losses with lower charge motion, or that improve mixture preparation with high injection pressures and an increased number of smaller injector nozzle holes.

8.4 Conclusions

Cold start performance has been investigated on a single cylinder, high pressure common rail, direct injection diesel engine at compression ratios 18.4:1 and 15.4:1. The conclusions that have been drawn from the investigations are considered applicable to multi-cylinder engines operating at cold start conditions, and therefore provide implications for future design and calibration.

Firstly, investigation at 18.4:1 resulted in the following conclusions when considering operation at 300 rpm, a speed just higher than cranking

- High indicated mean effective pressure (up to 10.5 bar $\overline{IMEP}g_5$ at $-20°C$) is possible with a single over-rich fuel injection, providing that main injection timing is just after TDC.
- A small pilot injection reduces the ignition delay and increases the peak rate of heat release. This extends the region of main injection timings which result in high work output from TDC to positions as retarded as 15°ATDC. Pilot injection does not increase work output when total fuel injected is sufficient for global $\phi > 1$, but up to 1 bar improvement is found when global $\phi < 1$.
- There is a strong relationship between total cumulative heat release and IMEPg. Indicated thermal efficiency does not vary greatly over the considered range of injection timings whereas combustion efficiency can rapidly drop to zero at timings after TDC.
- Low temperatures result in increased peak IMEPg, mainly due to greater oxygen availability and longer combustion duration enabling more complete fuel burn. The highest IMEPg achieved at $10°C$ was ≈ 8.5 bar, rising to ≈ 10.5 bar at $-20°C$.

Cold idle operation was approximated by motoring the engine to speeds in the range 600–1500 rpm. Indicated work output was adjusted to match expected frictional demands at each test temperature. The following conclusions, still at 18.4:1, were obtained from these studies

- A pilot injection is necessary to obtain significant positive work output at all temperatures between $10°C$ and $-20°C$.
- With a pilot, cycle-to-cycle variation of IMEPg becomes worse as temperature is reduced. At $-20°C$ it was impossible to achieve $\mathrm{CoV}_{\mathrm{IMEPg}} < 10\%$.
- Twin pilot injection increases work output by $\approx 25\%$ for a given fuelling at $-20°C$. This is a result of reduced ignition delay and increased peak rate of heat release. Stability in terms of $\mathrm{CoV}_{\mathrm{IMEPg}}$ also improved so that a range of timings gave $\mathrm{CoV}_{\mathrm{IMEPg}} < 10\%$. The principle reason for this was the introduction of a second phase of accelerating combustion after poor initial heat release which would previously have resulted in low IMEPg for that cycle. A simple triple pilot injection strategy was found to maximise this benefit, resulting in low $\mathrm{CoV}_{\mathrm{IMEPg}}$ values over a broad range of injection timings and engine speeds at $-20°C$. A further pilot injection resulted in the re-introduction of poor cycles.
- A CFD investigation was performed to reveal any differences in fuel/air mixing with multiple pilots. The results indicate that multiple small pilots provide a more homogeneous fuel distribution throughout the bowl before main injection than either single main injection or larger pilots injected at advanced timings.

A reduction in compression ratio to 15.4:1 was achieved by replacing the piston with one of the same design, but with a larger bowl volume. The trends observed were generally similar to those at 18.4:1, but with the following significant differences.

- Peak compression pressure at 300 rpm reduced from ≈ 40 bar to ≈ 33 bar at $-10°C$.
- Using the Ideal Gas Law to calculate in-cylinder temperature with measured cylinder pressure, and assuming no (or identical) mass loss, 15.4:1 in-cylinder temperature was found to be higher at all points after TDC at speeds below 600 rpm.
- Losses to heat transfer and blowby increase rapidly at the lowest engine speeds due to extending time under high pressure conditions. Heat transfer loss prediction using

the Hohenberg correlation decreased by $\approx 14\%$ when lowering compression ratio. A simple blowby model predicted a similar reduction in blowby energy and mass loss. Attempts to measure blowby mass directly resulted in much variation, but on average 15.4:1 blowby was 30% lower than 18.4:1 at 300 rpm.

- At 300 rpm cold start conditions, 15.4:1 is capable of ≈ 2 bar increase in peak IMEPg at all test temperatures. This is partially due to reduced losses, but also due to reduced peak rates of heat release and longer combustion durations allowing more thorough fuel mixing and greater cumulative heat release.

- At cold idle speeds, $-20°C$, the general performance of 15.4:1 is significantly worse than 18.4:1. 10 mm^3/str more fuel was required for similar IMEPg. Work output and CoV_{IMEPg} worsen greatly with speed, especially above 1000 rpm. The best CoV_{IMEPg} obtained was $\approx 20\%$, twice the level defined as acceptable for this investigation.

- Multiple pilot does not benefit 15.4:1 cold idle. Some cycles experience increased work output as found at 18.4:1, whilst others do not, worsening the spread of possible IMEPg values.

The following key observations relating to glow plug operation were made. Experiments were performed at both compression ratios. Ceramic glow plugs enabled investigation of the effect of glow plug temperature on cold start performance.

- At 18.4:1, 300 rpm cold start, the glow plug is not required for high work output operation at $10°C$, but there were some misfiring cycles at $-10°C$. The glow plug is crucial for combustion initiation at $-10°C$, 15.4:1.

- At 1000 rpm for the more stable 18.4:1, the glow plug was not required at $10°C$, but there was potential for increased variability at $0°C$ (10% $CoV_{IMEPg} \rightarrow 30\%$). Further reduction in temperature led to near total misfire without glow plug operation. Multiple pilot injection did not improve stability without glow plug operation. The glow plug is a requirement for cold idle; multiple pilot merely improves performance. It is not possible to directly compare these findings to 15.4:1 as no comparable experiments

were performed. All indications are that 15.4:1 cold idle operation without glow plug operation would be significantly worse than 18.4:1 at these temperatures.

- At 300 rpm, $-10°C$, 15.4:1, high initial work output could be achieved on every cycle with glow plug core temperature of $900°C$. In was necessary to increase core temperature to $950°C$ at $-20°C$. Poor 15.4:1 cold idle stability at $-20°C$ could be improved with higher glow plug temperatures. Steel glow plugs gave $\mathrm{CoV_{IMEPg}}$ in the region of 20%. Similar performance was obtained when glow plug internal temperature was $950°C$. An increase to $1100°C$ improved $\mathrm{CoV_{IMEPg}}$ to 10%. $\overline{IMEP}g_{10}$ also improved from 3.5 bar to 4.5 bar.

- Increasing glow plug temperature produced a reduced and less variable ignition delay, especially for the first fired cycles before there has been significant heat input from previous cycles. There is an accompanying increase in peak rate of heat release, especially for the poor cycles, as glow plug temperature is increased.

- Glow plug placement is crucial for reliable cold idle operation. A 25% reduction in glow plug protrusion at 18.4:1, $-20°C$ increased $\mathrm{CoV_{IMEPg}}$ from 10% to 25%. Any further reduction in protrusion led to rapid degredation in performance with onset of misfire.

References

[1] Carfolio. Automotive technical data and specifications. Technical report, www.carfolio.com, accessed 11/03/2008.

[2] Neumann Petroleum Pty Ltd. Unleaded petrol material safety data sheet.

[3] Phillips Petroleum Company. No. 2 diesel fuel material safety data sheet.

[4] Editor: Horst Bauer. *Diesel Engine Management 4th edition.* Robert Bosch GmbH, 2005.

[5] United Nations. Kyoto protocol to the united nations framework convention on climate change. Technical report, United Nations, 1998.

[6] Ritt Bjerregaard. Commission Recommendation of 5 February 1999 on the reduction of CO_2 emissions from passenger cars. *Official Journal of the European Communities 1999/125/EC*, 1999.

[7] European Union. Press release ip/07/155, 2007.

[8] R Teichmann and S Bernet. UK new car registrations by CO_2 performance: Report on the 2005 market. Technical report, The Society of Motor Manufacturers and Traders Limited, 2006.

[9] Efthimios Zervas and Christos Lazarou. CO_2 benefit from the increasing percentage of diesel passenger cars in Sweden. *International Journal of Energy Research*, 31:192–203, 2007.

[10] Peter Schmidt. Diesel Car Prospects to 2008. Technical report, Automotive Industry Data, 2002.

[11] J. A. Wünning and J. G. Wünning. Flameless oxidation to reduce thermal NO-formation. *Progress of Energy Combustion Science*, 23:81–94, 1997.

[12] M. Badami, F. Mallamo, F. Millo, and E. E. Rossi. Influence of multiple injection strategies on emissions, combustion noise and BSFC of a DI common-rail diesel engine. *SAE Paper 2002-01-0503*, 2002.

[13] G. M. Bianchi, P. Pelloni, F. E. Corcione, and F. Luppino. Numerical analysis of passenger car HSDI diesel engines with the 2nd generation of common-rail injection systems: The effect of multiple injections on emissions. *SAE Paper 2001-01-1068*, 2001.

[14] S. Kevin Chen. Simultaneous reduction of NO_x and particulate emissions by using multiple injections in a small diesel engine. *SAE Paper 2000-01-3084*, 2000.

[15] Felice E. Corcione, Bianca M. Vaglieco, Giuseppe E. Corcione, M. Lavorgna, and Rosario Lanzafame. Study of the combustion system of a new small DI diesel engine with advanced common-rail injection system. *SAE Paper 2003-01-1782*, 2003.

[16] Jin ha Lee, Yuichi Goto, and Matsuo Odaka. Measurement of the diesel exhaust particle reduction effect and particle size distribution in a transient cycle mode with an installed diesel particulate filter (DPF). *SAE Paper 2002-01-1005*, 2002.

[17] P. Richards, B. Terry, and D. Pye. Demonstration of the benefits of DPF/FBC systems on London black cabs. *SAE Paper 2003-01-0375*, 2003.

[18] K. Y. Cheng, P. J. Shayler, and M. Murphy. The influence of blow-by on indicated work output from a diesel engine under cold start conditions. *Proc. IMechE - Part D*, 218(3):333–340, 2004.

[19] Isao Osuka, Masataka Nishimura, Yasushi Tanaka, and Masahiko Miyaki. Benefits of new fuel injection system technology on cold startability of diesel engines - improvements on cold startability and white smoke reduction by means of multi injection with common rail fuel system (ECD-U2). *SAE Paper 940586*, 1994.

[20] K. Shen, R. D. Matthews, J. P. Chiu, M. H. Darden, R. W. Faidley, S. P. Nichols, and W. F. Weldon. Initial study of railplugs as an aid for cold starting of diesels. *SAE Paper 940108*, 1994.

[21] Ruonan Sun, E. Jack Sweet, J. R. Zurio, and William C. Pfefferie. Diesel engine cold starting with catalytically ignited recirculated exhaust gas. *SAE Paper 940086*, 1994.

[22] John E. Dec. A conceptual model of DI diesel combustion based on laser-sheet imaging. *SAE Paper 970873*, 1997.

[23] John B. Heywood. *Internal Combustion Engine Fundamentals*. McGraw Hill Book Company, 1988.

[24] W. M. Studzinski, P. M. Liiva, P. J. Choate, W. P. Acker, M. Smooke K., Brezinsky, T. Litzinger, and S. Bower. A computational and experimental study of combustion chamber deposit effects on NO_x emissions. *SAE Paper 970873*, 1997.

[25] L. M. Pickett1, J. A. Caton, M. P. B. Musculus, and A. E. Lutz. Evaluation of the equivalence ratiotemperature region of diesel soot precursor formation using a two-stage Lagrangian model. *International Journal of Energy Research*, 7:349–370, 2006.

[26] Sanghoon Kook, Chongsik Bae, Paul C. Miles, Dae Choi, and Lyle M. Pickett. The influence of charge dilution and injection timing on low-temperature diesel combustion and emissions. *SAE Paper 2005-01-3837*, 2005.

[27] N. Ladommatos, S. M. Abdelhalim, H. Zhao, and Z. Hu. The dilution, chemical, and thermal effects of exhaust gas recirculation on diesel engine emissions - part 1: Effect of reducing inlet charge oxygen. *SAE Paper 961165*, 1996.

[28] D. T. Hountalas, T. C. Zannis, and G. C. Mavropoulos. Potential benefits in heavy duty diesel engine performance and emissions from the use of variable compression ratio. *SAE Paper 2006-01-0081*, 2006.

[29] M. M. Abou Al-Sood, A. M. Ibrahim, and A. A. Abdel-Latif. Optimum compression ratio variation of a 4-stroke, direct-injection diesel engine for minimum BSFC. *SAE Paper 1999-01-2519*, 1999.

[30] Adnan Parlak, Halit Yasar, and Bahri Sahin. Performance and exhaust emission characteristics of a lower compression ratio LHR diesel engine. *Energy Conversion and Management*, 44:163–175, 2003.

[31] Evert Rosseel and Roger Sierens. The physical and the chemical part of the ignition delay in diesel engines. *SAE Paper 961123*, 1996.

[32] C. B. Dicksee. Some problems connected with high-speed compression ignition engine development. *Proc. IMechE*, 26:309–382, 1932.

[33] C. Crua, D. A. Kennaird, S. S. Sazhin, M. R. Heikal, and M. R. Gold. Diesel autoignition at elevated in-cylinder pressures. *International journal of Engine Research*, 5(4):365–374, 2004.

[34] Manuel A. Gonzalez, Gary L. Borman, and Rolf D. Reitz. A study of diesel cold starting using both cycle analysis and multidimensional calculations. *SAE Paper 910180*, 1991.

[35] M. Caron, M. Goethals, G. De Smedt, J. Berghmans, S. Vliegen, E. Van't Oost, and A. van den Aarssen. Pressure dependence of the auto-ignition temperature of methane/air mixtures. *Journal of Hazardous Materials*, 65(3):233–244, 1999.

[36] V. Bermúdez, J. M. García, E. Juliá, and S. Martínez. Engine with optically accessible cylinder head: A research tool for injection and combustion processes. *SAE Paper 2003-01-1110*, 2003.

[37] Ming-Chia Lai, Naeim A. Henein, Xingbin Xie, Tsan-Hai Chue, Yasuhiko Itoh, and Walter Bryzik. Diesel cold-starting study using optically accessible engines. *SAE Paper 952366*, 1995.

[38] Charles E. Solbrig and T. A. Litzinger. The effect of intake charge temperature on combustion and emissions in an optically accessible DI diesel engine with and without swirl. *SAE Paper 902060*, 1990.

[39] Monish Darda, Anup Sable, G. V. J. Sastry, and Harish Chandra. Detailed engine mapping using E-DACS for thorough performance analysis. *SAE Paper 950012*, 1995.

[40] Katsumi Kataoka, Masahiro Tsurusaki, and Toshikazu Kadota. Effect of fuel properties on the combustion process and NO emission in spark ignition engine. *SAE Paper 931940*, 1993.

[41] R. Worret, S. Bernhardt, F. Schwarz, and U. Spicher. Application of different cylinder-pressure-based knock detection methods in spark ignition engines. *SAE Paper 2002-01-1668*, 2002.

[42] Brian Higgins, Dennis Siebers, and Allen Aradi. Diesel-spray ignition and premixed-burn behavior. *SAE Paper 2000-01-0940*, 2000.

[43] L. J. Spadaccini abd J. A. Tevelde. Autoignition characteristics of aircraft-type fuels. *Combustion and Flame*, 46:286–300, 1983.

[44] F. W. Stringer, A. E. Clarke, and J. S. Clarke. The spontaneous ignition of hydrocarbon fuels in a flowing system. *Proc. IMechE*, 184(3J):212–225, 1970.

[45] H. H. Wolfer. Ignition lag in diesel engines. *VDI-Forschungsheft, Translated by Royal Aircraft Establishment, August 1959*, (392), 1983.

[46] H. Hiroyasu, T. Kadota, and M. Arai. Supplementary comments: Fuel spray characterization in diesel engines. *from "Combustion Modelling in Reciprocating Engines" by J. N. Mattavi and C. A. Amann, New York: Plenum Press*, pages 369–408, 1980.

[47] N. Watson, A. D. Pilley, and M. Marzouk. A combustion correlation for diesel engine simulation. *SAE Paper 800029*, 1980.

[48] H. O. Hardenburg and F. W. Hase. An empirical formula for computing the pressure rise delay or a fuel from its cetane number and from the relevant parameters of direct injection diesel engines. *SAE Paper 790493*, 1979.

[49] Beru AG. Beru glow plugs - faster, more reliable diesel cold starting, even at low temperatures. Internet, http://www.beru.com/download/produkte/endverbraucher_gk_e.pdf, 2003.

[50] Pierre Pacaud, Hervé Perrin, and Olivier Laget. Cold start on diesel engine: Is low compression ratio compatible with cold start requirements? *SAE Paper 2008-01-3726*, 2008.

[51] N. M. F. Vulliamydnan. Matching a diesel engine to light road vehicles. *Proceedings of the Institution of Mechanical Engineers, Automobile Division*, 1954:225–245, 1954.

[52] Akram Zahdeh, Naeim Henein, and Walter Bryzik. Diesel cold starting - actual cycle analysis under border-line conditions. *SAE Paper 900441*, 1990.

[53] Paul J. Shayler, David K. W. Leong, and Michael Murphy. Contributions to engine friction during cold, low-speed running and the dependence on oil viscosity. *SAE Paper 2005-01-1654*, 2005.

[54] J. A. Burrows. *An Investigation into the Performance of Cold Start Diesel Engines.* PhD thesis, University of Nottingham, 1998.

[55] C. R. Tindle. *An Investigation of Factors which Influence the Cold Start Performance of Diesel Engines.* PhD thesis, University of Nottingham, 2000.

[56] Lurun Zhong, Steve Gruenewald, and Naeim A. Henein. Lower temperature limits for cold starting of diesel engine with a common rail fuel injection system. *SAE Paper 2007-01-0934*, 2007.

[57] Jincai Zheng, David L. Miller, Nicholas P. Cernansky, Dexin Liu, Yong Li, Xiujing Shang, and Mingxian Zhang. Two types of autoignition and their engine applications. *SAE Paper 2005-01-0178*, 2005.

[58] Zhiping Han, Naeim Henein, Bogdan Nitu, and Walter Bryzik. Diesel engine cold-start combustion instability and control strategy. *SAE Paper 2001-01-1237*, 2001.

[59] Ken Mitchell. The cold performance of diesel engines. *SAE Paper 932768*, 1993.

[60] A. J. Davies. Injection characteristics and diesel knock. *Proc. IMechE, Automobile Division*, 1951:214–223, 1951.

[61] P. Carlucci, A. Ficarella, and D. Laforgia. Effects on combustion and emissions of early and pilot fuel injections in diesel engines. *International Journal of Engine Research*, 6(1):43–60, 2005.

[62] Masahiro Ishida, Zhi-Li Chen, Gui-Feng Luo, and Hironobu Ueki. The effect of pilot injection on combustion in a turbocharged D.I. diesel engine. *SAE Paper 941692*, 1994.

[63] M. Gairing, J. M. Marriott, K. H. Reders, A. A. Reglitzky, and P. E. Wolveridge. The effect of modern additive technology on diesel fuel performance. *SAE Paper 950252*, 1995.

[64] Bruno Lindl and Heinz-Georg Schmitz. Cold-start equipment for diesel direct-injection engines. *SAE Paper 1999-01-1244*, 1999.

[65] Oskar Schatz. Cold start improvement by use of latent heat stores. *SAE Paper 921605*, 1992.

[66] Xiang Dong Chen and Martin Roskilly. A crank angular velocity based method for engine IMEP measurement for idle quality investigation and adaptive ignition time trimming to improve idle quality. *SAE Paper 1999-01-0855*, 1999.

[67] U. Di Martino, G. Formisano, and G. Lucignano. Combustion stability at idle: A non-indicated methodology for analysis. *SAE Paper 2003-01-0640*, 2003.

[68] Charlie Teng. Evaluation of idle combustion stability using flywheel acceleration. *SAE Paper 2003-01-1673*, 2003.

[69] P. C. Hinze and W. K Cheng. Assessing the factors affecting SI engine cycle-to-cycle variations at idle. In *27th Symposium (International) on Combustion*, Pittsburgh, 1998. The Combustion Institute.

[70] Kuo-Chiang Chen, Koen Dewitte, and Wai K. Cheng. Fuel effects and enrichment effects on engine starting and warm-up behavior. *SAE Paper 9500650*, 1995.

[71] S. Jabez Dhinagar, B. Nagalingam, and K. V. Gopalakrishnan. Spark assisted diesel operation in a low compression ratio low heat rejection engine. *SAE Paper 920545*, 1992.

[72] O. Laguitton, C. Crua, T. Cowell, M.R. Heikal, and M.R. Gold. The effect of compression ratio on exhaust emissions from a PCCI Diesel engine. *Energy Conversion and Management*, 48:2918–2924, 2007.

[73] Lingen Chen, Junxing Lin, Jun Luo, Fengrui Sun, and Chih Wu. Friction effect on the characteristic performance of diesel engines. *International Journal of Engine Research*, 26: 965–971, 2002.

[74] Souvik Bhattacharyya. Optimizing an irreversible diesel cycle - fine tuning of compression ratio and cut-off ratio. *Energy Conversion and Management*, 41:847–854, 2000.

[75] Optifluid CS cold start fuel data sheet.

[76] N. Brown, V. Gupta, A. La Rocca, P. J. Shayler, M. Murphy, I. Pegg, and M. Watts. Effects of injection strategies on the cold start up of DI diesel engines. *Proc. IMechE*, 221(Part D): 1415–1423, 2007.

[77] John E. Dec and Dale R. Tree. Diffusion-flame / wall interactions in a heavy-duty DI diesel engine. *SAE Paper 2001-01-1295*, 2001.

[78] Chao F. Daniels and Brian M. Scilzo. The effects of electrode design on mixture ignitability. *SAE Paper 960606*, 1996.

[79] Tomohiro Kanda, Takazo Hakozaki, Tatsuya Uchimoto, Jyunichi Hatano, Naoto Kitayama, and Hiroshi Sono. PCCI operation with early injection of conventional diesel fuel. *SAE Paper 2005-01-0378*, 2005.

[80] Fanhua Ma, Yu Wang, Haiquan Liu, Yong Li, Junjun Wang, and Shangfen Ding. Effects of hydrogen addition on cycle-by-cycle variations in a lean burn natural gas spark-ignition engine. *International Journal of Hydrogen Energy*, 33(2):823–831, 2008.

[81] Michael F. J. Brunt and Kieron C.Platts. Calculation of heat release in direct injection diesel engines. *SAE Paper 1999-01-0187*, 1999.

[82] Michael F. J. Brunt, Harjit Rai, and Andrew L. Emtage. The calculation of heat release energy from engine cylinder pressure data. *SAE Paper 981052*, 1998.

[83] J.A. Gatowski, E.N. Balles, F.E. Nelson, J.A. Ekchian, and J.B. Heywood. Heat release analysis of engine pressure data. *SAE Paper 841359*, 1984.

[84] G. J. Pugh. *The Analysis of Heat Release in the Investigation of Split Main Fuel Injection in a Diesel Engine.* PhD thesis, University of Nottingham, 2004.

[85] Günter Hohenberg. Advanced approaches for heat transfer calculations. *SAE Paper 790825*, 1979.

[86] K. Cheng. *Proceses Influencing the Indicated Work Output of Direct Injection Diesel Engines During Cold Starting.* PhD thesis, University of Nottingham, 2002.

[87] Alessandro Catanese. *Emission Characterisation and Cylinder Pressure Information for Applications in the Electronic Engine Management of Diesel Engines.* PhD thesis, University of Nottingham, 2006.

[88] U. Mathis, M. Mohr, and A. Forss. Comprehensive particle characterization of modern gasoline and diesel passenger cars at low ambient temperatures. *Atmospheric Environment*, 39(Part D):107–117, 2005.

[89] F. Schwarz and U. Spicher. Determination of residual gas fraction in IC engines. *SAE Paper 2003-01-3148*, 2003.

[90] Seokhwan Lee, Choongsik Bae, Robert Prucka, Gerald Fernandes, Zoran S. Filipi, and Dennis N. Assanis. Quantification of thermal shock in a piezoelectric pressure transducer. *SAE Paper 2005-01-2092*, 2005.

[91] Paulius V. Puzinauskas, Joseph C. Eves, and Nohr F. Tillman. Measuring absolute-cylinder pressure and pressure drop across intake valves of firing engines. *SAE Paper 941881*, 1994.

[92] Harjit S. Rai, Michael F. J. Brunt, and Colin P. Loader. Quantification and reduction of IMEP errors resulting from pressure transducer thermal shock in an S.I. engine. *SAE Paper 1999-01-1329*, 1999.

[93] Terunao Kawai, Takayuki Hirose, Syuuzou Miyake, Jiro Senda, and Hajime Fujimoto. Detection of luminescence from pre-autoignition reaction zone in S.I. engine. *SAE Paper 970508*, 1997.

[94] H.K. Ng. *The Simulation of Combustion in Diesel Engines using KIVA-3V on a PC Platform.* PhD thesis, University of Nottingham, 2003.

[95] P.J. Shayler and H.K. Ng. Simulation studies of the effect of fuel injection pattern on NO and soot formation in diesel engines. *SAE Paper 2004-01-0116*, 2004.

[96] Patrick F. Flynn, Russell P. Durrett, Gary L. Hunter, Axel O. zur Loye, O. C. Akinyemi, John E. Dec, and Charles K. Westbrook. Diesel combustion: An integrated view combining laser diagnostics, chemical kinetics, and empirical validation. *SAE Paper 1999-01-0509*, 1999.

[97] J. J. Zheng, J. H. Wang, B. Wang, and Z. H. Huang. Effect of the compression ratio on the performance and combustion of a natural-gas direct-injection engine. *Proc. IMechE - Part D*, 223(1):85–98, 2009.

[98] Takuji Ishiyama, Masahiro Shiojiand Tadayoshi Ihara, and Akihiro Katsuura. Modelling and experiments on ignition of fuel sprays considering the interaction between fuel-air mixing and chemical reactions. *SAE Paper 2003-01-1071*, 2003.

[99] Hajime Fujimoto, Jiro Senda, Masahiro Nagae, Yoshiaki Asou, and Kazushi Tsurutani. Combustion in a small DI diesel engine at starting. *SAE Paper 920697*, 1992.

[100] Naeim A. Henein, Akram R. Zahdeh, Mahmoud K. Yassine, and Walter Bryzik. Diesel engine cold starting: Combustion instability. *SAE Paper 920005*, 1992.

[101] Gordon E. Andrews, Grant Zhu, Hu Li, Alex Simpson, James A. Wylie, Margaret Bell, and James Tate. The effect of ambient temperature on cold start urban traffic emissions for a real world SI car. *SAE Paper 2004-01-2903*, 2004.

[102] European Union. Directive 2001/100/ec, 2001.

[103] Delphi Corporation. Worldwide emissions standards - passenger cars & light duty trucks. Internet, hard copy available on request, http://delphi.com/pdf/emissions/2008_Delphi_PC.pdf, 2008.

[104] Hanho Yun and Rolf D. Reitz. An experimental investigation on the effect of post-injection strategies on combustion and emissions in the low-temperature diesel combustion regime. *Transactions of the ASME*, 129:279–286, 2007.

[105] Nicolas Dronniou, Marc Lejeune, Iyad Balloul, and Pascal Higelin. Combination of high EGR rates and multiple injection strategies to reduce pollutant emissions. *SAE Paper 2005-01-3726*, 2005.

[106] F. Payri, X. Margot, A. Gil, and J. Martin. Computational study of heat transfer to the walls of a DI diesel engine. *SAE Paper 2005-01-0210*, 2005.

[107] Kazutoshi Mori, Hiroshi Jyoutaki, Kenji Kawai, and Kenji Sakai. New quiescent combustion system for heavy-duty diesel engines to overcome exhaust emissions and fuel consumption trade-off. *SAE Paper 2000-01-1811*, 2001.

[108] C. Espey, J. A. Pinson, and T. A. Litzinger. Swirl effects on mixing and flame evolution in a research DI diesel engine. *SAE Paper 902076*, 1992.

[109] Sung Wook Park and Rolf D. Reitz. Optimization of fuel/air mixture formation for stoichiometric diesel combustion using a 2-spray-angle group-hole nozzle. *Fuel*, 88:843–852, 2009.

[110] W Zhang, K Nishida, J Gao, and D Miura. An experimental study on flat-wall-impinging spray of microhole nozzles under ultra-high injection pressures. *Proc. IMechE - Part D*, 222: 1731–1741, 2008.

Appendix

A.1 Fuelling Tests

Figure a gives an overview of a variety of experiments where differing quantities of fuel were injected at a variety of timings and test temperatures for a 300 rpm engine speed. Fuel was collected over a period of time from three injectors firing into a bomb, which was in turn connected to a measuring cylinder on a digital scales. Typically, 100 ml+ of fuel was collected to ensure experimental and measurement errors were kept to a minimum. As can be seen, fuel delivery is very close to demand until very high fuel delivery, where a saturation of fuel quantity around 90 mm^3/str is reached before significant error occurs. If multiple injections are to be used, there must be a gap of 5° between injections or excess fuel is delivered (insufficient dwell time for full closure/de-energising). This was later found to increase in line with engine speed, as would be expected. There does not seem to be a temperature dependency for fuelling.

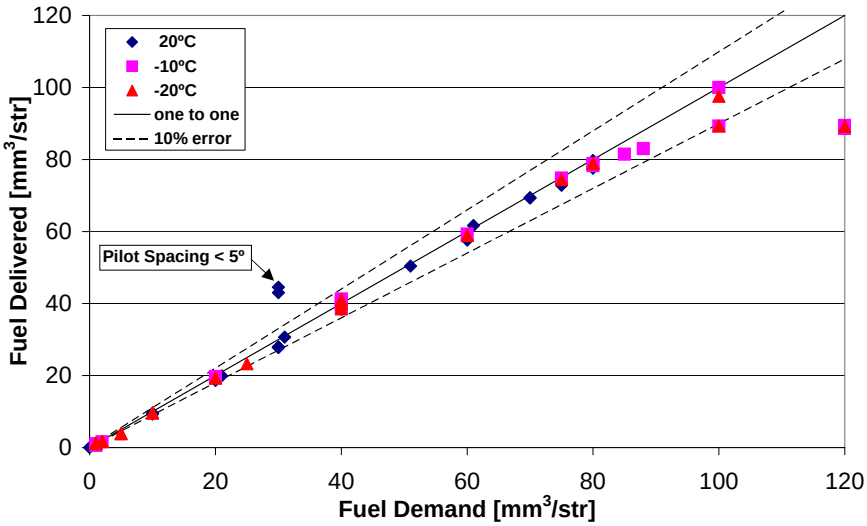

Figure a: Fuelling tests at three different temperatures

A.2 System Schematics

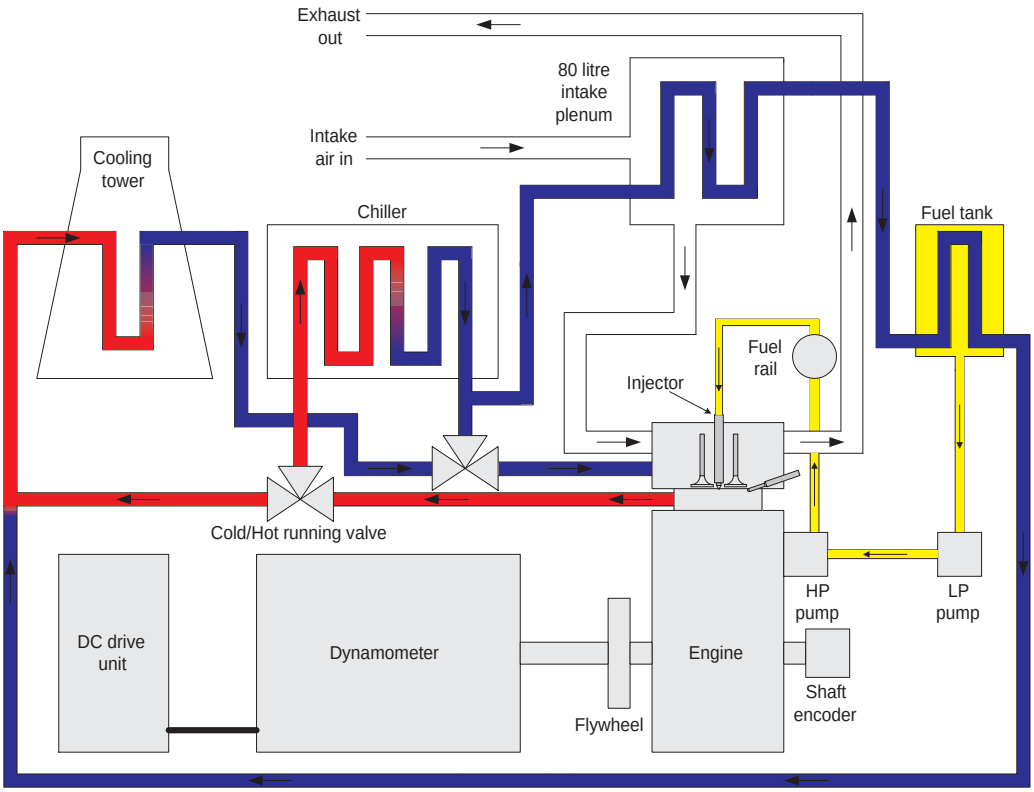

Figure b: Coolant flow through the system

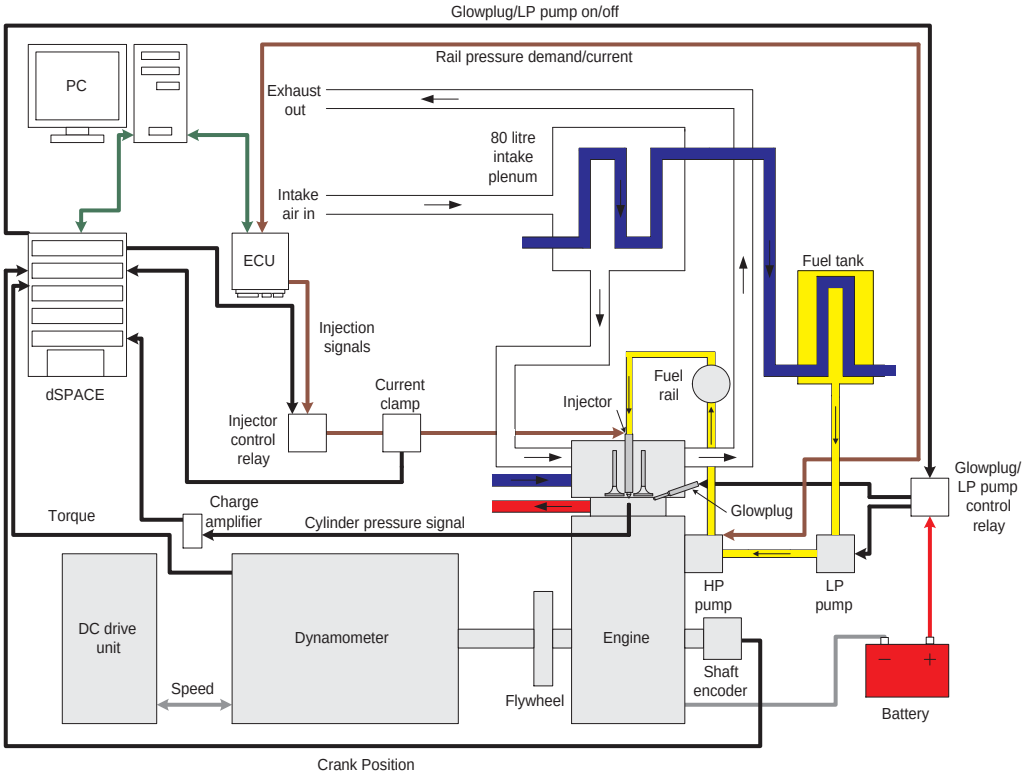

Figure c: Principal power and signal flows through the system

A.3 Start-of-Day Pre-Test Procedure

- Power up all electrical equipment.
- Turn on oil pump.
- Ensure cooling circuit engaged for cold operation.
- Turn on chiller cooling pump.
- Turn on chiller and set to desired operation temperature.
- Place insulation on engine if targeting $-20°C$ operation.
- Run through three cleaning point tests.
- Position the piston at bottom dead centre intake.
- Allow one hour for engine to soak at the desired temperature.

- Perform and record three first test of the day points at 15 minute intervals.

A.4 End-of-Day Conditioning Procedure

- Turn off chiller and chiller pump.
- Engage cooling circuit for hot operation.
- Turn on hot circuit cooling tower.
- Turn on oil and water heaters.
- Allow oil and coolant temperatures to rise to around $30°C$.
- Motor engine to approximately 1000 rpm.
- Engage fuelling at low level until temperatures exceed $60°C$.
- Increase engine speed to 1500 rpm and increase fuelling.
- Allow engine temperatures to reach steady-state with cooling at around 80–$90°C$.
- Continue operation for a further 20 minutes of hot operation.
- Gradually reduce fuelling to zero.
- Motor engine for two minutes.
- Stop engine and turn off pumps+electrical equipment.

A.5 Traditional First Law Heat Release Derivation

Equation 4.7 is rewritten below as the genera net heat release rate ignoring losses with respect to crank angle degrees

$$\frac{dQ_{net}}{d\theta} = \frac{dW}{d\theta} + \frac{dU_s}{d\theta} \tag{A.1}$$

and as work done, assuming constant pressure, is $p\,dV$ and internal energy for an ideal gas is given by mc_vT

$$\frac{dQ_{net}}{d\theta} = p\frac{dV}{d\theta} + mc_v\frac{dT}{d\theta} \tag{A.2}$$

The Ideal Gas Law states

$$pV = mRT \tag{A.3}$$

which can be written

$$\frac{d(pV)}{d\theta} = mR\frac{dT}{d\theta} \tag{A.4}$$

enabling equation A.2 to be rewritten as

$$\frac{dQ_{net}}{d\theta} = p\frac{dV}{d\theta} + \frac{c_v}{R}\frac{d(pV)}{d\theta} \tag{A.5}$$

or

$$\frac{dQ_{net}}{d\theta} = \left(1 + \frac{c_v}{R}\right)p\frac{dV}{d\theta} + \frac{c_v}{R}V\frac{dp}{d\theta} \tag{A.6}$$

$R = c_p - c_v$, which may be rewritten

$$\frac{c_p}{c_v} = \frac{c_v}{c_v} + \frac{R}{c_v} \tag{A.7}$$

and γ is defined as the ratio of specific heats, $\frac{c_p}{c_v}$ therefore

$$\gamma = 1 + \frac{R}{c_v} \tag{A.8}$$

meaning the $\frac{c_v}{R}$ term in equation A.6 may be replaced with

$$\frac{c_v}{R} = \frac{1}{\gamma - 1} \tag{A.9}$$

and $(1 + \frac{c_v}{R})$ can also be substituted with a relationship as follows

$$1 + \frac{c_v}{R} = \frac{\gamma - 1}{\gamma - 1} + \frac{1}{\gamma - 1} \tag{A.10}$$

which simplifies to

$$1 + \frac{c_v}{R} = \frac{\gamma}{\gamma - 1} \tag{A.11}$$

Equations A.9 and A.11 allow Equation A.6 to be written in its final form:

$$\frac{dQ_{net}}{d\theta} = \frac{\gamma}{\gamma - 1}p\frac{dV}{d\theta} + \frac{1}{\gamma - 1}V\frac{dp}{d\theta} \tag{A.12}$$

A.6 Output from AVL Blowby Meter

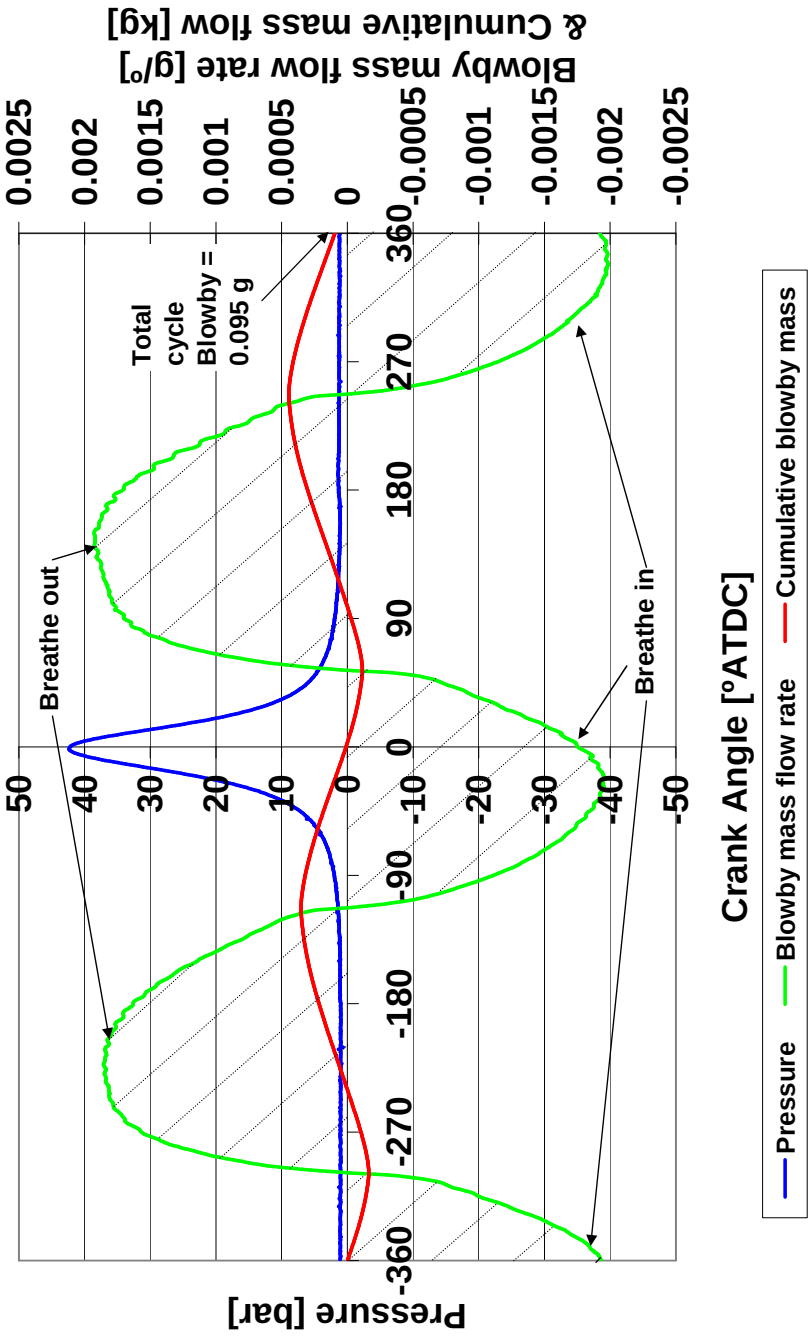

Figure d: Typical 300 rpm motored cycle with crank angle resolved AVL blowby meter readings in kg/CA and cumulative total showing 0.095 g blowby mass for this cycle.

A.7 Ceramic Glow Plug Supplied Calibration Sheet

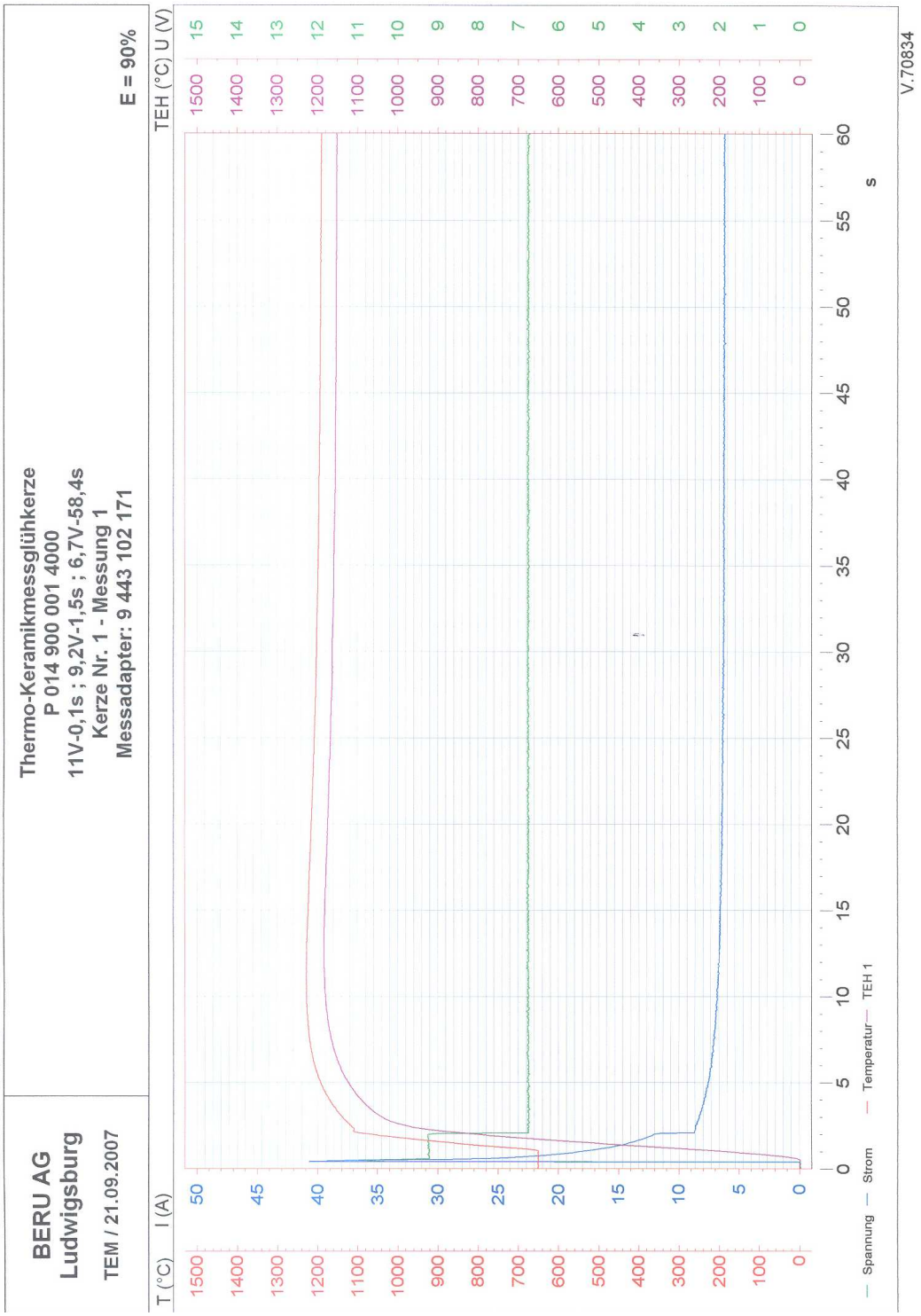

Figure e: Ceramic glow plug service power supply and internal/external temperature readings